Thermoresponsive polymer desiccants for water harvesting

A thesis submitted for the degree of Doctor of Philosophy of
The Australian National University

by

Moki Korakot Thanusing

August 2025

Australian National University

Research School of Chemistry
Canberra, Australia

Declaration

I declare that the material presented in this thesis, to the best of my knowledge, represents the result of original work carried out by the author from 2022 to 2025, and has not been presented for examination or credit towards any other degree or qualification. This thesis does not exceed 100,000 words in length. Established information, ideas, and methodologies have been acknowledged, wherever possible, by citation of the original publications from which they derive.

Moki Thanusing

August 2025

“Brevity is the soul of wit.”

- Hamlet, Act 2 Scene 2
  William Shakespeare

Acknowledgements

First and foremost, it is with pleasure that I thank my supervisor Professor Luke Connal for his consistent guidance and unwavering support throughout my candidature. Your open-minded and principled approach to science (and life) is one I will take with me into the future. I would also like to express my gratitude for my panel members, Em. Prof. Penelope Brothers, Assoc. Prof. Annie Colebatch, and Dr. Brett Pollard.

I also thank the present members of the Connal group for their camaraderie and willingness to share their knowledge: Dr. Brett Pollard (who mentored me closely throughout my candidature), Peidong Shen, Lillian Boton, Jason Buchanan, Md. Saifur Rahaman, Sandra Jestin, Rimaz Toto, Shraddha Bhat, and Kalyanshi Ubnare. I am also grateful to the past Connal group members, and would like to make special mention of Isaac Hampton, who passed away suddenly during my candidature. I further extend my gratitude to those who have collaborated on the research presented in this thesis.

This work is presented as an academic achievement, but it is accompanied by four years of personal growth as a young adult. Many valuable human lessons were taught alongside the academic ones – I am thankful for receiving both.

Finally, I am eternally grateful to my family and friends for their unending love and support, and without them this journey could never have happened.

Publications and Presentations

The following list details publications and presentations resulting from research that was conducted during the candidature of the Doctor of Philosophy.

Published

- **Thanusing, M.K.**; Shen, P; Pollard, B.L.; Connal, L.A. Rational design of water-harvesting hydrogels. *Mol. Syst. Des. Eng.*, **2024**, *9*, 63-72
- Zhang, F; Zhang, Y.; **Thanusing, M.K.**; Yu, Q.; Connal, L.A.; Lipiński, W.; Wang, X. CO2 hydrate formation in superabsorbent hydrogels for carbon capture—A comparison of water-confined framework vs non-water framework. *Chem Eng J*, **2024**, *500*, 157422
- **Thanusing, M.K.**; Pollard, B.L.; Connal, L.A. Arginine-functionalised hydrogels as a novel atmospheric water-harvesting material. *RSC Appl. Polym.*, **2025**, *3*, 480-487
- Zhang, Y.; **Thanusing, M.K.**; Rahaman, M.S.; Wang, F.; Alexander, K.; Connal, L.A.; Zhang, F; Wang, X. Zwitterionic polymeric hydrogels promote CO_2 hydrate formation kinetics: An experimental study. *Fuel*, **2025**, *396*, 135329
- Pollard, B.L.; **Thanusing, M.K.**; Connal, L.A. WHO Said What? Non-Robust Standards in Citing WHO and EPA Drinking Water Guidelines. *Mol. Syst. Des. Eng.*, **2026**, *11*, 147-153
- **Thanusing, M.K.**; Pollard, B.L.; Connal, L.A. Hygroscopic, creatine-functionalised microgels for efficient desiccants and water harvesting. *ACS Appl. Polym. Mater.,* **2026**

Presentations

- The 17th Pacific Polymer Conference, **Poster Presentation**, Water Harvesting Polymers (13th December 2022)
- The 38th Australasian Polymer Symposium, **Oral Seminar**, Water Harvesting Polymers (20th February 2024)

Abstract

Atmospheric water is a ubiquitous yet underutilised source of potable water. Polymeric desiccants are a particularly promising candidate for atmospheric water harvesting given their adaptability and scalability. However, the relative nascency of the field leaves many classes of polymers yet unexplored. This thesis details efforts into developing novel polymeric desiccants for atmospheric water harvesting while establishing frameworks for their rational design. The focus is primarily on thermoresponsive polymers, a particularly useful class of materials enabling the low energy release of sorbed water. Despite this property these materials have been largely overlooked for water harvesting applications. In **Chapter 1**, the current literature in atmospheric water harvesting is described, giving context to the experimental work reported within. In **Chapter 2**, a thermoresponsive copolymer library was synthesised to examine how differences in composition, crosslinker density and crosslinker length affected water harvesting properties. These insights into the relationship between polymer structure and water harvesting properties lay the groundwork for future rational design. **Chapter 3** details the development of a novel desiccant utilising *L*-arginine post-functionalisation of a thermoresponsive polymer. The resulting desiccant was highly hygroscopic while retaining its thermoresponsive properties. The kinetics of its water harvesting allowed for rapid harvesting cycles and increased yield. Finally, **Chapter 4** presents improved desiccants culminating from insights gained in the preceding chapters. The use of microgel structures and creatine functionalisation further improved water harvesting kinetics. In addition to highlighting the potential of microgels as a class of polymeric desiccants, these materials outperform many of those in existing literature.

Abbreviations

The following abbreviations have been used throughout this thesis.

µg	microgram(s)
µL	microlitre(s)
AA	acrylic acid
AIBN	2,2′-azobis(2-methylpropionitrile)
Alg	sodium alginate
APS	ammonium persulfate
Arg	arginine
AWH	atmospheric water harvesting
b	broad
BHT	butylated hydroxytoluene
BIS	*N*,*N*-methylenebisacrylamide
bmt	billion metric tonnes
cm	centimetre(s)
CMC	critical micelle concentration
CNT	carbon nanotube
COF	covalent organic framework
CTP	4-cyano-4-(phenyl-carbonothioylthio)pentanoic acid
d	doublet
Đ	dispersity
Da	dalton
DCM	dichloromethane
DEA	diethylamine
DLS	dynamic light scattering
DMAc	*N*,*N*-dimethylacetamide
DMAP	4-dimethylaminopyridine
DMF	*N*,*N*-dimethylformamide
DMSO	dimethylsulfoxide
DSC	differential scanning calorimetry
e.g.	*exempli gratia* (for example)
EDC	*N*-(3-dimethylaminopropyl)-*N*′-ethylcarbodiimide hydrochloride

EDU	1-(3-(dimethylamino)propyl)-3-ethylurea
EGDMA	ethylene glycol dimethacrylate
eq.	equivalents
et al.	*et alia* (and others)
EtOAc	ethyl acetate
FESEM	field emission scanning electron microscopy
Fmoc	fluorenylmethoxycarbonyl
FTIR	Fourier transform infrared
g	gram(s)
GPC	gel permeation chromatography
h	hour(s)
HEMA	2-hydroxyethyl methacrylate
HPC	hydroxypropylcellulose
HPMC	hydroxymethylpropylcellulose
i.e.	*id est* (that is)
IPN	interpenetrating polymer network
kDa	kilodalton(s)
kJ	kilojoule(s)
L	litre(s)
LCST	lower critical solution temperature
m	multiplet
M	molar
MAA	methacrylic acid
MeHQ	4-methoxyphenol
mg	milligram(s)
MHz	megahertz
min	minute(s)
mL	millilitre(s)
mmol	millimole(s)
Mn	number average molecular weight
MOF	metal organic framework
mol	mole(s)
mol%	mole percent

mW	milliwatt(s)
NIPAAm	*N*-isopropylacrylamide
nm	nanometre(s)
NMR	nuclear magnetic resonance
PAAS	poly(sodium acrylate)
PAN	polyacrylonitrile
Pbf	2,2,4,6,7-pentamethyldihydrobenzofuran-5-sulfonyl
PDI	polydispersity index
PEG	poly(ethylene glycol)
PEGDMA	poly(ethylene glycol) dimethacrylate
PEGMA	poly(ethylene glycol) methyl ether methacrylate
pKa	acid dissociation constant
POP	porous organic polymer
PPy	polypyrrole
PVCL	poly(*N*-vinylcaprolactam)
RAFT	reversible addition-fragmentation chain transfer
RH	relative humidity
RO	reverse osmosis
RT	room temperature
s	singlet
SAWH	sorption-based atmospheric water harvesting
SDS	sodium dodecyl sulfate
SEM	scanning electron microscopy
t	triplet
T_{cp}	cloud point temperature
TEA	triethylamine
TFA	trifluoroacetic acid
T_g	glass transition temperature
THF	tetrahydrofuran
TIPS	triisopropylsilane
UCST	upper critical solution temperature
VCL	*N*-vinylcaprolactam
viz.	*videlicet* (namely)

VPTT	volume phase transition temperature
w.r.t.	with respect to
wt%	weight percent
δ	chemical shift (parts per million)
ΔG_{mix}	Gibbs free energy of mixing
ΔH_{mix}	enthalpy of mixing
ΔS_{mix}	entropy of mixing

Table of Contents

Chapter One – Introduction

Water scarcity is a pressing global issue that requires urgent intervention. Approximately two thirds of the global population experiences severe water scarcity for at least one month per year.[1] Droughts caused by water scarcity cost an estimated $307 billion USD in damages yearly.[2] There are many causes of water scarcity, including mismatched supply and demand, subpar infrastructure, or lack of governance. A growing world population also commands an increasing demand, which is currently unmet by any comparable growth in freshwater supply.[3] One method of alleviating water scarcity is to utilise new sources of freshwater. The most prominent of these efforts has been utilising seawater through desalination. Seawater comprises over 96% of global water and is essentially limitless compared to human requirements.[4] However, desalination is currently energy-intensive, laborious, limited to coastal areas, and carries its own negative environmental impacts.[5] The environmental impacts of desalination are severe, including disturbance of aquatic ecosystems and production of highly saline byproducts.

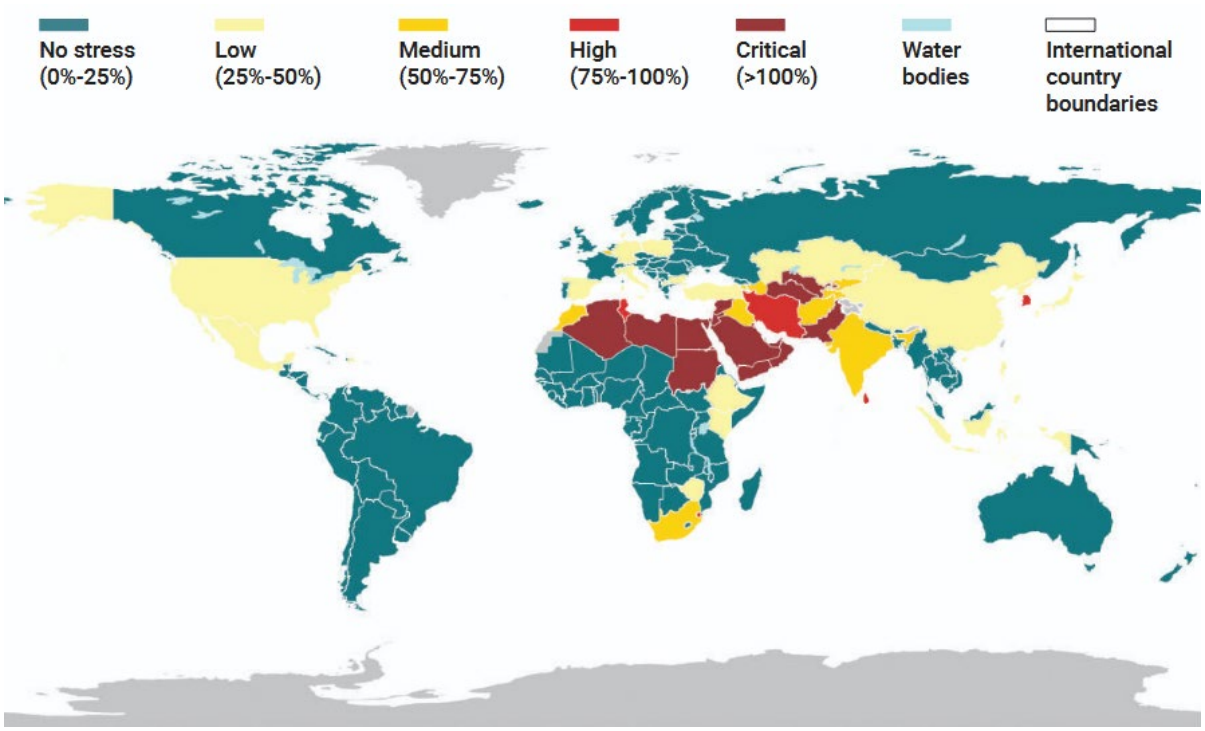

Figure 1: Map of water stress (withdrawn freshwater relative to renewable freshwater resources) by country, 2021. Reproduced from UN Water.[6]

Atmospheric water is another promising renewable freshwater reservoir. The hydrologic cycle is the natural movement of water in different forms on Earth.[7] An estimated 45.5 trillion

metric tonnes of water is moved by the hydrologic cycle every year, which greatly exceeds the global freshwater usage.[8] All water used by humans eventually returns to the hydrologic cycle, albeit in forms that are not easily accessible (e.g. soil via irrigation) or require processing to use (e.g. wastewater, seawater). Being a core reservoir of the hydrologic cycle, the total amount of atmospheric water is estimated to be around 12.9 trillion metric tonnes, which is over five times more than the amount of water in the world's rivers.[9] Atmospheric water has an average residence time of 9 days, that is, the average water molecule spends 9 days as atmospheric water before moving along the hydrologic cycle.[10] Exact residence times are dependent on season and location but are always in the order of days. In contrast, rivers, lakes, and groundwater, which are the most utilised freshwater sources, generally have longer residence times.[11, 12] Residence times are typically calculated by the rate at which water enters or exits a reservoir. Atmospheric water is therefore replenished more rapidly than other water sources, making it a robust potential water source. An additional advantage of atmospheric water is its ubiquity in all climates.[13] There are many situations where decentralised water harvesting can be beneficial. Communities where freshwater is not otherwise accessible (e.g. arid climates) can still harvest atmospheric water.[14] Portable harvesting systems can allow atmospheric water to be harvested *in situ*, which removes the need for water transport for long journeys or disaster zones.[15, 16] Atmospheric water is also generally clean, reducing the need for treatments such as filtrations or sterilisations typical of other water sources.[17]

Despite the appeal of atmospheric water harvesting (AWH), it still has not been adopted beyond small-scale commercial systems. One of the obstacles to AWH usage has been energy demand, especially critical in locations where solar energy is not available in abundance.[18-20] Energy and water are mutually dependent on each other; this relationship is called the water-energy nexus.[21] The yield of water from an AWH system comes with an energy cost to produce and operate that system which in turn has a water cost. A viable AWH system must therefore be energy-efficient in both production and operation. It is likely that large-scale adoption of AWH (or any other new water harvesting method) will only proceed after extensive analysis of cost, energy usage and environmental impact.

AWH technologies can be divided into two categories based on their mechanism of harvesting: cooling and desiccating. Cooling technologies depend on cooling and subsequent condensing of liquid water from the air, while desiccant technologies use desiccating

materials to gather water for later extraction. These categories can be further subdivided based on energy input, *viz.* active or passive.

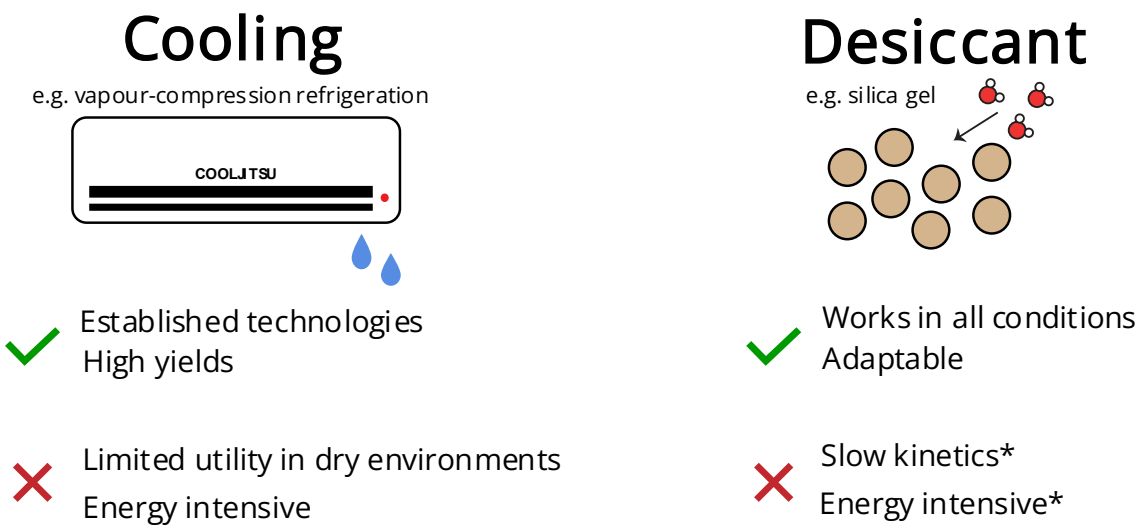

Figure 2: Advantages and disadvantages between cooling and desiccant-based AWH technologies. (*depending on desiccant)

Commercially, cooling technologies are the most prominent AWH strategy. Active cooling methods use existing refrigeration technologies, principally vapour compression, thermoelectric or adsorption/absorption cooling. These methods are adjusted to maximise condensation which is normally a byproduct of air conditioning or dehumidification.[22] The temperature difference needed to form condensation is dependent on relative humidity (RH) and ambient temperature. At 80% RH and 25°C, condensation will happen on a surface that is about 21.3°C. When the humidity halved is to 40% RH at the same ambient temperature, the surface will need to be 10.5°C for condensation.[23] Condensation temperature and ambient temperature increase proportionally at constant RH. The mathematical relationships between humidity parameters relevant to water harvesting are elaborated upon further in other sources.[23, 24] The energy usage for cooling increases significantly in hotter, drier areas, which makes this technology unsuitable for arid climates. Passive (energy free) cooling technologies include fog and dew harvesting. Water vapour can spontaneously form droplets in the air (in the case of fog) or on a surface (in the case of dew). Fog nets and dew farms have been developed to harness these natural phase change phenomena though yields are highly dependent on location and weather conditions.[25, 26] Cooling AWH technologies require specific environmental conditions to operate efficiently and cannot be adapted universally. Other authors have written reviews covering cooling AWH technologies in more detail.[18, 22, 25-28]

Desiccants present an attractive alternate pathway via sorption-based AWH (SAWH). Moisture is gathered spontaneously into a desiccating material, which can later be extracted. In many systems extraction is done by vaporising the captured moisture and condensing it into liquid water. This step renews the desiccant for more harvesting. Unlike pure cooling AWH systems, this condensation step is more localised and therefore more energy efficient. SAWH can be adapted to a wide variety of climates, including arid. To yield useable water, SAWH systems usually require the desiccant material to be heated enough for captured water to vaporise and be condensed separately. This step is energy-intensive; the heat of vaporisation of pure water is 40.66 kJ/mol.[29] As water becomes more favourably bound to a material, the necessary energy for desorption increases further. For example, water in zeolite 13X requires temperatures above 120°C for full desorption.[30] The major categories of SAWH desiccants vary by author discretion, but the following covers the most prevalent groups of materials: inorganic solids (e.g. silica gel and zeolites), hygroscopic salts (mainly lithium or calcium chloride), metal-organic frameworks (MOFs), porous organic polymers (POPs), and hydrogels.[31-38]

Some desiccants are already produced at scale, though there are disadvantages to their use in SAWH. Inorganic materials and hygroscopic salts are already produced at scale for dehumidification but have disadvantages for SAWH.[39, 40] Briefly, these usually have slow adsorption rates and require high temperatures to desorb efficiently.[41, 42] For AWH, hygroscopic salts can uptake significant amounts of water even in low humidity environments.[43-45] However, their ability to deliquesce necessitates an appropriate vessel or substrate to prevent leaching into harvested water. Hydration kinetics are also slowed by particle agglomeration, and concentrated salt solutions can be corrosive, reducing the longevity of AWH systems.[46-49]

In the context of SAWH, the scope of polymer design allows for tailoring to specific climates, making them an attractive alternative to existing desiccants. MOFs and POPs show promising AWH performance yet generally involve expensive reagents or days-long syntheses in extreme reaction conditions.[35-37, 50, 51] The synthetic methods for these materials are also not readily scalable scale despite recent advances.

Hydrogels are especially promising for SAWH given their adaptability and scalability. Many hydrogels can be made from sustainably sourced reagents in mild reaction conditions. This makes them the most promising material for large-scale SAWH**;** even when focusing on

hydrogel-based SAWH materials, there has been a sharp increase in published literature in the last decade.

The polymer network in SAWH hydrogels is critical to the water harvesting properties of the final material. Water uptake can be improved with charged polymers. A study by Feng and coworkers illustrated this well by comparing 7 different hydrogels for SAWH.[52] The charged polymers all showed superior uptake to neutral hydrogels. Poly(2-acrylamido-2-methylpropane sulfonic acid) (PAMPS) was identified as the best candidate for water harvesting based on its balanced water uptake and release kinetics. The related monomer, AMPS, and the sulfonate moiety in general, has demonstrated strong SAWH performance elsewhere.[53-55]

Functional additives feature significantly in SAWH hydrogel literature. Hygroscopic salts like lithium chloride and calcium chloride are often added to enhance water uptake, especially in low RH conditions. The disadvantages that come from the deliquescence of these materials can be mitigated by distributing salt crystals within a polymer matrix.[56-59] In one example, Shan and coworkers used LiCl to enhance the water uptake of a PAMPS hydrogel.[60] The sulfonate groups on the PAMPS formed ionic bonds with the LiCl, immobilising the salt within the hydrogel and minimising salt leakage. Water uptake reached 2 g/g after 1 h at 90% RH, however desorption at 90°C for 6 h left about 0.5 g/g within the polymer. In another example, Aleid and coworkers used a zwitterionic polymer, poly(2-(methacryloyloxy)ethyldimethyl-(3-sulfopropyl)ammonium hydroxide) (PDMAPS), to immobilise both ions from LiCl.[61] PDMAPS itself is not soluble in water because polymer self-association is more favourable. When LiCl is added, ionic bonds are formed between the polymer chains and the salt ions. These salt-polymer interactions are more energetically favourable than the polymer self-association. This gives rise to a “salting-in” effect, allowing PDMAPS to “solvate” or hydrogen bond with water. Water uptake of PDMAPS hydrogel was improved about fivefold after the addition of the LiCl, up to 0.75 g/g after 1 h at 60% RH. Beyond hygroscopic additives, photothermal additives are often used in SAWH polymers. Photothermal functionality enhances water release by converting light into additional heat energy.[62, 63] Many SAWH materials are intended for outdoor usage. The abundance of solar energy enhances the effectiveness of photothermal additives. The most common photothermal additives used in SAWH are carbonaceous fillers like carbon nanotubes (CNTs), graphene, and carbon black.[35, 64-69] One study utilising photothermal functionality incorporated CNTs into a system with polyacrylamide (PAM) and $CaCl_2$.[70] About 0.3 g/g of

water uptake was observed after 1 h at 60% RH. The use of CNTs greatly increased the local temperature of the material during solar irradiation up to 75°C.

Modified, naturally derived polymers are also candidates for SAWH, including sodium alginate (Alg), cellulose, starch, silk fibroin and chitosan.[71-75] Compared to fully synthetic systems, natural polymers generally required more processing before use. The main exception is Alg, which can be made easily through ionic crosslinking. Alg is already produced sustainably on an industrial scale, making it one of the most promising natural polymers for scalable SAWH materials.[76, 77] One possible concern with Alg-based hydrogels is their durability. Alg is crosslinked through ionic bonds whereas many hydrogels are crosslinked through covalent bonds. With the constant movement of water through a SAWH hydrogel, it is worth considering the effectiveness of an ionic bond in the long term. Ion exchange would occur with the use of additives like hygroscopic salts. This was capitalised upon by Entezari and coworkers with their dual-ion Alg system. A combination of Li and Ca ions was found to be optimal for SAWH performance.[78] About 2 g/g of uptake can be observed after 1 h at 70% RH.

Multiple polymers can be utilised at once to form more complex SAWH hydrogels. One approach is using an interpenetrating polymer network (IPN) to combine functional polymers. In the context of SAWH this typically consists of a thermoresponsive polymer and a hydrophilic/hygroscopic polymer.[79-81] The thermoresponsive polymer undergoes a hydrophilic/hydrophobic transition with a change in temperature which assists in water release. However, the IPN structure with a hydrophilic polymer impedes the release of water. Another approach to combining multiple polymer functionalities is using layered structures, particularly when introducing photothermal additives. One study by Yu and coworkers used a hydrophobic and photothermal polydimethylsiloxane (PDMS) layer on the outside of a salt-impregnated cellulose-based material. The PDMS layer did not impede water uptake, but it did minimise leakage of the hygroscopic salt during water release.[82] About 0.4 g/g of uptake was observed after 1 h at 60% RH. PDMS was also used as a photothermal layer in a polyacrylonitrile-based (PAN) material by the same research group.[83] Water uptake reached 2.5 g/g after 1 h at 60% RH. These studies highlight the scope of polymer synthesis in incorporating multiple functionalities.

SAWH performance can also be enhanced through maximising surface area. This is typically demonstrated through optimising porosity. Lyu and coworkers formed macroporous

hydrogels by using poly(ethylene glycol) (PEG) as a pore-foaming template.[67] The large pores enhanced the speed of water uptake compared to a chemically identical oven-dried polymer. Water uptake reached about 0.7 g/g after 1 h at 70% RH. Another approach to improving porosity optimises the tortuosity of the polymer matrix. Tortuosity is a parameter of porous media describing the ratio between the shortest possible pathway and the distance between two points.[84] For SAWH, minimising tortuosity can optimise the mass and heat transfer of water in a porous medium. Wang and coworkers formed a polymer with a honeycomb-like structure and vertical channels.[66] Surface area in the inside of this hydrogel was more accessible, increasing the uptake by over 200%, up to 0.4 g/g at 30% RH, in 1 h compared to a hydrogel without channels. Water release would likewise be enhanced by the accessible surface area of the channels though this was not explicitly tested in the study.

Many additional avenues for SAWH hydrogel design have emerged in literature. While hygroscopic salts and carbonaceous fillers are the most common additives in SAWH hydrogels, other additives for water uptake and release have been recorded.[74, 85, 86] These additives can include other polymers, like how Zhou and coworkers dispersed chitosan chains within a PAM network.[87] Some synthetic methods have only been explored in a limited capacity. Two studies by Mohanrao and coworkers are the only examples of topochemical synthesis that could be found for SAWH hydrogels.[88, 89] Emulsion polymerisation is also underrepresented in this space, with the only SAWH example found being a study by Guan and coworkers.[90] Hybrid SAWH materials also exist between major categories. MOFs have been integrated into hydrogels as functional crosslinkers.[75, 91] A flexible chitosan-silica composite was made by Song and coworkers that could release water through mechanical compression.[92] These studies highlight a wider range of exciting materials and methods left to be explored for SAWH.

The dependence of SAWH hydrogels on functional additives is a cause for concern. Many AWH studies claim to yield potable water, including SAWH studies with functional additives. Such a claim would necessitate that these additives are benign or otherwise safe in dilute concentrations. The most concerning of the common additives is LiCl. Lithium is one of the trace metals essential for human health, though negative side effects can be observed at therapeutic doses.[93, 94] Lithium can easily become toxic to the human body, affecting renal and thyroid function. Despite this, lithium concentrations in drinking water are not currently regulated in any jurisdiction. The most recent drinking water guidelines from the WHO in 2022 make no mention of lithium, and the US Environmental Protection Agency (US EPA)

recommends a health reference level of 10 µg/L.[95, 96] This lack of clear guidelines makes any claim of cleanliness impossible to substantiate with the presence of lithium.

Materials chemistry research is usually conducted with specific applications in mind, rendering rational design necessary for efficient material development. Rational design in the context of SAWH hydrogels necessitates understanding how specific polymer structures affect water harvesting properties, or put more simply, the structure-property relationship. However, as I have presented, recent literature pertaining to SAWH hydrogels has focused heavily on the use of additives, specifically hygroscopic salts and carbonaceous fillers. Additives were used in all but one of the studies referenced thus far.[81] While this general (if somewhat myopic) approach has presented immediately attractive water harvesting performance, there has been a wide knowledge gap left behind. The use of additives obfuscates exact structure-property relationships for the fundamental polymer systems, hindering rational design choices.

The structure-property relationships for SAWH polymers are still not deeply understood. Many polymer properties are interdependent, making it difficult to identify the exact relationship between polymer structure and desired water harvesting behaviour. One such unknown is the effects of crosslinking on SAWH, as, *a priori*, properties like crosslinker length or density should have some observable effect. Despite the great number of unknowns, there are still some universal (if lower-order) desirable traits. A high surface area enhances the rate of both water uptake and release. For water uptake, there needs to be hydrophilic or charged moieties in the system, whether that is part of the polymer chain or in an additive. These properties generally correlate with hygroscopicity. Hydrophilicity also assists in water storage within the polymer. However, this hydrophilicity will act against us in the release process; the energy needed to break the polymer-water interactions increases with polymer hydrophilicity.[97] Hydrophilicity therefore needs to be balanced to allow water uptake but also efficient water release.

Thermoresponsive polymers require less energy for water release without compromising water uptake. Reducing the intrinsic energy demand of water release without compromising water uptake is possible with stimulus-responsive polymers. Of these, thermoresponsive polymers are the most well-known, and have already shown promise for drug delivery applications.[98, 99] These polymers undergo a reversible and discontinuous change in properties (a phase transition) as a function of temperature. The phase transition is generally described

as a hydrophilic-hydrophobic or coil-to-globule transition, with the hydrophilic "coil" interacting freely with solvent (i.e. being soluble) and the hydrophobic "globule" maximising interactions with itself (i.e. being insoluble) (**Figure 3**). An amphiphilic structure is hence necessary for thermoresponsive properties.

A polymer solution that separates into two phases upon heating displays a lower critical solution temperature (LCST). When this separation happens upon cooling, the polymer has an upper critical solution temperature (UCST). Most known thermoresponsive polymers only display LCST behaviour, though some display an UCST or both.[100] The most well-known thermoresponsive polymer is made with *N*-isopropylacrylamide (NIPAAm). The reason poly(NIPAAm) (PNIPAAm) continues to garner strong research interest is due to its relatively low LCST, being close to the human body temperature at only 32°C.[101, 102]

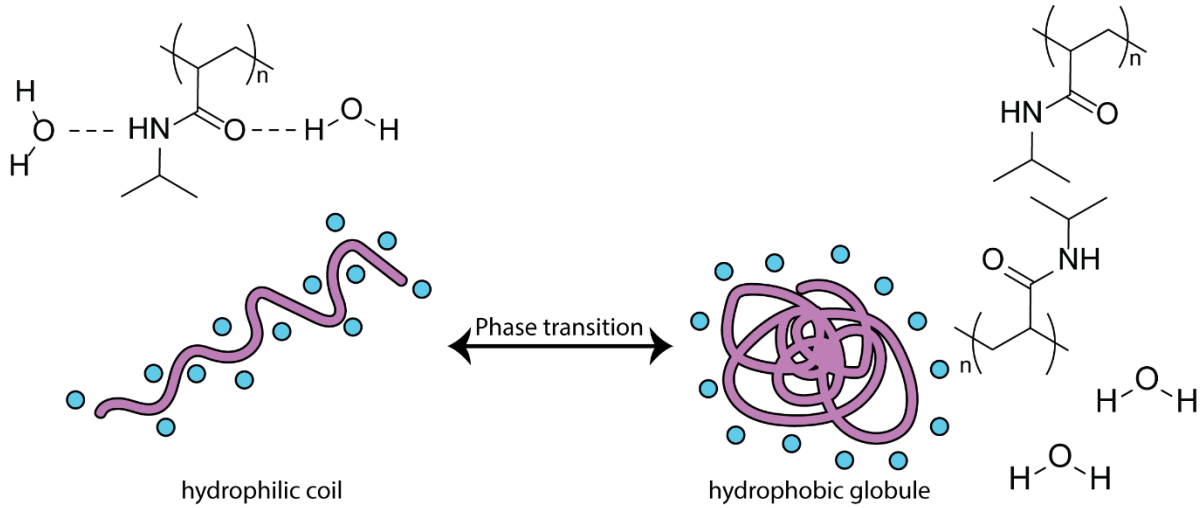

Figure 3: Reversible phase transition of thermoresponsive polymers, using PNIPAAm as an example. In the hydrophilic state (below LCST in the case of PNIPAAm), polymer-solvent interactions are favoured. In the hydrophobic state (above LCST for PNIPAAm), polymer-polymer and solvent-solvent interactions are favoured.

The phase transition temperature is determined by the thermodynamic relationship between polymer and solvent. As LCST behaviour is more relevant to SAWH, future references to thermoresponsive polymers within this chapter will assume LCST behaviour unless stated otherwise. Considering the Gibbs free energy of mixing (ΔG_{mix}), both entropic and enthalpic factors are necessary to explain thermoresponsive behaviour:

$$\Delta G_{mix} = \Delta H_{mix} - T\Delta S_{mix} \quad (1)$$

Equation 1: Gibbs free energy of mixing.

In an ideal solution mixing is always favourable. There is no enthalpy of mixing (ΔH_{mix}), hence the entropy of mixing (ΔS_{mix}) is also always favourable.[103] However, polymer solutions are not ideal. When a polymer is solvated, solvent molecules interact with and are ordered along a polymer chain. As temperature increases, this ordering becomes less entropically favourable. Any polymer solution, thermoresponsive or not, will have less favourable entropy as temperature increases. By necessity, the magnitude of entropic contributions increases with temperature to the ΔG_{mix}. The deciding factor for observable thermoresponsive behaviour is therefore the ΔH_{mix} between polymer and solvent. To display LCST behaviour, the interactions between polymer and solvent (i.e. ΔH_{mix}) need to become less favourable with increasing temperature relative to polymer-polymer and solvent-solvent interactions.

A diverse range of structures can provide thermoresponsive polymers, enabling for a great degree of freedom in system design. Thermoresponsive behaviour is only dependent on overall polymer amphiphilicity. For example, NIPAAm has both a hydrophilic (amide bond) and hydrophobic moiety (isopropyl group), making PNIPAAm thermoresponsive. In contrast, ethylene glycol-based monomers are comparatively hydrophilic and still form thermoresponsive polymers.[104, 105] Foster and coworkers recognised two statistically significant clusters of thermoresponsive homopolymers based on monomer hydrophobicity.[106] One set of monomers had both hydrophilic and hydrophobic moieties while the other was more hydrophilic. The amphiphilic nature of thermoresponsive polymers made from hydrophilic monomers comes from the hydrophobic hydrocarbon polymer backbone.[107, 108] By extension, monomers for non-responsive homopolymers could be combined to give the necessary amphiphilicity for thermoresponsive behaviour.[109-111]

Thermoresponsivity is sensitive to a variety of factors. The temperature at which a phase transition occurs is concentration dependent, known as the cloud point, T_{cp}. The LCST occurs at the lowest possible T_{cp} on a temperature-composition phase diagram (**Figure 4**). LCST is specific to a polymer and solvent system regardless of its concentration in solution.[112] The term is often used as a general indicator of thermoresponsive properties. An increase in polymer length enhances the negative entropic effect on ΔG_{mix} and so reduces the LCST.[113, 114] Increased polymer hydrophilicity reduces ΔH_{mix} which increases LCST, and conversely the opposite applies for hydrophobicity, which decreases LCST.[107, 108, 110, 111] The hydrophilic-hydrophobic balance is most often adjusted by copolymerisation. The existence of charge, whether on the polymer chain or in solution, can dampen thermoresponsive behaviour.[115] Other solution additives like surfactant can also change LCST.[116]

Thermoresponsive behaviour can be tuned to differing degrees depending on the specific polymer system.

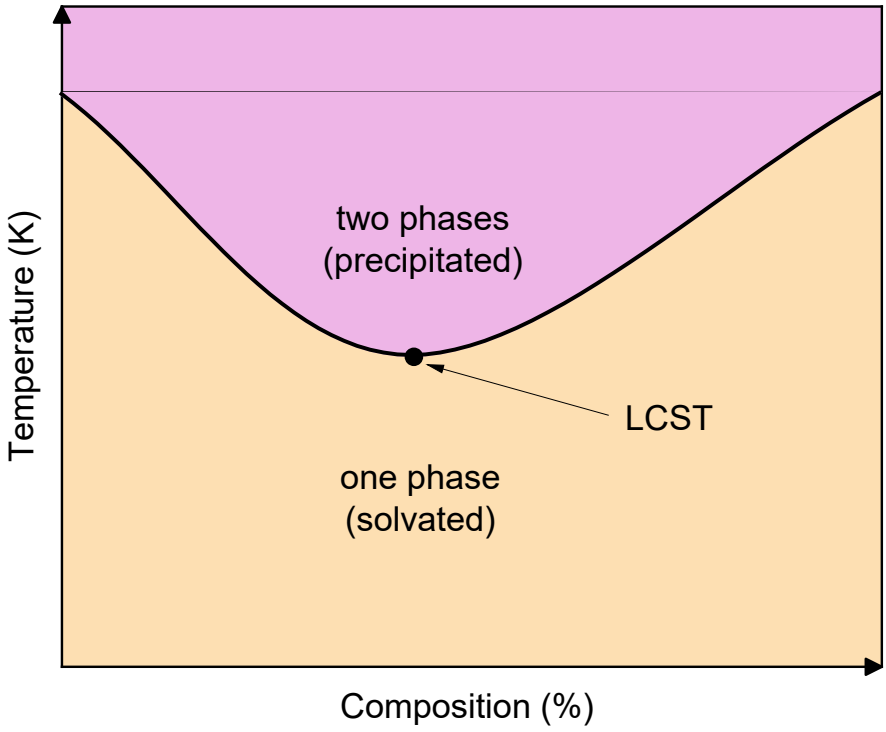

Figure 4: A general temperature-composition phase diagram of a polymer solution exhibiting LCST behaviour. LCST is defined as the lowest temperature on the phase diagram where phase transition can occur.

Overall, there are many avenues through which thermoresponsive polymers can be adjusted for specific applications. Thermoresponsive polymers can be hygroscopic and hence show promise for SAWH applications. The typical SAWH material requires the vaporisation and subsequent condensation of harvested water. Even with the abundance of energy provided by solar power, vaporising liquid water only to condense it again is a method that could be further optimised. Effective condensation temperatures are much lower in hot environments, meaning that the energy requirements of a SAWH system become more demanding in hot environments.[23] Thermoresponsive polymers can bypass the need to vaporise (and therefore condense) harvested water. A polymer with LCST behaviour has a hydrophilic-hydrophobic transition as temperature increases. Captured water inside a thermoresponsive SAWH material would therefore be expelled in liquid form above a specific temperature. As LCST is specific to phase transitions in solution, the analogous transition for a solid material is known as the volume phase transition temperature (VPTT).[117] As no vaporisation of water is happening, the energy requirements for water release are just the amount to heat the desiccant

to a suitable desorption temperature. After the harvested water has been taken, a reduction in ambient temperature below the VPTT will renew a thermoresponsive SAWH material ready for more harvesting. These polymers are therefore promising for a lower-energy SAWH system.

Thermoresponsive polymers have featured in several SAWH hydrogel materials, largely focusing on PNIPAAm, although also on cellulose derivatives and poly(*N*-vinylcaprolactam) (PVCL) to lesser extents. Earlier examples of thermoresponsive SAWH materials used an interpenetrating polymer network (IPN) to combine desirable functionalities. A study from Matsumoto and coworkers presented an IPN with hydrophilic and thermoresponsive networks.[81] PNIPAAm and Alg were used in the IPN. The addition of the Alg network allowed for 300% improved water absorption compared to the PNIPAAm by itself. 0.4 g/g of water could be absorbed in 1 h at 80% RH. Additionally, the thermoresponsive behaviour of PNIPAAm was preserved in the IPN. Even though the VPTT of the polymer was close to the LCST of PNIPAAm (being 32°C), the investigators report that a temperature of 50°C was required to maximise water release. While the phase transition temperature is the lowest necessary amount of energy to break polymer-water hydrogen bonds, more strongly bound water molecules require higher amounts of energy. Supplying excess energy guarantees a higher amount of desorption as more strongly bound water molecules can be desorbed reliably. Uptake-release cycles of this polymer also only yielded up to 20% of absorbed water per cycle. Water release was impeded by the hydrophilicity of the Alg despite the hydrophilic-hydrophobic transition from PNIPAAm. Despite this, full water release is not always necessary for a working SAWH system. Another IPN-based water harvester by Lee and coworkers retained much of its moisture but could continuously harvest and release water.[80] This cactus-inspired system had a polymer IPN “mucilage” made from networks of agarose, Alg, and PNIPAAm. Water uptake was assisted by a copper mesh “cuticle” on the outside of the polymer cylinder which nucleated water droplets for absorption while preventing undesirable evaporation from the polymer. Water release could be conducted at 40°C with visible droplet formation. The yield of water per harvesting cycle was minimal (40 mg), given the hydrophilic Alg and agarose networks in the IPN, though cycles were under 10 minutes in total. Photothermal additives can increase the yield of water release. Chang and coworkers used PNIPAAm/Alg IPN beads for irrigation, adding black dye to the mixture for photothermal functionality.[118] Water uptake reached 1 g/g after 1 hour at 60% RH. Field testing of this material yielded 2.3 g/g (~80% total absorbed water, 14 h uptake) of released

water over 9 daylight hours. Notably, only 4 of those hours had ambient temperatures above the LCST of PNIPAAm. The photothermal black dye increased the local temperature of the polymer when there was sufficient sunlight and allowed for water release over time.

In these PNIPAAm systems, water release during SAWH can be maximised by optimising polymer structure. The main disadvantage of an IPN structure is that the non-responsive networks impede collapse, which also impedes water release. One workaround is to utilise smaller hygroscopic additives which will not impede the movement of thermoresponsive polymers. In a study by Zhao and coworkers, hygroscopic polypyrrole (PPy) particles were incorporated into a porous PNIPAAm hydrogel.[119] Water uptake reached 3 g/g at 60% RH after 24 h. During water release the PNIPAAm could collapse easily around the polypyrrole particles, greatly maximising water release. About 50% of absorbed water was released after 20 minutes at 40°C. Another small hygroscopic additive is hygroscopic salts, which feature in many SAWH hydrogel materials.[120] Wang and coworkers, using PNIPAAm and graphene oxide, used a calcium chloride solution to incorporate the salt into the hydrogel. This material could uptake 1.5 g/g water after 1 hour at 90% RH.[121] About 80% of sorbed water could be released after 2-3 hours under solar light irradiation. Another alternative to the IPN structure is utilising functional layers. Zhang and coworkers made a hydrogel with a thermoresponsive PNIPAAm core and a hygroscopic/photothermal polydopamine-sodium polyacrylate (PDA-PAAS) shell.[122] LiCl was dispersed evenly within the hydrogel to enhance water uptake. The core-shell structure was crucial to minimise LiCl leakage from the hydrogel. Any expelled liquid water would have LiCl within, necessitating the release of water by condensation for this polymer. (Interestingly, Li ions were still found in collected water.) Water uptake reached up to 1.2 g/g at 90% RH. Almost all absorbed water was released under 12 h natural solar irradiation. The same research group adapted this method for another study where flax yarn was coated with PNIPAAm then PDA-PPy.[123] $CaCl_2$ was used instead of LiCl, yielding a water uptake after 1 h of 0.75 g/g at 70% RH. While water uptake performance was similar to the last material, complete water release could be achieved after 6 hours at 50°C. A thermoresponsive shell around a hydrophilic core was made by Maity and coworkers.[53] Water uptake reached 2.5 g/g after 1 h at 75% RH. During water release the thermoresponsive shell squeezed the core, extracting liquid water from the hydrogel. About 80% of water could be released after 15 minutes of heating at 70°C. Ma and Zheng used a thermoresponsive PNIPAAm shell over a silica gel core instead, supplemented by LiCl.[124] About 1 g/g water was absorbed at 70% RH after 1 h. Up to 65% of water could be released from these

composites after an hour at 50°C, with the remainder staying within the system. Water release from silica gel requires high-energy conditions, meaning that the released water is likely exclusively from the grafted PNIPAAm. While functionality was not layered in this case, one study from Zheng and coworkers used PNIPAAm as a grafted side chain on an Alg-based network.[86] About 0.5 g/g of water was absorbed in 2 h at 80% RH. It is not clear what effects PNIPAAm grafting had on water uptake or release. The effectiveness of grafted thermoresponsive polymers for SAWH is still a topic that could be explored.

Desorption for PNIPAAm-based systems may not always benefit from full polymer network collapse. For a porous polymer, this collapse is associated with a reduction in porosity as the thermoresponsive polymer network undergoes phase transition. Reduced porosity impedes the movement of water within the polymer out of the system. Lu and coworkers made a shrinkage-resistant SAWH hydrogel by reinforcing a PNIPAAm hydrogel with cellulose nanofibers.[125] Water uptake reached 2 g/g after 1 h at 80% RH. Porosity was retained when the polymer was heated, allowing for faster water release. This polymer, also containing LiCl and photothermal CNTs, was capable of 80% water release after 20–30 minutes, and full release after 1 h of solar irradiation.

The use of hygroscopic salts in PNIPAAm-based SAWH hydrogels improves water uptake but causes salt leaching. The working life of salt-impregnated SAWH polymers is hence limited if leaching is not controlled. One approach to minimise leaching is to ionically bond the salt to a charged polymer like PDMAPS, like was done in a study by Guan and coworkers.[90] The strong charges made LiCl less likely to leach out during water release while still allowing hygroscopicity. After 1 h at 60% RH, 1 g/g of water was absorbed by the polymer. Almost all absorbed water was released after 30 minutes of solar irradiation, but only about 70% was collected by condensation. Inductively coupled plasma mass spectrometry (ICP-MS) analysis of the harvested water showed a Li concentration of about 7 μg/L. This concentration is one of the lowest recorded in SAWH literature, and is below the US EPA's reference level of 10 μg/L.[96]

Apart from PNIPAAm, cellulose derivatives have been employed as the thermoresponsive component of a SAWH hydrogel. Cellulose is naturally derived and biodegradable, making it an attractive choice for sustainable chemistry applications.[126, 127] Some modified cellulose ethers display thermoresponsive properties. Hydroxypropyl cellulose (HPC) is one such cellulose derivative which has many industrial applications.[128-131] HPC has a LCST of around

43°C. HPC can be used as a functional matrix for additives like hygroscopic salts. A LiCl supplemented HPC porous polymer was made by Yu and coworkers.[132] Water capture reached up to 0.5 g/g after 1 h at 70% RH in the samples containing the most LiCl. Most of the captured water could be released from these materials after 30 minutes of heating at 50°C. While the LCST of HPC is higher than that of PNIPAAm, there seems to be little difference in the energy needed for full water desorption. Water release could be improved by altering the physical properties of the hydrogel. HPC with dispersed LiCl was crosslinked with divinyl sulfone to form microgel beads.[133] The reduced physical dimensions of the microgel maximised surface area, adsorption, and desorption. These microgels could absorb 0.8 g/g water after 1 h at 30% RH. They could also release 90% of water after 20 minutes, confirming surface area contributions to both water uptake and release. Alternatively, HPC could be used in conjunction with other functional polymers. A polymer film consisting of HPC, hydrophilic konjac glucomannan and LiCl was made by Guo and coworkers.[79] The use of glucomannan formed large pores after gelation which facilitate the movement of water into the polymer. This translates to a 1.5 g/g water uptake after 1 h at 60% RH. After 30 minutes of heating at 60°C, 80% of absorbed water could be collected. The VPTT of the film was calculated to be 44°C, but full desorption required higher temperatures. Wang and coworkers used HPC in conjunction with PNIPAAm and while phase transition behaviour was not studied, the material was likely thermoresponsive. Water uptake on the final material reached 0.9 g/g after 1 h at 70% RH.[134] Hydroxypropyl methylcellulose (HPMC, a.k.a. hypromellose) is closely related to HPC but has additional methyl ether modifications on the cellulose hydroxyl groups. Despite the hydrophobicity imparted from additional methyl groups, HPMC has a LCST of about 60–80°C.[135, 136] Yang and coworkers used HPMC in conjunction with poly(sodium acrylate) (PAAS), LiCl and photothermal TiN nanoparticles.[137] An interconnected porous structure was formed using a foaming-drying method. This polymer was able uptake about 1.7 g/g in 1 h at 60% RH, and release almost 90% of water after 30 minutes of solar irradiation.

PVCL is another thermoresponsive polymer that has been studied for SAWH purposes. Its biocompatibility allows PVCL to be used in biomedical and environmental applications.[138] The LCST has been reported in a range from 25°C to 50°C.[139] The observed phase transitions of PVCL are more sensitive to synthetic factors like molecular weight compared to PNIPAAm.[140] Kim and Choi showcased a functional copolymer of VCL and acrylic acid (AA) as a core-shell nanofiber.[141] AA added hydrophilicity and self-crosslinking capabilities.

The core of these nanofibers was made from PAN which allowed for increased mechanical strength. Electrospinning yielded a network of core-shell nanofibers that showed mechanical strength while retaining porosity. Water uptake was around 0.2 g/g after 1 h at 80% RH. Water release could be observed above 40°C, however the efficiency of water release relative to total uptake was not stated. Another P(VCL-AA) nanofiber by the same research group took a different approach by using additives.[142] Electrospun P(VCL-AA) nanofibers were loaded with LiCl before being coated with photothermal graphene oxide. Uptake was about 1 g/g after 1 h at 60% RH, and 85% of absorbed water could be recovered after 3 h of heating. The LCST of the functionalised nanofibers was around 36°C, though desorption was conducted at 50°C.

The ethylene glycol-based thermoresponsive polymers are underrepresented in SAWH hydrogel literature. No studies involving these polymers in the field have been conducted as of present, though one polymer made for wastewater purification was noted to have SAWH potential.[143] This polymer utilised (2-methoxyethoxy)ethyl methacrylate (MEO_2MA), the homopolymer of which exhibits a LCST of 28°C.[108] One trait of MEO_2MA that could be utilised for SAWH is its lack of hydrogen bond donors. As a result of this trait, MEO_2MA and other ether-capped ethylene glycol-based polymers lack any hysteresis in heating or cooling during phase transition.[144-146] In contrast, PNIPAAm has a noticeable hysteresis when cooling. Polymer collapse causes polymer-polymer hydrogen bonds to form, which must be broken during cooling and re-solvation. The effects of phase transition hysteresis on SAWH may be significant, though they are currently difficult to extrapolate from existing data.

Thermoresponsive SAWH hydrogels have shown promising water harvesting performance, warranting further exploration. Two avenues can immediately be identified. Firstly, polymers other than PNIPAAm have had few or no relevant SAWH studies. Additionally, like other SAWH hydrogels, the liberal use of functional additives obfuscates the polymer-specific effects on water harvesting.

Despite the promise of SAWH hydrogels for large-scale water harvesting, there are unanswered questions in the field: principally, how can polymers perform competitively without relying on additives? The SAWH advantages offered by additives could be replicated by direct polymer modification. Any desired polymer functionality can be imparted by a suite of tools including copolymerisation or post-functionalisation. For example, highly hydrophilic moieties like guanidine, carboxylates or amines could be covalently linked to a

polymer in lieu of using a hygroscopic salt. As another solution, thermoresponsive polymers can bypass the trade-off between efficient water uptake and release, making them promising as the basis of a fully polymeric and high-performing SAWH system.

The focus of this thesis is on the development of additive-free, thermoresponsive SAWH hydrogels with comparable water uptake performance to existing desiccants (**Table 1**). It is presented as a compilation of three research chapters, two of which have been published and the last of which is a manuscript prepared for publication.

Reference	*Water uptake after 1 hour (g/g)*	*Relative Humidity (% RH)*	*Hygroscopic component*
53	2.5	75	LiCl
79	2.5	60	LiCl
81	0.4	80	Alg
90	1	60	LiCl
118	1	60	Alg
119	1	60	PPy-Cl
120	1.2	60	LiCl
122	0.5	70	LiCl
123	0.75	70	$CaCl_2$
124	1	70	LiCl, silica gel
125	2	80	LiCl
125	1.3	60	LiCl
134	0.9	70	LiCl
137	1.7	60	LiCl, PAAS
141	0.2	80	P(VCL-AA) polymer
142	1	60	LiCl

Table 1: References used in determining an appropriate benchmark for water harvesting.

After assessment of previous studies, we determined a competitive additive-free SAWH hydrogel would exceed a water uptake of 1 g/g after 1 h at 60–70% RH. The major caveat for direct comparison is that the aforementioned SAWH hydrogels all contain some sort of functional additive. Hygroscopic salts are able to adsorb water appreciably from about 10–20% RH, whereas a hydrogel requires higher humidity conditions for efficient sorption.[147] Many SAWH hydrogels are tested exclusively in low RH conditions (because of their salt usage), excluding these studies from our benchmark. On the other end, tests conducted at 90% RH are common yet could lead to an overly optimistic assessment of a polymer's water harvesting capabilities in different conditions. We decided to aim for tests conducted at 60–70% RH as a compromise between the two extremes.

No benchmark could easily be established based on water release. Ideally, one would be based on total energy usage in water release. Most studies that were examined conducted desorption under an excess of energy (like natural or artificial solar irradiation), making the necessary amount of energy for desorption impossible to determine.

Rational design requires a detailed examination of relevant structure-property relationships. In **Chapter 2**, a thermoresponsive copolymer library was synthesised to examine how differences in composition, crosslinking density and crosslinker length affected water harvesting properties.[148] The thermoresponsive component of this polymer system was poly(ethylene glycol) methyl ether methacrylate (PEGMA), which was the first time this system had been reported for the purpose of SAWH. Changes in water uptake (i.e. sorption) occurred with logical causal relationships to synthetic differences, establishing a baseline understanding of polymer-specific relationships with water harvesting.

In **Chapter 3**, the rational design strategy developed in **Chapter 2** was used to prepare a novel thermoresponsive SAWH hydrogel utilising arginine post-functionalisation.[149] Post-functionalisation of a polymer was used to add sensitive functional groups that cannot withstand polymerisation reaction conditions. One hygroscopic moiety that had not yet been used in SAWH hydrogels was guanidine. Many guanidine-containing molecules, including arginine, are noted to be hygroscopic.[150-152] *L*-arginine was specifically chosen in this chapter for its abundance and biocompatibility. *L*-arginine functionalisation greatly increased water uptake while allowing the material to retain thermoresponsive properties. Additionally, the improved water uptake kinetics could be utilised in faster water uptake-release cycles, increasing potential daily yield.

Chapter 4 consolidates the insights earned in **Chapters 2** and **3**, culminating in a SAWH hydrogel that was simpler to prepare and more effective at harvesting. This is presented in a manuscript prepared for publication. Both physical and chemical considerations were accounted for in the rational design of this improved SAWH material. Chief among the physical properties was surface area, which was maximised by forming polymer microgels through precipitation polymerisation. The *L*-arginine functionalisation in **Chapter 3** was replaced with a more streamlined and atom efficient method using creatine, which is accessible, structurally similar and biocompatible. In this work, these considerations translated to a high-performing SAWH hydrogel with rapid sorption kinetics. New insights into microgel-specific structure-property relationships for SAWH are also reported.

The race to water harvesting has left many unexplored avenues in its wake. This thesis presents further efforts to broaden this field of study and explore an underutilised class of SAWH polymers.

References

(1) Mekonnen, M. M.; Hoekstra, A. Y. Four billion people facing severe water scarcity. *Science Advances* **2016**, *2* (2), e1500323. DOI: doi:10.1126/sciadv.1500323.
(2) Thomas, R. D., J.; King, C.; Kruse, J.; Schauer, M.; Bisom, N.; Tsegai, D.; Madani, K. *Economics of Drought: Investing in Nature-Based Solutions for Drought Resilience – Proaction Pays*; Bonn, Germany; Toronto, Canada, 2024. DOI: 10.53328/INR24CCD001.
(3) Koncagül, E. C., R.; Abete, V. *The United Nations World Water Development Report 2024: water for prosperity and peace; facts, figures and action examples*; WWAP/SC-2024/PI/1; France, 2024. https://unesdoc.unesco.org/ark:/48223/pf0000388952.
(4) Gleick, P. H.; Pacific Institute for Studies in Development, E.; Security; Stockholm Environment, I. *Water in crisis : a guide to the world's fresh water resources*; Oxford University Press, 1993.
(5) Zolghadr-Asli, B.; McIntyre, N.; Djordjevic, S.; Farmani, R.; Pagliero, L.; Martínez-Alvarez, V.; Maestre-Valero, J. F. A review of limitations and potentials of desalination as a sustainable source of water. *Environmental Science and Pollution Research* **2023**, *30* (56), 118161-118174. DOI: 10.1007/s11356-023-30662-x.
(6) UN-Water, F. *Progress on the level of water stress – Mid-term status of SDG Indicator 6.4.2 and acceleration needs, with special focus on food security - 2024*; FAO, Rome, 2024. DOI: https://doi.org/10.4060/cd2179en.
(7) Oki, T.; Kanae, S. Global Hydrological Cycles and World Water Resources. *Science* **2006**, *313* (5790), 1068-1072. DOI: 10.1126/science.1128845.
(8) Steffen, W.; Broadgate, W.; Deutsch, L.; Gaffney, O.; Ludwig, C. The trajectory of the Anthropocene: The Great Acceleration. *The Anthropocene Review* **2015**, *2* (1), 81-98. DOI: 10.1177/2053019614564785.
(9) Shiklomanov, I. A. World fresh water resources. In *Water in Crisis: A Guide to the World's Fresh Water Resources*, Gleick, P. H. Ed.; Oxford University Press, 1993; pp 13-24.
(10) van der Ent, R. J.; Tuinenburg, O. A. The residence time of water in the atmosphere revisited. *Hydrol. Earth Syst. Sci.* **2017**, *21* (2), 779-790. DOI: 10.5194/hess-21-779-2017.
(11) Rueda, F.; Moreno-Ostos, E.; Armengol, J. The residence time of river water in reservoirs. *Ecological Modelling* **2006**, *191* (2), 260-274. DOI: https://doi.org/10.1016/j.ecolmodel.2005.04.030.
(12) Kralik, M. How to Estimate Mean Residence Times of Groundwater. *Procedia Earth and Planetary Science* **2015**, *13*, 301-306. DOI: https://doi.org/10.1016/j.proeps.2015.07.070.
(13) Wahlgren, R. V. Atmospheric water vapour processor designs for potable water production: a review. *Water Research* **2001**, *35* (1), 1-22. DOI: https://doi.org/10.1016/S0043-1354(00)00247-5.
(14) Ansari, E.; Ferber, N. L.; Milošević, T.; Barron, J.; Karanikolos, G. N.; AlMarzooqi, F.; Dumée, L. F.; Calvet, N. Atmospheric water generation in arid regions – A perspective on deployment challenges for the Middle East. *Journal of Water Process Engineering* **2022**, *49*, 103163. DOI: https://doi.org/10.1016/j.jwpe.2022.103163.
(15) Chen, Z.; Deng, F.; Yang, X.; Shao, Z.; Du, S.; Wang, R. Highly efficient portable atmospheric water harvester with integrated structure design for high yield water production. *Energy* **2024**, *293*, 130749. DOI: https://doi.org/10.1016/j.energy.2024.130749.
(16) Loo, S.-L.; Fane, A. G.; Krantz, W. B.; Lim, T.-T. Emergency water supply: A review of potential technologies and selection criteria. *Water Research* **2012**, *46* (10), 3125-3151. DOI: https://doi.org/10.1016/j.watres.2012.03.030.
(17) Kaplan, A.; Ronen-Eliraz, G.; Ratner, S.; Aviv, Y.; Wolanov, Y.; Avisar, D. Impact of industrial air pollution on the quality of atmospheric water production. *Environmental Pollution* **2023**, *325*, 121447. DOI: https://doi.org/10.1016/j.envpol.2023.121447.
(18) Ahrestani, Z.; Sadeghzadeh, S.; Motejadded Emrooz, H. B. An overview of atmospheric water harvesting methods, the inevitable path of the future in water supply. *RSC Advances* **2023**, *13* (15), 10273-10307. DOI: 10.1039/D2RA07733G.
(19) Mittal, H.; Al Alili, A.; Alhassan, S. M.; Naushad, M. Advances in the role of natural gums-based hydrogels in water purification, desalination and atmospheric-water harvesting. *International Journal of Biological Macromolecules* **2022**, *222*, 2888-2921. DOI: https://doi.org/10.1016/j.ijbiomac.2022.10.067.

(20) Poredoš, P.; Shan, H.; Wang, C.; Deng, F.; Wang, R. Sustainable water generation: grand challenges in continuous atmospheric water harvesting. *Energy & Environmental Science* **2022**, *15* (8), 3223-3235. DOI: 10.1039/D2EE01234K.
(21) IEA. Water-Energy Nexus. 2016.
(22) Tu, R.; Hwang, Y. Reviews of atmospheric water harvesting technologies. *Energy* **2020**, *201*, 117630. DOI: https://doi.org/10.1016/j.energy.2020.117630.
(23) Peeters, R.; Vanderschaeghe, H.; Rongé, J.; Martens, J. A. Energy performance and climate dependency of technologies for fresh water production from atmospheric water vapour. *Environ. Sci.: Water Res. Technol.* **2020**, *6* (8), 2016-2034. DOI: 10.1039/D0EW00128G.
(24) Çengel, Y. A.; Boles, M. A. *Thermodynamics : an engineering approach*; McGraw-Hill, 2011.
(25) Tu, Y.; Wang, R.; Zhang, Y.; Wang, J. Progress and Expectation of Atmospheric Water Harvesting. *Joule* **2018**, *2* (8), 1452-1475. DOI: 10.1016/j.joule.2018.07.015.
(26) Thavalengal, M. S.; Jamil, M. A.; Mehroz, M.; Xu, B. B.; Yaqoob, H.; Sultan, M.; Imtiaz, N.; Shahzad, M. W. Progress and Prospects of Air Water Harvesting System for Remote Areas: A Comprehensive Review. *Energies* **2023**, *16* (6), 2686.
(27) Shafeian, N.; Ranjbar, A. A.; Gorji, T. B. Progress in atmospheric water generation systems: A review. *Renewable and Sustainable Energy Reviews* **2022**, *161*, 112325. DOI: https://doi.org/10.1016/j.rser.2022.112325.
(28) Wang, M.; Liu, E.; Jin, T.; Zafar, S.-u.; Mei, X.; Fauconnier, M.-L.; De Clerck, C. Towards a better understanding of atmospheric water harvesting (AWH) technology. *Water Research* **2024**, *250*, 121052. DOI: https://doi.org/10.1016/j.watres.2023.121052.
(29) Datt, P. Latent Heat of Vaporization/Condensation. In *Encyclopedia of Snow, Ice and Glaciers*, Singh, V. P., Singh, P., Haritashya, U. K. Eds.; Springer Netherlands, 2011; pp 703-703.
(30) Hanikel, N.; Prévot, M. S.; Fathieh, F.; Kapustin, E. A.; Lyu, H.; Wang, H.; Diercks, N. J.; Glover, T. G.; Yaghi, O. M. Rapid Cycling and Exceptional Yield in a Metal-Organic Framework Water Harvester. *ACS Cent Sci* **2019**, *5* (10), 1699-1706. DOI: 10.1021/acscentsci.9b00745 PubMed.
(31) Bilal, M.; Sultan, M.; Morosuk, T.; Den, W.; Sajjad, U.; Aslam, M. M. A.; Shahzad, M. W.; Farooq, M. Adsorption-based atmospheric water harvesting: A review of adsorbents and systems. *International Communications in Heat and Mass Transfer* **2022**, *133*, 105961. DOI: https://doi.org/10.1016/j.icheatmasstransfer.2022.105961.
(32) Gao, S.; Wang, Y.; Zhang, C.; Jiang, M.; Wang, S.; Wang, Z. Tailoring interfaces for atmospheric water harvesting: Fundamentals and applications. *Matter* **2023**, *6* (7), 2182-2205. DOI: https://doi.org/10.1016/j.matt.2023.04.008.
(33) Yang, K.; Pan, T.; Lei, Q.; Dong, X.; Cheng, Q.; Han, Y. A Roadmap to Sorption-Based Atmospheric Water Harvesting: From Molecular Sorption Mechanism to Sorbent Design and System Optimization. *Environmental Science & Technology* **2021**, *55* (10), 6542-6560. DOI: 10.1021/acs.est.1c00257.
(34) Chen, Z.; Song, S.; Ma, B.; Li, Y.; Shao, Y.; Shi, J.; Liu, M.; Jin, H.; Jing, D. Recent progress on sorption/desorption-based atmospheric water harvesting powered by solar energy. *Solar Energy Materials and Solar Cells* **2021**, *230*, 111233. DOI: https://doi.org/10.1016/j.solmat.2021.111233.
(35) Zhang, S.; Fu, J.; Xing, G.; Zhu, W.; Ben, T. Recent advances in porous adsorbent assisted atmospheric water harvesting: a review of adsorbent materials. *Chemical Synthesis* **2023**, *3* (2), 10.
(36) Schweng, P.; Woodward, R. T. Challenging POPular opinion: Porous organic polymers for atmospheric water harvesting. *Reactive and Functional Polymers* **2024**, *203*, 106014. DOI: https://doi.org/10.1016/j.reactfunctpolym.2024.106014.
(37) Byun, Y.; Je, S. H.; Talapaneni, S. N.; Coskun, A. Advances in Porous Organic Polymers for Efficient Water Capture. *Chemistry – A European Journal* **2019**, *25* (44), 10262-10283. DOI: https://doi.org/10.1002/chem.201900940.
(38) Shi, Y.; Feng, A.; Mao, S.; Onggowarsito, C.; Stella Zhang, X.; Guo, W.; Fu, Q. Hydrogels in solar-driven water and energy production: Recent advances and future perspectives. *Chemical Engineering Journal* **2024**, *492*, 152303. DOI: https://doi.org/10.1016/j.cej.2024.152303.
(39) Sharma, S. D.; Kitano, H.; Sagara, K. Phase change materials for low temperature solar thermal applications. *Res. Rep. Fac. Eng. Mie Univ* **2004**, *29* (1), 31-64.

(40) Carlsson, B. Phase change behaviour of some latent heat storage media based on calcium chloride hexahydrate. *Solar Energy* **2009**, *83* (4), 485-500. DOI: https://doi.org/10.1016/j.solener.2008.09.004.
(41) Ng, E.-P.; Mintova, S. Nanoporous materials with enhanced hydrophilicity and high water sorption capacity. *Microporous and Mesoporous Materials* **2008**, *114* (1), 1-26. DOI: https://doi.org/10.1016/j.micromeso.2007.12.022.
(42) Wynnyk, K. G.; Hojjati, B.; Marriott, R. A. High-Pressure Sour Gas and Water Adsorption on Zeolite 13X. *Industrial & Engineering Chemistry Research* **2018**, *57* (45), 15357-15365. DOI: 10.1021/acs.iecr.8b03317.
(43) Polyachenok, O. G.; Dudkina, E. N.; Branovitskaya, N. V.; Polyachenok, L. D. Formation of super disperse phase and its influence on equilibrium and thermodynamics of thermal dehydration. *Thermochimica Acta* **2008**, *467* (1), 44-53. DOI: https://doi.org/10.1016/j.tca.2007.11.005.
(44) Luo, Y.; Tan, B.; Liang, X.; Wang, S.; Gao, X.; Zhang, Z.; Fang, Y. Investigation on water vapor adsorption performance of LiCl@MIL-100(Fe) composite adsorbent for adsorption heat pumps. *International Journal of Energy Research* **2020**, *44* (7), 5895-5904. DOI: https://doi.org/10.1002/er.5361.
(45) Li, R.; Shi, Y.; Shi, L.; Alsaedi, M.; Wang, P. Harvesting Water from Air: Using Anhydrous Salt with Sunlight. *Environmental Science & Technology* **2018**, *52* (9), 5398-5406. DOI: 10.1021/acs.est.7b06373.
(46) Kallenberger, P. A.; Fröba, M. Water harvesting from air with a hygroscopic salt in a hydrogel–derived matrix. *Communications Chemistry* **2018**, *1* (1), 28. DOI: 10.1038/s42004-018-0028-9.
(47) Arya, A.; Beving, M.; Mahmoudi, A.; Donkers, P. A. J.; Brem, G.; Shahi, M. Quantifying volume variation and agglomeration in thermochemical materials: An in-situ measurement methodology. *Journal of Energy Storage* **2025**, *124*, 116877. DOI: https://doi.org/10.1016/j.est.2025.116877.
(48) Sim, J.-H.; Kim, Y.-S.; Cho, I.-J. Corrosion behavior induced by LiCl-KCl in type 304 and 316 stainless steel and copper at low temperature. *Nuclear Engineering and Technology* **2017**, *49* (4), 769-775. DOI: https://doi.org/10.1016/j.net.2017.02.007.
(49) Ruozzi, A.; Vainio, E.; Kinnunen, H.; Hupa, L. Cold-end corrosion in biomass combustion – Role of calcium chloride in the deposit. *Fuel* **2023**, *349*, 128344. DOI: https://doi.org/10.1016/j.fuel.2023.128344.
(50) Li, D.; Yadav, A.; Zhou, H.; Roy, K.; Thanasekaran, P.; Lee, C. Advances and Applications of Metal-Organic Frameworks (MOFs) in Emerging Technologies: A Comprehensive Review. *Global Challenges* **2024**, *8* (2), 2300244. DOI: https://doi.org/10.1002/gch2.202300244.
(51) Zeggai, F. z.; Ait-Touchente, Z.; Bachari, K.; Elaissari, A. Investigation of Metal-Organic Frameworks (MOFs): Synthesis, Properties, and Applications - An In-Depth Review. *Chemical Physics Impact* **2025**, *10*, 100864. DOI: https://doi.org/10.1016/j.chphi.2025.100864.
(52) Feng, A.; Shi, Y.; Onggowarsito, C.; Zhang, X. S.; Mao, S.; Johir, M. A. H.; Fu, Q.; Nghiem, L. D. Structure-Property Relationships of Hydrogel-based Atmospheric Water Harvesting Systems. *ChemSusChem* **2024**, *17* (11), e202301905. DOI: https://doi.org/10.1002/cssc.202301905.
(53) Maity, D.; Teixeira, A. P.; Fussenegger, M. Hydratable Core–Shell Polymer Networks for Atmospheric Water Harvesting Powered by Sunlight. *Small* **2023**, *19* (47), 2301427. DOI: https://doi.org/10.1002/smll.202301427.
(54) Schweng, P.; Mayer, F.; Galehdari, D.; Weiland, K.; Woodward, R. T. A Robust and Low-Cost Sulfonated Hypercrosslinked Polymer for Atmospheric Water Harvesting. *Small* **2023**, *19* (50), 2304562. DOI: https://doi.org/10.1002/smll.202304562.
(55) Zhang, S.; Fu, J.; Das, S.; Ye, K.; Zhu, W.; Ben, T. Crystalline Porous Organic Salt for Ultrarapid Adsorption/Desorption-Based Atmospheric Water Harvesting by Dual Hydrogen Bond System. *Angewandte Chemie International Edition* **2022**, *61* (40), e202208660. DOI: https://doi.org/10.1002/anie.202208660.
(56) Pu, S.; Fu, J.; Liao, Y.; Ge, L.; Zhou, Y.; Zhang, S.; Zhao, S.; Liu, X.; Hu, X.; Liu, K.; et al. Promoting Energy Efficiency via a Self-Adaptive Evaporative Cooling Hydrogel. *Advanced Materials* **2020**, *32* (17), 1907307. DOI: https://doi.org/10.1002/adma.201907307.
(57) Graeber, G.; Díaz-Marín, C. D.; Gaugler, L. C.; Zhong, Y.; El Fil, B.; Liu, X.; Wang, E. N. Extreme Water Uptake of Hygroscopic Hydrogels through Maximized Swelling-Induced Salt Loading. *Advanced Materials* **2024**, *36* (12), 2211783. DOI: https://doi.org/10.1002/adma.202211783.

(58) Nah, S. H.; Lee, Y.; Yu, K.-H.; Chi, Y.; Lee, H.; Chen, B.; Patel, M.; Wang, K.; Yang, S. Moisture Absorbing and Water Self-Releasing from Hybrid Hydrogel Desiccants. *Advanced Functional Materials* **2024**, *34* (19), 2313881. DOI: https://doi.org/10.1002/adfm.202313881.
(59) Lu, H.; Shi, W.; Zhang, J. H.; Chen, A. C.; Guan, W.; Lei, C.; Greer, J. R.; Boriskina, S. V.; Yu, G. Tailoring the Desorption Behavior of Hygroscopic Gels for Atmospheric Water Harvesting in Arid Climates. *Advanced Materials* **2022**, *34* (37), 2205344. DOI: https://doi.org/10.1002/adma.202205344.
(60) Shan, H.; Poredoš, P.; Ye, Z.; Qu, H.; Zhang, Y.; Zhou, M.; Wang, R.; Tan, S. C. All-Day Multicyclic Atmospheric Water Harvesting Enabled by Polyelectrolyte Hydrogel with Hybrid Desorption Mode. *Advanced Materials* **2023**, *35* (35), 2302038. DOI: https://doi.org/10.1002/adma.202302038.
(61) Aleid, S.; Wu, M.; Li, R.; Wang, W.; Zhang, C.; Zhang, L.; Wang, P. Salting-in Effect of Zwitterionic Polymer Hydrogel Facilitates Atmospheric Water Harvesting. *ACS Materials Letters* **2022**, *4* (3), 511-520. DOI: 10.1021/acsmaterialslett.1c00723.
(62) Thakur, A. K.; Hazra, S. K.; Saleque, A. M.; Bhattarai, S.; Hwang, J.-Y.; Ahamed, M. S. Toward Sustainable Water Solutions: A Review of Nanomaterials for Solar-Driven Water Harvesting. *ACS ES&T Water* **2024**, *4* (11), 4741-4757. DOI: 10.1021/acsestwater.4c00620.
(63) Cui, X.; Ruan, Q.; Zhuo, X.; Xia, X.; Hu, J.; Fu, R.; Li, Y.; Wang, J.; Xu, H. Photothermal Nanomaterials: A Powerful Light-to-Heat Converter. *Chemical Reviews* **2023**, *123* (11), 6891-6952. DOI: 10.1021/acs.chemrev.3c00159.
(64) Chen, B.; Zhao, X.; Yang, Y. Superelastic Graphene Nanocomposite for High Cycle-Stability Water Capture–Release under Sunlight. *ACS Applied Materials & Interfaces* **2019**, *11* (17), 15616-15622. DOI: 10.1021/acsami.9b02215.
(65) Li, R.; Shi, Y.; Wu, M.; Hong, S.; Wang, P. Photovoltaic panel cooling by atmospheric water sorption–evaporation cycle. *Nature Sustainability* **2020**, *3* (8), 636-643. DOI: 10.1038/s41893-020-0535-4.
(66) Wang, J.; Deng, C.; Zhong, G.; Ying, W.; Li, C.; Wang, S.; Liu, Y.; Wang, R.; Zhang, H. High-yield and scalable water harvesting of honeycomb hygroscopic polymer driven by natural sunlight. *Cell Reports Physical Science* **2022**, *3* (7), 100954. DOI: https://doi.org/10.1016/j.xcrp.2022.100954.
(67) Lyu, T.; Wang, Z.; Liu, R.; Chen, K.; Liu, H.; Tian, Y. Macroporous Hydrogel for High-Performance Atmospheric Water Harvesting. *ACS Applied Materials & Interfaces* **2022**, *14* (28), 32433-32443. DOI: 10.1021/acsami.2c04228.
(68) Liu, Y.; Liu, Z.; Wang, Z.; Sun, W.; Kong, F. Photovoltaic passive cooling via water vapor sorption-evaporation by hydrogel. *Applied Thermal Engineering* **2024**, *240*, 122185. DOI: https://doi.org/10.1016/j.applthermaleng.2023.122185.
(69) Ni, F.; Qiu, N.; Xiao, P.; Zhang, C.; Jian, Y.; Liang, Y.; Xie, W.; Yan, L.; Chen, T. Tillandsia-Inspired Hygroscopic Photothermal Organogels for Efficient Atmospheric Water Harvesting. *Angewandte Chemie International Edition* **2020**, *59* (43), 19237-19246. DOI: https://doi.org/10.1002/anie.202007885.
(70) Li, R.; Shi, Y.; Alsaedi, M.; Wu, M.; Shi, L.; Wang, P. Hybrid Hydrogel with High Water Vapor Harvesting Capacity for Deployable Solar-Driven Atmospheric Water Generator. *Environmental Science & Technology* **2018**, *52* (19), 11367-11377. DOI: 10.1021/acs.est.8b02852.
(71) Song, M.; Shao, F.; Wang, L.; Xie, H.; Yu, W. Biomass-derived porous carbon aerogels for effective solar thermal energy storage and atmospheric water harvesting. *Solar Energy Materials and Solar Cells* **2023**, *262*, 112532. DOI: https://doi.org/10.1016/j.solmat.2023.112532.
(72) Park, H.; Haechler, I.; Schnoering, G.; Ponte, M. D.; Schutzius, T. M.; Poulikakos, D. Enhanced Atmospheric Water Harvesting with Sunlight-Activated Sorption Ratcheting. *ACS Applied Materials & Interfaces* **2022**, *14* (1), 2237-2245. DOI: 10.1021/acsami.1c18852.
(73) Zhang, H.; Zhou, Z.; Du, J.; Pei, X.; Zhou, L. Starch-derived photoresponsive high-efficientcy hygroscopic hydrogel for all-weather atmospheric water harvesting. *Journal of Cleaner Production* **2023**, *416*, 137897. DOI: https://doi.org/10.1016/j.jclepro.2023.137897.
(74) Nong, Y.; Fan, B.; Bao, X.; Xu, B.; Zhou, M.; Yu, Y.; Wang, Q.; Wang, P. Fabrication of hygroscopic photothermal fibroin-based aerogels for dehumidification and solar-driven water harvesting. *Materials Today Communications* **2022**, *32*, 103984. DOI: https://doi.org/10.1016/j.mtcomm.2022.103984.

(75) Luo, Q.; Chen, M.; Yu, D.; Zhang, T.; Zhao, J.; Zhang, L.; Han, X.; Zhou, M.; Hou, Y.; Zheng, Y. An Atmospheric Water-Harvester with Ultrahigh Uptake-Release Efficiency at Low Humidity. *ACS Nano* **2024**, *18* (22), 14650-14660. DOI: 10.1021/acsnano.4c02866.
(76) Hecht, H.; Srebnik, S. Structural Characterization of Sodium Alginate and Calcium Alginate. *Biomacromolecules* **2016**, *17* (6), 2160-2167. DOI: 10.1021/acs.biomac.6b00378.
(77) Akagi, T.; Yasuda, K.; Tajima, M.; Suzuki, K.; Inomata, M.; Shiraishi, N.; Sato, Y.; Kitano, S. Sodium alginate as an ideal submucosal injection material for endoscopic submucosal resection: preliminary experimental and clinical study. *Gastrointestinal Endoscopy* **2011**, *74* (5), 1026-1032. DOI: https://doi.org/10.1016/j.gie.2011.07.042.
(78) Entezari, A.; Ejeian, M.; Wang, R. Super Atmospheric Water Harvesting Hydrogel with Alginate Chains Modified with Binary Salts. *ACS Materials Letters* **2020**, *2* (5), 471-477. DOI: 10.1021/acsmaterialslett.9b00315.
(79) Guo, Y.; Guan, W.; Lei, C.; Lu, H.; Shi, W.; Yu, G. Scalable super hygroscopic polymer films for sustainable moisture harvesting in arid environments. *Nature Communications* **2022**, *13* (1), 2761. DOI: 10.1038/s41467-022-30505-2.
(80) Lee, S. J.; Ha, N.; Kim, H. Superhydrophilic–Superhydrophobic Water Harvester Inspired by Wetting Property of Cactus Stem. *ACS Sustainable Chem. Eng.* **2019**, *7* (12), 10561-10569. DOI: 10.1021/acssuschemeng.9b01113.
(81) Matsumoto, K.; Sakikawa, N.; Miyata, T. Thermo-responsive gels that absorb moisture and ooze water. *Nat. Commun.* **2018**, *9* (1), 2315. DOI: 10.1038/s41467-018-04810-8.
(82) Yu, Z.; Li, S.; Su, J.; Zhang, J.; Zhang, D.; Zhou, Z.; Qin, Z.; Liu, X.; Lai, Y.; Fu, S. Bio-inspired core-shell structural aerogel with programmable water release capacity for efficient solar thermoelectricity-freshwater cogeneration. *Matter* **2023**, *6* (10), 3509-3525. DOI: https://doi.org/10.1016/j.matt.2023.07.015.
(83) Yu, Z.; Li, S.; Zhang, J.; Tang, C.; Qin, Z.; Liu, X.; Zhou, Z.; Lai, Y.; Fu, S. Phospholipid Bilayer Inspired Sandwich Structural Nanofibrous Membrane for Atmospheric Water Harvesting and Selective Release. *Nano Letters* **2024**, *24* (8), 2629-2636. DOI: 10.1021/acs.nanolett.3c04658.
(84) Fu, J.; Thomas, H. R.; Li, C. Tortuosity of porous media: Image analysis and physical simulation. *Earth-Science Reviews* **2021**, *212*, 103439. DOI: https://doi.org/10.1016/j.earscirev.2020.103439.
(85) Mittal, H.; Al Alili, A.; Alhassan, S. M. Solid polymer desiccants based on poly(acrylic acid-co-acrylamide) and Laponite RD: Adsorption isotherm and kinetics studies. *Colloids and Surfaces A: Physicochemical and Engineering Aspects* **2020**, *599*, 124813. DOI: https://doi.org/10.1016/j.colsurfa.2020.124813.
(86) Zheng, D.; Xu, X.; Zhu, J.; Bai, B.; Wang, Q.; Shi, W.; Li, J. Humidity capture and solar-driven water collection behaviors of alginate-g-PNIPAm-based hydrogel. *Journal of Environmental Chemical Engineering* **2023**, *11* (1), 109247. DOI: https://doi.org/10.1016/j.jece.2022.109247.
(87) Zhou, Z.; Wang, G.; Pei, X.; Zhou, L. Solar-driven MXene aerogels with high water vapor harvesting capacity for atmospheric water harvesting. *Chemical Engineering Journal* **2023**, *474*, 145605. DOI: https://doi.org/10.1016/j.cej.2023.145605.
(88) Mohanrao, R.; Sureshan, K. M. Synthesis and Reversible Hydration of a Pseudoprotein, a Fully Organic Polymeric Desiccant by Multiple Single-Crystal-to-Single-Crystal Transformations. *Angewandte Chemie International Edition* **2018**, *57* (38), 12435-12439. DOI: https://doi.org/10.1002/anie.201806451.
(89) Mohanrao, R.; Hema, K.; Sureshan, K. M. Scalable Topochemical Synthesis of a Pseudoprotein in Aerogel for Water-Capturing Applications. *ACS Applied Polymer Materials* **2020**, *2* (11), 4985-4992. DOI: 10.1021/acsapm.0c00849.
(90) Guan, W.; Zhao, Y.; Lei, C.; Yu, G. Molecularly confined hydration in thermoresponsive hydrogels for efficient atmospheric water harvesting. *Proceedings of the National Academy of Sciences* **2023**, *120* (38), e2308969120. DOI: doi:10.1073/pnas.2308969120.
(91) Liu, X.; Zeng, W.; Ding, W.; Yang, C.; Li, J.; Liu, P.; Litaor, M. I.; Lei, Z. Solar-powered porous polymer materials-enabled rapid atmospheric water harvesting and storage of liquid water. *Materials Today Chemistry* **2024**, *38*, 102083. DOI: https://doi.org/10.1016/j.mtchem.2024.102083.
(92) Song, J.; Liu, Z.; Boñgol, J. P.; Zhang, Z.; Yeung, K. L. An atmospheric water harvester with fast and energy-saving water removal and recovery. *Biosurface and Biotribology* **2023**, *9* (1), 9-16. DOI: https://doi.org/10.1049/bsb2.12056.

(93) Gitlin, M. Lithium side effects and toxicity: prevalence and management strategies. *International Journal of Bipolar Disorders* **2016**, *4* (1), 27. DOI: 10.1186/s40345-016-0068-y.
(94) Schrauzer, G. N. Lithium: Occurrence, Dietary Intakes, Nutritional Essentiality. *Journal of the American College of Nutrition* **2002**, *21* (1), 14-21. DOI: 10.1080/07315724.2002.10719188.
(95) World Health Organisation *Guidelines for drinking-water quality: fourth edition incorporating the first and second addenda*; 2022.
(96) U.S. Environmental Protection Agency *Technical Fact Sheet: Lithium in Drinking Water*; EPA 815-F-23-007; 2023. https://www.epa.gov/system/files/documents/2023-11/ucmr5-technical-fact-sheet-lithium-in-drinking-water.pdf.
(97) Sugiyama, H.; Katoh, K.-i.; Sekine, N.; Sekine, Y.; Watanabe, T.; Ikeda-Fukazawa, T. Effects of hydrophilic groups of polymer on change in hydrogen-bonding structure of water in hydrogels during dehydration. *Chemical Physics Letters* **2024**, *856*, 141655. DOI: https://doi.org/10.1016/j.cplett.2024.141655.
(98) Yuan, Y.; Raheja, K.; Milbrandt, N. B.; Beilharz, S.; Tene, S.; Oshabaheebwa, S.; Gurkan, U. A.; Samia, A. C. S.; Karayilan, M. Thermoresponsive polymers with LCST transition: synthesis, characterization, and their impact on biomedical frontiers. *RSC Applied Polymers* **2023**, *1* (2), 158-189. DOI: 10.1039/D3LP00114H.
(99) Hogan, K. J.; Mikos, A. G. Biodegradable thermoresponsive polymers: Applications in drug delivery and tissue engineering. *Polymer* **2020**, *211*, 123063. DOI: https://doi.org/10.1016/j.polymer.2020.123063.
(100) Roy, D.; Brooks, W. L. A.; Sumerlin, B. S. New directions in thermoresponsive polymers. *Chemical Society Reviews* **2013**, *42* (17), 7214-7243. DOI: 10.1039/C3CS35499G.
(101) Throat, S.; Bhattacharya, S. Macromolecular Poly(N-isopropylacrylamide) (PNIPAM) in Cancer Treatment and Beyond. *Advances in Polymer Technology* **2024**, *2024* (1), 1444990. DOI: https://doi.org/10.1155/2024/1444990.
(102) Rana, M. M.; De la Hoz Siegler, H. Tuning the Properties of PNIPAm-Based Hydrogel Scaffolds for Cartilage Tissue Engineering. *Polymers* **2021**, *13* (18), 3154.
(103) Atkins, P. W.; De Paula, J.; Keeler, J. *Atkins' physical chemistry*; Oxford University Press, 2014.
(104) Peng, B.; Grishkewich, N.; Yao, Z.; Han, X.; Liu, H.; Tam, K. C. Self-Assembly Behavior of Thermoresponsive Oligo(ethylene glycol) Methacrylates Random Copolymer. *ACS Macro Letters* **2012**, *1* (5), 632-635. DOI: 10.1021/mz300135x.
(105) Vancoillie, G.; Frank, D.; Hoogenboom, R. Thermoresponsive poly(oligo ethylene glycol acrylates). *Progress in Polymer Science* **2014**, *39* (6), 1074-1095. DOI: https://doi.org/10.1016/j.progpolymsci.2014.02.005.
(106) Foster, J. C.; Akar, I.; Grocott, M. C.; Pearce, A. K.; Mathers, R. T.; O'Reilly, R. K. 100th Anniversary of Macromolecular Science Viewpoint: The Role of Hydrophobicity in Polymer Phenomena. *ACS Macro Letters* **2020**, *9* (11), 1700-1707. DOI: 10.1021/acsmacrolett.0c00645.
(107) Ishizone, T.; Seki, A.; Hagiwara, M.; Han, S.; Yokoyama, H.; Oyane, A.; Deffieux, A.; Carlotti, S. Anionic Polymerizations of Oligo(ethylene glycol) Alkyl Ether Methacrylates: Effect of Side Chain Length and ω-Alkyl Group of Side Chain on Cloud Point in Water. *Macromolecules* **2008**, *41* (8), 2963-2967. DOI: 10.1021/ma702828n.
(108) Han, S.; Hagiwara, M.; Ishizone, T. Synthesis of Thermally Sensitive Water-Soluble Polymethacrylates by Living Anionic Polymerizations of Oligo(ethylene glycol) Methyl Ether Methacrylates. *Macromolecules* **2003**, *36* (22), 8312-8319. DOI: 10.1021/ma0347971.
(109) Ida, S.; Kawahara, T.; Fujita, Y.; Tanimoto, S.; Hirokawa, Y. Thermoresponsive Properties of Copolymer Gels Induced by Appropriate Hydrophilic/Hydrophobic Balance of Monomer Combination. *Macromolecular Symposia* **2015**, *350* (1), 14-21. DOI: https://doi.org/10.1002/masy.201400020.
(110) Akar, I.; Foster, J. C.; Leng, X.; Pearce, A. K.; Mathers, R. T.; O'Reilly, R. K. Log Poct/SA Predicts the Thermoresponsive Behavior of P(DMA-co-RA) Statistical Copolymers. *ACS Macro Letters* **2022**, *11* (4), 498-503. DOI: 10.1021/acsmacrolett.1c00776.
(111) Ida, S.; Nishisako, D.; Fujiseki, A.; Kanaoka, S. Thermoresponsive properties of polymer hydrogels induced by copolymerization of hydrophilic and hydrophobic monomers: comprehensive study of monomer sequence and water affinity. *Soft Matter* **2021**, *17* (25), 6063-6072. DOI: 10.1039/D1SM00596K.

(112) Seuring, J.; Agarwal, S. Polymers with Upper Critical Solution Temperature in Aqueous Solution. *Macromolecular Rapid Communications* **2012**, *33* (22), 1898-1920. DOI: https://doi.org/10.1002/marc.201200433.
(113) Lessard, D. G.; Ousalem, M.; Zhu, X. X. Effect of the molecular weight on the lower critical solution temperature of poly(N,N-diethylacrylamide) in aqueous solutions. *Canadian Journal of Chemistry* **2001**, *79* (12), 1870-1874. DOI: 10.1139/v01-180.
(114) Ieong, N. S.; Hasan, M.; Phillips, D. J.; Saaka, Y.; O'Reilly, R. K.; Gibson, M. I. Polymers with molecular weight dependent LCSTs are essential for cooperative behaviour. *Polymer Chemistry* **2012**, *3* (3), 794-799. DOI: 10.1039/C2PY00604A.
(115) Ng, W. S.; Forbes, E.; Franks, G. V.; Connal, L. A. Xanthate-Functional Temperature-Responsive Polymers: Effect on Lower Critical Solution Temperature Behavior and Affinity toward Sulfide Surfaces. *Langmuir* **2016**, *32* (30), 7443-7451. DOI: 10.1021/acs.langmuir.6b00211.
(116) Guo, Y.; Dong, X.; Ruan, W.; Shang, Y.; Liu, H. A thermo-sensitive OEGMA-based polymer: synthesis, characterization and interactions with surfactants in aqueous solutions with and without salt. *Colloid and Polymer Science* **2017**, *295* (2), 327-340. DOI: 10.1007/s00396-016-4006-4.
(117) Dušek, K.; Dušková-Smrčková, M. Volume Phase Transition in Gels: Its Discovery and Development. *Gels* **2020**, *6* (3), 22.
(118) Chang, X.; Li, S.; Li, N.; Wang, S.; Li, J.; Guo, C.; Yu, L.; Murto, P.; Xu, X. Marine biomass-derived, hygroscopic and temperature-responsive hydrogel beads for atmospheric water harvesting and solar-powered irrigation. *Journal of Materials Chemistry A* **2022**, *10* (35), 18170-18184. DOI: 10.1039/D2TA04919H.
(119) Zhao, F.; Zhou, X.; Liu, Y.; Shi, Y.; Dai, Y.; Yu, G. Super Moisture-Absorbent Gels for All-Weather Atmospheric Water Harvesting. *Advanced Materials* **2019**, *31* (10), 1806446. DOI: https://doi.org/10.1002/adma.201806446.
(120) Wang, J.; Ying, W.; Lin, B.; Li, C.; Deng, C.; Zhang, H.; Wang, S.; Wang, R. Tillandsia-Inspired Ultra-Efficient Thermo-Responsive Hygroscopic Nanofibers for Solar-Driven Atmospheric Water Harvesting. *Advanced Materials* **2025**, *37* (3), 2408977. DOI: https://doi.org/10.1002/adma.202408977.
(121) Wang, X.; Yang, D.; Zhang, M.; Hu, Q.; Gao, K.; Zhou, J.; Yu, Z.-Z. Super-Hygroscopic Calcium Chloride/Graphene Oxide/Poly(N-isopropylacrylamide) Gels for Spontaneous Harvesting of Atmospheric Water and Solar-Driven Water Release. *ACS Applied Materials & Interfaces* **2022**, *14* (29), 33881-33891. DOI: 10.1021/acsami.2c08591.
(122) Zhang, Z.; Wang, Y.; Li, Z.; Fu, H.; Huang, J.; Xu, Z.; Lai, Y.; Qian, X.; Zhang, S. Sustainable Hierarchical-Pored PAAS–PNIPAAm Hydrogel with Core–Shell Structure Tailored for Highly Efficient Atmospheric Water Harvesting. *ACS Applied Materials & Interfaces* **2022**, *14* (49), 55295-55306. DOI: 10.1021/acsami.2c19840.
(123) Zhang, Z.; Wang, X.; Li, H.; Liu, G.; Zhao, K.; Wang, Y.; Li, Z.; Huang, J.; Xu, Z.; Lai, Y.; et al. A humidity/thermal dual response 3D-fabric with porous poly(N-isopropyl acrylamide) hydrogel towards efficient atmospheric water harvesting. *Journal of Colloid and Interface Science* **2024**, *653*, 1040-1051. DOI: https://doi.org/10.1016/j.jcis.2023.09.116.
(124) Ma, Q.; Zheng, X. Preparation and characterization of thermo-responsive composite for adsorption-based dehumidification and water harvesting. *Chemical Engineering Journal* **2022**, *429*, 132498. DOI: https://doi.org/10.1016/j.cej.2021.132498.
(125) Lu, J.; Yan, J.; Pei, F.; Niu, Z.; Li, J.; Han, G.; Wang, D.; Yue, Y.; Cheng, W. Shrinkage-Resistant Thermo-Responsive Hygroscopic Hydrogel Toward Ultra-Rapid Cycling Atmospheric Water Harvesting. *Advanced Functional Materials* **2025**, *n/a* (n/a), 2505359. DOI: https://doi.org/10.1002/adfm.202505359.
(126) Kostag, M.; Gericke, M.; Heinze, T.; El Seoud, O. A. Twenty-five years of cellulose chemistry: innovations in the dissolution of the biopolymer and its transformation into esters and ethers. *Cellulose* **2019**, *26* (1), 139-184. DOI: 10.1007/s10570-018-2198-0.
(127) Carolin C, F.; Kamalesh, T.; Kumar, P. S.; Hemavathy, R. V.; Rangasamy, G. A critical review on sustainable cellulose materials and its multifaceted applications. *Industrial Crops and Products* **2023**, *203*, 117221. DOI: https://doi.org/10.1016/j.indcrop.2023.117221.

(128) Kamel, S.; Ali, N.; Jahangir, K.; Shah, S. M.; El-Gendy, A. A. Pharmaceutical significance of cellulose: A review. *Express Polymer Letters* **2008**, *2*, 758-778. DOI: 10.3144/expresspolymlett.2008.90.
(129) Rodu, B.; Russell, C. M. Performance of a hydroxypropyl cellulose film former in normal and ulcerated oral mucosa. *Oral Surgery, Oral Medicine, Oral Pathology* **1988**, *65* (6), 699-703. DOI: https://doi.org/10.1016/0030-4220(88)90013-8.
(130) Walters, C. M.; Boott, C. E.; Nguyen, T.-D.; Hamad, W. Y.; MacLachlan, M. J. Iridescent Cellulose Nanocrystal Films Modified with Hydroxypropyl Cellulose. *Biomacromolecules* **2020**, *21* (3), 1295-1302. DOI: 10.1021/acs.biomac.0c00056.
(131) Weißenborn, E.; Braunschweig, B. Hydroxypropyl cellulose as a green polymer for thermo-responsive aqueous foams. *Soft Matter* **2019**, *15* (13), 2876-2883. DOI: 10.1039/C9SM00093C.
(132) Yu, Y.; Gu, W.; Sui, K. Thermoresponsive Aerogel Enabling Ultrafast Adsorption-Release Cycles for Atmospheric Harvesting. *ACS Applied Materials & Interfaces* **2025**, *17* (22), 32906-32913. DOI: 10.1021/acsami.5c05485.
(133) Guan, W.; Lei, C.; Guo, Y.; Shi, W.; Yu, G. Hygroscopic-Microgels-Enabled Rapid Water Extraction from Arid Air. *Advanced Materials* **2024**, *36* (12), 2207786. DOI: https://doi.org/10.1002/adma.202207786.
(134) Wang, X.; Ma, G.; Cui, S.; Sun, K.; Li, W.; Peng, H. Title High Solar-Thermal Conversion Aerogel for Efficient Atmospheric Water Harvesting. *Small* **2024**, *20* (12), 2307416. DOI: https://doi.org/10.1002/smll.202307416.
(135) Joshi, S. C. Sol-Gel Behavior of Hydroxypropyl Methylcellulose (HPMC) in Ionic Media Including Drug Release. *Materials* **2011**, *4* (10), 1861-1905.
(136) Knarr, M.; Rogers, T. L.; Petermann, O.; Adden, R. Investigation and rank-ordering of hydroxypropyl methylcellulose (HPMC) properties impacting controlled release performance. *Journal of Drug Delivery Science and Technology* **2025**, *104*, 106425. DOI: https://doi.org/10.1016/j.jddst.2024.106425.
(137) Yang, X.; Chen, Z.; Xiang, C.; Shan, H.; Wang, R. Enhanced continuous atmospheric water harvesting with scalable hygroscopic gel driven by natural sunlight and wind. *Nature Communications* **2024**, *15* (1), 7678. DOI: 10.1038/s41467-024-52137-4.
(138) Cortez-Lemus, N. A.; Licea-Claverie, A. Poly(N-vinylcaprolactam), a comprehensive review on a thermoresponsive polymer becoming popular. *Progress in Polymer Science* **2016**, *53*, 1-51. DOI: https://doi.org/10.1016/j.progpolymsci.2015.08.001.
(139) Vihola, H.; Laukkanen, A.; Valtola, L.; Tenhu, H.; Hirvonen, J. Cytotoxicity of thermosensitive polymers poly(N-isopropylacrylamide), poly(N-vinylcaprolactam) and amphiphilically modified poly(N-vinylcaprolactam). *Biomaterials* **2005**, *26* (16), 3055-3064. DOI: https://doi.org/10.1016/j.biomaterials.2004.09.008.
(140) Liu, J.; Debuigne, A.; Detrembleur, C.; Jérôme, C. Poly(N-vinylcaprolactam): A Thermoresponsive Macromolecule with Promising Future in Biomedical Field. *Advanced Healthcare Materials* **2014**, *3* (12), 1941-1968. DOI: https://doi.org/10.1002/adhm.201400371.
(141) Kim, S.; Choi, H. Switchable Wettability of Thermoresponsive Core–Shell Nanofibers for Water Capture and Release. *ACS Sustainable Chemistry & Engineering* **2019**, *7* (24), 19870-19879. DOI: 10.1021/acssuschemeng.9b05273.
(142) Kim, S.; Liang, Y.; Kang, S.; Choi, H. Solar-assisted smart nanofibrous membranes for atmospheric water harvesting. *Chemical Engineering Journal* **2021**, *425*, 131601. DOI: https://doi.org/10.1016/j.cej.2021.131601.
(143) Combita, D.; Ahmed, M. Thermoresponsive and antifouling hydrogels as a radiative energy driven water harvesting system. *Materials Chemistry Frontiers* **2021**, *5* (2), 917-928. DOI: 10.1039/D0QM00584C.
(144) Lutz, J.-F.; Akdemir, Ö.; Hoth, A. Point by Point Comparison of Two Thermosensitive Polymers Exhibiting a Similar LCST: Is the Age of Poly(NIPAM) Over? *Journal of the American Chemical Society* **2006**, *128* (40), 13046-13047. DOI: 10.1021/ja065324n.
(145) Liu, L.; Li, W.; Liu, K.; Yan, J.; Hu, G.; Zhang, A. Comblike Thermoresponsive Polymers with Sharp Transitions: Synthesis, Characterization, and Their Use as Sensitive Colorimetric Sensors. *Macromolecules* **2011**, *44* (21), 8614-8621. DOI: 10.1021/ma201874c.

(146) Tao, X.; Liu, K.; Li, W.; Zhang, A. Remarkable structure effects on thermoresponsive properties of dendritic macromolecules. *Polymer* **2014**, *55* (16), 3672-3679. DOI: https://doi.org/10.1016/j.polymer.2014.06.010.
(147) Díaz-Marín, C. D.; Zhang, L.; Lu, Z.; Alshrah, M.; Grossman, J. C.; Wang, E. N. Kinetics of Sorption in Hygroscopic Hydrogels. *Nano Letters* **2022**, *22* (3), 1100-1107. DOI: 10.1021/acs.nanolett.1c04216.
(148) Thanusing, M. K.; Shen, P.; Pollard, B. L.; Connal, L. A. Rational design of water-harvesting hydrogels. *Molecular Systems Design & Engineering* **2024**, *9* (1), 63-72. DOI: 10.1039/D3ME00132F.
(149) Thanusing, M. K.; Pollard, B. L.; Connal, L. A. Arginine-functionalised hydrogels as a novel atmospheric water-harvesting material. *RSC Applied Polymers* **2025**, *3* (2), 480-487. DOI: 10.1039/D4LP00373J.
(150) Hackl, E.; Darkwah, J.; Smith, G.; Ermolina, I. Effect of Arginine on the Aggregation of Protein in Freeze-Dried Formulations Containing Sugars and Polyol: 1—Formulation Development. *AAPS PharmSciTech* **2018**, *19* (2), 896-911. DOI: 10.1208/s12249-017-0884-0.
(151) Gutiérrez-Hellín, J.; Del Coso, J.; Franco-Andrés, A.; Gamonales, J. M.; Espada, M. C.; González-García, J.; López-Moreno, M.; Varillas-Delgado, D. Creatine Supplementation Beyond Athletics: Benefits of Different Types of Creatine for Women, Vegans, and Clinical Populations—A Narrative Review. *Nutrients* **2025**, *17* (1), 95.
(152) American Chemical Society *Guanidine*. 2020. https://www.acs.org/molecule-of-the-week/archive/g/guanidine.html (accessed 2025 21/08).

Chapter Two

Rational design of water-harvesting hydrogels

Moki K. Thanusing, Peidong Shen, Brett L. Pollard, Luke A. Connal

Mol. Syst. Des. Eng., 2024, **9**, 63-72

Australian National University

Statement of Contribution

This thesis is submitted as a Thesis by Compilation in accordance with https://policies.anu.edu.au/ppl/document/ANUP_003405

I declare that the research presented in this Thesis represents original work that I carried out during my candidature at the Australian National University, except for contributions to multi-author papers incorporated in the Thesis where my contributions are specified in this Statement of Contribution.

Title: Rational design of water-harvesting hydrogels

Authors: Moki K. Thanusing, Peidong Shen, Brett L. Pollard, Luke A. Connal

Current status of paper: Published

Publication Outlet: Molecular Systems Design & Engineering, **2024**, *9*, 63-72

Contribution to paper: This is a full paper and the candidate conducted all of the experimental work reported within. In addition, all spectral data presented in the Supporting Information document was collected and formatted by the candidate. The candidate also wrote the entirety of the manuscript and experimental section and conducted relevant literature surveys. A preliminary outline was generated and revised by the candidate.

Senior author or collaborating authors endorsement: Peidong Shen

Moki Thanusing		25/08/25
Candidate – Print Name	Signature	Date

Endorsed

Luke Connal		26/08/25
Chair of Supervisory Panel – Print Name	Signature	Date
Mark Humphrey		28/08/25
Delegated Authority – Print Name	Signature	Date

Foreword

This thesis focuses on the development of additive-free, thermoresponsive SAWH hydrogels. Without a robust rational design framework, this development cannot meaningfully proceed. In this chapter, I examine structure-property relationships which can inform future design decisions. A thermoresponsive copolymer library, using methacrylic acid and poly(ethylene glycol) methyl ether methacrylate (PEGMA) as monomers, was synthesised with variations to composition, crosslinking density and crosslinker length. The causal relationships between these synthetic changes and water harvesting are reported, thus establishing a baseline understanding that can be applied to later chapters.

This chapter was published in the January 2024 edition of Molecular Systems Design and Engineering, where I am its first author. My contribution to the manuscript includes designing and conducting experiments, characterisation of resulting materials, data analysis as well as preparing and revising the manuscript and figures (overall 75%). The published version of the manuscript is presented here. Peidong Shen and Brett L. Pollard edited and revised the manuscript. Luke A. Connal contributed to experimental design, supervised the project, and edited and revised the manuscript and figures.

Introduction

Water scarcity is one of the perennial problems impacting the human population. The hydrological cycle (which interconverts fresh and saline water) redistributes 455,000 billion metric tonnes (bmt) of water globally per annum.[1] Humans, in comparison, consume around 4,000 bmt in the same period, with groundwater, rivers and lakes being the most used water sources. The uneven distribution of the hydrological cycle gives rise to local water scarcity.[1, 2] Atmospheric water, while also considered easily accessible, has been largely neglected. Representing around 10,000 bmt of water, it would be more than sufficient for global fresh water needs while also having several major advantages. Atmospheric water is ubiquitous and can be captured locally, eliminating the need for transportation. Unlike groundwater, atmospheric water is clean and can be used immediately upon collection. The hydrological cycle replenishes atmospheric water quickly, which makes it an almost inexhaustible source of water.[1, 3, 4] Hence, using atmospheric water as a resource is an attractive solution to location-specific water shortages.

Desiccants have significant potential as a water-harvesting technology.[5, 6] These can be solid (zeolites, MOFs, silica gel) or liquid (salt solutions like LiCl).[4, 7-9] Existing materials show impressive water harvesting performance. Xu *et al.* used hygroscopic LiCl salt in a MOF matrix with 0.77 g g^{-1} sorption in 12 hours in low humidity conditions.[10] Comparable performance is seen in LiCl-impregnated macroporous polyacrylamide, made by Lyu *et al*. This material absorbs water rapidly, reaching 0.32 g g^{-1} in the first hour in high humidity conditions.[11, 12] While desiccants can easily absorb water from the air, their high affinity for water in turn makes the water release phase more energy-intensive. Some materials, like zeolites, require temperatures far above the vaporisation temperature of water in order to extract the harvested water.[7, 13] For a desiccant to be viable as a water-harvesting material, therefore, water uptake needs to be sufficiently rapid without requiring a prohibitively energy-intensive water release. Desiccants based off thermoresponsive polymers fit these criteria; their switchable affinity for water reduces the energy required for water release without negative effects on water uptake. These polymers exhibit drastic and discontinuous changes in properties with a change in temperature and hence can liberate water more easily.[14-16] Some prominent examples include Lee *et al.*'s cactus-inspired solar still, which includes PNIPAAm as the thermoresponsive component, and Guo *et al.*'s porous films made

with sustainable raw materials, which use hydroxypropyl cellulose.[12, 17] These materials can yield 209 mg cm^{-2} h^{-1} at 80% RH and up to 0.96 g g^{-1} at 30% RH respectively.

When considering the thermoresponsive behaviour of hydrogels (or crosslinked networks), the point at which the polymer switches from hydrophilic to hydrophobic (and *vice versa*) is known as the volume phase transition temperature (VPTT). The mechanism of this phase transition is similar to that of a non-crosslinked polymer. In the context of water harvesting, thermoresponsive polymers absorb atmospheric water by way of their hygroscopicity, before subsequent physical contraction to release liquid water upon heating above the VPTT. This is a renewable process as water capture and release can theoretically be cycled indefinitely. The release of liquid water gives thermoresponsive polymers an advantage over other desiccants, which must release water as a vapour.[12, 18, 19] The water-harvesting thermoresponsive polymer is therefore a material of great interest in this space (**Figure 1**).

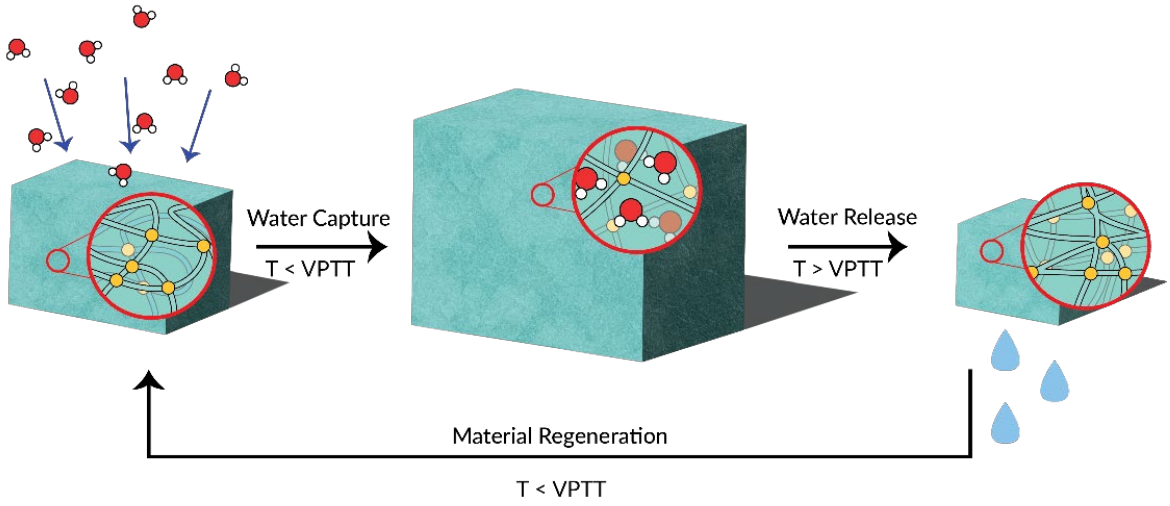

Figure 1: A graphical depiction of a thermoresponsive water-harvesting polymer. Water is absorbed into the hydrogel (left, middle). The system is heated above the hydrogel's volume phase transition temperature (VPTT), triggering a hydrophilic-hydrophobic transformation. As the hydrogel becomes hydrophobic, water molecules within the network aggregate and are expelled as liquid water (right). The material is renewed as the temperature is brought back below the VPTT, rendering the hydrogel hydrophilic and ready for another water-harvesting cycle.

Herein, we developed a new candidate polymer with water-harvesting potential: poly(methacrylic acid-*co*-poly(ethylene glycol) methyl ether methacrylate) (poly(MAA-*co*-PEGMA)) and its related hydrogels. We chose this material due to its hydrophilic nature and

its impressive thermoresponsive, mechanical and self-healing properties.[20] Currently, poly(*N*-isopropylacrylamide) (PNIPAAm) polymers see the most use for atmospheric water harvesting polymers in current research.[12, 18, 19, 21, 22] PEGMA exhibits appreciable thermoresponsive behaviour and hydrophilicity.[23] MAA is also natively hygroscopic; this is contrasted with current literature where deliquescent salts are used as the primary source of hygroscopic properties.[19, 22, 24-26] MAA can also be easily functionalised like NIPAAm which allows for customisation of physical and chemical properties.[27, 28] The use of a copolymer allows for all desired functionality to be incorporated into a single polymer network. Properties such as thermoresponsive behaviour can be tuned easily by modifying the composition of the polymer. The structure-property relationships with respect to water uptake and release are investigated, which we anticipate will be critical in directing future efforts to design water-harvesting polymers.

Results and Discussion

The development of polymer systems that could reversibly capture and release water at a critical temperature switch could drastically reduce the energy to harvest water from desiccant systems (**Figure 1**). We initially developed a library of soluble poly(MAA-*co*-PEGMA) copolymers to understand the impact of composition on the resulting copolymer water uptake potential and thermoresponsitivity. MAA was chosen as the hygroscopic component of the copolymer, while PEGMA imparted thermoresponsive properties. These findings were then used to design a series of copolymer gels. Reversible addition-fragmentation transfer (RAFT) polymerisation was conducted to afford a series of copolymers (**Scheme S1**). ^{1}H NMR spectroscopy was used to characterise the poly(MAA-*co*-PEGMA) system (**Figure S1**). The following compositions were prepared and analysed further: poly(MAA_{27}-*co*-$PEGMA_{20}$), poly(MAA_{38}-*co*-$PEGMA_{16}$), poly(MAA_{40}-*co*-$PEGMA_{15}$), and poly(MAA_{203}-*co*-$PEGMA_{50}$).

We initially screened the library in terms of ease of handling as we wanted to make consistent films to test the material's water uptake. Incremental changes in feed ratio of 10% showed marked differences in the resulting polymers's physical properties. The copolymer became physically softer with increasing PEGMA content, owing to the reduced T_g, reduced packing density between the long ethylene glycol chains of the parent monomer, as well as its strong solvation effects.[20, 29] Near-proportional changes to T_g with increasing PEGMA content were

observed by Jones *et al.* in a similar MAA-*co*-PEGMA material, which corresponds with the appreciably different physical properties of our own materials when varying PEGMA content.[29] We cast films from *N,N*-dimethylformamide (DMF) and then oven dried these films at 50°C over 24 hours. Films cast from poly(MAA_{27}-*co*-$PEGMA_{20}$) were essentially low viscosity liquids and could not be easily handled. Hence, this composition was considered impractical for further investigation in this case. Gratifyingly, poly(MAA_{38}-*co*-$PEGMA_{16}$) could be readily shaped in a mould after casting and drying. Films cast from poly(MAA_{40}-*co*-$PEGMA_{15}$) were glassy but became flexible after exposure to humidity. All the aforementioned compositions were soluble in water. Finally, attempts to cast films from poly(MAA_{203}-*co*-$PEGMA_{50}$) were unsuccessful as the material only became viscous on attempts to dissolve. As a result, this material was not studied further.

Water uptake experiments were then conducted on the most promising compositions, namely poly(MAA_{38}-*co*-$PEGMA_{16}$) and poly(MAA_{40}-*co*-$PEGMA_{15}$). Dried samples were stored under humid conditions (70% relative humidity) in a closed environment for one day, with water uptake determined by recording their change in mass over time. There was a considerable difference in the rate of water uptake between the samples, with poly(MAA_{38}-*co*-$PEGMA_{16}$) showing faster water uptake in the first 400 minutes. Over 24 hours both copolymer compositions approached a similar water uptake **(Figure 2)**. The reduced packing caused by the long sidechains of PEGMA likely the atmospheric water easier access to the polymer backbone and hydrophilic side chains.

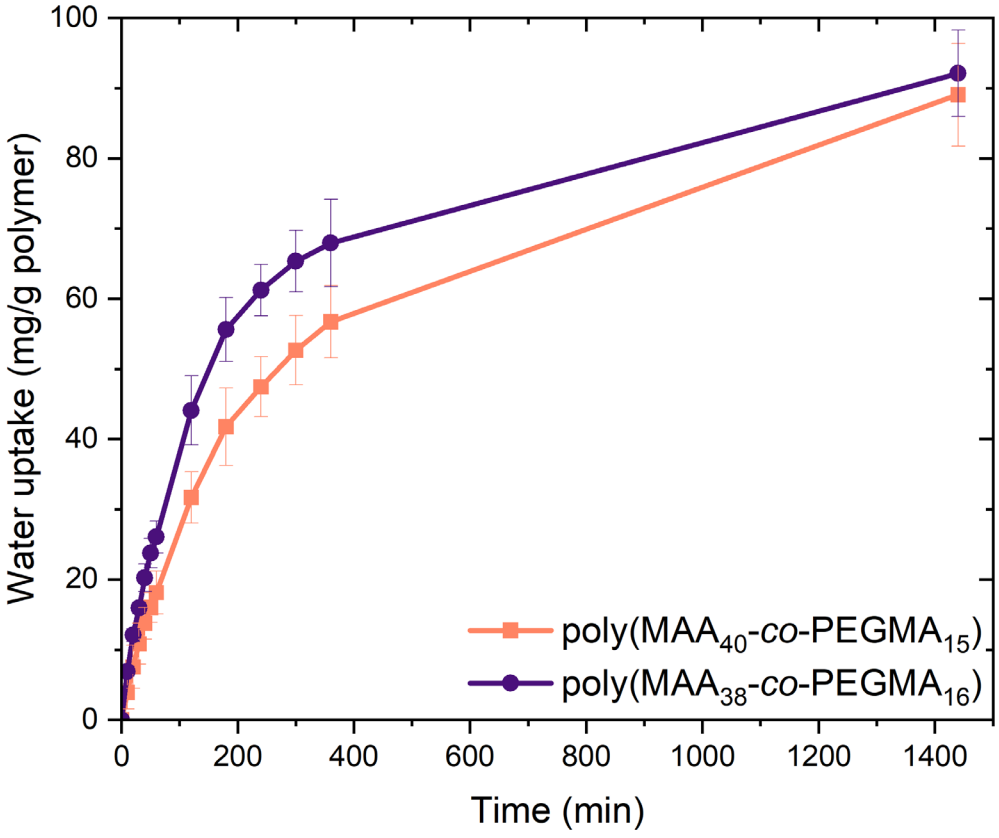

Figure 2: Water uptake measured over 24 hours for poly(MAA_{40}-*co*-$PEGMA_{15}$) and poly(MAA_{38}-*co*-$PEGMA_{16}$), illustrating the effects of MAA:PEGMA feed ratio. Poly(MAA_{40}-*co*-$PEGMA_{15}$) reached 89 mg water/g polymer after 24 hours, while poly(MAA_{38}-*co*-$PEGMA_{16}$) reached 92 mg/g. Rate of uptake was also affected, evidenced by poly(MAA_{38}-*co*-$PEGMA_{16}$) absorbing 68 mg/g by 360 minutes while poly(MAA_{40}-*co*-$PEGMA_{15}$) absorbed 57 mg/g in comparison.

With the above copolymer systems, we have confirmed the potential of the copolymers to absorb water. However, in a practical water harvesting system, crosslinking is required, thereby increasing the stability and applicability to water uptake and release.[26, 30] Thus, we next designed a covalently crosslinked hydrogel system that drew on our knowledge of the water-soluble poly(MAA-*co*-PEGMA) copolymer system. The general scheme for hydrogel synthesis is given below (**Scheme 1)**. In our synthetic strategy, we utilised RAFT polymerisation to create gels with varying crosslinking density (***G1*** - ***G3***), PEGMA composition (***G1*** and ***G4***) and crosslinker length (***G1***, ***G5***, ***G6***, ***G8***, ***G9***) (**Table 1**). We used various crosslinkers, including ethylene glycol dimethacrylate (EGDMA) and multiple lengths of poly(ethylene glycol) dimethacrylate (PEGDMA). Methacrylate crosslinkers were

chosen as to keep the inter- and intramolecular interactions within the hydrogel consistent with those within the copolymer.

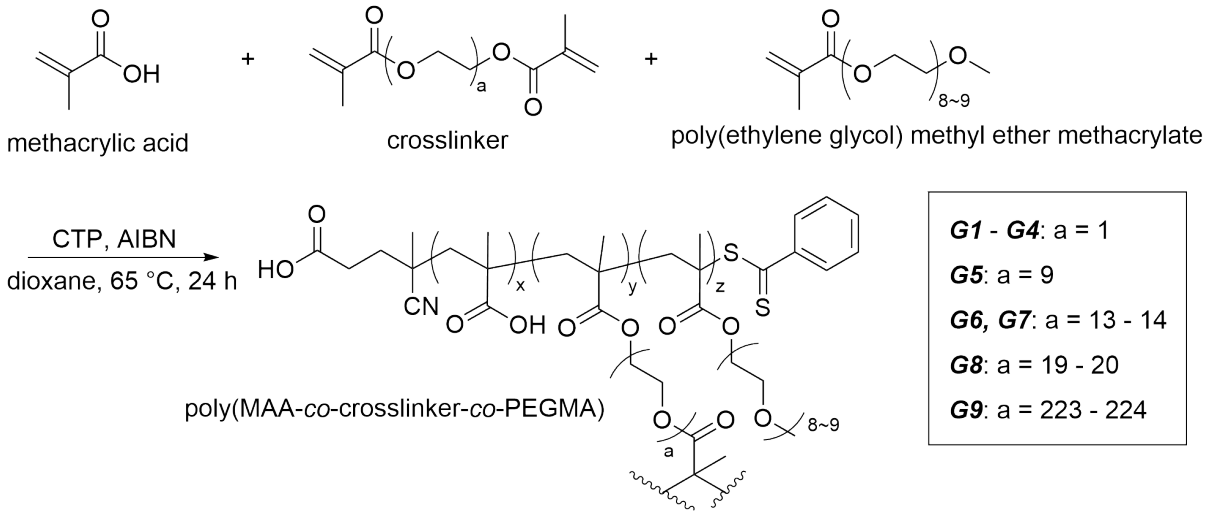

Scheme 1: Generalised scheme for the poly(MAA-*co*-PEGMA) hydrogel.

Label	*Composition (MAA:crosslinker:PEGMA)*	*Crosslinker*	*VPTT (°C)*
G1	75:5:20	EGDMA	65.3
G2	74:6:20		54.7
G3	73:7:20		52.3
G4	65:5:30		65.1
G5	75:5:20	PEGDMA 550	63.5
G6	75:5:20	PEGDMA 750	57.2
G7	75:5:20 (pristine)		59.7
G8	75:5:20	PEGDMA 1000	70.6
G9	75:5:20	PEGDMA 10000	71.3

Table 1: Summary of poly(MAA-*co*-PEGMA)-based hydrogels synthesised according to **Scheme 1**. Composition is given as MAA:crosslinker:PEGMA molar ratio.

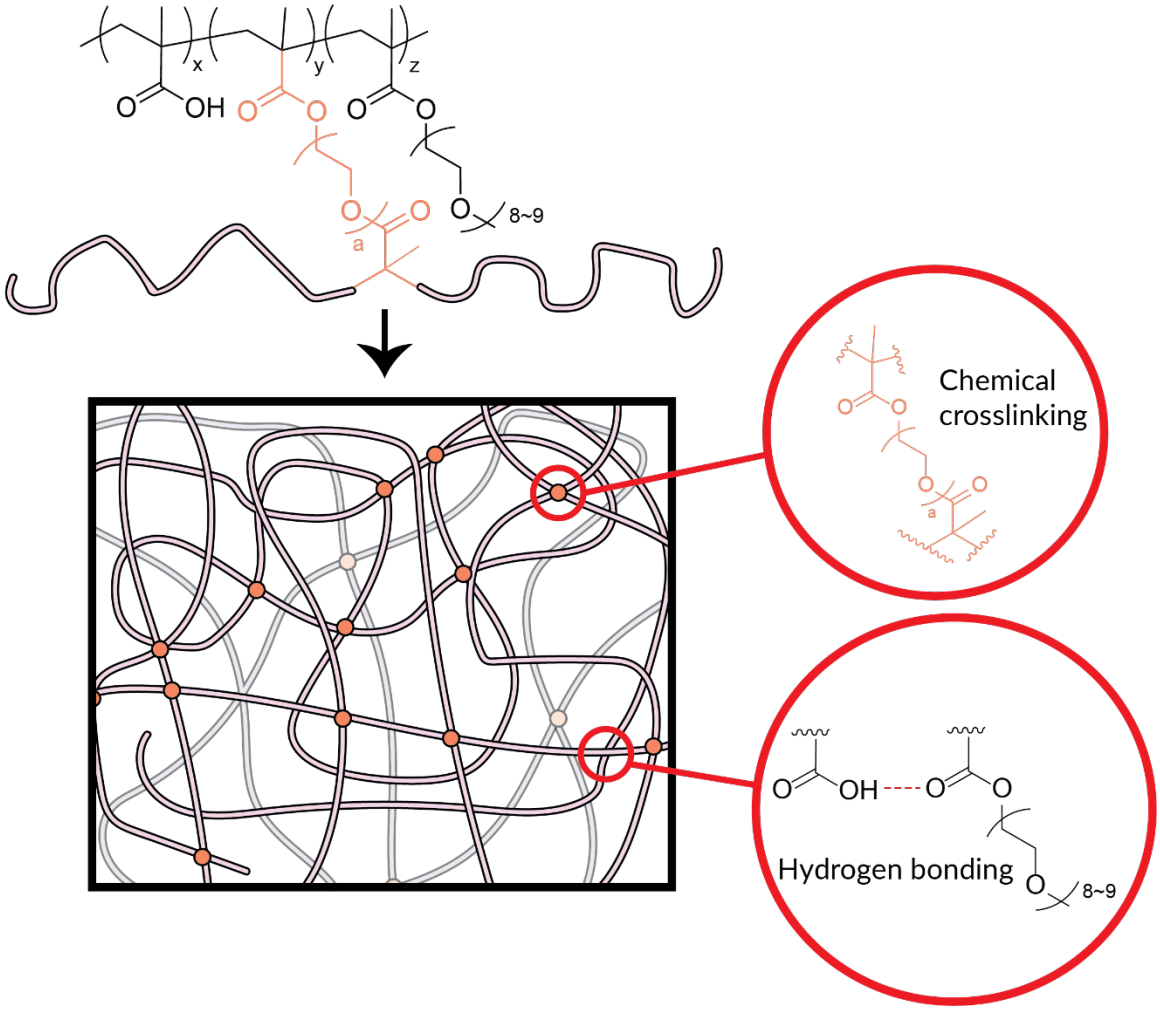

Figure 3: Illustration of the design of the poly(MAA-*co*-PEGMA)-based hydrogel. The network is held together by both chemical and physical crosslinking. Chemical crosslinking comes from the use of the dimethacrylate crosslinkers (**Scheme 1**, **Table 1**) within the hydrogel. Physical crosslinking comes principally from hydrogen bonding that occurs between the hydrogen-bond donors on the MAA units and various possible hydrogen-bond acceptors on the PEGMA or crosslinker chains.

The poly(MAA-*co*-PEGMA)-based hydrogel was designed for stability on exposure to water using chemical crosslinking. Crosslinking already exists within the copolymer in the form of physical entanglement and hydrogen bonding. The desired application, atmospheric water-harvesting, involves consistent contact with water in vapour or liquid form. Hydrogen bonding between polymer and water is favourable during the water uptake phase, which reduces the hydrogen bonding between polymer chains and therefore the physical crosslinking. This can be observed as with increased exposure to humid conditions, copolymer samples visibly "melted". Additionally, as water enters the copolymer system, individual polymer chains have more freedom of movement which loosens physical

entanglement in the water uptake phase. Upon water release, the observed deformities in the samples were shown to be permanent. It is not practical for the desired application to have a material which readily deforms with use. The introduction of a chemical crosslinker is the simplest remedy. Chemical crosslinking is stable to water, which allows for water harvesting without deformation of the polymer.

We initially studied the effect of crosslinking density on water uptake. Dried crosslinked films (***G1***–***G3***) were held in a humid environment (70% RH) for 48 h and the weight of the gels were measured periodically. Water uptake was rapid until around the 24 hour mark, at which point water capacity was reached and the water content entered an equilibrium with the relative humidity of the environment (~70% relative humidity (RH)). This behaviour was observed with all gels. All data was taken up to 24 hours for this reason. The gel with the highest water absorbing capacity was ***G1***, with the lowest crosslinking density. Increasing the crosslinking density decreased the water absorption capacity (***G2***–***G3***) (**Figure 4a**). The trend was expected: as crosslinking density increases, there is less network mobility and hence water permeation and absorption are decreased. Despite this, the difference in uptake for this series was more marginal than expected.

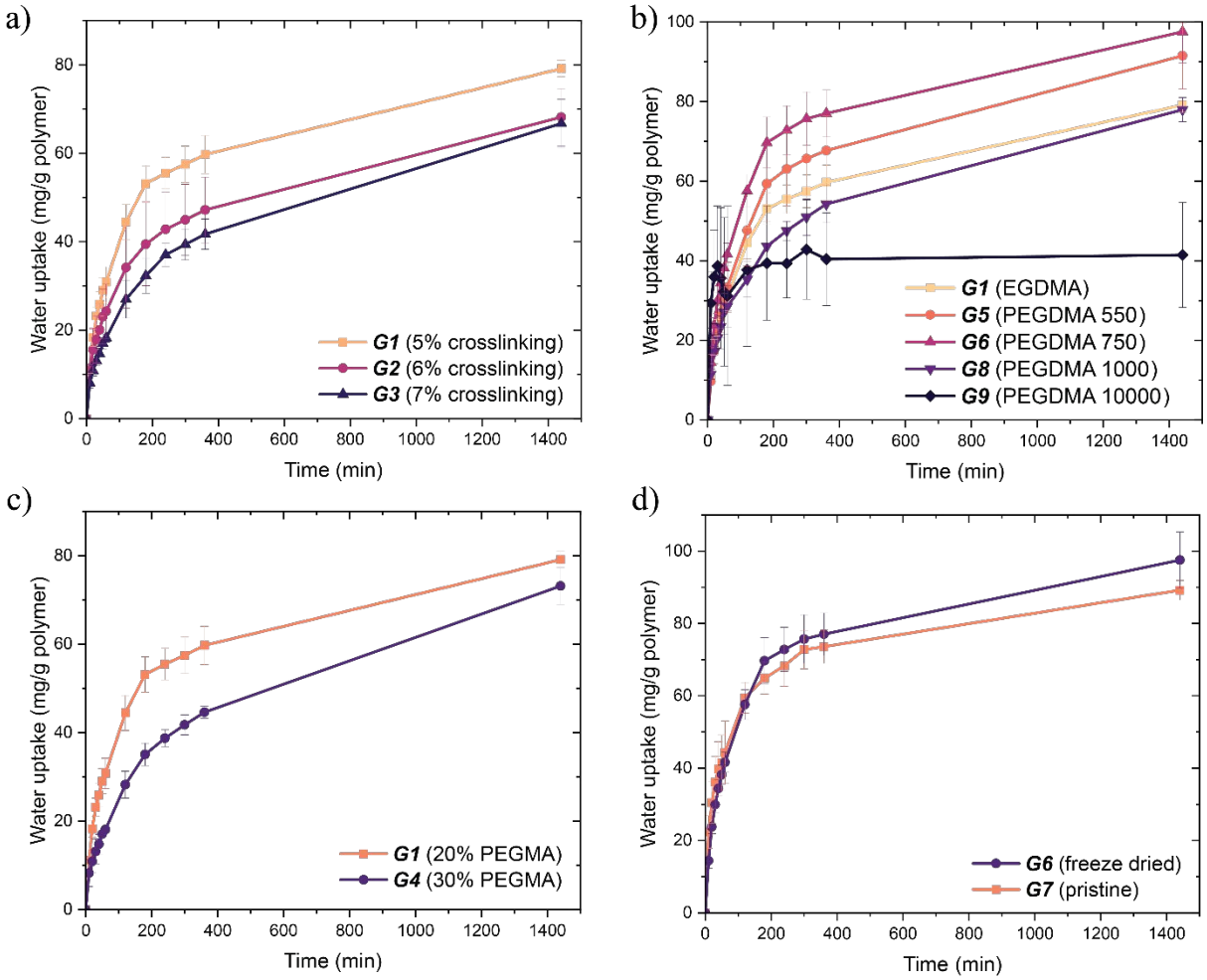

Figure 4: Water uptake over 24 hours of poly(MAA-*co*-PEGMA)-based hydrogels: a) uptake using ***G1***, ***G2*** and ***G3***, comparing crosslinking density, demonstrating a decrease in crosslinking density increases uptake capacity; b) uptake using ***G1***, ***G5***, ***G6***, ***G8***, and ***G9***, comparing crosslinker length, demonstrating a non-linear relationship between crosslinker length and water uptake; c) uptake using ***G1*** and ***G4***, comparing PEGMA content demonstrating increasing MAA content increases uptake ; d) uptake using ***G6*** and ***G7***, comparing effects of freeze-drying demonstrating additional porosity imparted by freeze drying allowed for an slight increase in water uptake after 24 hours.

The effects of crosslinker length on water uptake were also investigated. The intermediate length PEGDMA 550 Da (***G5***) and 750 Da (***G6***) crosslinkers showed increased water capacity after 24 hours compared to both shorter and longer crosslinkers. The short chain EGDMA (***G1***) crosslinked network displayed the next best water uptake kinetics. (**Figure 4c**). Surprisingly, the gels with the longer PEGDMA crosslinkers (1000 Da and 10,000 Da, ***G8*** and ***G9*** respectively) showed the lowest water uptake.

The non-linear change of water uptake with length suggests the combination of several effects. Firstly, there is the positive effect on water uptake from a looser polymer network, as demonstrated above (**Figure 4a**). The increase in water uptake can be seen from EGDMA to PEGDMA 750 Da, showing the positive effect of a looser network. However, the positive effect does not increase linearly with length. As water is a small molecule, the increase in the degree of freedom provided to the solvent within the polymer network decreases with crosslinker length. There is therefore a reduced increase of the positive effect on water uptake as crosslinker length increases. At the point of PEGDMA 10,000 Da, the positive effect of length on water uptake would be minimal, if not negligible.

There is a simultaneous negative effect on water uptake with crosslinker length. This is due to the mass fraction of MAA units decreasing with the increasing length and molecular weight of the crosslinker. PEGDMA is less hygroscopic than MAA, so as the proportion of PEGDMA by weight increases, decreasing hygroscopicity of the polymer is expected (**Figure S2**). We tested the hypothesis that the low water uptake of ***G9*** was observed because of the smaller mass fraction of MAA units to PEGMA and PEGDMA in the system. A sample of hydrogel replacing the PEGMA in ***G9*** with MAA (leading to a 95:5 feed ratio poly(MAA-co-PEGDMA)) was prepared (***GS1***). The water uptake of ***GS1*** is increased in comparison to ***G9*** **(Figure S2)**. This confirms our assumption that MAA is the hygroscopic element of the polymer system and that the reduced proportion of MAA in ***G9*** was the cause of the reduced water uptake.[31, 32] The negative effect increases proportionally to the reduction of MAA mass fraction in the polymer, i.e. with increasing crosslinker length. The combination of both positive and negative effects explains the increase then decrease in water uptake with crosslinker length.

We then investigated the effect of composition of PEGMA and MAA on the water absorbing capacity. Gels (***G1*** and ***G4***) were placed in a humid environment and their mass was recorded periodically. Again, a sharp increase followed by a plateau was observed in the first 24 hours (**Figure 4b**). The gel with the highest composition of MAA showed both a faster water absorption and a larger water absorbing capacity. The equivalent copolymers in **Figure 2** showed the opposite results where increasing MAA decreased the water absorbing capacity. A looser network resulting from increased PEGMA content would still be observed in the crosslinked gel, implying a positive correlation between PEGMA content and water uptake. However, MAA is the primary component of the hygroscopic polymer system (**Figure S2**), which implies a positive correlation between MAA content and water uptake. If both

correlations occur simultaneously, it can be concluded that the effect of each relationship changes with crosslinking of the poly(MAA-*co*-PEGMA) system. The loosening of the polymer network is minimal between ***G1*** and ***G4***; the crosslinking density remains the same. Thus, the positive correlation between water uptake and MAA content takes precedence over that with PEGMA, and we observe ***G1*** (with lower PEGMA content, i.e. higher MAA content) having more water capacity than ***G4***.

The effects of porosity on water uptake were also studied. Freeze drying is an effective method to produce porous materials.[20] We conducted freeze drying on the majority of the synthesised hydrogels. Freeze drying-induced porosity allows a greater surface area of hydrogel to be exposed to humid air and should increase the rate of water absorption. Increased surface area via porosity is easily observable between ***G6*** and ***G7***: ***G6*** has visible pores in the range of 1–10 μm while ***G7*** is smooth with no discernible pores (**Figure 5**). However, there is little difference between the freeze-dried and pristine samples in the first two hours of water uptake (**Figure 4d**). Slightly increased water capacity in the freeze-dried sample was observed after two hours, owing to the more rapid absorption and diffusion of water into the system via porosity. Since the hydrogels were hard and brittle, the porosity imparted by freeze drying was appreciable yet could be improved further. Freeze drying is more effective in hydrogels with less crosslinking density (i.e. a smaller proportion of added crosslinker or the use of a longer crosslinker), and this increased porosity results in clearer changes in water harvesting behaviour in the first 6 hours. Increased water uptake is generally attributed to increased surface area of a material.[7, 9, 17] Therefore, these results show more about the material itself rather than the relationship between surface area and water uptake. No substantial difference in water capacity between freeze-dried and pristine samples was expected because the only difference was surface area through porosity. However, there was a 10% increase with 10 mg/g difference in water capacity after 24 hours (**Figure 4d**). This demonstrates the importance of surface area in water uptake as well as its relationship with diffusivity within the polymer network.

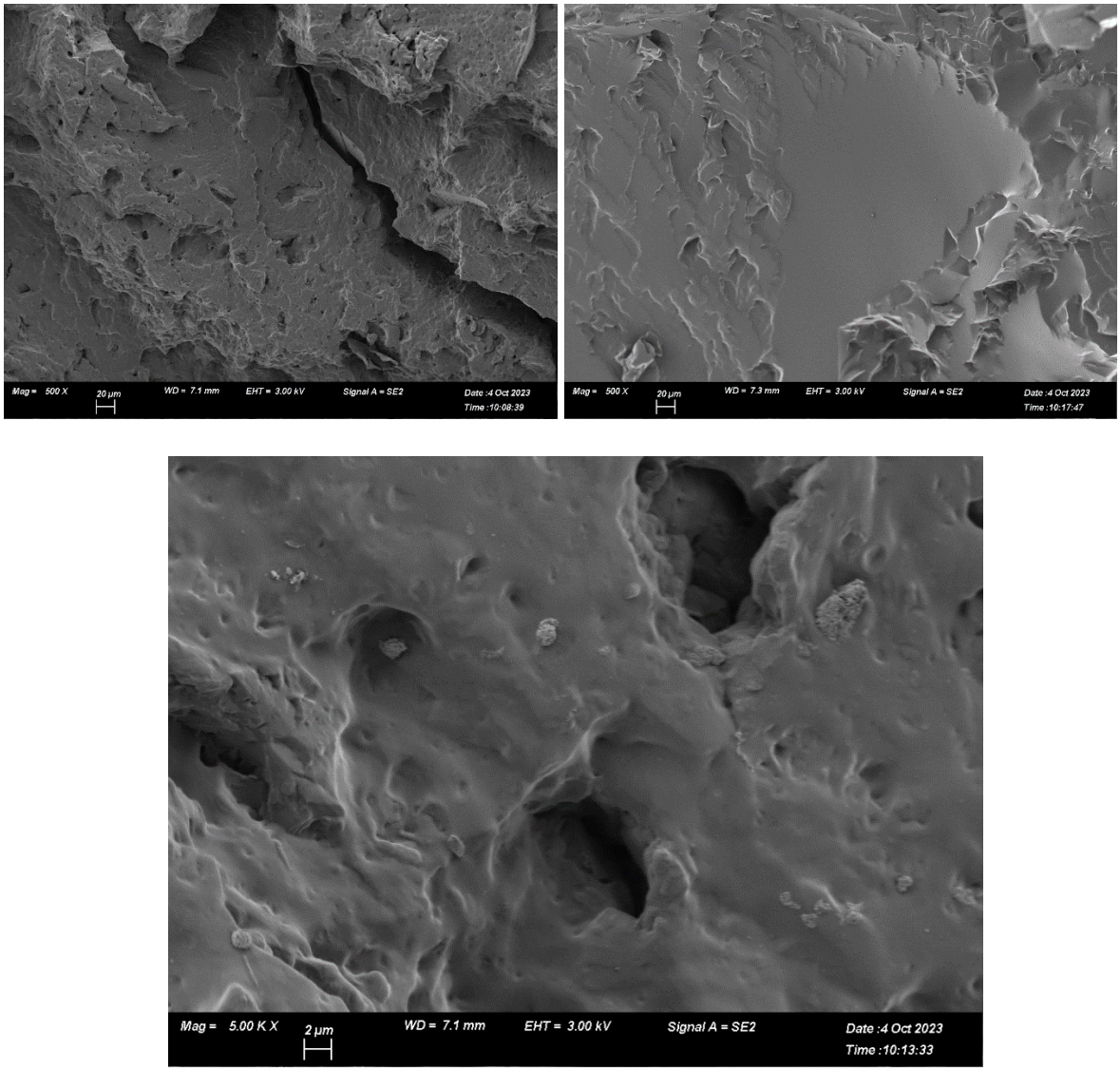

Figure 5: SEM images of ***G6*** and ***G7***, showing differences in porosity between freeze-dried (top left) and non-freeze-dried samples (top right). Pores in ***G6*** are around 1 – 10 µm in size (bottom). Scale bars are 20 µm (top left and right) and 2 µm respectively.

Next, the water release behaviour of the hydrogels was studied. We initially measured the VPTT by conducting differential scanning calorimetry (DSC) on hydrogel samples up to 100°C (**Table 1**), where VPTT can be detected as an endothermic peak.[33] This endothermic change in heat flow corresponds to the temperature at which the polymer-water hydrogen bonds become less favourable than the polymer-polymer and water-water hydrogen bonds, resulting in the release of water. Over 100°C, the vaporisation of water as well as the phase transition of the hydrogel are taken into account. Temperatures beyond this point would not only yield less accurate VPTT measurements, but would also negate the benefits of exploiting the VPTT for water release.

Increasing crosslinker length was associated with a decrease a non-linear change in VPTT, where VPTT lowered with length until PEGDMA 750 Da and then increased up to 71.3°C for PEGDMA 10,000 Da. While increasing length of PEGMA pendant groups is generally associated with increasing lower critical solution temperature (LCST), it should be recognised that different interactions would exist within hydrogels which plausibly gives rise to differing LCST/VPTT behaviour.[34-38]

There are possibly both negative and positive entropic effects on VPTT with increasing crosslinker length. Dissolution of larger polymers requires the ordering of many solvent molecules along the polymer chain and is generally entropically unfavourable. The effect on entropy increases with the size of the polymer. Lower critical solution temperature (LCST) is entropically controlled, considering TΔS comprises more of the Gibbs free energy of mixing as temperature increases.[39] This means that dissolution of larger polymers becomes entropically unfavourable at lower temperatures.[40-46] While this explanation directly contradicts existing literature on PEGMA pendant group effects on LCST, it should be noted that these papers do not include pendant chains more than eight or nine ethylene glycol units long. At over two hundred ethylene glycol units in PEGDMA 10,000 Da, the ordering of water molecules along the crosslinker chain should have an appreciable negative effect on entropy, thus increasing the VPTT. However, there is a positive effect on entropy that should also be considered as crosslinker length increases. Longer crosslinker chains means an overall looser network, that is, an increased number of configurations of the crosslinker chain.

In a similar vein of logic, both positive and negative enthalpic effects are possible for VPTT with increasing crosslinker length. Increasing hydrophilicity with crosslinker length is analogous to increasing pendant group length in soluble polymers, thus having a positive effect on VPTT. Additionally, as crosslinker length increases, so too does the number of hydrogen bond acceptors within the polymer system, while the proportion of hydrogen bond donating MAA carboxyl units is decreased. At very high crosslinker lengths, the material experiences a large deficit in the number of hydrogen bond donors relative to the hydrogen bond acceptors. This causes the polymer-polymer hydrogen bonds that would occur above the VPTT to be less energetically favourable, thus increasing the VPTT needed to allow the phase transition to occur.[47] The closer the number of hydrogen bond donors and acceptors in the polymer system, the less positive (if not outright negative) this enthalpic effect will be. It

is currently unclear whether all or some of these entropic and enthalpic effects on VPTT are present. Nonetheless, the observed non-linear trend indicates the interplay of positive and negative effects on VPTT.

We found that increasing crosslinking density also correlated with a decrease in VPTT. Tighter polymer networks have fewer possible configurations in solvent than looser networks, making them less entropically favourable. The temperature at which mixing of polymer and solvent becomes unfavourable has a positive correlation with entropic favourability. Hence, there is a correlation between increasing crosslinking density and decreasing VPTT.

Interestingly, increasing the proportion of PEGMA in polymer composition has negligible effects on VPTT. ***G1*** and ***G4*** have a composition of 75:5:20 and 65:5:30 ratios of MAA:EGDMA:PEGMA, with a VPTT of 65.3°C and 65.1°C respectively. A similar change in the soluble copolymer yielded a 14°C increase in LCST with increased PEGMA content (**Table S1**). This result implies the greater influence of crosslinking density on VPTT compared to composition.

Finally, we investigated the cycling of water uptake and release. We demonstrated this property with ***G6*** with multiple cycles of water uptake (70% RH, 24 h) and then water release (60°C, 1 h). ***G6*** had the highest-measured water uptake after 24 hours, and thus was chosen for this experiment. Cycling experiments conducted showed only a marginal loss in water uptake capacity over multiple uptake/release cycles (**Figure 5**). This shows that poly(MAA-*co*-PEGMA) hydrogels are capable of repeated uptake/release cycles and hence offer a lengthy functional lifespan. Critically, the water release temperature requirement is only above that of the VPTT, which is significantly lower than the energy required to release water from traditional desiccants.

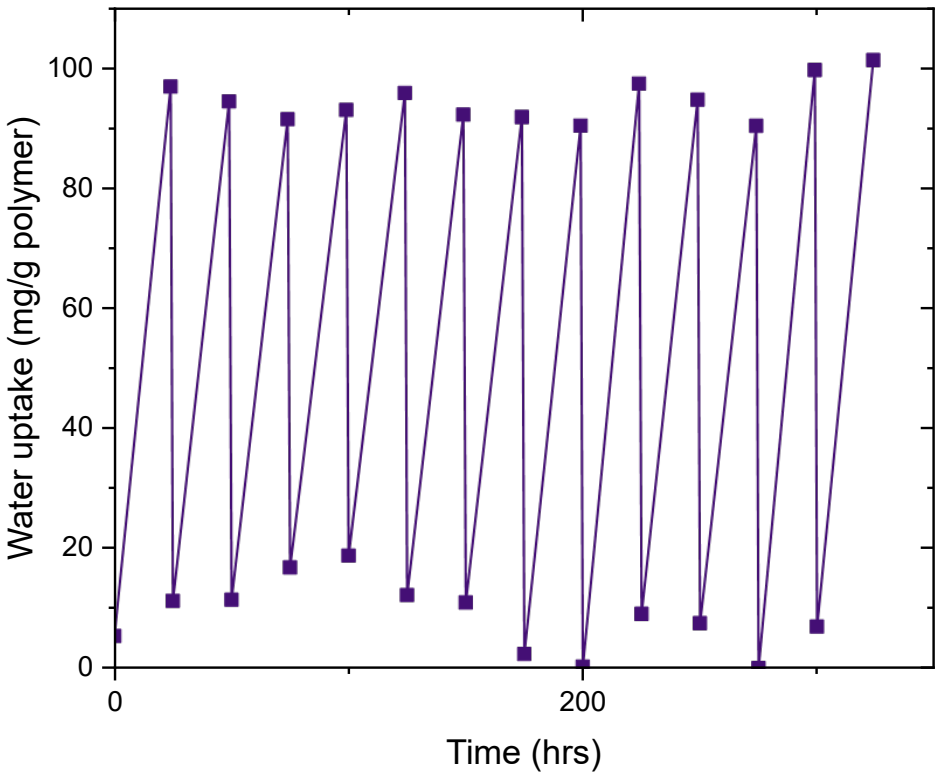

Figure 6: Cycling data of ***G6***, showing no loss in water uptake capacity over 12 uptake/release cycles. Water uptake was consistent at an average of 95 mg/g for each cycle.

Conclusion

In summary, we have demonstrated in-depth structure-property relationships for water-harvesting polymer gels. We assessed the water uptake and release capabilities of a library of poly(MAA-*co*-PEGMA)-based hydrogels. Most notably, longer crosslinkers generally improved the water uptake of hydrogels, up to a total of around 200 mg water (per gram of polymer) after 24 hours exposure to 70% RH air. We also found that this must be balanced with the proportion of hygroscopic material within the hydrogel, which offers insight into the rational design of water-harvesting polymer systems. Porosity of the hydrogels induced by freeze-drying was also observed to promote rapid water uptake in the first 6 hours. The hydrogels were not only thermoresponsive, but retained their water-harvesting capabilities over several water uptake and release cycles. These insights into the structure-property

relationships of water-harvesting polymers will allow for a more streamlined approach to their rational design.

Experimental section

All chemicals were purchased from Sigma-Aldrich and were used as supplied. Monomers supplied with inhibitors (BHT and MEHQ) were subjected to basic-alumina chromatography to remove inhibitors prior to polymerisation. ^{1}H NMR spectra were obtained at 298 K on a Bruker Ascend 400 at 400 MHz, using DMSO-d_6 as solvent. FTIR spectroscopy was conducted on a Perkin Elmer Spectrum 2. DSC experiments were conducted using a Perkin-Elmer DSC8500 apparatus. Humidity was measured inside a custom set-up as shown in **Figure S3**. Humidity and ambient temperature were measured using a RS-1260 humidity temperature meter. The humidity box operated on a constant flow of compressed air (CA) (**1**). Two adjustable lines of air are controlled by a flow meter (**2**): the "dry" air coming directly off the CA, and the "wet" air which is percolated through a flask of water (**3**). The proportions of each air flow were adjusted manually using valves. Field emission electron scanning microscopy (FESEM) images were taken at 3 kV using a Zeiss UltraPlus analytical FESEM. Samples were desiccated and coated with platinum before analysis.

Synthesis of Poly(MAA-*co*-PEGMA)

RAFT polymerisation was conducted with MAA and PEGMA 500 monomers, 2,2′-azobis(2-methylpropionitrile) (AIBN) initiator and 4-cyano-4-(phenyl-carbonothioylthio)pentanoic acid (CTP) chain transfer agent in anhydrous DMF. The solution was allowed to react at 65°C for 24 h before the reaction vessel was exposed to air.

A detailed procedure for poly(MAA_{80}-*co*-$PEGMA_{20}$) is provided. CTP (40.4 mg, 0.14 mmol), MAA (1.38 g, 16 mmol), PEGMA 500 (2.00 g, 4.0 mmol), AIBN (0.2 M in toluene; 1.64 mg, 0.01 mmol) and 6.0 mL of anhydrous *N,N*-dimethylformamide (DMF) were charged into a 25 mL round bottom flask. The mixture was maintained at 0°C and degassed with nitrogen for 20 minutes. The flask was then carefully sealed and stirred at 65°C in an oil bath for 24 hours. After cooling, the resultant mixture was precipitated into chilled diethyl ether (180 mL), forming a pink, solid mass. After air drying overnight, the product was precipitated in chilled *n*-hexane (180 mL) using THF as a carrier solvent. The polymer product was dried at 50°C to afford a pink solid (41%).

^{1}H NMR (poly(MAA$_{60}$-*co*-PEGMA$_{40}$), 400 MHz, DMSO-d$_6$) δ 12.33 (b, 200*1H), 4.00 (s, 133*2H), 3.51, 3.44, 3.43, 3.24 (m, 133*18H), 3.07 (s, 2H), 2.89 (s, 2H), 1.70 (b, 133*2H + 200*2H), 0.94 (b, 133*3H + 200*3H).

^{1}H NMR (poly(MAA$_{70}$-*co*-PEGMA$_{30}$), 400 MHz, DMSO-d$_6$) δ 12.33 (b, 156*1H), 4.01, 3.60, 3.44, 3.43 (m, 67*18H), 3.24 (s, 67*3H), 2.90 (s, 2H), 2.74 (s, 2H), 1.71 (b, 67*2H + 156*2H), 0.94 (b, 67*3H + 156*3H).

^{1}H NMR (poly(MAA$_{80}$-*co*-PEGMA$_{20}$), 400 MHz, DMSO-d$_6$) δ 12.33 (b, 133*1H), 4.00, 3.61, 3.52, 3.44, 3.43 (m, 33*18H), 3.24 (s, 33*3H), 3.06 (s, 2H), 2.67 (s, 2H), 1.71 (b, 33*2H + 133*2H), 0.94 (b, 33*3H + 133*3H).

^{1}H NMR (poly(MAA$_{90}$-*co*-PEGMA$_{10}$), 400 MHz, DMSO-d$_6$) δ 12.34 (b, 150*1H), 4.01, 3.62, 3.52, 3.46 (m, 17*18H), 3.24 (s, 17*3H), 3.07 (s, 2H), 2.74 (s, 2H), 1.70 (b, 17*2H + 150*2H), 0.94 (b, 17*3H + 150*3H).

General procedure for the synthesis of crosslinked poly(MAA-*co*-PEGMA) hydrogels

RAFT polymerisation was conducted using MAA and PEGMA 500 monomers, crosslinker, AIBN initiator and 4-cyano-4-(phenyl-carbonothioylthio)pentanoic acid (CTP) chain transfer agent in anhydrous dioxane. The solution was allowed to react at 65°C for 24 h, with stirring, before the vessel was opened and exposed to air. The gel product obtained was then freeze-dried for 48 hours.

A detailed procedure for poly(MAA-*co*-EGDMA-*co*-PEGMA) with a feed ratio of 75:5:20 (***G1***) is provided. CTP (40.4 mg, 0.14 mmol), MAA (1.29 g, 15 mmol), PEGMA (2.00 g, 4.0 mmol), EGDMA (198 mg, 1.0 mmol), AIBN (0.2M in toluene; 1.64 mg, 0.01 mmol) and 6 mL of anhydrous dioxane were charged into a 25 mL round bottom flask. The mixture was maintained at 0°C and degassed with nitrogen for 15 minutes. The flask was then carefully sealed and gently stirred at 65°C in an oil bath for 24 hours. After mechanically breaking the resultant solid into small chunks, the product was submerged in RO water over two days to leach unreacted monomers, with the water changed daily. After purification, the product was freeze-dried for 2 days to afford an orange or pink glassy solid.

G7 was prepared with a modified version of the above method. After purification, freeze-drying was not conducted. The product was then dried at 50 °C to afford an orange gel.

VPTT measurements

The VPTT of hydrogel products was determined using DSC. The surface of water-swollen gels were blotted dry with filter paper and a small piece (5–15 mg) was loaded into a hermetically sealed aluminium pan. Two cycles were run from ambient temperature to 80°C, with a heating rate of 3°C per minute. Endothermic phase transition peaks were defined by the peak maxima of the endotherm. Reported data is from the second cycle.

Water Uptake

Dried polymer samples were maintained at 50°C before experiments were conducted. Petri dishes containing samples were placed into the humidity box shown in **Figure S3**. Humidity was adjusted to approximately 70% RH. Samples were removed, weighed and returned to the box as quickly as possible. Water content was determined as mass of water per gram of polymer. For the first hour, measurements were taken every ten minutes, then every hour for the next six hours, then a final measurement 24 hours after commencing the experiment.

Cycling experiments

G6 was kept maintained at 50°C before experiments were conducted. The water uptake method described above was followed, with the exception of measurements only being taken after 24 hours. After this, the sample was placed into an oven maintained at the sample's VPTT (i.e. 60°C). After 1 hour, the sample was weighed. This uptake-release cycle was repeated for another twelve cycles.

Supporting Information

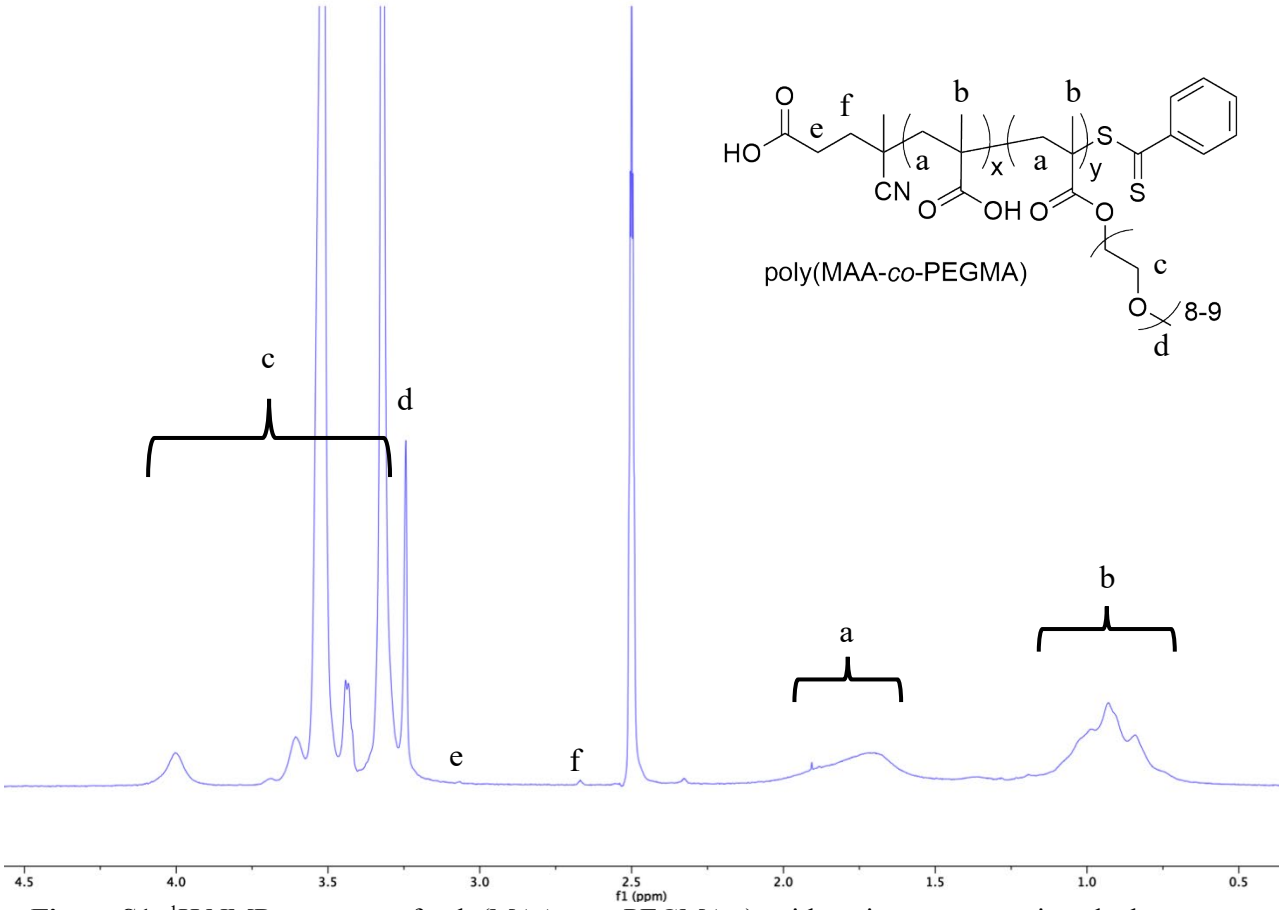

Figure S1: ^{1}H NMR spectrum of poly(MAA$_{80}$-*co*-PEGMA$_{20}$), with major protons assigned where possible.

Sample	*Mn(kDa)*	*Notes*	*LCST (°C)*
poly(MAA$_{27}$-*co*-PEGMA$_{20}$)	12.6	Viscous liquid	68
poly(MAA$_{38}$-*co*-PEGMA$_{16}$)	11.5	Malleable	52
poly(MAA$_{40}$-*co*-PEGMA$_{15}$)	11.3	Malleable yet glassy	38
poly(MAA$_{203}$-*co*-PEGMA$_{50}$)	26.1	Brittle	Not soluble

Table S1: M_n of poly(MAA-*co*-PEGMA) as calculated using ^{1}H NMR spectroscopy (by way of integration). Additional notes on appearance of samples are provided.

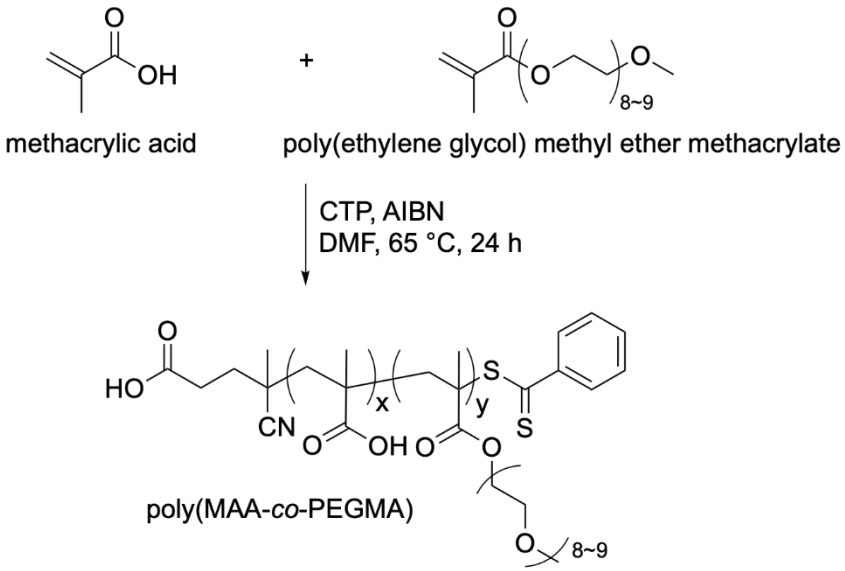

Scheme S1: Pathway to synthesis of poly(MAA-*co*-PEGMA) temperature-responsive co-polymers.

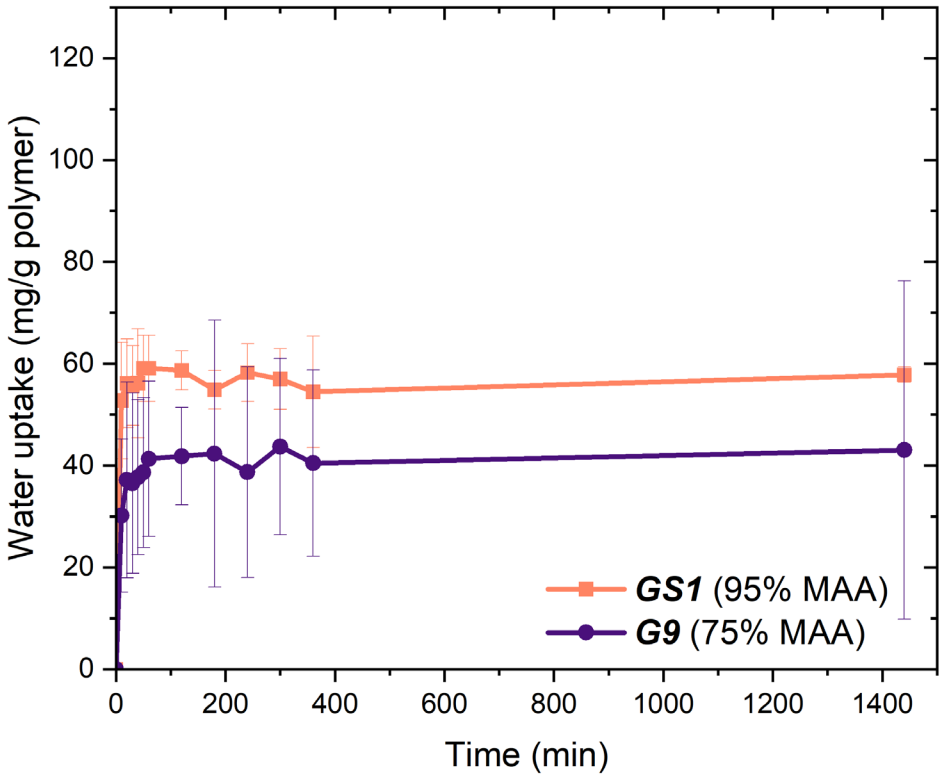

Figure S2: Water uptake over 24 hours of ***GS1*** and ***G9***, comparing MAA content. ***GS1*** used a 95:5 ratio of MAA to PEGDMA (10,000 Da).

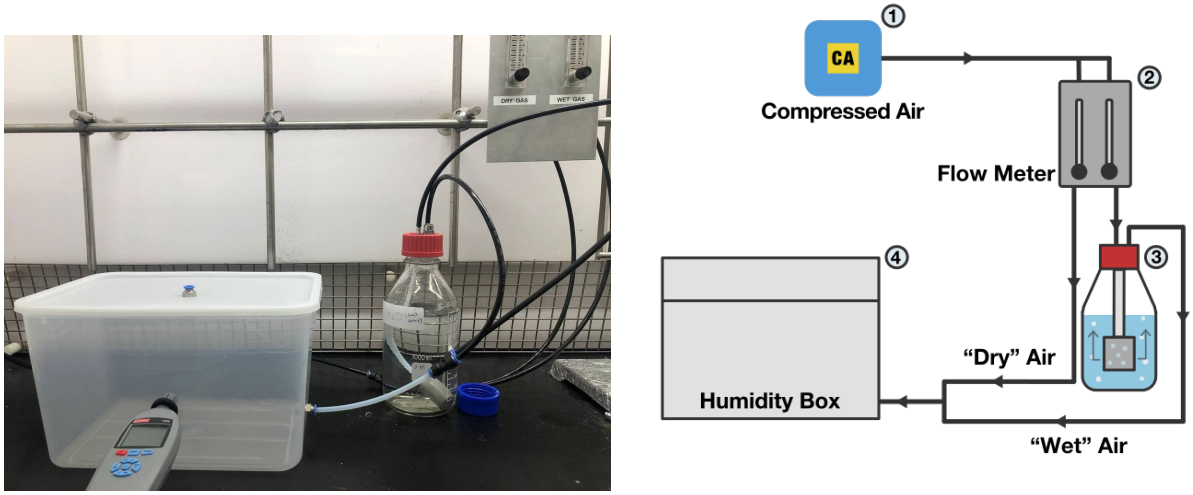

Figure S3: A photograph of the humidity box (left) and a schematic of the system (right).

For **Figures S4** to **S12**, the exotherm points downwards.

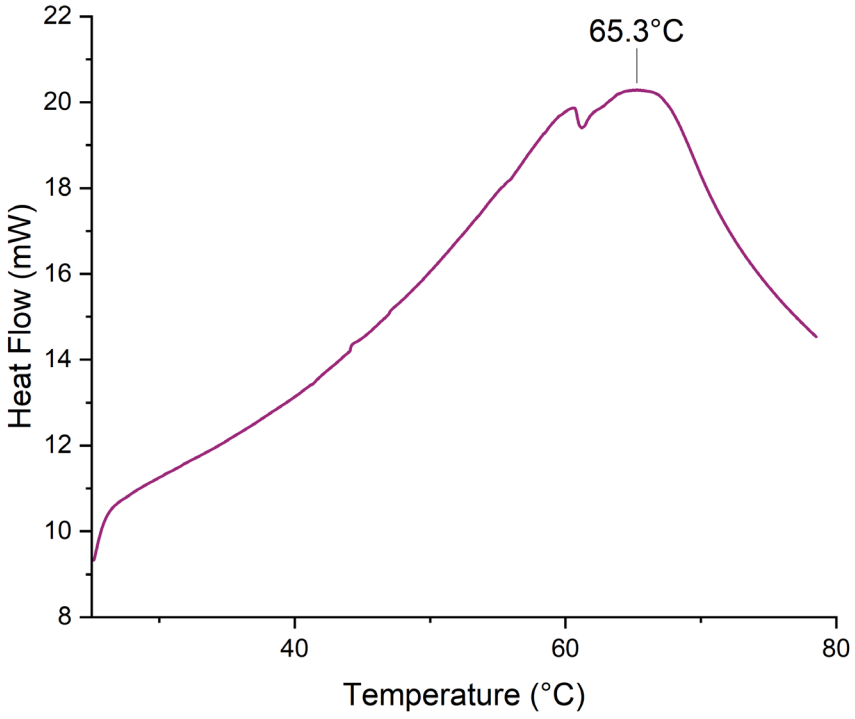

Figure S4: DSC curve for ***G1*** from 25°C to 80°C with VPTT marked.

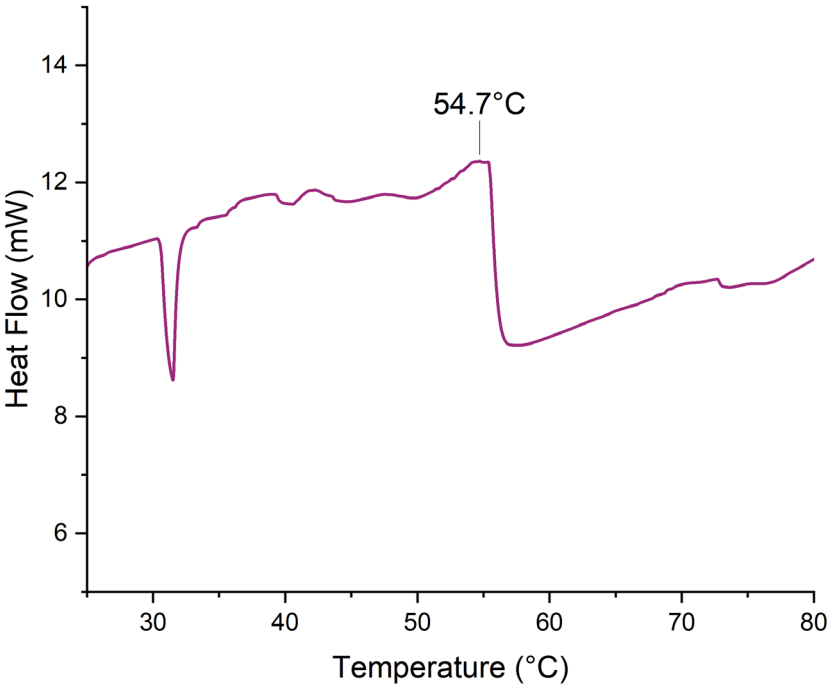

Figure S5: DSC curve for ***G2*** from 25°C to 80°C with VPTT marked.

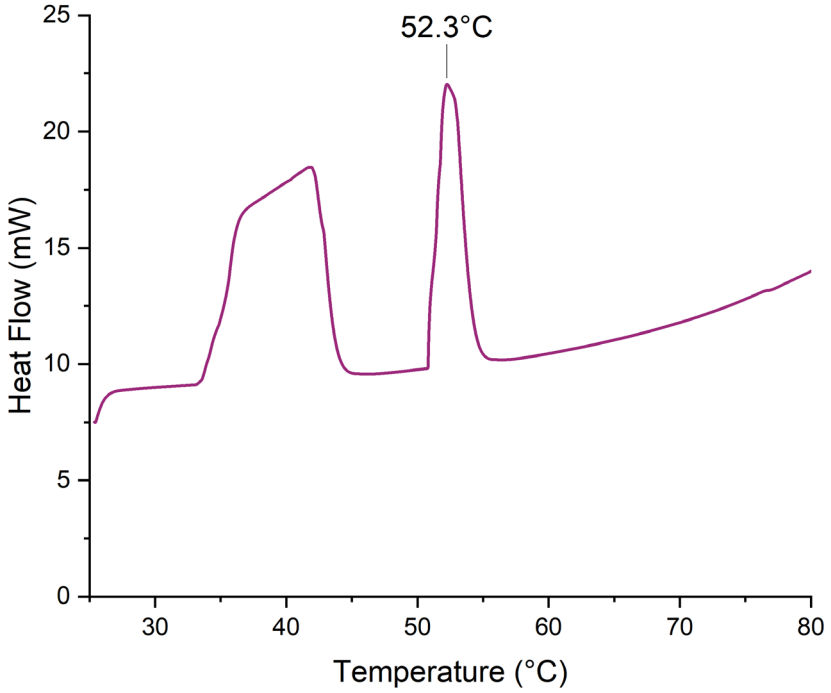

Figure S6: DSC curve for ***G3*** from 25°C to 80°C with VPTT marked.

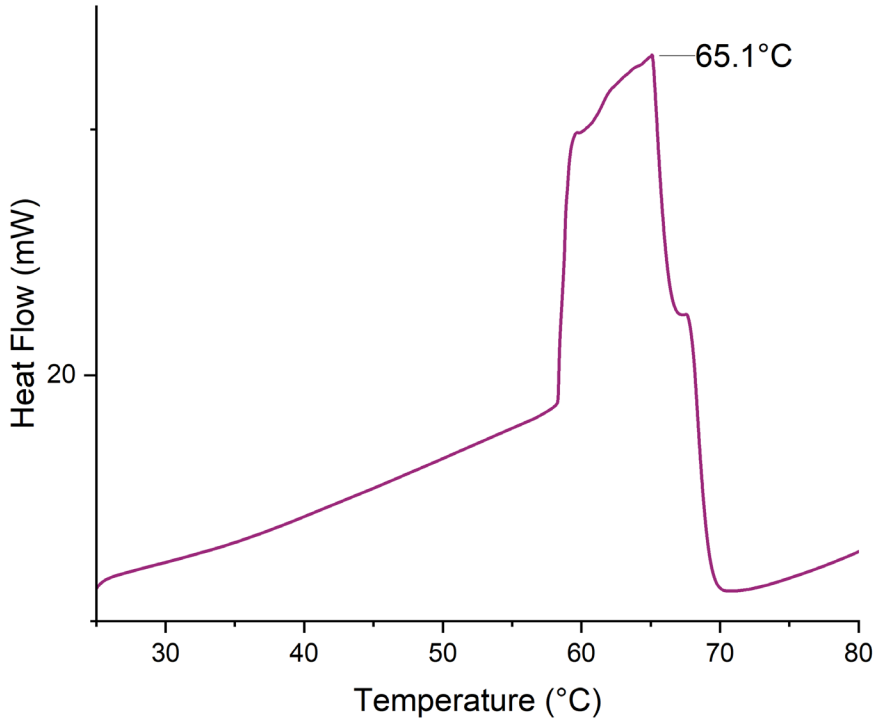

Figure S7: DSC curve for ***G4*** from 25°C to 80°C with VPTT marked.

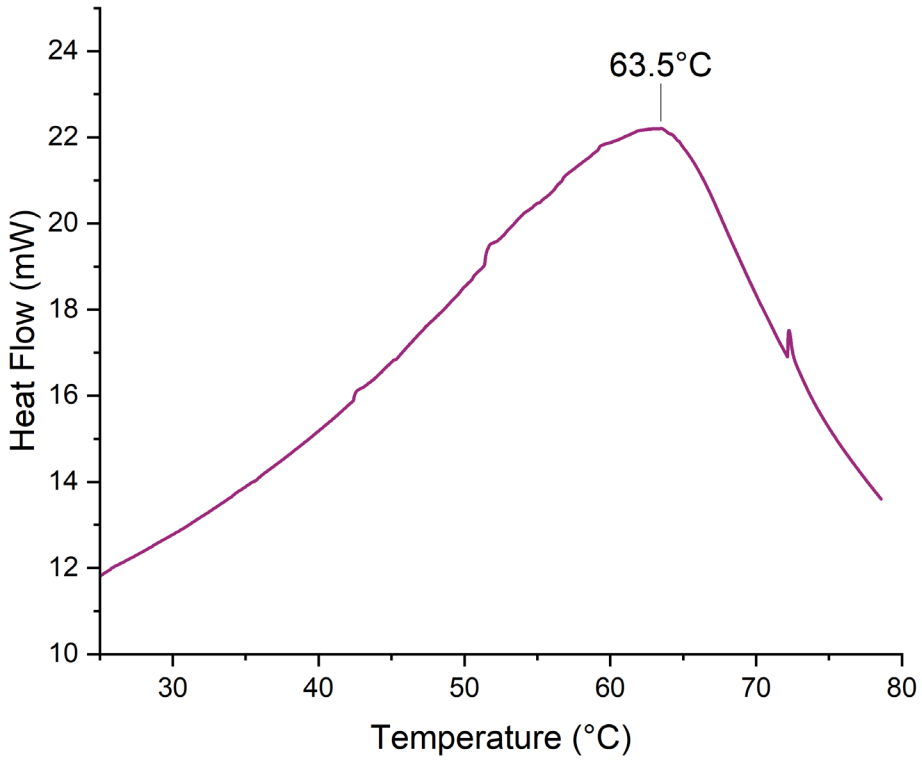

Figure S8: DSC curve for ***G5*** from 25°C to 80°C with VPTT marked.

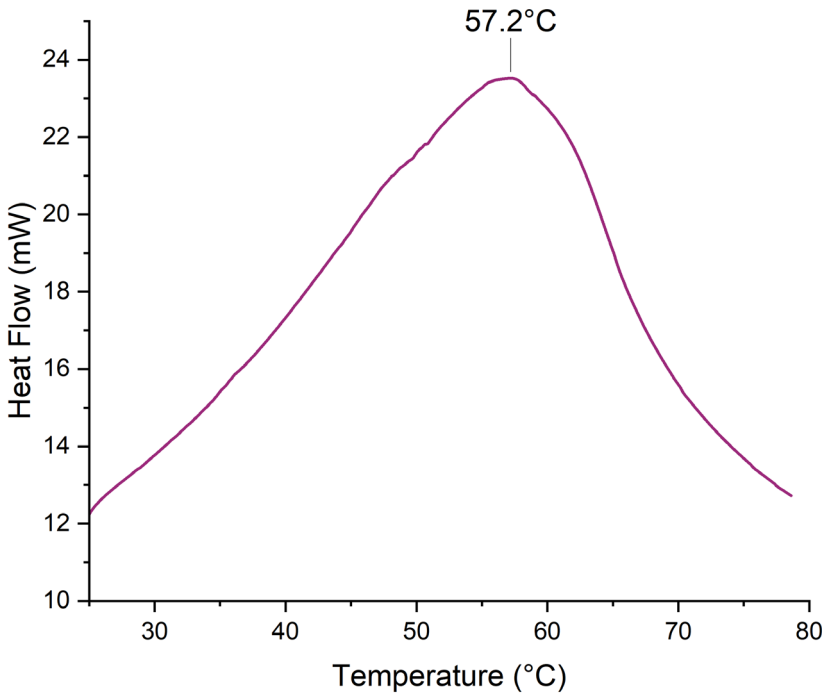

Figure S9: DSC curve for ***G6*** from 25°C to 80°C with VPTT marked.

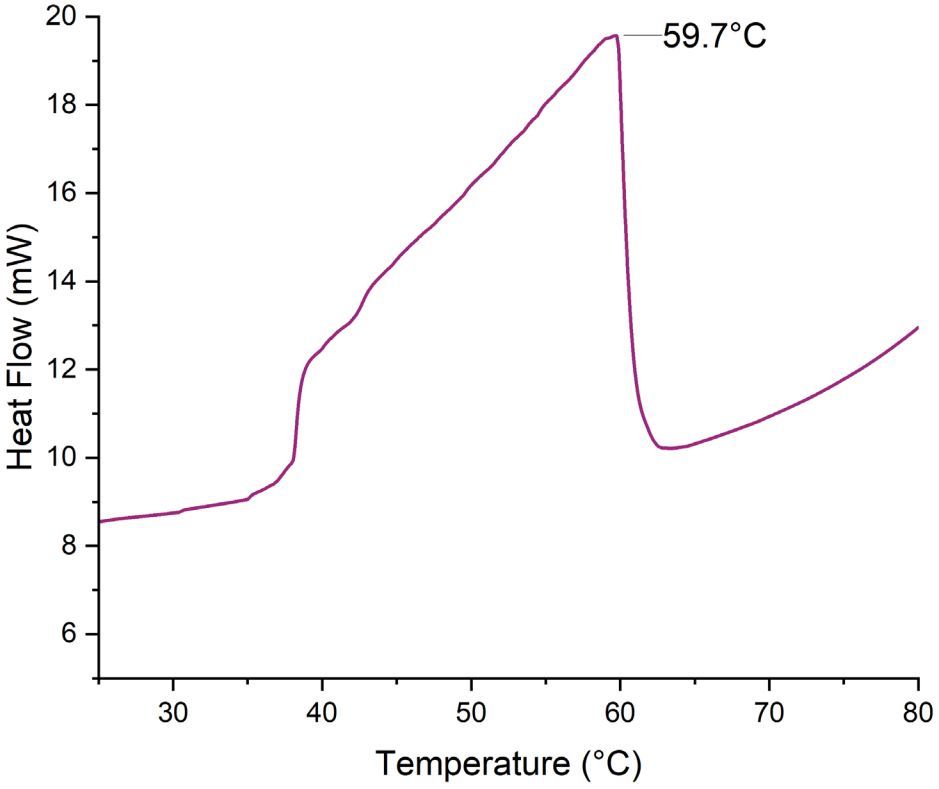

Figure S10: DSC curve for ***G7*** from 25°C to 80°C with VPTT marked.

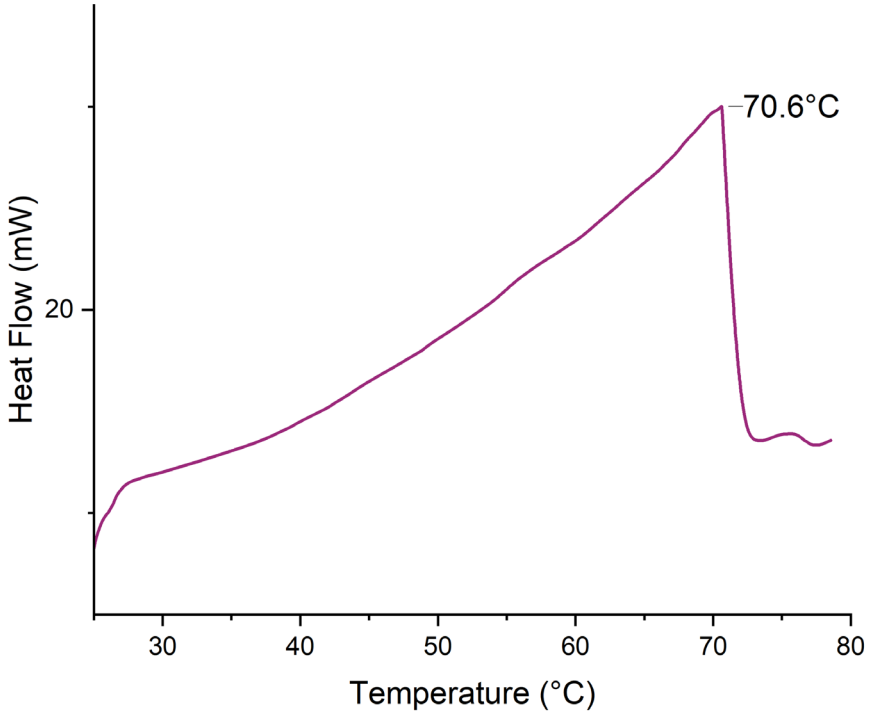

Figure S11: DSC curve for ***G8*** from 25°C to 80°C with VPTT marked.

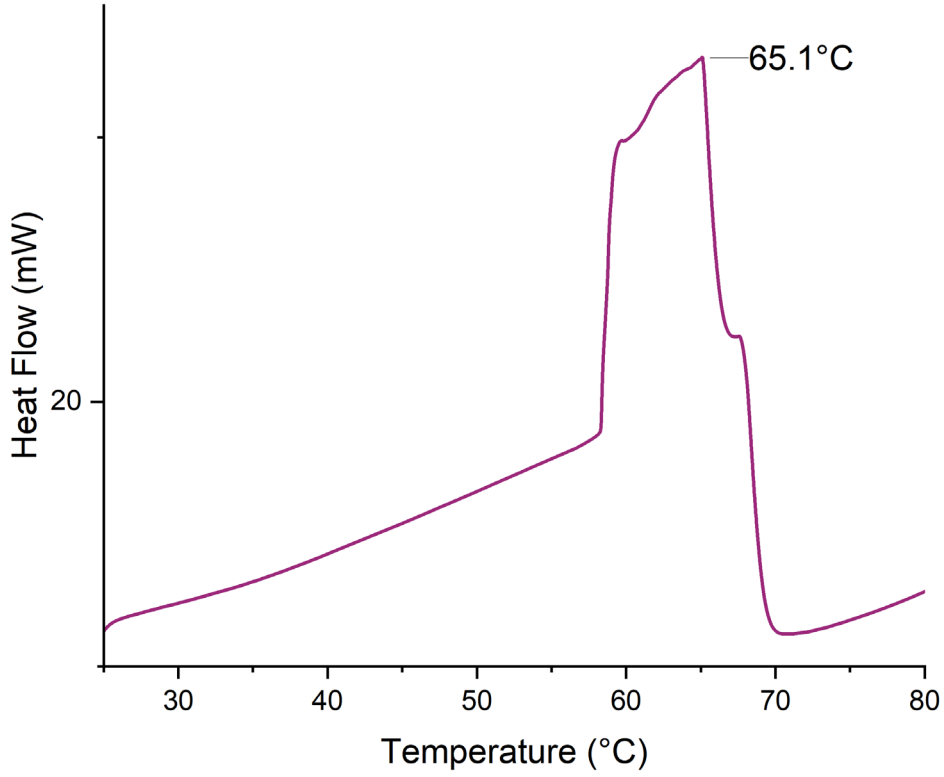

Figure S12: DSC curve for ***G9*** from 25°C to 80°C with VPTT marked.

References

(1) IEA. *Water-Energy Nexus*; Paris, 2016. https://iea.blob.core.windows.net/assets/e4a7e1a5-b6ed-4f36-911f-b0111e49aab9/WorldEnergyOutlook2016ExcerptWaterEnergyNexus.pdf (accessed December 5, 2021).
(2) Oki, T.; Kanae, S. Global Hydrological Cycles and World Water Resources. *Science* **2006**, *313* (5790), 1068-1072. DOI: 10.1126/science.1128845.
(3) Shiklomanov, I. A. World fresh water resources. In *Water in Crisis: A Guide to the World's Fresh Water Resources*, Gleick, P. H. Ed.; Oxford University Press, 1993; pp 13-24.
(4) Gad, H. E.; Hamed, A. M.; El-Sharkawy, I. I. Application of a solar desiccant/collector system for water recovery from atmospheric air. *Renewable Energy* **2001**, *22* (4), 541-556. DOI: https://doi.org/10.1016/S0960-1481(00)00112-9.
(5) Peeters, R.; Vanderschaeghe, H.; Rongé, J.; Martens, J. A. Energy performance and climate dependency of technologies for fresh water production from atmospheric water vapour. *Environ. Sci.: Water Res. Technol.* **2020**, *6* (8), 2016-2034. DOI: 10.1039/D0EW00128G.
(6) Lu, H.; Shi, W.; Guo, Y.; Guan, W.; Lei, C.; Yu, G. Materials Engineering for Atmospheric Water Harvesting: Progress and Perspectives. *Advanced Materials* **2022**, *34* (12), 2110079. DOI: https://doi.org/10.1002/adma.202110079.
(7) Sayılgan, Ş. Ç.; Mobedi, M.; Ülkü, S. Effect of regeneration temperature on adsorption equilibria and mass diffusivity of zeolite 13x-water pair. *Microporous Mesoporous Mater.* **2016**, *224*, 9-16. DOI: https://doi.org/10.1016/j.micromeso.2015.10.041.
(8) Wang, J. Y.; Wang, R. Z.; Wang, L. W.; Liu, J. Y. A high efficient semi-open system for fresh water production from atmosphere. *Energy* **2017**, *138*, 542-551. DOI: https://doi.org/10.1016/j.energy.2017.07.106.
(9) Kim, H.; Yang, S.; Rao, S. R.; Narayanan, S.; Kapustin, E. A.; Furukawa, H.; Umans, A. S.; Yaghi, O. M.; Wang, E. N. Water harvesting from air with metal-organic frameworks powered by natural sunlight. *Science* **2017**, *356* (6336), 430-434. DOI: 10.1126/science.aam8743.
(10) Xu, J.; Li, T.; Chao, J.; Wu, S.; Yan, T.; Li, W.; Cao, B.; Wang, R. Efficient Solar-Driven Water Harvesting from Arid Air with Metal–Organic Frameworks Modified by Hygroscopic Salt. *Angewandte Chemie International Edition* **2020**, *59* (13), 5202-5210. DOI: https://doi.org/10.1002/anie.201915170.
(11) Lyu, T.; Wang, Z.; Liu, R.; Chen, K.; Liu, H.; Tian, Y. Macroporous Hydrogel for High-Performance Atmospheric Water Harvesting. *ACS Applied Materials & Interfaces* **2022**, *14* (28), 32433-32443. DOI: 10.1021/acsami.2c04228.
(12) Lee, S. J.; Ha, N.; Kim, H. Superhydrophilic–Superhydrophobic Water Harvester Inspired by Wetting Property of Cactus Stem. *ACS Sustainable Chem. Eng.* **2019**, *7* (12), 10561-10569. DOI: 10.1021/acssuschemeng.9b01113.
(13) Hanikel, N.; Prévot, M. S.; Fathieh, F.; Kapustin, E. A.; Lyu, H.; Wang, H.; Diercks, N. J.; Glover, T. G.; Yaghi, O. M. Rapid Cycling and Exceptional Yield in a Metal-Organic Framework Water Harvester. *ACS Cent Sci* **2019**, *5* (10), 1699-1706. DOI: 10.1021/acscentsci.9b00745 PubMed.
(14) Wei, M.; Gao, Y.; Li, X.; Serpe, M. J. Stimuli-responsive polymers and their applications. *Polym. Chem.* **2017**, *8* (1), 127-143, 10.1039/C6PY01585A. DOI: 10.1039/C6PY01585A.
(15) Patel, G. C.; Parmar, V. K.; Patel, P. S. 17 - Stimuli-responsive polymers for ocular therapy. In *Stimuli Responsive Polymeric Nanocarriers for Drug Delivery Applications*, Makhlouf, A. S. H., Abu-Thabit, N. Y. Eds.; Woodhead Publishing, 2019; pp 463-489.
(16) Haq, M. A.; Su, Y.; Wang, D. Mechanical properties of PNIPAM based hydrogels: A review. *Mater. Sci. Eng. C* **2017**, *70*, 842-855. DOI: https://doi.org/10.1016/j.msec.2016.09.081.
(17) Guo, Y.; Guan, W.; Lei, C.; Lu, H.; Shi, W.; Yu, G. Scalable super hygroscopic polymer films for sustainable moisture harvesting in arid environments. *Nature Communications* **2022**, *13* (1), 2761. DOI: 10.1038/s41467-022-30505-2.
(18) Matsumoto, K.; Sakikawa, N.; Miyata, T. Thermo-responsive gels that absorb moisture and ooze water. *Nat. Commun.* **2018**, *9* (1), 2315. DOI: 10.1038/s41467-018-04810-8.

(19) Zhao, F.; Zhou, X.; Liu, Y.; Shi, Y.; Dai, Y.; Yu, G. Super Moisture-Absorbent Gels for All-Weather Atmospheric Water Harvesting. *Adv. Mater.* **2019**, *31* (10), 1806446. DOI: https://doi.org/10.1002/adma.201806446.
(20) Jiang, Z.; Diggle, B.; Shackleford, I. C. G.; Connal, L. A. Tough, Self-Healing Hydrogels Capable of Ultrafast Shape Changing. *Adv. Mater.* **2019**, *31* (48), 1904956. DOI: https://doi.org/10.1002/adma.201904956.
(21) Zhang, Z.; Wang, Y.; Li, Z.; Fu, H.; Huang, J.; Xu, Z.; Lai, Y.; Qian, X.; Zhang, S. Sustainable Hierarchical-Pored PAAS–PNIPAAm Hydrogel with Core–Shell Structure Tailored for Highly Efficient Atmospheric Water Harvesting. *ACS Applied Materials & Interfaces* **2022**, *14* (49), 55295-55306. DOI: 10.1021/acsami.2c19840.
(22) Zheng, D.; Xu, X.; Zhu, J.; Bai, B.; Wang, Q.; Shi, W.; Li, J. Humidity capture and solar-driven water collection behaviors of alginate-g-PNIPAm-based hydrogel. *Journal of Environmental Chemical Engineering* **2023**, *11* (1), 109247. DOI: https://doi.org/10.1016/j.jece.2022.109247.
(23) Israelachvili, J. The different faces of poly(ethylene glycol). *Proc Natl Acad Sci U S A* **1997**, *94* (16), 8378-8379. DOI: 10.1073/pnas.94.16.8378 From NLM.
(24) Aleid, S.; Wu, M.; Li, R.; Wang, W.; Zhang, C.; Zhang, L.; Wang, P. Salting-in Effect of Zwitterionic Polymer Hydrogel Facilitates Atmospheric Water Harvesting. *ACS Materials Letters* **2022**, *4* (3), 511-520. DOI: 10.1021/acsmaterialslett.1c00723.
(25) Li, C.; Wang, J.; Deng, C.; Wang, R.; Zhang, H. Protocol for atmospheric water harvesting using in situ polymerization honeycomb hygroscopic polymers. *STAR Protocols* **2022**, *3* (4), 101780. DOI: https://doi.org/10.1016/j.xpro.2022.101780.
(26) Deng, F.; Chen, Z.; Wang, C.; Xiang, C.; Poredoš, P.; Wang, R. Hygroscopic Porous Polymer for Sorption-Based Atmospheric Water Harvesting. *Advanced Science* **2022**, *9* (33), 2204724. DOI: https://doi.org/10.1002/advs.202204724.
(27) Schmeling, N.; Hunger, K.; Engler, G.; Breiten, B.; Rölling, P.; Mixa, A.; Staudt, C.; Kleinermanns, K. Photo-crosslinking of poly[ethene-stat-(methacrylic acid)] functionalised with maleimide side groups. *Polymer International* **2009**, *58* (7), 720-727. DOI: https://doi.org/10.1002/pi.2583.
(28) Drain, B. A.; Becer, C. R. Synthetic approaches on conjugation of poly(2-oxazoline)s with vinyl based polymers. *European Polymer Journal* **2019**, *119*, 344-351. DOI: https://doi.org/10.1016/j.eurpolymj.2019.07.047.
(29) Jones, J. A.; Novo, N.; Flagler, K.; Pagnucco, C. D.; Carew, S.; Cheong, C.; Kong, X. Z.; Burke, N. A. D.; Stöver, H. D. H. Thermoresponsive copolymers of methacrylic acid and poly(ethylene glycol) methyl ether methacrylate. *J. Polym. Sci., Part A: Polym. Chem.* **2005**, *43* (23), 6095-6104. DOI: https://doi.org/10.1002/pola.21099.
(30) Zhang, Y.; Nandakumar, D. K.; Tan, S. C. Digestion of Ambient Humidity for Energy Generation. *Joule* **2020**, *4* (12), 2532-2536. DOI: https://doi.org/10.1016/j.joule.2020.10.003.
(31) Ulasan, M.; Yavuz, E.; Bagriacik, E. U.; Cengeloglu, Y.; Yavuz, M. S. Biocompatible thermoresponsive PEGMA nanoparticles crosslinked with cleavable disulfide-based crosslinker for dual drug release. *J. Biomed. Mater. Res., Part A* **2015**, *103* (1), 243-251. DOI: https://doi.org/10.1002/jbm.a.35146.
(32) Victor, S. P.; Sharma, C. P. Stimuli Sensitive Polymethacrylic Acid Microparticles (PMAA) – Oral Insulin Delivery. *J. Biomater. Appl.* **2002**, *17* (2), 125-134. DOI: 10.1106/088532802028583.
(33) Fei, R.; George, J. T.; Park, J.; Means, A. K.; Grunlan, M. A. Ultra-strong thermoresponsive double network hydrogels. *Soft Matter* **2013**, *9* (10), 2912-2919. DOI: 10.1039/C3SM27226E.
(34) Lutz, J.-F. Polymerization of oligo(ethylene glycol) (meth)acrylates: Toward new generations of smart biocompatible materials. *Journal of Polymer Science Part A: Polymer Chemistry* **2008**, *46* (11), 3459-3470. DOI: https://doi.org/10.1002/pola.22706.
(35) Han, S.; Hagiwara, M.; Ishizone, T. Synthesis of Thermally Sensitive Water-Soluble Polymethacrylates by Living Anionic Polymerizations of Oligo(ethylene glycol) Methyl Ether Methacrylates. *Macromolecules* **2003**, *36* (22), 8312-8319. DOI: 10.1021/ma0347971.
(36) Zhao, B.; Li, D.; Hua, F.; Green, D. R. Synthesis of Thermosensitive Water-Soluble Polystyrenics with Pendant Methoxyoligo(ethylene glycol) Groups by Nitroxide-Mediated Radical Polymerization. *Macromolecules* **2005**, *38* (23), 9509-9517. DOI: 10.1021/ma0514572.

(37) Lutz, J.-F.; Hoth, A. Preparation of ideal PEG analogues with a tunable thermosensitivity by controlled radical copolymerization of 2-(2-methoxyethoxy) ethyl methacrylate and oligo (ethylene glycol) methacrylate. *Macromolecules* **2006**, *39* (2), 893-896.
(38) Jonas, A. M.; Glinel, K.; Oren, R.; Nysten, B.; Huck, W. T. S. Thermo-Responsive Polymer Brushes with Tunable Collapse Temperatures in the Physiological Range. *Macromolecules* **2007**, *40* (13), 4403-4405. DOI: 10.1021/ma070897l.
(39) Ward, M. A.; Georgiou, T. K. Thermoresponsive Polymers for Biomedical Applications. *Polymers* **2011**, *3* (3), 1215-1242.
(40) Trongsatitkul, T.; Budhlall, B. M. Temperature dependence of serum protein adsorption in PEGylated PNIPAm microgels. *Colloids and Surfaces B: Biointerfaces* **2013**, *103*, 244-252. DOI: https://doi.org/10.1016/j.colsurfb.2012.10.053.
(41) Li, Z.; Kim, Y.-H.; Min, H. S.; Han, C.-K.; Huh, K. M. Molecular weight and end group effects on the thermo-responsive property of oligomeric N-isopropylacrylamide. *Macromolecular Research* **2010**, *18* (6), 618-621. DOI: 10.1007/s13233-010-0609-7.
(42) Furyk, S.; Zhang, Y.; Ortiz-Acosta, D.; Cremer, P. S.; Bergbreiter, D. E. Effects of end group polarity and molecular weight on the lower critical solution temperature of poly(N-isopropylacrylamide). *Journal of Polymer Science Part A: Polymer Chemistry* **2006**, *44* (4), 1492-1501. DOI: https://doi.org/10.1002/pola.21256.
(43) Zhang, Y.; Furyk, S.; Bergbreiter, D. E.; Cremer, P. S. Specific Ion Effects on the Water Solubility of Macromolecules: PNIPAM and the Hofmeister Series. *Journal of the American Chemical Society* **2005**, *127* (41), 14505-14510. DOI: 10.1021/ja0546424.
(44) Patterson, D. Free Volume and Polymer Solubility. A Qualitative View. *Macromolecules* **1969**, *2* (6), 672-677. DOI: 10.1021/ma60012a021.
(45) Lessard, D. G.; Ousalem, M.; Zhu, X. X. Effect of the molecular weight on the lower critical solution temperature of poly(N,N-diethylacrylamide) in aqueous solutions. *Canadian Journal of Chemistry* **2001**, *79* (12), 1870-1874. DOI: 10.1139/v01-180 (acccessed 2023/06/12).
(46) Ieong, N. S.; Hasan, M.; Phillips, D. J.; Saaka, Y.; O'Reilly, R. K.; Gibson, M. I. Polymers with molecular weight dependent LCSTs are essential for cooperative behaviour. *Polymer Chemistry* **2012**, *3* (3), 794-799. DOI: 10.1039/C2PY00604A.
(47) Drozdov, A. D.; Christiansen, J. d. Modulation of the volume phase transition temperature of thermo-responsive gels. *Journal of the Mechanical Behavior of Biomedical Materials* **2021**, *114*, 104215. DOI: https://doi.org/10.1016/j.jmbbm.2020.104215.

Chapter Three

Arginine-functionalised hydrogels as a novel atmospheric water-harvesting material

Moki K. Thanusing, Brett L. Pollard, Luke A. Connal

RSC Appl. Polym., 2025, **3**, 480-487

Australian National University

Statement of Contribution

This thesis is submitted as a Thesis by Compilation in accordance with https://policies.anu.edu.au/ppl/document/ANUP_003405

I declare that the research presented in this Thesis represents original work that I carried out during my candidature at the Australian National University, except for contributions to multi-author papers incorporated in the Thesis where my contributions are specified in this Statement of Contribution.

Title: Arginine-functionalised hydrogels as a novel atmospheric water-harvesting material

Authors: Moki K. Thanusing, Brett L. Pollard, Luke A. Connal

Current status of paper: Published

Publication Outlet: RSC Applied Polymers, **2025**, *3*, 480-487

Contribution to paper: This is a full paper and the candidate conducted all of the experimental work reported within. In addition, all spectral data presented in the Supporting Information document was collected and formatted by the candidate. The candidate also wrote the entirety of the manuscript and experimental section and conducted relevant literature surveys. A preliminary outline was generated and revised by the candidate.

Senior author or collaborating authors endorsement: 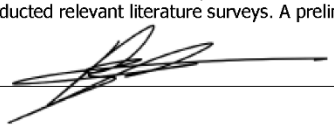

Moki Thanusing		25/08/25
Candidate – Print Name	Signature	Date

Endorsed

Luke Connal		26/08/25
Chair of Supervisory Panel – Print Name	Signature	Date
Mark Humphrey		28/8/25
Delegated Authority – Print Name	Signature	Date

Foreword

This chapter details the development of a thermoresponsive SAWH hydrogel using the previously established rational design framework. *L*-arginine was identified as a hygroscopic molecule yet to be used for SAWH. Post-functionalisation of a SAWH hydrogel with *L*-arginine greatly increased water uptake while preserving thermoresponsive properties. Additionally, improved water uptake kinetics showed potential for faster harvesting and therefore increased potential yield.

This chapter was published in the March 2025 edition of RSC Applied Polymers, where I am its first author. My contribution to the manuscript includes designing and conducting experiments, characterisation of resulting materials, data analysis as well as preparing and revising the manuscript and figures (overall 75%). The published version of the manuscript is presented here. Brett L. Pollard contributed to experimental design, and edited and revised the manuscript. Luke A. Connal contributed to experimental design, supervised the project, and edited and revised the manuscript and figures.

Introduction

Polymer desiccants are an interesting and diverse class of atmospheric water harvesting (AWH) materials. Atmospheric water is found in all climates, notably arid climates with few other accessible water sources, making it a promising avenue for alleviating water scarcity. The large scope of functionalities and synthetic methods available allows for the fine-tuning of desired properties. The rate of water uptake is generally the bottleneck of the water-harvesting process, however, and as a result many existing polymeric materials use hygroscopic additives to enhance uptake.[1-5] Lithium chloride is the most commonly used in current literature given its high water-uptake ability.[6] Such materials harvest water at low humidities and can be renewed at low temperatures (and low energy inputs), visibly improving upon current AWH technologies. However, there are clear drawbacks, especially when considering future commercial and industrial use. There is a growing industrial demand for LiCl, most notably for the production of lithium-ion batteries.[7] Another more general drawback for additives in water-harvesting systems is leaching over time, effectively decreasing the material efficiency. Scaling up the production of a LiCl-dependent water-harvesting material is therefore impractical.

Identifying hygroscopic functionalities which can be covalently bonded to the polymer backbone therefore represents an attractive target. Although the relationship between chemical structure and hygroscopicity (or water sorption) is complex and not precisely understood, charge is a rough indicator for hygroscopic behaviour and can help direct the identification of promising AWH material candidates.[8-12] This was well demonstrated with the poly([2-(acryloyloxy)ethyl]trimethylammonium acetate) (PAETA-Ac) system of Wu *et al.*, where the polymer network's intrinsic charge was used for water harvesting to capture ~0.53 g g^{-1}/day.[13] Natural polymers have also been used for AWH, like in the Park *et al.* alginate/acrylamide/carbon nanotube composite system which gave a daily yield of 1.81 g g^{-1}/day.[14] However, this material used $CaCl_2$ as a hygroscopic additive, meaning leaching (however minimal) would result in reduced performance over time. Even though polymeric AWH materials have only been studied in earnest within the last two decades, there are already a wide variety of approaches published to literature, including using MOFs, COFs, and more bioinspired systems.[15-17] The ubiquity of atmospheric water compared to other water sources allows for AWH to fill environmental niches not available to other water harvesting methods. Given its relative novelty, we feel drawn to AWH focusing on expanding

the breadth of chemical structures and functionalities, synthetic methods, and harvesting environments rather than the optimisation of known systems.

One well-known hygroscopic moiety that has not yet been utilised for AWH materials is the guanidinium moiety, sustainably (and affordably) available in the form of arginine. Arginine, being an amino acid, also offers convenient routes for functionalisation that do not interfere with the guanidinium side chain. In this work, we report our efforts to design, prepare and characterise an additive-free water-harvesting polymer system using hygroscopic guanidinium moieties attached by esterification of *L*-arginine.

Results and Discussion

We designed a synthetic pathway to understand polymer structure-property relationships by copolymer functionality, specifically with guanidinium (via arginine) in this study. To form a parent polymer for functionalisation with arginine groups, we first prepared poly(2-hydroxyethyl methacrylate-*co*-poly(ethylene glycol) methyl ether methacrylate) (poly(HEMA-*co*-PEGMA)) (***P1***, **Scheme S1**). This was done using reverse addition fragmentation transfer (RAFT) polymerisation to control dispersity. HEMA is thermoresponsive, hydrophilic, and can be readily modified through the side chain alcohol. The poly(HEMA) homopolymer is, however, brittle and insoluble in common solvents, rendering further processing impractical. The addition of PEGMA allows for a more soluble and flexible material, as well as maintaining thermoresponsivity. The final molar composition of the polymer, as calculated by ^{1}H nuclear magnetic resonance (^{1}H NMR) spectroscopy, was found to be 81:19 HEMA:PEGMA with a theoretical molecular weight of around 21 kDa. Gel permeation chromatography (GPC) data obtained indicated a M_n of 58 kDa and a dispersity around 6. Polymeric inter- and intramolecular hydrogen-bonding interactions can inflate dispersity measurements; this is indicated by FTIR data and a broad, multimodal GPC trace (**Figures S5, S14**).[18] Dispersity is significant when considering size-dependent properties such as thermal phase transitions; a narrow molecular weight distribution allows for a faster phase transition over a smaller temperature range.[19] However, the effects of molecular weight (and dispersity) on other water harvesting properties is unclear, and so in the context of this study we performed measurements using a singular batch of bulk sample so as to retain molecular weight as a controlled variable.

Steglich esterification was then conducted to attach N-terminus and side group protected-arginine to the HEMA sidechain (***P2***, **Scheme 1**). The amine was protected with fluorenylmethoxycarbonyl (Fmoc) and 2,2,4,6,7-pentamethyldihydrobenzofuran-5-sulfonyl (Pbf) protected the guanidine group. *N*-(3-dimethylaminopropyl)-*N*′-ethylcarbodiimide hydrochloride (EDC) was selected as the byproduct 1-(3-(dimethylamino)propyl)-3-ethylurea (EDU) is soluble in water and enables facile purification. Functionalisation was confirmed via ^{1}H NMR analysis which indicated that ca. 50% of HEMA groups had been converted. The overall composition of the functionalised polymer ***P2*** was hence determined to be poly((Fmoc-Arg(Pbf))MA$_{40}$-*co*-HEMA$_{40}$-*co*-PEGMA$_{20}$). The mild conditions of Steglich esterification were expected to minimise the undesired deprotection of Fmoc during the reaction, though we still observed some cleavage by ^{1}H NMR analysis. A change in the material colour also indicated that the RAFT chain transfer agent end groups were removed during the esterification. ***P2*** was also insoluble in water, likely due to the presence of the bulky protecting groups.

The orthogonality of the deprotection chemistry enables us to reveal the polar groups sequentially. Initially, we removed Fmoc to liberate the primary amine. Some Fmoc had already been removed during the esterification and so the complete removal of Fmoc was conducted (***P3***, **Scheme 1**). We next removed the Pbf group to liberate the guanidine group (***P4***, **Scheme 1**). Characterisation using ^{1}H NMR spectroscopy confirmed the successful removal of the protecting groups. As expected, the polymer composition stayed consistent to that calculated from ***P2***, indicating that the deprotection conditions did not cause any unwanted side reactions or degradation.

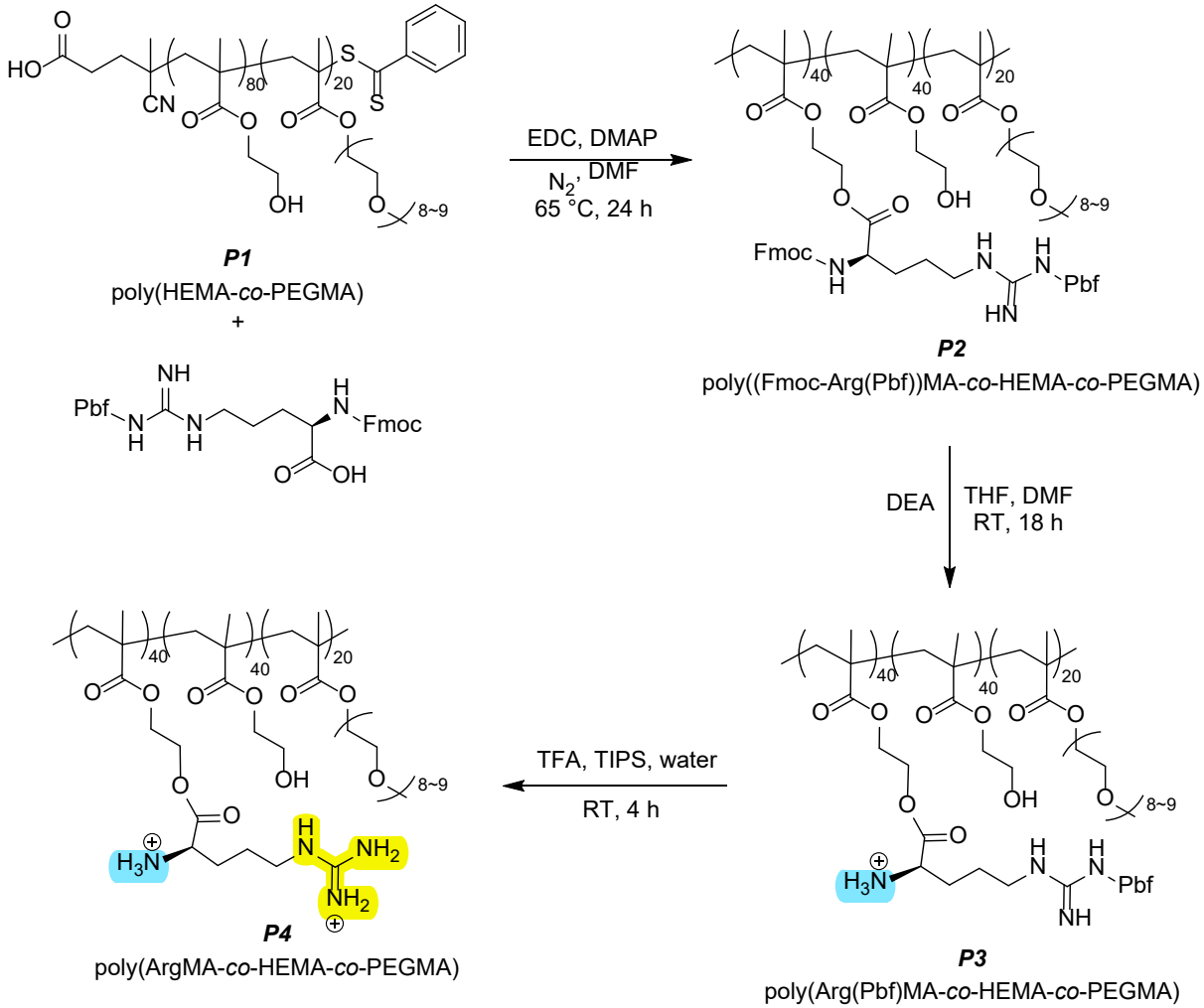

Scheme 1: Scheme depicting functionalisation of ***P1*** via Steglich esterification (top) and sequential deprotection of side chain Fmoc-Arg(Pbf) (right and bottom). Highlighted are side-chain arginine primary amine (blue) and guanidine (yellow) exposed after deprotection.

With our controlled deprotection we had 4 polymers with varying polarity and functional groups: the parent polymer (***P1***), with HEMA and PEGMA; ***P2***, with fully protected arginine; ***P3*** with free primary amine and protected guanidine; and ***P4*** with free amine and guanidine. We next set about measuring the water uptake for products ***P1***–***P4*** over a period of 24 hours (**Figure 1a**). The fully deprotected arginine-functionalised polymer (***P4***) had increased water uptake at 24 hours from 92 mg/g to 134 mg/g water to polymer; a 46% increase compared to the base polymer ***P1***. Considering that approximately 50% of HEMA groups were functionalised (i.e. 40% of the polymer by molar ratio), this shows arginine has around twice the water uptake capacity as HEMA. In terms of sequential deprotection, there was a 150% increase in water uptake after 24 hours from ***P2*** to ***P3***, then a 77% increase from ***P3*** to ***P4***. While the guanidine group is known to be hygroscopic and was expected to be the main contributor to increasing water uptake, the first deprotection of Fmoc (exposing the primary

amine) appeared more impactful by percentage increase in uptake. However, the sequential improvements in water uptake are contributed to by both the removal of bulky protecting groups and the exposure of hydrophilic/hygroscopic functional groups on the arginine side chain.

When comparing ***P1*** and ***P4***, the arginine side chain greatly increased the initial rate of uptake compared to HEMA (**Figure 1b**). The rapid water uptake within the first 3 hours for ***P4*** highlights the possibility of applications tailored toward more rapid cycling. ***P2*** and ***P3*** showed similar changes of rate to ***P4***, however this is more likely due to bulky protecting groups hindering water uptake. The bulky and hydrophobic protecting groups reduce the adsorption capacity of the polymer. Interestingly, functionalised samples ***P2***–***P4*** showed a sudden decrease in the rate of water uptake at around 120–180 minutes, contrasted with a more gradual attenuation for ***P1***. Rapid surface adsorption of water vapour followed by a relatively slow diffusion of water into the polymer network are the main mechanisms of water uptake in these materials.[20, 21] The decrease in water uptake rate likely indicates saturation of surface hygroscopic groups, with further water uptake depending on the rate of diffusion. The relative rates of diffusion are unclear from the data, though over short time periods this would be less relevant.

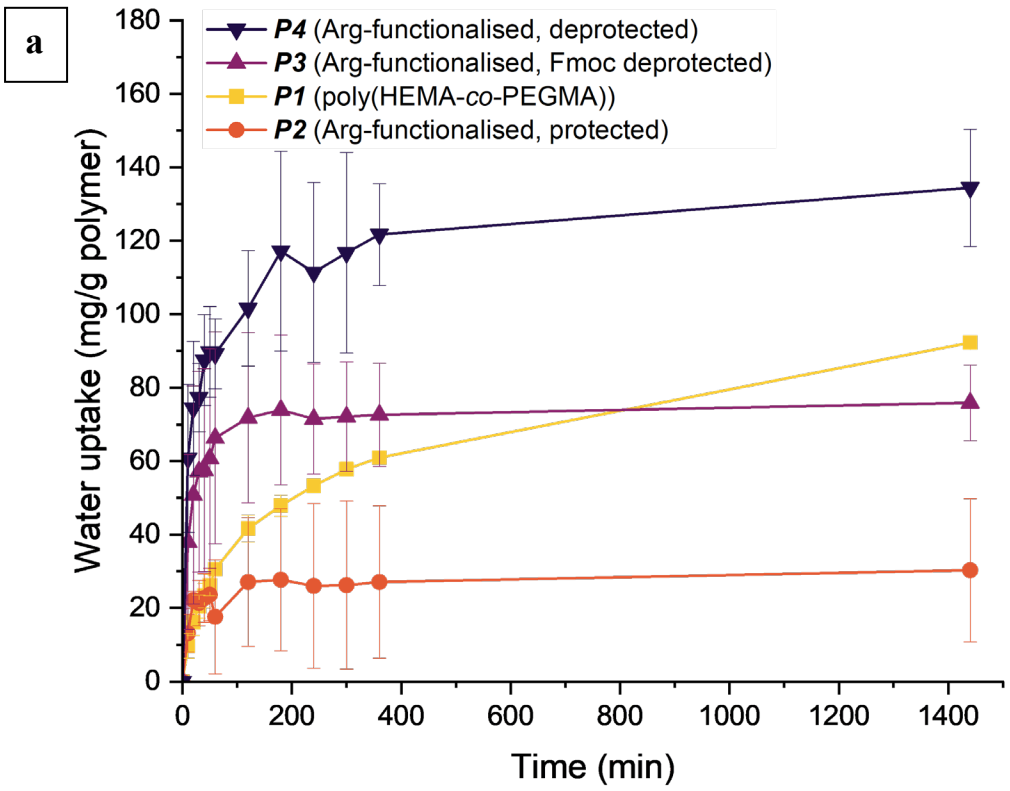

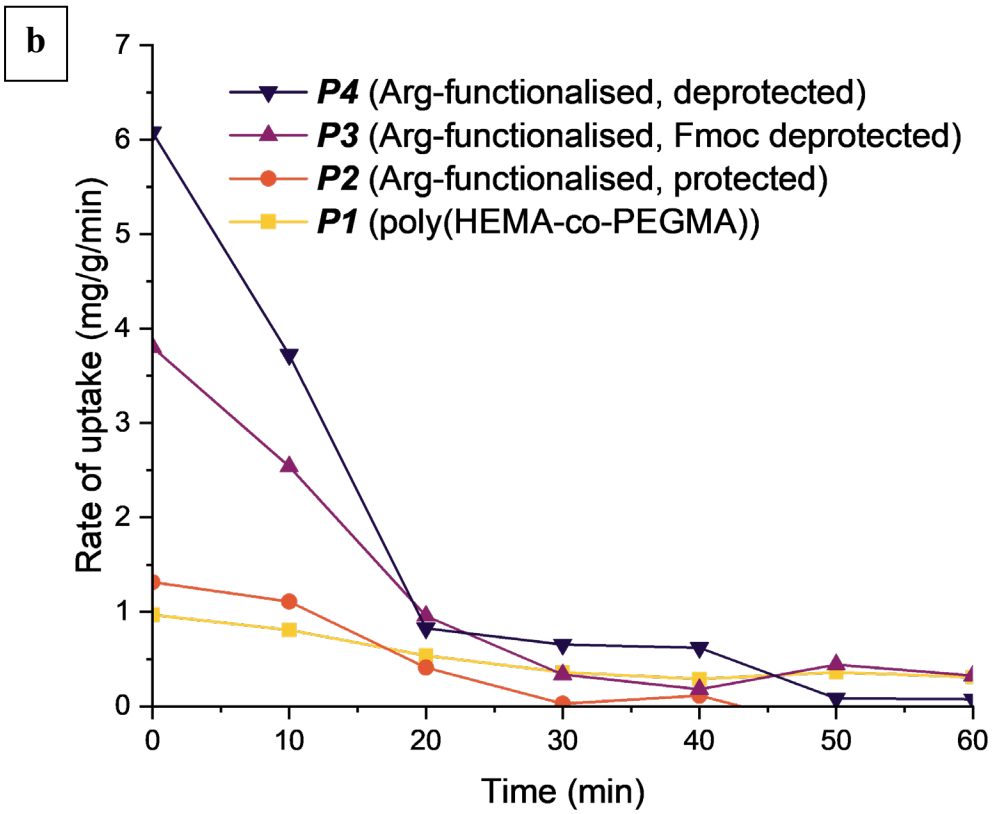

Figure 1: (a) Water uptake over 24 hours, showing the effects of arginine functionalisation and sequential deprotection. (b) First derivative of water uptake over 1 hour, highlighting the different rates of change in water uptake with functionalisation and sequential deprotection.

While the linear, soluble polymer is useful for characterisation, it would be solubilised in water-harvesting applications and hence contaminate the harvested water. Crosslinking eliminates any polymer solubility in water, alleviating these concerns. A hydrogel system based on the arginine-functionalised polymers above is shown in **Figure 2**. This was synthesised with a 75:5:20 molar feed ratio of HEMA, poly(ethylene glycol) dimethacrylate (PEGDMA) 750 crosslinker and PEGMA (**Scheme S2**). PEGDMA 750 was selected because of its similarity in structure to PEGMA and its positive contributions to water uptake observed in our past work.[22] Functionalisation and deprotection were conducted using the same methods employed for the linear polymer to afford base gel ***G1*** and arginine-functionalised gel ***G2*** (**Scheme S2**). Given the insolubility of hydrogel products, characterisation of the resulting gel products was performed using FTIR spectroscopy. Disappearance of the free HEMA alcohol O-H stretch at 3670 cm^{-1}, the splitting of the alkane C-H stretch at around 2900 cm^{-1}, as well as the appearance of amine peaks between 3100 cm^{-1} and 3350 cm^{-1}, indicated that functionalisation was successful (**Figures S9**, **S10**). After lyophilisation, ***G2*** takes on a powdery appearance, and although the porosity is minimal (as

shown by SEM imaging, **Figure 2c**), the polymer was still found to have a large surface area. While the powdery, crumbly nature of ***G2*** was not amenable to mechanical testing, its high surface area rendered it particularly suitable for water-harvesting applications.

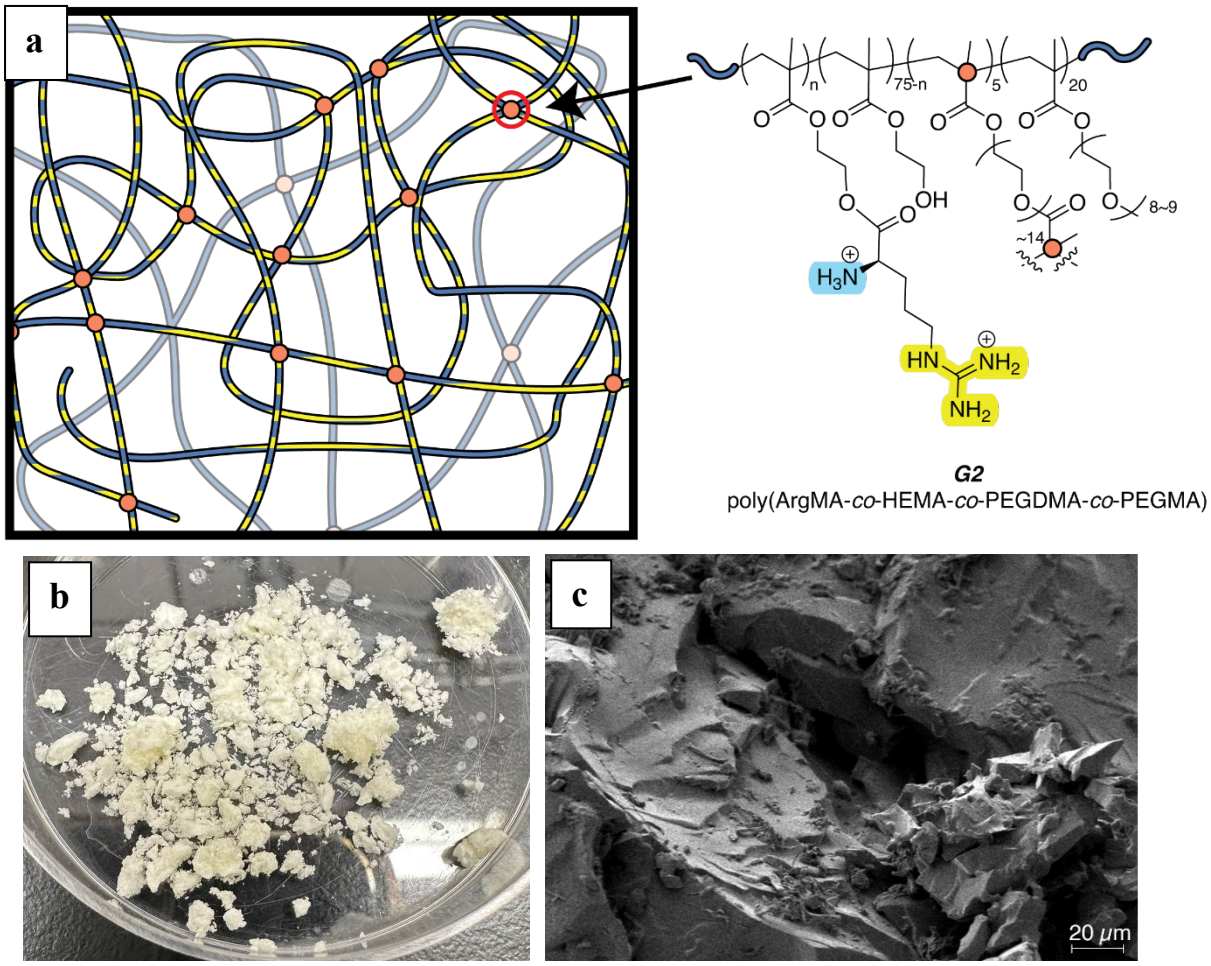

Figure 2: (a) Graphical representation and chemical structure of the functionalised hydrogel ***G2***, showing its single-network structure, PEGDMA 750 crosslinking, and interspersion of the arginine-functionalised sidechain. (b) Photo of ***G2*** after lyophilisation. (c) SEM image of ***G2*** (scale bar 20 µm).

Because the fully deprotected polymer was the lead candidate in terms of water uptake, we went straight to investigating the fully deprotected gel ***G2***. The gel, like its linear counterparts, showed rapid water uptake which plateaued after 2 hours. After 24 hours, ***G2*** absorbed a total of 149 mg/g water compared to ***P4***'s 134 mg/g, showing that, as in our previous study, the addition of PEGDMA crosslinker did not negatively affect water uptake (**Figure 3**).[22]

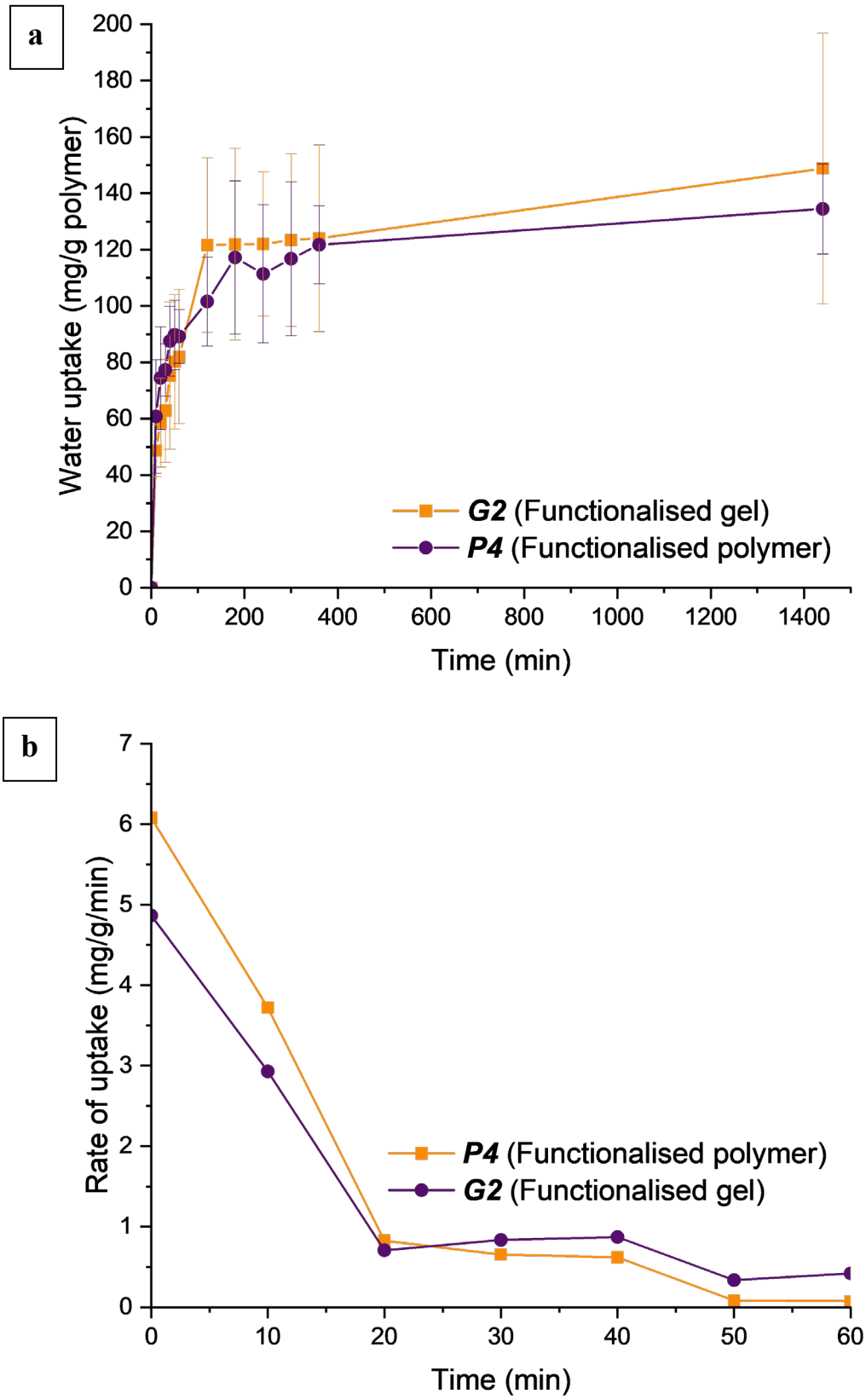

Figure 3: (a) Water uptake over 24 hours of ***G2*** and ***P4***, showing that crosslinking with PEGDMA 750 had no negative effects on water uptake. (b) First derivative of water uptake over 1 hour of ***G2*** and ***P4***, showing the minimal impact of crosslinking.

We next turned our attention to water release. Thermoresponsive polymers allow for the energy-efficient harvesting of water at low temperatures. HEMA and PEGMA homopolymers are both thermoresponsive, as well as the copolymer ***P1***, with a cloud point close to 56 °C at a concentration of 10 mg/mL in water, and a 69.5°C lower critical solution temperature (LCST) after swelling.[23-25] Differential scanning calorimetry (DSC) was used to determine phase transition temperatures to account for varying solubility of products and allow for direct comparison. We determined ***P4*** to have a LCST of 81.9°C, meaning that the incorporation of arginine greatly increases the temperature required for water release. Arginine is cationic at neutral pH, hindering the thermal transition change and increasing the LCST.[23] In contrast to its linear counterpart, ***G2*** has a volume phase transition temperature (VPTT) of 62.2°C, which is more amenable to the desired application of water harvesting. While we were satisfied with our measured VPTT, it is well known that this property is dependent on the specific hydrophilic/hydrophobic balance of a system and so could be further tuned by adjusting the polymer composition and the degree of arginine functionalisation.[26, 27]

A cycling experiment was then conducted on ***G2*** to evaluate the combined uptake and release abilities over time (**Figure 4**). ***G2*** lends itself to short cycle times as the initial rapid adsorption slows at around 120 minutes. After calculating total output based on uptake and cycle times, we decided that a 60-minute uptake and 10-minute release cycle would be most optimal. Gratifyingly, after conducting 25 cycles we observed no loss of uptake or release capacity. The scale of these experiments was in the sub-gram range, hence some water loss would be attributed to evaporation. However, the ability to renew the material quickly at low temperatures nonetheless is promising for future water harvesting applications.

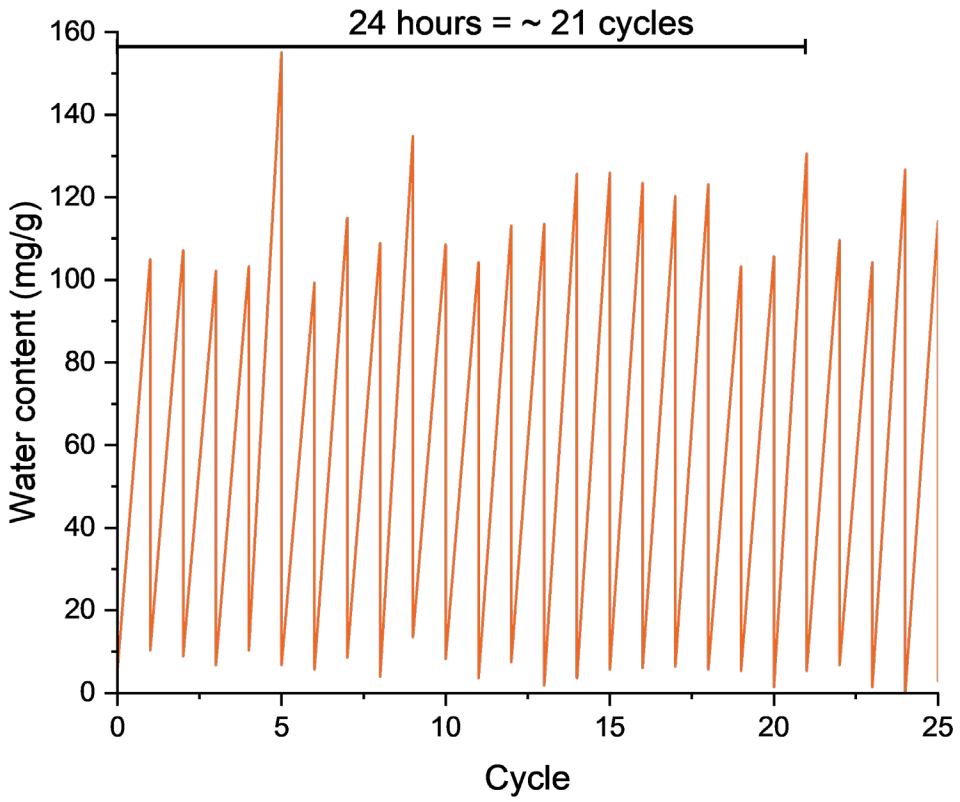

Figure 4: Water harvesting cycling data of ***G2***, showing minimal/no decay of performance. Uptake cycles were conducted at 70% RH at around 25°C for 1 hour, while release cycles were conducted in a 70°C oven for 10 minutes.

Conclusions

In summary, we have demonstrated the water-harvesting potential of *L*-arginine-functionalised polymers and a novel use of the hygroscopic guanidine moiety. Notably, arginine-functionalised polymers exhibited around 140 mg/g of uptake after 24 hours at 70% RH without any additives. We demonstrated that the primary amine group has positive effects on water harvesting but an even greater effect when combined with the guanidine group. Rapid cycling behaviour has also been demonstrated, with 70-minute cycles potentially yielding 2 g/g of water after 24 hours. Water uptake and release properties were retained over an extended period of time. Side-chain functionalisation was also demonstrated to affect physical properties such as thermal phase transitions, allowing another avenue for the material tunability required for specialised applications. Additional studies on this work would include changes in copolymerisation ratios and arginine conversion, as well as

investigations into more efficient post-functionalisation methods. These outcomes highlight the expansive potential for new hygroscopic moieties and underutilised synthetic methods in the water-harvesting material space, in particular, the further study of arginine and other guanidinium-containing molecules.

Experimental Section

Fmoc-Arg(Pbf)-OH was purchased from GL Biochem. All other chemicals were purchased from Sigma-Aldrich and were used as purchased with the following exceptions: poly(ethylene glycol) methyl ether methacrylate (PEGMA, average Mn 500, containing 200 ppm butylated hydroxytoluene (BHT), 100 ppm 4-methoxyhenol (MEHQ) as inhibitor), 2-hydroxyethyl methacrylate (HEMA, containing ≤50 ppm MEHQ as inhibitor), and poly(ethylene glycol) dimethacrylate (PEGDMA average Mn 750, containing 80–120 ppm MEHQ as inhibitor, 270–330 ppm BHT as inhibitor). For these, basic-alumina chromatography was conducted to remove inhibitors immediately prior to polymerisation.

Gel permeation chromatography (GPC) was performed with an Agilent 1260 Infinity II, using *N,N*-dimethylacetamide (DMAc) as solvent with a 1.00 mL/min flow rate and a column temperature of 30°C. Molecular weights were calibrated against polyethylene oxide/glycol EasiVirals® (Agilent Technologies, U.K.) standards that covered an average molecular mass range from 1,576,000 to 106 g/mol. ^{1}H NMR spectra were obtained at 298 K on a Bruker Ascend 400 at 400 MHz using DMSO-d_6 as solvent. FTIR spectroscopy was conducted on a Perkin Elmer Spectrum 2 using lyophilised samples. Humidity was measured inside a custom set-up as shown in **Figure S15**.[22] Humidity and ambient temperature were measured using a RS Pro RS-1260 humidity temperature meter. DSC experiments were conducted using a Perkin-Elmer DSC8500 apparatus.

Synthesis of poly(HEMA-*co*-PEGMA) copolymer

CTP chain transfer agent (4-cyano-4-(phenyl-carbonothioylthio)pentanoic acid) (27.9 mg, 0.10 mmol), HEMA (2.08 g, 16.00 mmol), PEGMA 500 (2.00 g, 4.00 mmol), 2,2′-azobis(2-methylpropionitrile) initiator (AIBN) (1.64 mg, 0.010 mmol) and 5 mL of anhydrous *N,N*-dimethylformamide (DMF) were charged into a 25 mL round bottom flask. Once dissolved, the solution was sealed with a rubber septum, magnetically stirred and maintained at 0°C while being degassed with nitrogen for 20 minutes. The flask was then magnetically stirred at 65°C in an oil bath for 24 hours. The resultant mixture was then precipitated into vigorously

stirred cold diethyl ether (80 mL) to afford a pink, solid mass. Further purification was conducted by dialysis in water over 3 days. The polymer product was lyophilised for 24 hours to afford a flexible pink film ***P1*** (poly(HEMA$_{80}$-*co*-PEGMA$_{20}$), 84%).

^{1}H NMR (poly(HEMA$_{80}$-*co*-PEGMA$_{20}$) (*P1*), 400 MHz, DMSO-d$_6$) δ 4.79 (s, 202*1H), 4.01 (s, 47*2H, signal overlapping), 3.90 (s, 202*2H, signal overlapping), 3.58-3.51 (s, 47*38H, signal overlapping), 3.44, 3.43, 3.42 (s, 202*2H), 3.24 (s, 47*3H), 2.53 (s, 47*2H), 1.78 (b, 202*2H, signal overlapping), 1.46 (b, 47*2H, signal overlapping), 0.94 (s, 47*3H, signal overlapping), 0.78 (202*3H, signal overlapping).

Synthesis of poly(HEMA-*co*-PEGDMA-*co*-PEGMA) hydrogel

CTP chain transfer agent (27.9 mg, 0.10 mmol), HEMA (1.95 g, 15.00 mmol), PEGMA 500 (2.00 g, 20.00 mmol), PEGDMA 750 (0.750 g, 1.00 mmol), AIBN initiator (1.64 mg, 0.010 mmol) and 6 mL of anhydrous DMF were charged into a 25 mL round bottom flask. The resulting solution was seal with a rubber septum and magnetically stirred at 0°C while being degassed with nitrogen for 20 minutes, with stirring. The flask was then magnetically stirred at 65°C in an oil bath for 24 hours, resulting in a solid pink gel. This product was broken into small chunks with a spatula. Excess monomer and other impurities were removed by soaking in water over 3 days. The polymer product was lyophilised for 24 hours to afford a soft pink solid ***G1*** (poly(HEMA$_{75}$-*co*-PEGDMA$_5$-*co*-PEGMA$_{20}$)).

Arginine functionalisation procedure

Steglich esterification was conducted with poly(HEMA-*co*-PEGMA) polymer (***P1***) or poly(HEMA-*co*-PEGDMA-*co*-PEGMA) gel (***G1***), Fmoc-Arg(Pbf)-OH, *N*-(3-dimethylaminopropyl)-*N*′-ethylcarbodiimide hydrochloride (EDC) and 4-dimethylaminopyridine (DMAP) catalyst in anhydrous DMF. The magnetically stirred solution was allowed to react at room temperature for 18 hours before the reaction vessel was exposed to air. Products ***P2*** and ***G1**** were afforded from this procedure.

A detailed procedure for poly(Fmoc-Arg(Pbf)MA-*co*-HEMA-*co*-PEGMA) (***P2***) is as follows: ***P1*** (303 mg, 43 wt% HEMA, 1.00 mmol HEMA), Fmoc-Arg(Pbf)-OH (649 mg, 1.00 mmol), EDC initiator (186 mg, 1.20 mmol), DMAP catalyst (36.7 mg, 0.30 mmol) and 7 mL of anhydrous DMF were charged into a 25 mL round bottom flask. The flask was sealed and magnetically stirred at room temperature overnight, with the solution going from clear, bright yellow to colourless. The resultant mixture was then precipitated into vigorously stirred cold water (80 mL) to afford an off-white precipitate. The precipitate was lyophilised for 24 h to

afford a beige powder ***P2*** (473 mg, approx. 50% HEMA conversion as determined by ^{1}H NMR).

^{1}H NMR (poly(Fmoc-Arg(Pbf)MA$_{40}$-*co*-HEMA$_{40}$-*co*-PEGMA$_{20}$) (*P2*), 400 MHz, DMSO-d$_6$) δ 7.89 (dt), 7.72 (d), 7.62 (dd), 7.43 (dtd), 4.75 (b), 4.29-4.19 (m, signal overlapping), 4.00 (s), 3.89 (s), 3.47 (s, signal overlapping), 3.21 (s, signal overlapping), 3.02-2.90 (m, signal overlapping), 2.48 (s, signal overlapping), 2.42 (s), 2.00, 1.99, 1.97 (t + s, signal overlapping), 1.65 (s, signal overlapping), 1.56 (s, signal overlapping), 1.45 (s, signal overlapping), 1.41, 1.39, 1.35 (t + s, signal overlapping), 0.92 (s, signal overlapping), 0.78 (s, signal overlapping).

Deprotection procedure

Fmoc protecting groups on Arg-functionalised products (***P2*** and ***G1****) were removed with diethylamine (DEA) in an equal volume of anhydrous tetrahydrofuran (THF). For ***G1****, 1 mL DMF was added to keep the gel swollen and to allow DEA to penetrate the network for deprotection. The mixture was stirred at room temperature for 18 hours, after which the contents were concentrated under reduced pressure and washed with cold diethyl ether. A tan solid was afforded after gravity filtration and air drying. Pbf protecting groups were removed with a mixture of trifluoroacetic acid, water and triisopropylsilane (95:2.5:2.5). The mixture was stirred at room temperature for 4 hours, after which the contents were washed with cold diethyl ether. A beige solid was afforded after lyophilisation.

Fmoc was removed from ***P2*** to afford ***P3*** (poly(Arg(Pbf)MA$_{40}$-*co*-HEMA$_{40}$-*co*-PEGMA$_{20}$)), and Pbf was removed from ***P3*** to afford ***P4*** (poly(ArgMA$_{40}$-*co*-HEMA$_{40}$-*co*-PEGMA$_{20}$)).

Both Fmoc and Pbf groups were removed from ***G1**** (poly(HEMA-*co*-Fmoc-Arg(Pbf)MA-*co*-PEGDMA-*co*-PEGMA)) to afford ***G2*** (poly(HEMA-*co*-ArgMA-*co*-PEGDMA-*co*-PEGMA)).

^{1}H NMR (poly(Arg(Pbf)MA$_{40}$-*co*-HEMA$_{40}$-*co*-PEGMA$_{20}$) (*P3*), 400 MHz, DMSO-d$_6$) δ 4.78 (b), 3.99, 3.90 (m + d, signal overlapping), 3.5 (s, signal overlapping), 3.23 (s, signal overlapping), 3.04 (s, signal overlapping), 2.96 (s, signal overlapping), 2.48 (s, signal overlapping), 2.42 (s, signal overlapping), 2.01 (s), 1.57 (m, signal overlapping), 1.41 (s, signal overlapping), 0.97 (s, signal overlapping), 0.79 (s, signal overlapping).

^{1}H NMR (poly(ArgMA$_{40}$-*co*-HEMA$_{40}$-*co*-PEGMA$_{20}$) (*P4*), 400 MHz, DMSO-d$_6$) δ 4.79 (b), 4.05, 3.90 (m + s, signal overlapping), 3.51 (s, signal overlapping), 3.44 (s, signal

overlapping), 3.24 (s, signal overlapping), 2.95, 2.93, 2.92, 2.89 (q, signal overlapping), 1.72, 1.54 (m + s + s, signal overlapping), 0.93 (s, signal overlapping), 0.78 (s, signal overlapping).

Water uptake measurement

Samples were lyophilised overnight right before water uptake experiments were conducted to minimise residual water. The humidity in the box was adjusted to approximately 70% RH. Room temperature was consistent at 23°C. Plastic petri dishes containing samples were placed into the humidity box shown in **Figure S15**. Samples were removed, weighed and returned to the box as quickly as possible. Water content was determined as the mass of water per gram of polymer. For the first hour, measurements were taken every ten minutes, then every hour for the next five hours, then once more 24 hours after the experiment was commenced. Mean values were taken from at least three trials for each sample.

LCST and VPTT measurement

The LCST of polymer products and VPTT of hydrogel products were determined using DSC. Water-swollen samples were blotted with filter paper and a small portion (~10 mg) was loaded into a hermetically sealed aluminium pan. One cycle was run from ambient temperature to 100°C. Endothermic phase transitions were defined by the peak of the endotherm.[24]

Cycling experiments

G2 was heated at 70°C for several hours before this experiment was commenced. The water uptake method described above was followed, with measurements taken after 1 hour. After this, the sample was placed into an oven maintained at 70°C. After 10 minutes, the sample was weighed then returned to the humidity box. This uptake-release cycle was repeated for another 24 cycles.

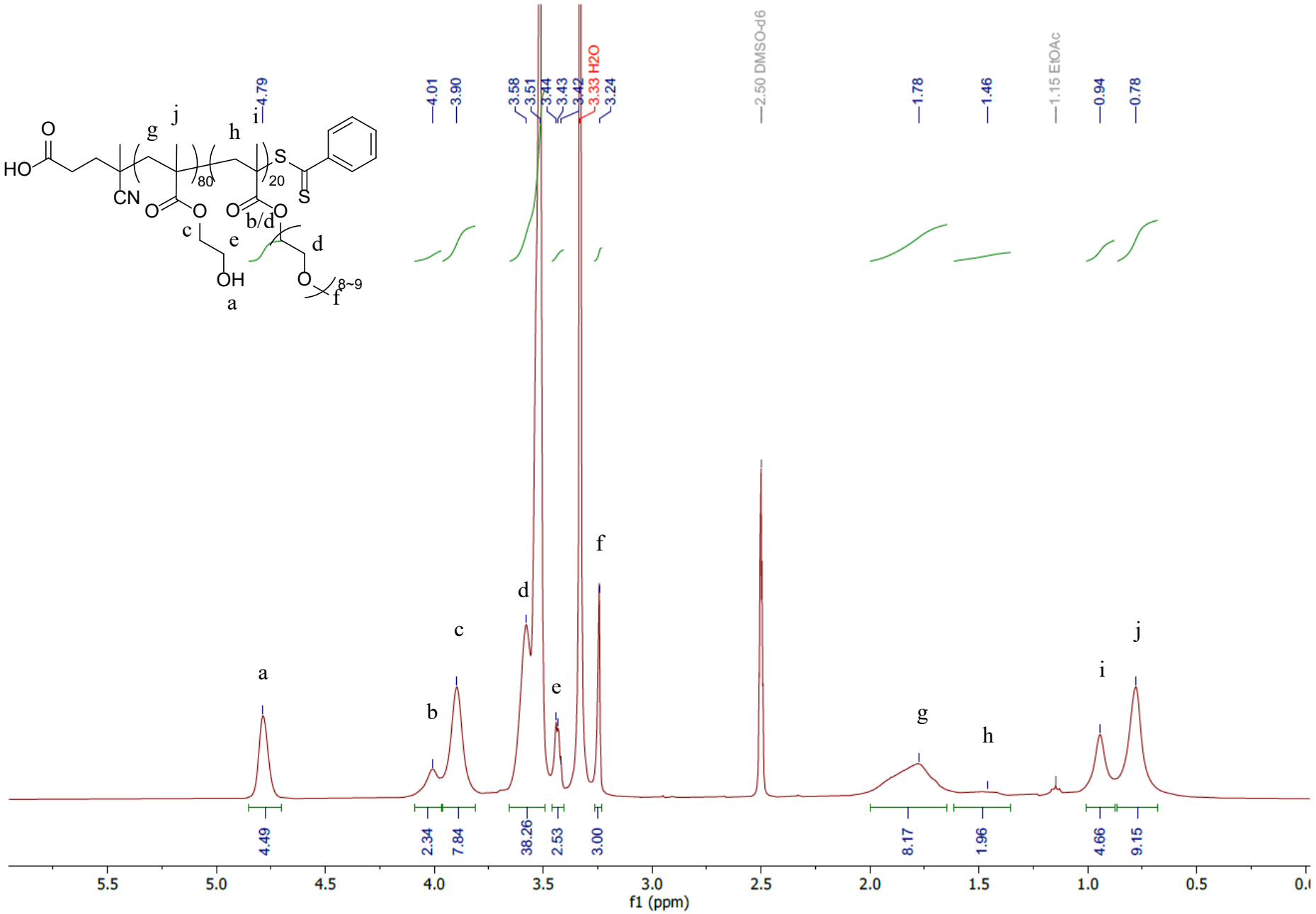

77 **Figure S1**: 400 MHz ^{1}H NMR of poly(HEMA$_{80}$-*co*-PEGMA$_{20}$) (***P1***) (Recorded in DMSO-d^{6})

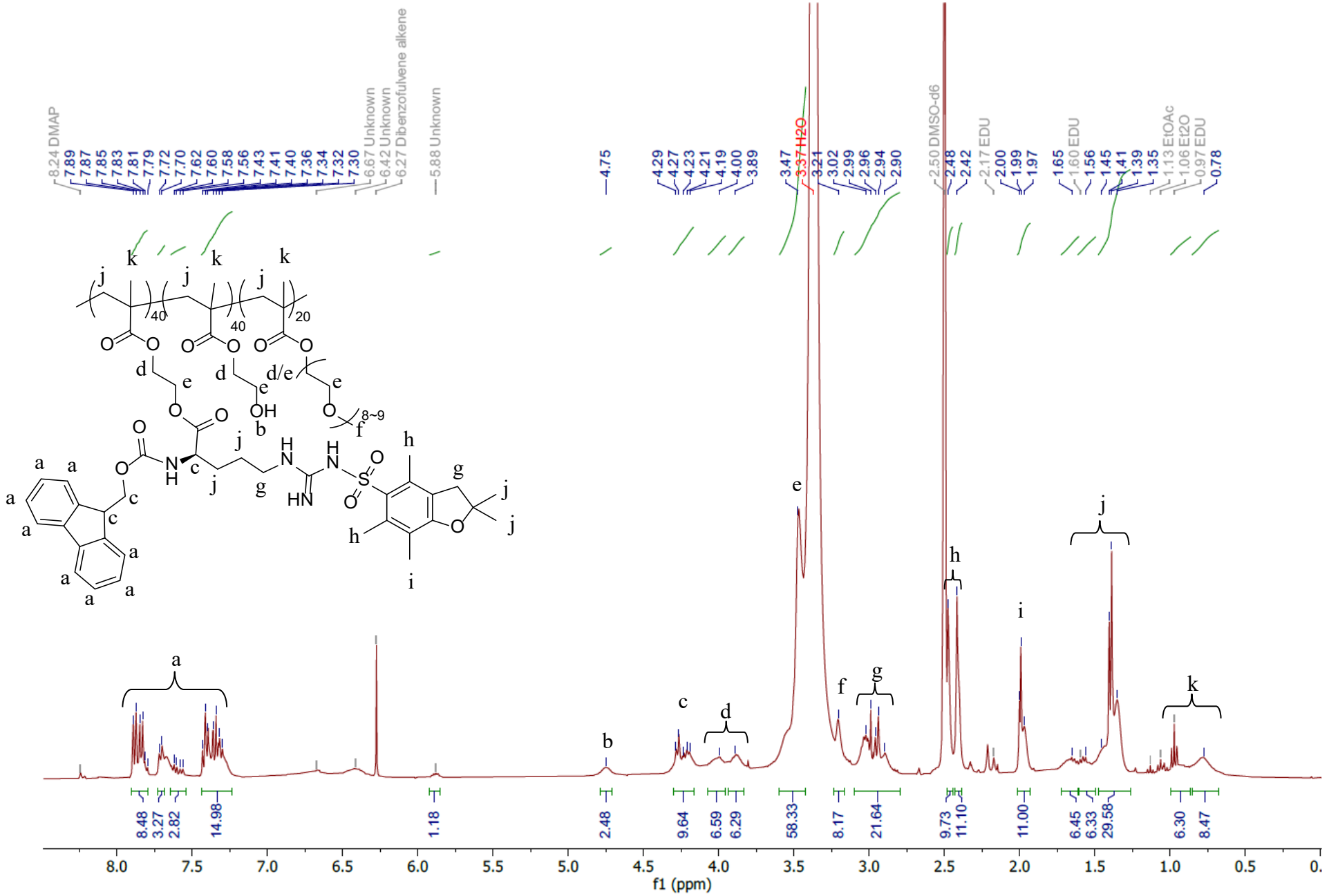

78 **Figure S2**: 400 MHz ^{1}H NMR of poly((Fmoc-Arg(Pbf))MA$_{40}$-*co*-HEMA$_{40}$-*co*-PEGMA$_{20}$) (***P2***) (Recorded in DMSO-d^{6})

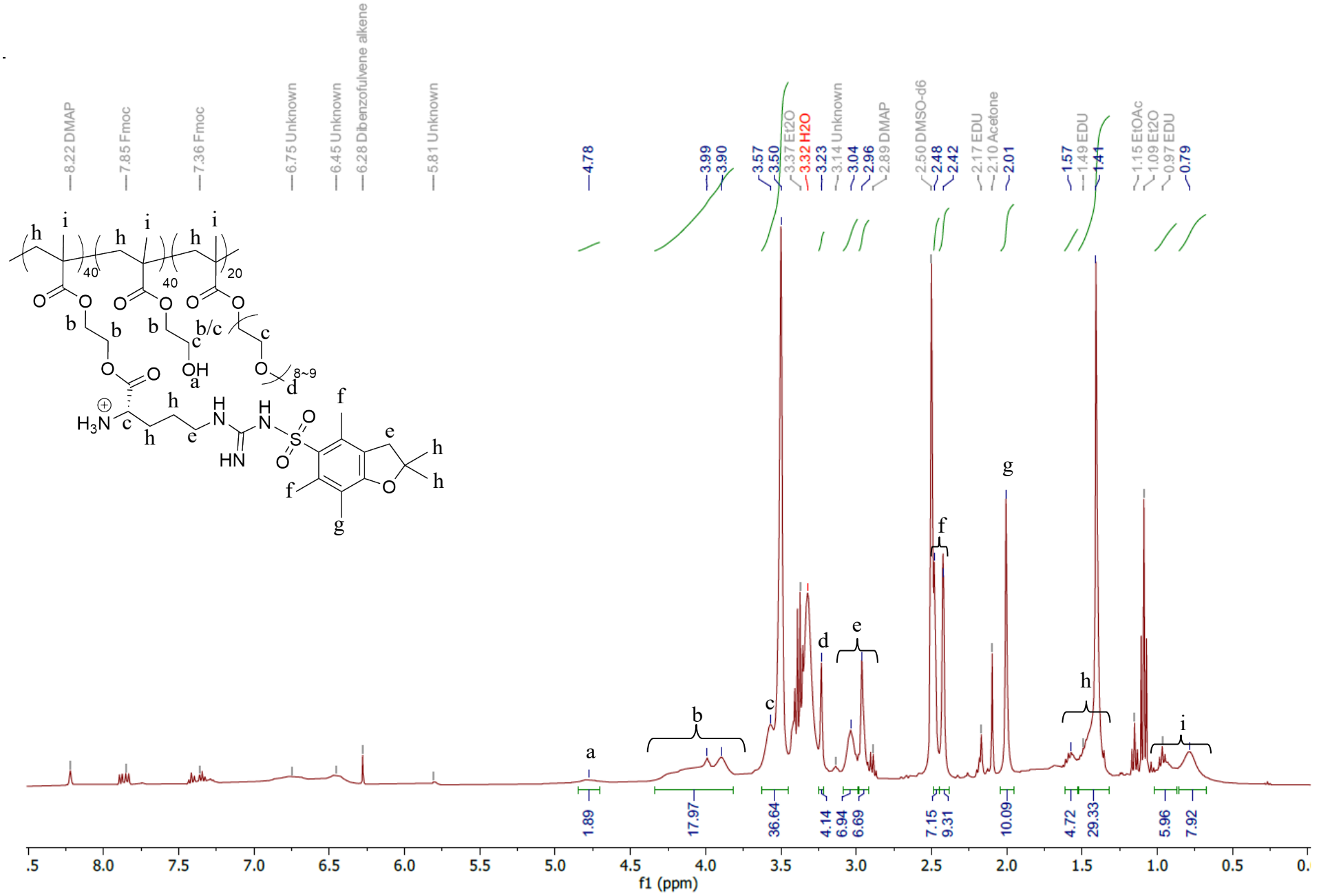

Figure S3: 400 MHz ^{1}H NMR of poly(Arg(Pbf)MA$_{40}$-*co*-HEMA$_{40}$-*co*-PEGMA$_{20}$) (***P3***) (Recorded in DMSO-d^{6})

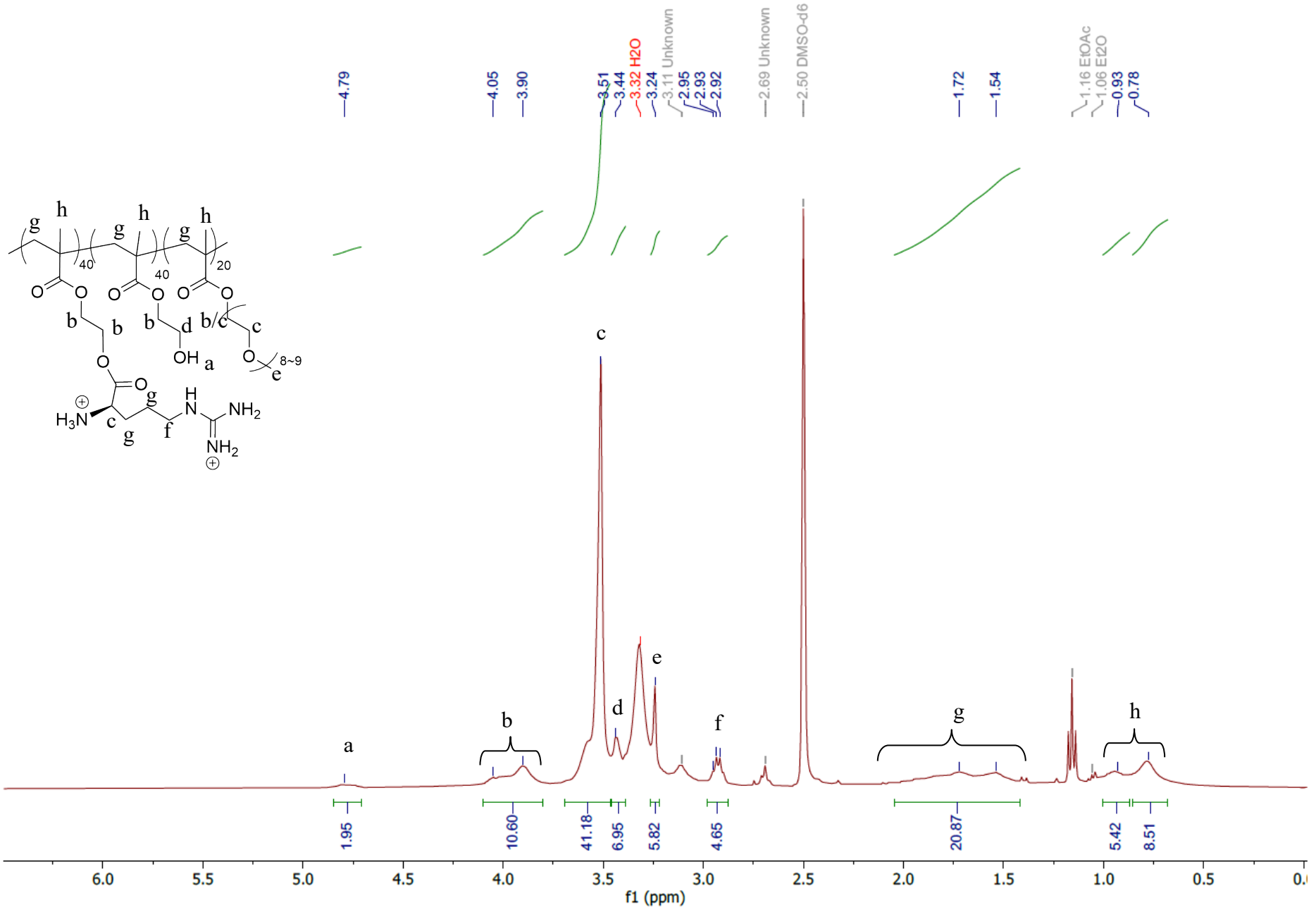

Figure S4: 400 MHz ^{1}H NMR of poly(ArgMA$_{40}$-*co*-HEMA$_{40}$-*co*-PEGMA$_{20}$) (***P4***) (Recorded in DMSO-d^{6})

FTIR Spectra

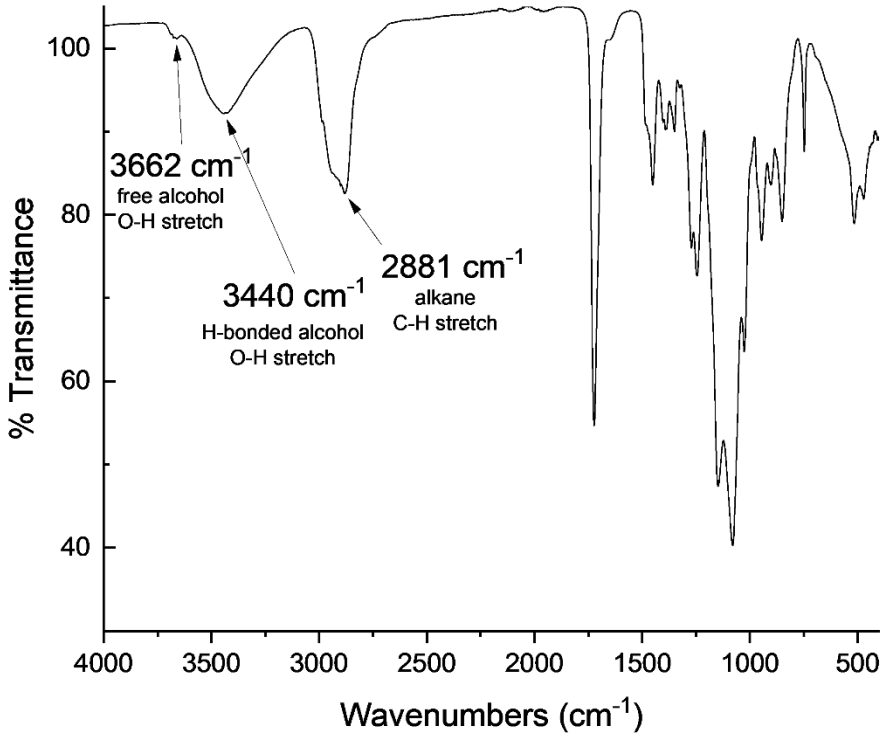

Figure S5: FTIR spectrum of poly(HEMA$_{80}$-*co*-PEGMA$_{20}$) (***P1***)

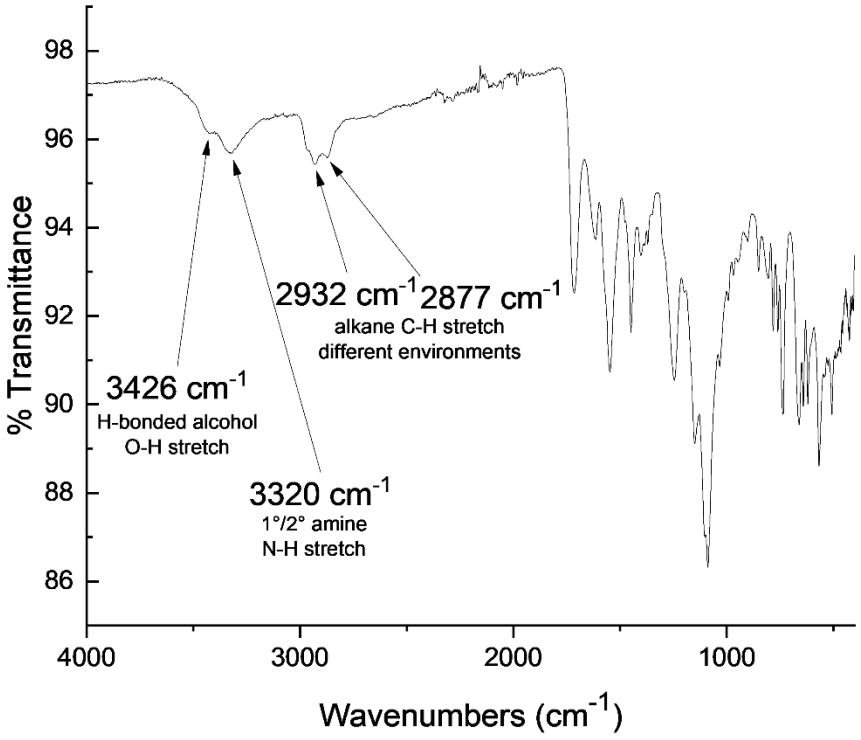

Figure S6: FTIR spectrum of poly((Fmoc-Arg(Pbf))MA$_{40}$-*co*-HEMA$_{40}$-*co*-PEGMA$_{20}$) (***P2***)

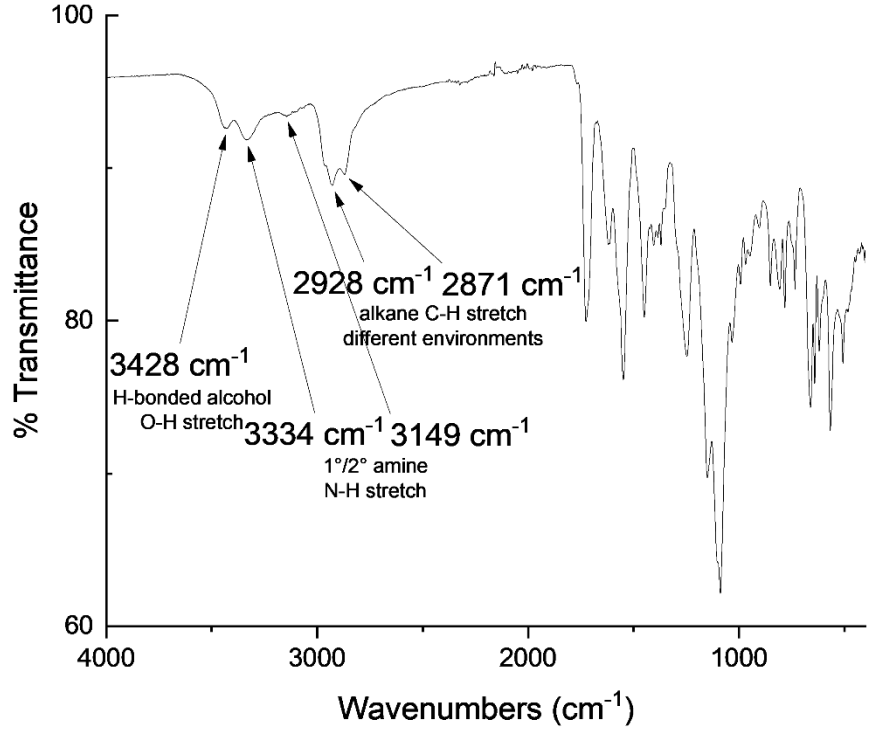

Figure S7: FTIR spectrum of poly(Arg(Pbf)MA$_{40}$-*co*-HEMA$_{40}$-*co*-PEGMA$_{20}$) (***P3***)

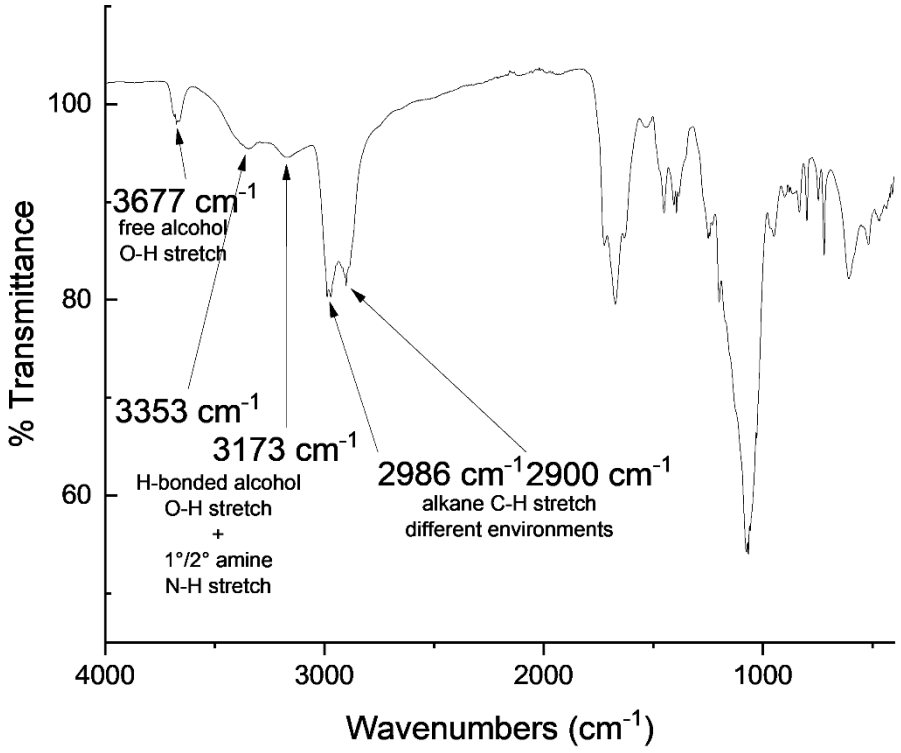

Figure S8: FTIR spectrum of poly(ArgMA$_{40}$-*co*-HEMA$_{40}$-*co*-PEGMA$_{20}$) (***P4***)

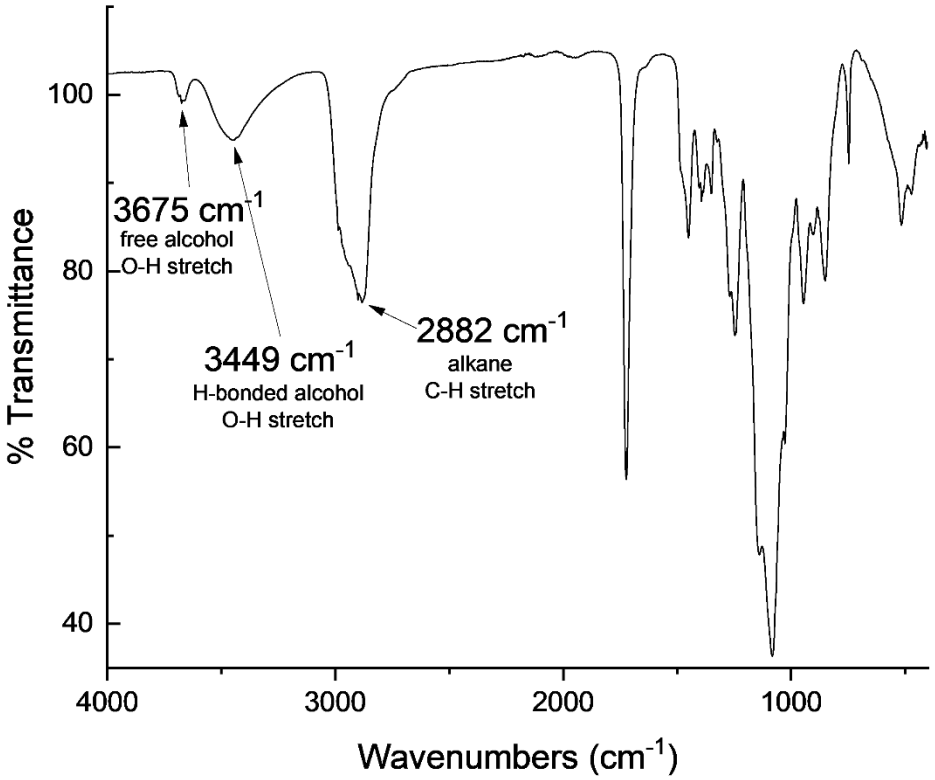

Figure S9: FTIR spectrum of poly(HEMA-*co*-PEGDMA-*co*-PEGMA) (***G1***)

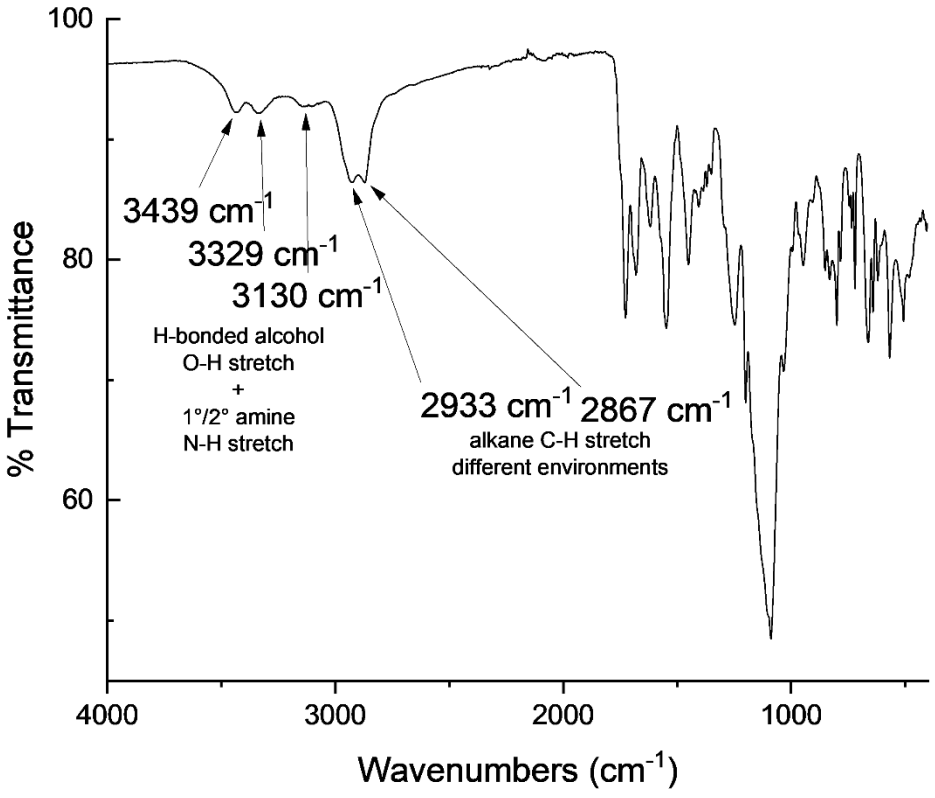

Figure S10: FTIR spectrum of poly(HEMA-*co*-ArgMA-*co*-PEGDMA-*co*-PEGMA) (***G2***)

DSC

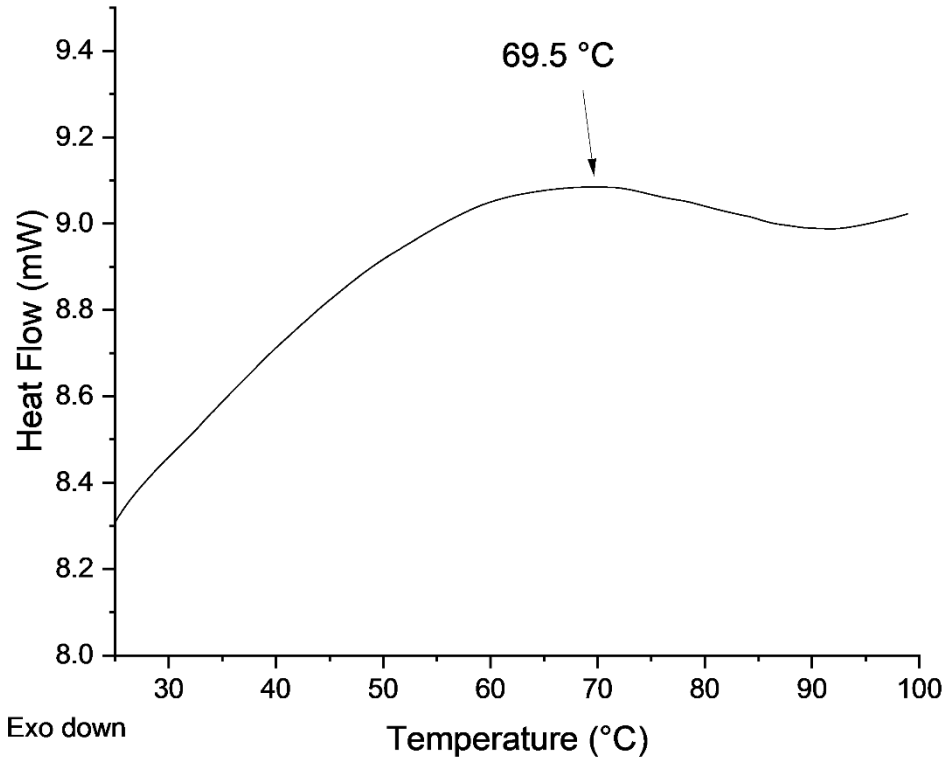

Figure S11: DSC trace of swollen poly(HEMA$_{80}$-*co*-PEGMA$_{20}$) (***P1***)

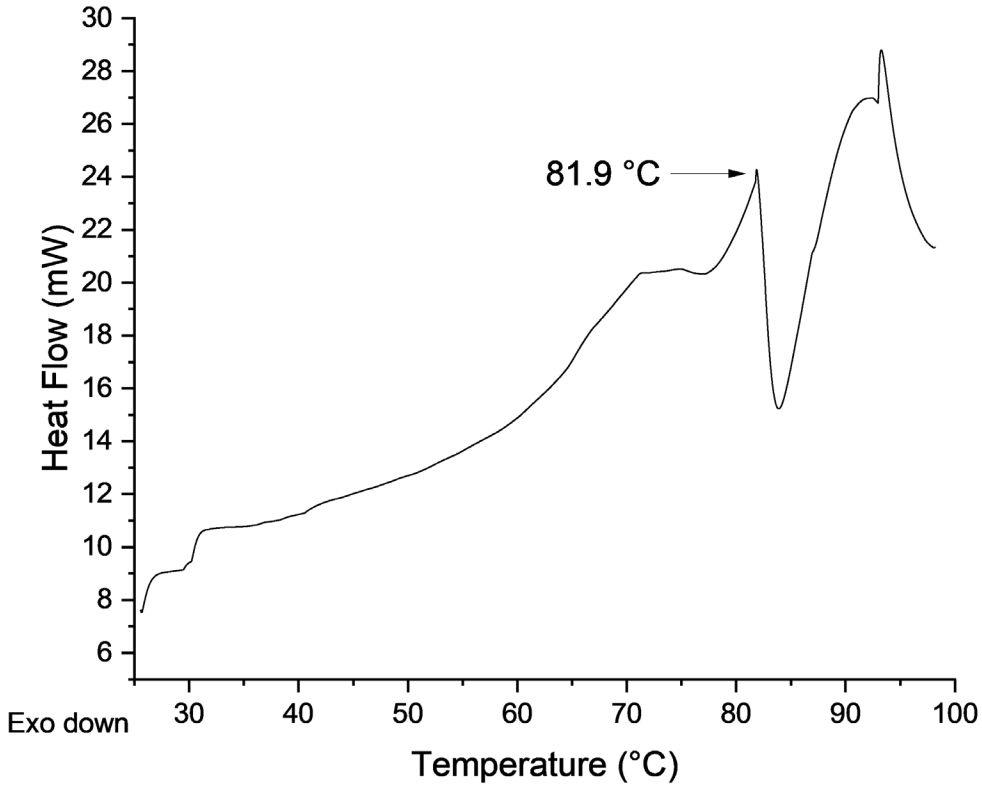

Figure S12: DSC trace of swollen poly(ArgMA$_{40}$-*co*-HEMA$_{40}$-*co*-PEGMA$_{20}$) (***P4***)

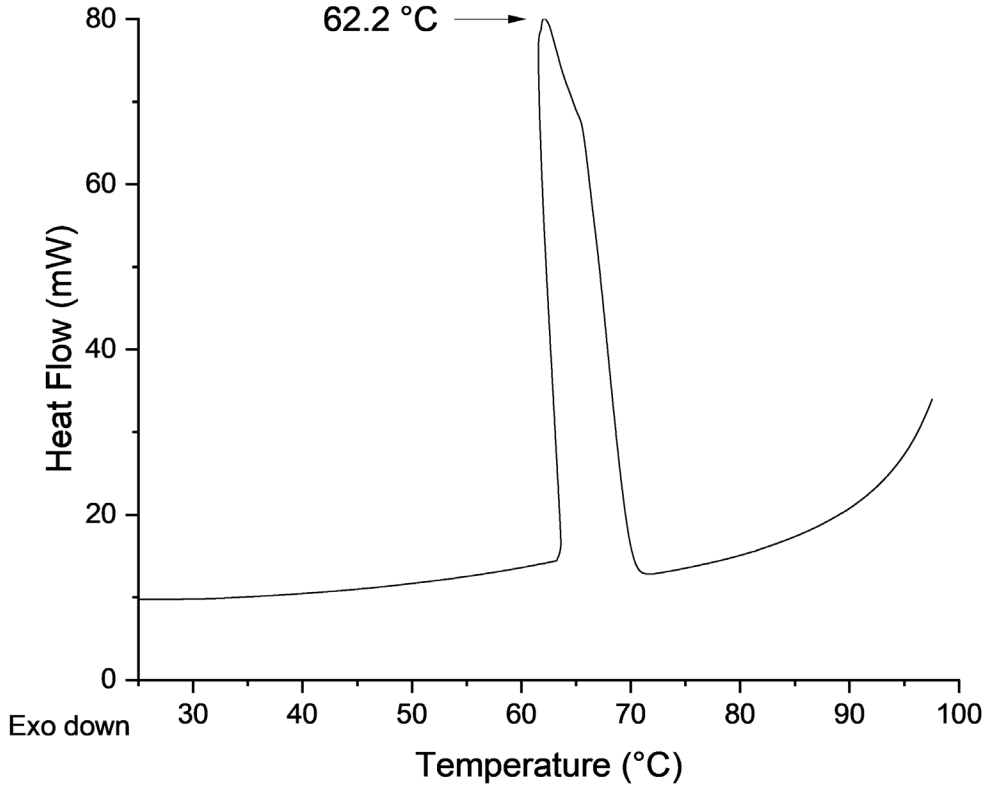

Figure S13: DSC trace of swollen poly(HEMA-*co*-ArgMA-*co*-PEGDMA-*co*-PEGMA) (***G2***)

GPC

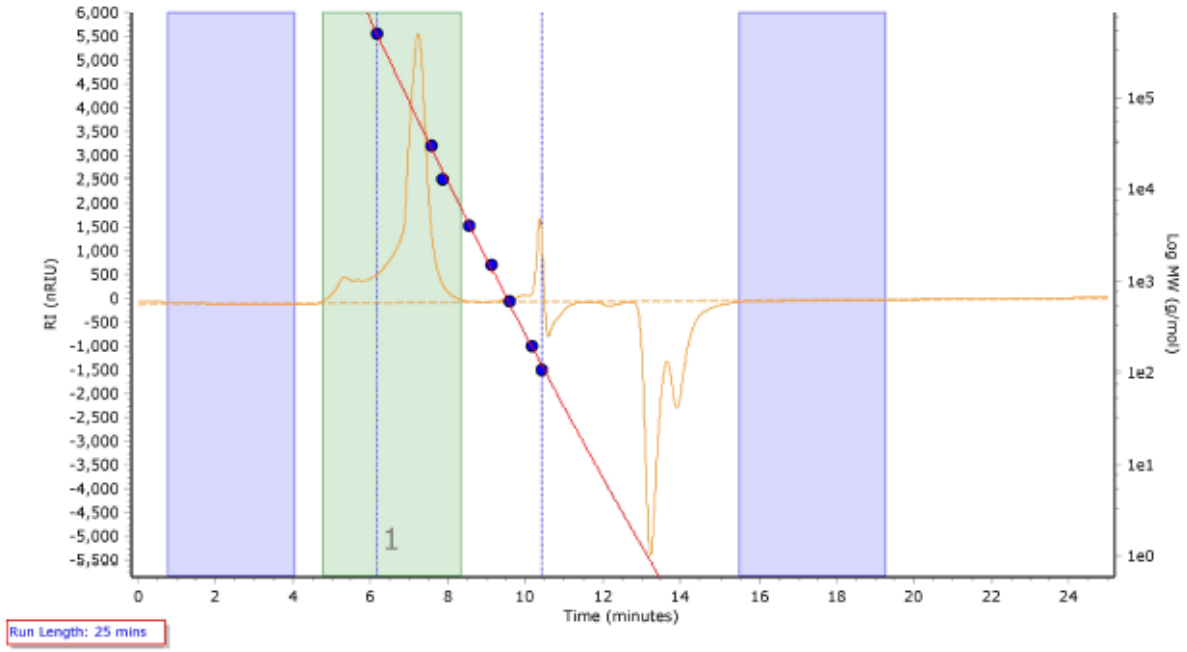

Molecular Weight Averages

Peak	Mp (g/mol)	Mn (g/mol)	Mw (g/mol)	Mz (g/mol)	Mz+1 (g/mol)	Mv (g/mol)	PD
Peak 1	54466	58604	355822	2706661	4600899	2381009	6.072

Figure S14: GPC trace derived from poly(HEMA$_{80}$-*co*-PEGMA$_{20}$) (***P1***) (*N*,*N*-dimethylacetamide used as eluting medium). Samples ***P2***–***P4*** do not dissolve in DMAc and thus could not be characterised with this method.

Reaction Schemes

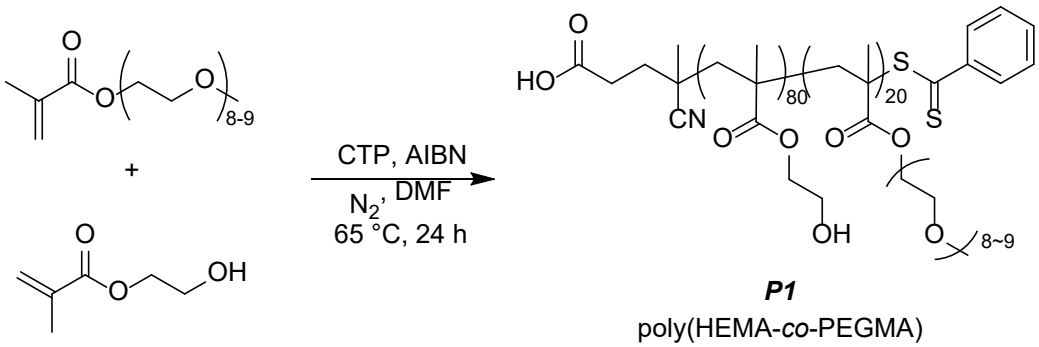

P1
poly(HEMA-*co*-PEGMA)

Scheme S1: Synthetic pathway for base poly(HEMA-*co*-PEGMA) copolymer.

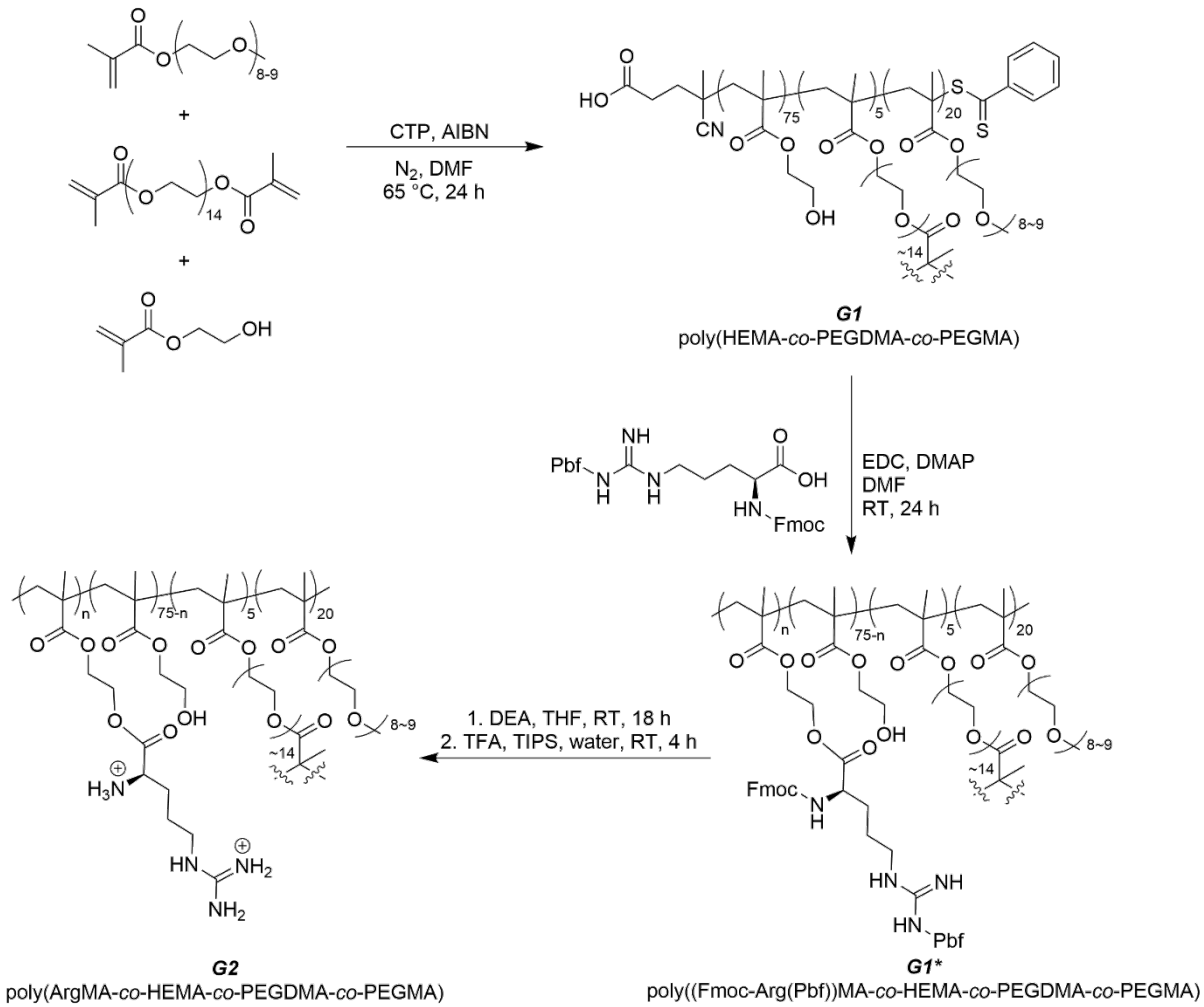

Scheme S2: Hydrogel synthesis (top), arginine functionalisation (right) and deprotection (bottom), analogous to copolymers ***P1***–***P4***

Humidity Apparatus

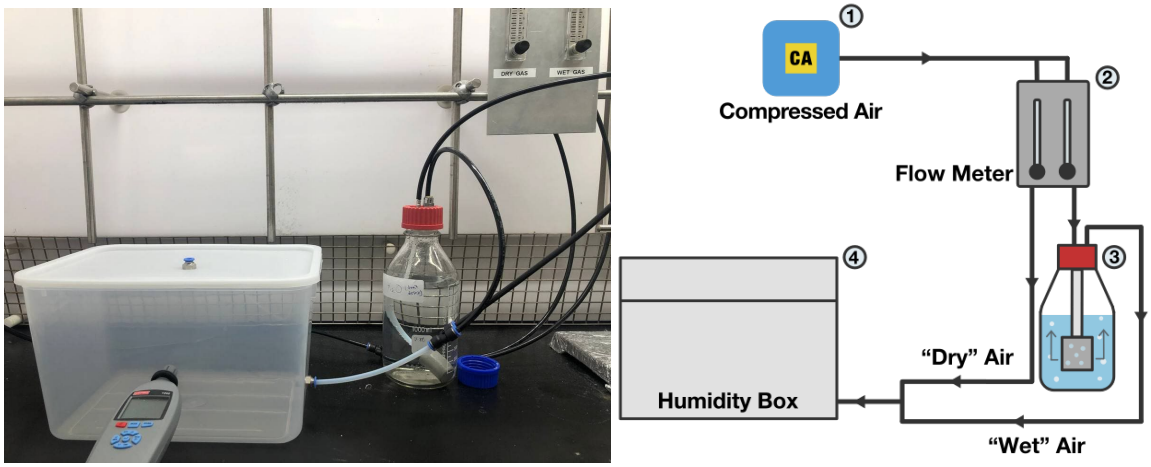

Figure S15: Custom humidity apparatus used for water uptake experiments, photo (left) and illustration (right).

The humidity box operates on a constant flow of compressed air (CA) (**1**). Two adjustable lines of air are controlled by a flow meter (**2**): the “dry” air coming directly off the CA, and the “wet” air which is bubbled through a bottle of water first (**3**). The proportions of each type of air can be adjusted at will. There is no need for insulation of the humidity box (**4**) as the constant positive flow of air through the system is sufficient to approximately maintain the environment in the box.

References

(1) Zhao, F.; Zhou, X.; Liu, Y.; Shi, Y.; Dai, Y.; Yu, G. Super Moisture-Absorbent Gels for All-Weather Atmospheric Water Harvesting. *Advanced Materials* **2019**, *31* (10), 1806446. DOI: https://doi.org/10.1002/adma.201806446.
(2) Guo, Y.; Guan, W.; Lei, C.; Lu, H.; Shi, W.; Yu, G. Scalable super hygroscopic polymer films for sustainable moisture harvesting in arid environments. *Nature Communications* **2022**, *13* (1), 2761. DOI: 10.1038/s41467-022-30505-2.
(3) Maity, D.; Teixeira, A. P.; Fussenegger, M. Hydratable Core–Shell Polymer Networks for Atmospheric Water Harvesting Powered by Sunlight. *Small* **2023**, *19* (47), 2301427. DOI: https://doi.org/10.1002/smll.202301427.
(4) Luo, Q.; Chen, M.; Yu, D.; Zhang, T.; Zhao, J.; Zhang, L.; Han, X.; Zhou, M.; Hou, Y.; Zheng, Y. An Atmospheric Water-Harvester with Ultrahigh Uptake-Release Efficiency at Low Humidity. *ACS Nano* **2024**, *18* (22), 14650-14660. DOI: 10.1021/acsnano.4c02866.
(5) Xu, J.; Li, T.; Yan, T.; Wu, S.; Wu, M.; Chao, J.; Huo, X.; Wang, P.; Wang, R. Ultrahigh solar-driven atmospheric water production enabled by scalable rapid-cycling water harvester with vertically aligned nanocomposite sorbent. *Energy & Environmental Science* **2021**, *14* (11), 5979-5994. DOI: 10.1039/D1EE01723C.
(6) Tereshchenko, A. G. Deliquescence: Hygroscopicity of Water-Soluble Crystalline Solids. *Journal of Pharmaceutical Sciences* **2015**, *104* (11), 3639-3652. DOI: https://doi.org/10.1002/jps.24589.
(7) Fortune Business Insights. *Lithium Chloride Market Size, Share & Industry Analysis, By Application (Batteries, Ceramics & Glass, Lubricants, Polymer Production, Air Treatment, and Others) and Regional Forecast, 2024-2032*; FBI108063; 2024. https://www.fortunebusinessinsights.com/lithium-chloride-market-108063.
(8) Hsiao, E.; Barnette, A. L.; Bradley, L. C.; Kim, S. H. Hydrophobic but Hygroscopic Polymer Films – Identifying Interfacial Species and Understanding Water Ingress Behavior. *ACS Applied Materials & Interfaces* **2011**, *3* (11), 4236-4241. DOI: 10.1021/am200894h.
(9) Cheng, Y.; Zhang, X.; Zhang, J.; He, Z.; Wang, Y.; Wang, J.; Zhang, J. Hygroscopic hydrophobic coatings from cellulose: Manipulation of the aggregation morphology of water. *Chemical Engineering Journal* **2022**, *441*, 136016. DOI: https://doi.org/10.1016/j.cej.2022.136016.
(10) Coughlin, J. E.; Reisch, A.; Markarian, M. Z.; Schlenoff, J. B. Sulfonation of polystyrene: Toward the "ideal" polyelectrolyte. *Journal of Polymer Science Part A: Polymer Chemistry* **2013**, *51* (11), 2416-2424. DOI: https://doi.org/10.1002/pola.26627.
(11) Schweng, P.; Mayer, F.; Galehdari, D.; Weiland, K.; Woodward, R. T. A Robust and Low-Cost Sulfonated Hypercrosslinked Polymer for Atmospheric Water Harvesting. *Small* **2023**, *19* (50), 2304562. DOI: https://doi.org/10.1002/smll.202304562.
(12) Mauer, L. J. Deliquescence of crystalline materials: mechanism and implications for foods. *Current Opinion in Food Science* **2022**, *46*, 100865. DOI: https://doi.org/10.1016/j.cofs.2022.100865.
(13) Wu, M.; Li, R.; Shi, Y.; Altunkaya, M.; Aleid, S.; Zhang, C.; Wang, W.; Wang, P. Metal- and halide-free, solid-state polymeric water vapor sorbents for efficient water-sorption-driven cooling and atmospheric water harvesting. *Materials Horizons* **2021**, *8* (5), 1518-1527. DOI: 10.1039/D0MH02051F.
(14) Park, H.; Haechler, I.; Schnoering, G.; Ponte, M. D.; Schutzius, T. M.; Poulikakos, D. Enhanced Atmospheric Water Harvesting with Sunlight-Activated Sorption Ratcheting. *ACS Applied Materials & Interfaces* **2022**, *14* (1), 2237-2245. DOI: 10.1021/acsami.1c18852.
(15) Lei, C.; Guan, W.; Zhao, Y.; Yu, G. Chemistries and materials for atmospheric water harvesting. *Chemical Society Reviews* **2024**, *53* (14), 7328-7362. DOI: 10.1039/D4CS00423J.
(16) Schweng, P.; Woodward, R. T. Challenging POPular opinion: Porous organic polymers for atmospheric water harvesting. *Reactive and Functional Polymers* **2024**, *203*, 106014. DOI: https://doi.org/10.1016/j.reactfunctpolym.2024.106014.
(17) Ni, F.; Qiu, N.; Xiao, P.; Zhang, C.; Jian, Y.; Liang, Y.; Xie, W.; Yan, L.; Chen, T. Tillandsia-Inspired Hygroscopic Photothermal Organogels for Efficient Atmospheric Water Harvesting. *Angewandte Chemie International Edition* **2020**, *59* (43), 19237-19246. DOI: https://doi.org/10.1002/anie.202007885.

(18) Diggle, B.; Jiang, Z.; Li, R. W.; Connal, L. A. Self-Healing Polymer Network with High Strength, Tunable Properties, and Biocompatibility. *Chemistry of Materials* **2021**, *33* (10), 3712-3720. DOI: 10.1021/acs.chemmater.1c00707.
(19) Ramkissoon-Ganorkar, C.; Feng, L.; Baudys, M.; Sung Wan, K. Effect of molecular weight and polydispersity on kinetics of dissolution and release from pH/temperature-sensitive polymers. *Journal of Biomaterials Science, Polymer Edition* **1999**, *10* (10), 1149-1161. DOI: 10.1163/156856299X00739.
(20) Newns, A. C. Sorption and Diffusion in Polymers. *Nature* **1968**, *218* (5139), 355-356. DOI: 10.1038/218355b0.
(21) Zhou, X.; Lu, H.; Zhao, F.; Yu, G. Atmospheric Water Harvesting: A Review of Material and Structural Designs. *ACS Materials Letters* **2020**, *2* (7), 671-684. DOI: 10.1021/acsmaterialslett.0c00130.
(22) Thanusing, M. K.; Shen, P.; Pollard, B. L.; Connal, L. A. Rational design of water-harvesting hydrogels. *Molecular Systems Design & Engineering* **2024**, *9* (1), 63-72. DOI: 10.1039/D3ME00132F.
(23) Ng, W. S.; Forbes, E.; Franks, G. V.; Connal, L. A. Xanthate-Functional Temperature-Responsive Polymers: Effect on Lower Critical Solution Temperature Behavior and Affinity toward Sulfide Surfaces. *Langmuir* **2016**, *32* (30), 7443-7451. DOI: 10.1021/acs.langmuir.6b00211.
(24) Fei, R.; George, J. T.; Park, J.; Means, A. K.; Grunlan, M. A. Ultra-strong thermoresponsive double network hydrogels. *Soft Matter* **2013**, *9* (10), 2912-2919. DOI: 10.1039/C3SM27226E.
(25) Singh, D.; Kuckling, D.; Choudhary, V.; Adler, H.-J.; Koul, V. Synthesis and characterization of poly(N-isopropylacrylamide) films by photopolymerization. *Polymers for Advanced Technologies* **2006**, *17* (3), 186-192. DOI: https://doi.org/10.1002/pat.713.
(26) Yuan, Y.; Raheja, K.; Milbrandt, N. B.; Beilharz, S.; Tene, S.; Oshabaheebwa, S.; Gurkan, U. A.; Samia, A. C. S.; Karayilan, M. Thermoresponsive polymers with LCST transition: synthesis, characterization, and their impact on biomedical frontiers. *RSC Applied Polymers* **2023**, *1* (2), 158-189. DOI: 10.1039/D3LP00114H.
(27) Singh, R.; Deshmukh, S. A.; Kamath, G.; Sankaranarayanan, S. K. R. S.; Balasubramanian, G. Controlling the aqueous solubility of PNIPAM with hydrophobic molecular units. *Computational Materials Science* **2017**, *126*, 191-203. DOI: https://doi.org/10.1016/j.commatsci.2016.09.030.

Chapter Four

Hygroscopic, creatine-functionalised microgels for efficient desiccants and water harvesting

Moki K. Thanusing, Brett L. Pollard, Luke A. Connal

***ACS Appl. Polym. Mater.**, 2026*

Australian National University

Statement of Contribution

This thesis is submitted as a Thesis by Compilation in accordance with https://policies.anu.edu.au/ppl/document/ANUP_003405

I declare that the research presented in this Thesis represents original work that I carried out during my candidature at the Australian National University, except for contributions to multi-author papers incorporated in the Thesis where my contributions are specified in this Statement of Contribution.

Title: Hygroscopic, creatine-functionalised microgels for efficient desiccants and water harvesting

Authors: Moki K. Thanusing, Brett L. Pollard, Luke A. Connal

Current status of paper: In Preparation

Contribution to paper: This is a full paper and the candidate conducted all of the experimental work reported within. In addition, all spectral data presented in the Supporting Information document was collected and formatted by the candidate. The candidate also wrote the entirety of the manuscript and experimental section and conducted relevant literature surveys. A preliminary outline was generated and revised by the candidate.

Senior author or collaborating authors endorsement: _____

Moki Thanusing	_____	25/08/25
Candidate – Print Name	Signature	Date

Endorsed

Luke Connal	_____	26/8/25
Chair of Supervisory Panel – Print Name	Signature	Date
Mark Humphrey	_____	28/08/25
Delegated Authority – Print Name	Signature	Date

Foreword

In this chapter, the insights earned in **Chapters 2** and **3** culminate in a further improved SAWH hydrogel. Both physical and chemical considerations were accounted for during the rational design process. Surface area, a critical physical property, was maximised by forming polymer microgels. The *L*-arginine post-functionalisation from the previous chapter was replaced with a more streamlined method using the structurally similar creatine. In addition to presenting a high-performing SAWH hydrogel, new insights into microgel-specific structure-property relationships for water harvesting are reported herein.

This chapter has been published in ACS Applied Polymer Materials, where I am the first author. My contribution to the manuscript includes designing and conducting experiments, characterisation of resulting materials, data analysis as well as preparing and revising the manuscript and figures (overall 75%). The manuscript prepared for submission is presented here. Brett L. Pollard and Luke A. Connal contributed to experimental design, supervised the project, and edited and revised the manuscript and figures.

Introduction

Atmospheric water harvesting (AWH) is one of the most promising avenues for alleviating water scarcity. The main advantage of atmospheric water as a freshwater source comes from its globally delocalised distribution. Atmospheric water can therefore be harvested from any location, including historically water-poor areas and arid environments. Polymer desiccants are one of the most promising classes of sorption-based AWH (SAWH) materials.

The sorption kinetics of SAWH materials can be improved by maximising surface area.[1] Surface interactions are rapid compared to diffusion of water inside a system. The typical approach is to improve porosity by controlling pore size, shape and distribution, however precise control can be laborious to execute and is prone to deformation upon hydration.[2-4] The alternative approach to maximising surface area is a general reduction in polymer dimensions. A thin film has a much larger surface area in proportion to its volume, allowing rapid water harvesting kinetics.[5] However, careful handling is required as these thin films are typically fragile. In contrast, a material comprised of a collection of small, spherical particles still offers a relatively high surface area in proportion to its volume without the structural constraints of a thin film. Despite this, there are only few reported examples of polymer microgel beads being utilised for SAWH purposes, leaving this avenue open for further exploration.[6-8] Microgels have already gained research interest in other areas of water harvesting, primarily as draw solutes in forward osmosis desalination.[9-12]

Poly(*N*-isopropylacrylamide-*co*-2-hydroxyethyl methacrylate) (poly(NIPAAm-*co*-HEMA)) microgels have been studied for biomedical applications.[13-16] We hypothesised that the combination of thermoresponsive and hydrophilic properties offered by the co-monomers in this system has strong potential for SAWH. Beyond this, the HEMA side chain alcohol provides scope for functionalisation and hence improved performance.

In our previous work, we showed the guanidinium moiety was able to enhance water harvesting properties.[17] This was done using esterification of *L*-arginine. The primary approach to improving water harvesting properties of SAWH polymers in the literature involves the incorporation of additives like lithium chloride and carbon nanotubes.[18, 19] Additives are prone to leaching in the long term, which has negative impacts on both the longevity and scalability of materials.[20] In contrast, post-functionalisation avoids these disadvantages. While functionalisation with arginine was highly effective in improving water uptake, we employed the use of protected arginine in order to control chemoselectivity and

hence required subsequent deprotection steps. We identified creatine as an alternative source of the hygroscopic/hydrophilic guanidinium moiety. While being similarly cheap, abundant and a well-known health supplement, we anticipated that creatine could be added in a more atom-efficient manner while still conferring improved SAWH properties. Creatine is a well-studied dietary supplement that is osmotically active and increases water retention in the first few days of supplementation.[21]

In this work, we present the use of poly(NIPAAm-*co*-HEMA) as a thermoresponsive SAWH material, including studies on the effect of various microgel sizes on water uptake and related properties, and investigations into the effects of creatine functionalisation on water harvesting performance.

Results and Discussion

To gain a baseline understanding of poly(NIPAAm-*co*-HEMA) properties and water harvesting capacity, we first synthesised a library of microgels with varying compositions (**Figure 1**). NIPAAm is well-known for its thermoresponsive properties and has already been used in SAWH applications.[6, 18, 22-24] HEMA was chosen as a hydrophilic monomer which could also be readily functionalised through its primary alcohol. Free radical precipitation polymerisation was used to synthesise the microgel library (**Scheme S1**). Compared to other methods of forming polymer microgels, such as emulsion or suspension polymerisation, precipitation polymerisation is relatively simple in its reagents and process.[25] Crucially, no stabiliser or surfactant is necessary for monodisperse microgels, although very dilute concentrations of the latter can be used for controlling size. Microgels were made with molar feed ratios of 7:3, 5:5, and 3:7 of NIPAAm and HEMA, labelled ***MG1***, ***MG2*** and ***MG3*** respectively. Successful polymerisation was confirmed with FTIR spectroscopy after purification and lyophilisation (**Figures S1**–**3**). While exact composition could not be confirmed, there were noticeable differences in composition between all three samples through FTIR spectroscopy. The relative sizes of NIPAAm-associated peaks (1724 cm^{-1} and 1536 cm^{-1}) to HEMA-associated peaks (1644 cm^{-1} and 1459 cm^{-1}) reduced with lower NIPAAm composition.

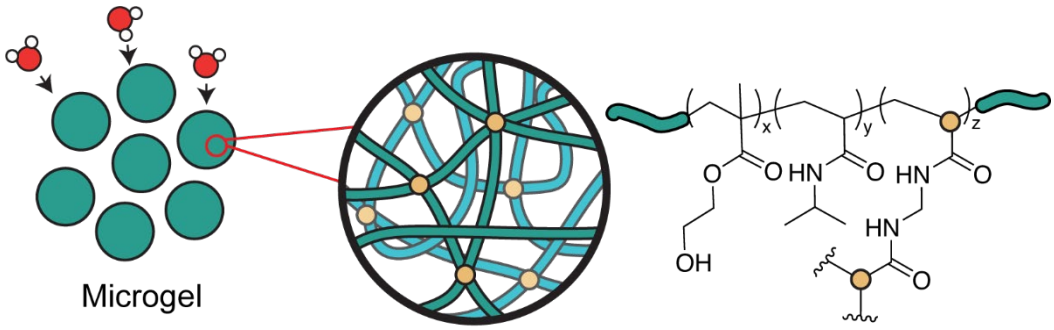

Figure 1: Graphical representation of poly(NIPAAm-*co*-HEMA) microgel with chemical structure.

The thermoresponsive properties of the microgels were examined through size analysis. Dynamic light scattering (DLS) was used to determine water suspended microgel size at temperatures from 5°C to 45°C (**Figure 2a**). PNIPAAm microgels undergo a rapid decrease in size as they pass the volume phase transition temperature (VPTT) at 32°C.[26] The phase transitions smoothed out and flattened with increasing HEMA content. In the 3:7 composition ***MG3*** microgel, the transition was difficult to distinguish. This trend was expected as thermoresponsive properties are proportional to thermoresponsive NIPAAm content. The VPTT of the microgels decreased slightly with increasing HEMA content. The 7:3 (***MG1***) composition showed a VPTT of around 31°C, 5:5 (***MG2***) at 27°C, and 3:7 (***MG3***) at 25–26°C. We had initially expected increasing polymer hydrophilicity with HEMA content, given that HEMA is more hydrophilic than NIPAAm. Typically, it is expected for phase transition temperatures to increase with increasing polymer hydrophilicity.[27] As a phase transition occurs, polymer-solvent interactions (with water as the typical solvent) are broken as the polymer starts interacting preferentially with itself. Since a more hydrophilic polymer would have more favourable polymer-solvent interactions, a higher temperature would be required to induce a thermoresponsive change. However, poly(NIPAAm-*co*-HEMA) has been shown to consistently have lower phase transition temperatures than pure PNIPAAm.[14, 26, 28] This increasing hydrophobic character would indicate that polymer-polymer interactions are more favourable than polymer-solvent interactions, which is plausible given poly(HEMA) has a tendency for strong self-association.[29] In the poly(NIPAAm-*co*-HEMA) microgel, the strong interactions between HEMA sidechains translate to an apparent increasing "hydrophobicity" with increasing HEMA content.

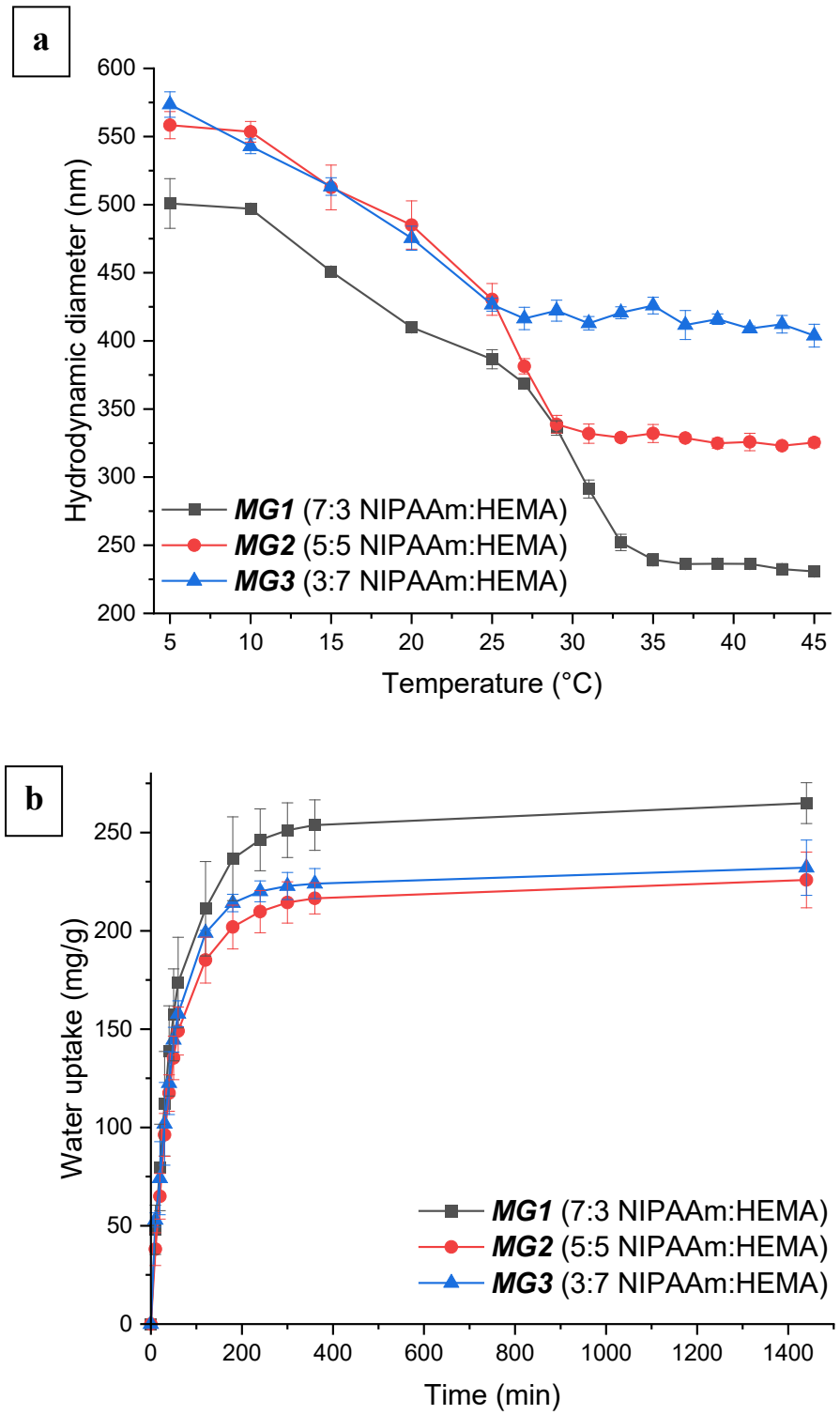

Figure 2: (a) Hydrodynamic diameter of ***MG1–MG3*** measured from 5°C to 45°C, showing how composition affected thermoresponsive behaviour. At 25°C, ***MG1*** had a hydrodynamic diameter of 390 nm, while ***MG2*** (5:5) and ***MG3*** (3:7) had a diameter of 430 nm. (b) Water uptake over 24 hours, showing the effects of microgel composition on water uptake.

There are other relationships between microgel composition and size beyond thermoresponsive properties. Generally, a higher composition of HEMA yielded larger microgels over the measured temperature range. The effects of composition on size were clearest above the VPTT, where the polymers had deswelled. HEMA already had strong self-association, thus above the VPTT there were fewer water molecules to expel from the microgel with higher HEMA content and less shrinking that could occur. Below the VPTT, the thermoresponsivity of NIPAAm caused a high degree of swelling in ***MG1***, which had the highest NIPAAm composition. Comparatively, the microgel size shrank 28%, 42% and 53% from 5°C to 35°C as NIPAAm content increased. ***MG1*** was consistently the smallest of the three compositions despite this large size change.

The water uptake for each lyophilised microgel was then measured over 24 hours (**Figure 2b**). ***MG1***, with a composition of 7:3 NIPAAm:HEMA, achieved an uptake of 265 mg water per gram of polymer after 24 hours and generally had a faster rate of uptake over the other two samples. The other microgel compositions could be considered to have the same uptake within error. From our previous work, we determined that slight changes in composition of a copolymer will confer large changes in water harvesting properties.[30] Specifically, more hydrophilic polymers have greater atmospheric water uptake. Given that apparent microgel hydrophilicity decreased with increasing HEMA content, water uptake was expected to decrease accordingly. However, given that microgel size changed with composition, it was impossible to identify the precise effect of composition on water uptake. Water uptake appears to correlate more closely with microgel size; both ***MG2*** and ***MG3*** had a diameter of 430 nm in suspension at 25°C while ***MG1*** was smaller. Intuitively, a smaller microgel should have superior water uptake given its higher surface area to volume ratio. The process of surface adsorption is faster than diffusion through the bulk polymer, thus a higher water uptake may be expected for a smaller microgel.[31, 32] This logic assumes densely packed, discrete and equally sized spheres. However, while individual microgel spheres were still apparent, SEM imaging showed these microgels packed tightly into sheets when dried, appearing fused without any visible inter-sphere voids (**Figure 3**). This macrostructure formation complicated the relationship between observed microgel size and water harvesting properties and required further examination.

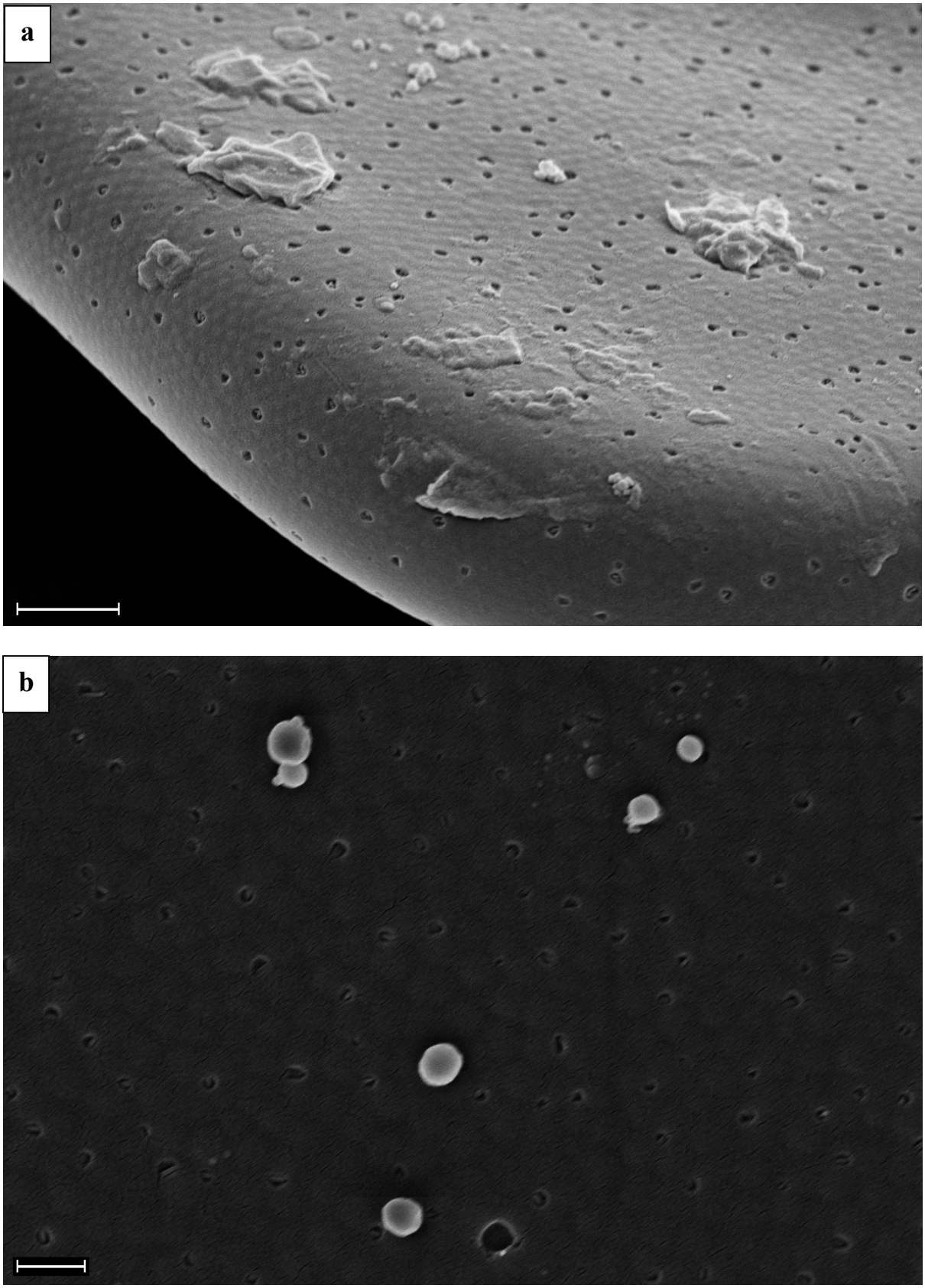

Figure 3: SEM images of dried ***MG1*** (a) and ***MG2*** (b), showing effects of composition. Scale bars are 1 μm and 500 nm respectively.

The rate of uptake of all microgel samples exhibited a plateau after approximately 3 hours, indicating a potential window for short water harvesting cycles.[33] This fast initial rate of uptake corresponds to saturation of surface functional groups. As these surface groups are occupied, the rate of water uptake becomes governed by the much slower process of diffusion into the polymer.[31, 32] Microgels were synthesised to maximise the surface area for rapid uptake while minimising the volume for diffusion. The rate of surface adsorption was estimated by the first hour of water uptake (**Table 1**). Diffusion effects became more prominent after 2 hours of uptake, and after 5 hours were the main contributor to water uptake. With short harvesting cycles, the effects of diffusion are limited. Notably, the rate of diffusion reduced with increasing HEMA composition, which is likely caused by strong HEMA self-association within the microgel. For rapid water cycling, uptakes should be conducted where surface adsorption is the dominant mechanism of water uptake. The ideal uptake time for these microgels during harvesting would therefore not exceed 1 hour.

Polymer	*Composition (NIPAAm:HEMA)*	*Initial uptake rate (mg/g/min)*	*Overall rate (mg/g/min)*
MG1	7:3	3.2	0.18
MG2	5:5	2.7	0.16
MG3	3:7	3.0	0.16

Table 1: Initial and overall uptake rate for ***MG1*** to ***MG3***. Initial uptake rate was calculated from the first hour of water uptake.

Understanding how size affected microgel water-harvesting behaviour was necessary for distinguishing the effects of other properties and synthetic changes. As the 7:3 microgel ***MG1*** showed the highest water uptake, we kept this feed ratio constant and varied the size of the microgels. In precipitation polymerisation, surfactant concentration can be used to control particle size.[34] During the reaction, polymer chains aggregate until a colloidally stable primary particle is formed. The primary particles serve as nucleation points for beads to grow and precipitate from the reaction mixture. Surfactant molecules stabilise polymer aggregates, allowing smaller and therefore more numerous primary particles to form.[35] The increased number of nucleation points reduces the final size of the resulting beads. Changes are appreciable even at surfactant concentrations far below the critical micelle concentration (CMC).[34] The previous set of microgels (***MG1***–***MG3***) were made with 2 mol% sodium dodecyl sulfate (SDS) (with respect to monomer), equivalent to ~25% of the CMC at room temperature. The molar ratio of surfactant used during polymerisation was reduced to form

two larger microgels: one was made using 1 mol% of surfactant w.r.t. monomer (***MG4***), and another with no surfactant (***MG5***).

Size analysis was used to further characterise this set of microgels as well as confirm thermoresponsive properties (**Figure 4a**). Reducing surfactant concentration was confirmed to cause increased microgel size. A linear relationship between surfactant concentration and microgel size was expected, though was not apparent in observed data.[34] The VPTT of all samples was identical (31°C), as would be expected due to their identical compositions of NIPAAm and HEMA. The largest microgel exhibited a slightly wider phase transition, fully deswelling at 35°C. As a microgel increases in size, the amount of energy to displace water for a thermoresponsive change increases, resulting in a wider phase transition.

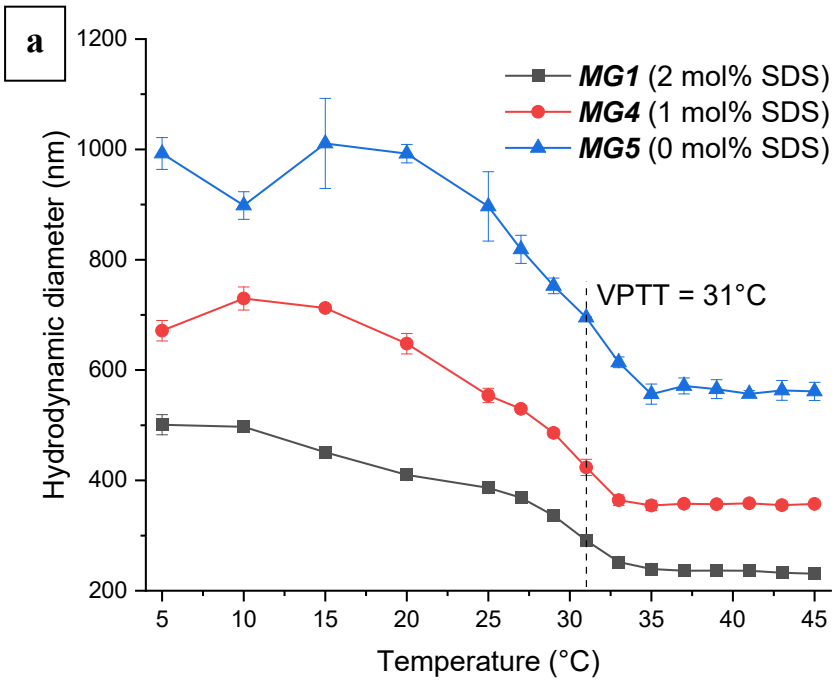

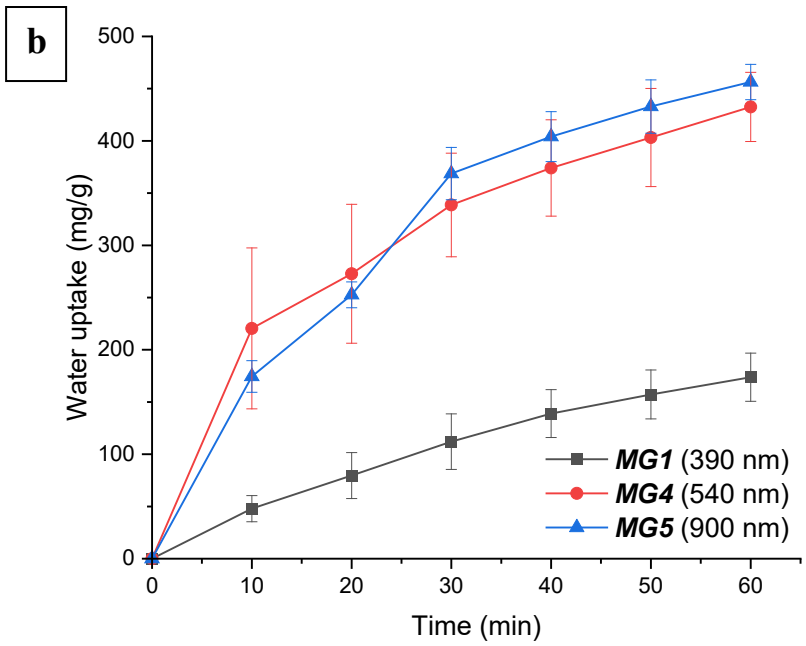

Figure 4: (a) Hydrodynamic diameter measured from 5°C to 45°C, showing how size affects thermoresponsive behaviour. (b) Water uptake over 1 hour, showing the effects of microgel size on water uptake.

The water uptake properties of these microgels relative to size were then recorded (**Figure 4b**). Water uptake was only recorded over 1 hour as this period was when the rate of uptake was governed by adsorption. Both the larger microgels absorbed over twice as much water as the 390 nm ***MG1*** microgel over 1 hour, around 450 mg/g. Over the hour, the 900 nm ***MG5*** microgel had a slightly higher rate of uptake over the 540 nm ***MG4*** (**Table 2**). The majority of water uptake in this timeframe was likely to be limited to surface adsorption, and therefore was fully dependent on exposed surface area. SEM images of all three microgels showed tight, almost fused packing of spheres with no visible inter-sphere voids (**Figure 5**). While ***MG1*** showed a mostly smooth surface, ***MG4*** and ***MG5*** had visible bumps, increasing their total surface area. Individual beads were observed to protrude more as microgel size increased. Water uptake is therefore dependent on surface area resulting from microgel packing, which is in turn affected by microgel size. It is likely that further increasing the microgel size of this system would continue to reduce the contact between each bead and therefore expose more surface area for water harvesting. At the same time, increasing microgel size would reduce the ratio of surface area to volume, decreasing the amount of rapid surface adsorption relative to diffusion. The optimal size for any microgel system must therefore account for these opposing trends.

Polymer	*Surfactant (mol%)*	*Uptake rate (mg/g/min)*	*Hydrodynamic diameter (nm)*
MG1	2	3.2	390
MG4	1	8.8	450
MG5	0	8.9	900

Table 2: Water uptake rate for ***MG1***, ***MG4*** and ***MG5***, showing effects of microgel size.

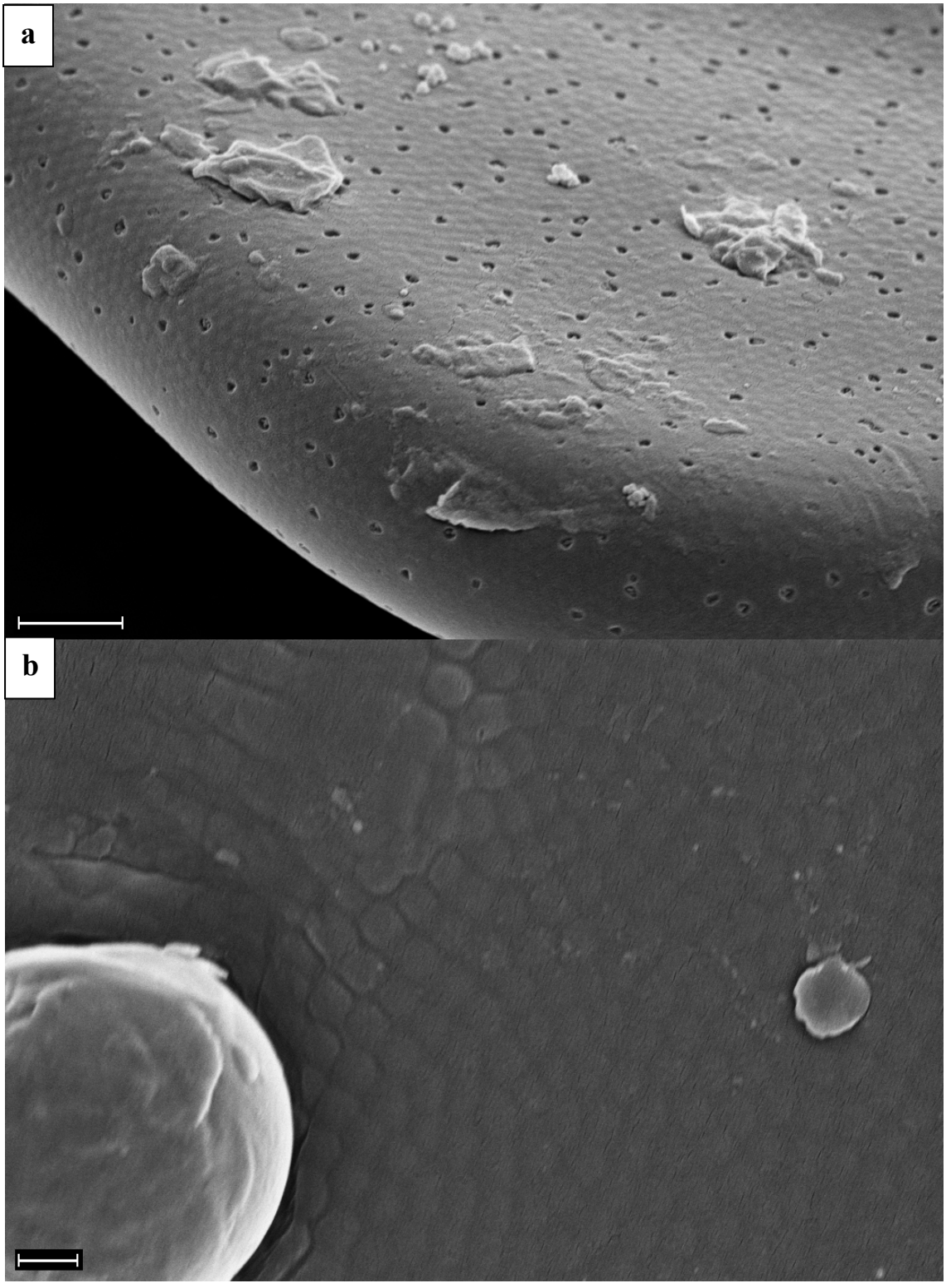
a
b

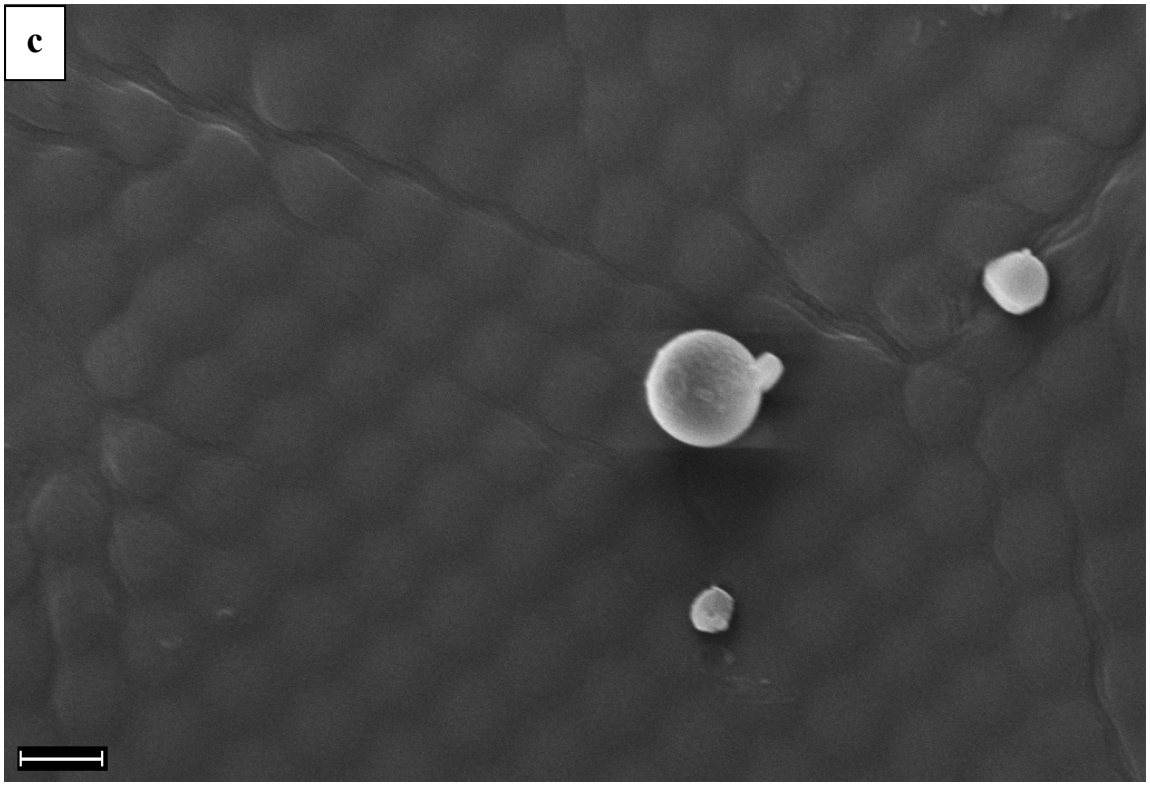

Figure 5: SEM images of dried ***MG1*** (a), ***MG4*** (b) and ***MG5*** (c), showing the effect of microgel size on packing. Scale bars are 1 μm, 400 nm and 400 nm respectively.

While this reveals that microgel size has a significant effect on water harvesting properties, precise control of size is difficult when varying other aspects of synthesis such as composition. In an ideal setting, microgel size would be kept consistent across other synthetic changes. There is a linear relationship between microgel size and surfactant concentration in precipitation polymerisation; however, this can only be determined experimentally for each polymer.[34] It would therefore be necessary to have a range of microgel sizes for each synthetic iteration before the target size could be achieved. For practicality in subsequent functionalisation experiments, microgel size was not controlled but still recorded.

We previously showed the ability of the guanidinium moiety to enhance water harvesting properties.[17] In that work, *L*-arginine was used as a source of guanidinium and was incorporated via post-functionalisation. Protection of the arginine was necessary to prevent self-polymerisation during functionalisation. While *L*-arginine functionalisation could easily be applied to these microgels in the same way, deprotection steps to liberate the hygroscopic functionalities were laborious and atom inefficient. Creatine was considered as a viable alternative for several reasons. Firstly, while its guanidinium moiety has an additional methyl group, the molecule is hygroscopic enough to spontaneously form a monohydrate under

ambient conditions.[36, 37] This hygroscopicity has not yet been utilised for SAWH purposes. Secondly, the use of creatine avoids the use of protecting groups. Thirdly, it increases muscle water retention in the short term (albeit by osmosis mechanisms).[21] Finally, it is safe, affordable and available in large quantities, opening the possibility for future scalability.

We hoped to preserve thermoresponsivity even with the addition of creatine to our microgels. ***MG1***, with the most NIPAAm, was more likely to preserve thermoresponsive properties after functionalisation. ***MG2***, with more HEMA, could be functionalised to a higher degree, which would greatly improve water uptake. ***MG1*** and ***MG2*** were therefore used as the basis of the functionalised microgels. Technically, ***MG3*** had the most available functionalisation handles as it had the most HEMA, however the baseline thermoresponsive properties were anticipated to provide a narrower window of tolerance to modification.

Using ***MG1*** and ***MG2***, we modified these with creatine, varying the degree of functionalisation on each (**Figure 6**, **Scheme S2**). We converted creatine (***1***) to its acyl chloride (***2***) as an effective route to esterification.[38] To account for the air and water sensitivity of ***2***, a slurry of the microgel with excess triethylamine (to neutralise HCl byproduct) in dry DCM was added to facilitate the acylation of microgel HEMA. Functionalisation was confirmed with FTIR spectroscopy after purification of the microgels (**Figures S6–9**). HEMA alcohol O-H stretches (~3300 cm^{-1}) were still visible after functionalisation, indicating functionalisation did not go to completion.

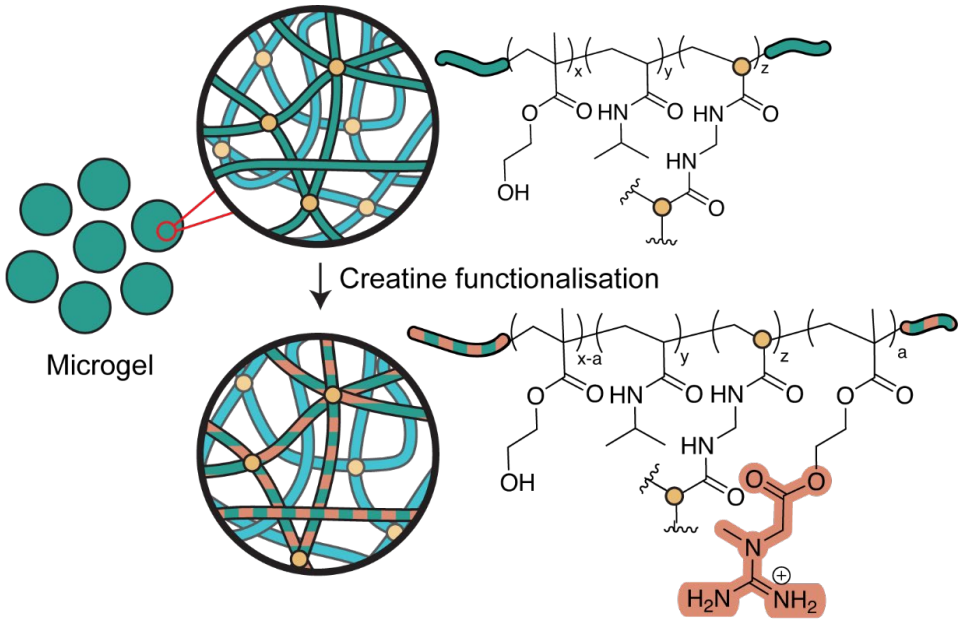

Figure 6: Graphical representation and chemical structure of microgels before and after creatine functionalisation.

We varied the degree of creatine functionalisation for each microgel composition. Given the insoluble nature of the microgels, it is difficult to directly quantify the degree of functionalisation; we thus conducted a range of reactions using varied equivalents of acyl chloride. This way, a qualitative comparison could be made between microgels with differing degrees of functionalisation. With respect to the calculated amount of HEMA that could be functionalised on the microgels, we elected to use 1.0 and 10 equivalents of creatine for functionalisation. From ***MG1*** (7:3 composition), this yielded ***MG6*** and ***MG7***, while ***MG2*** (5:5) yielded ***MG8*** and ***MG9***. This large range of functionalisation was expected to illustrate differences in properties of the esterified gels. Additionally, a tenfold excess of ***2*** was expected to guarantee complete or near-complete functionalisation of the microgels, thus we treated ***MG7*** and ***MG9*** as such. Unfortunately, given the insoluble nature of these microgels, no viable means of quantitative analysis for determining the actual degree of functionalisation was available to us, and so we instead focused on assessing the changes in the physical properties of the gels, particularly particle size, thermal responsivity and hygroscopicity.

Size analysis was then conducted on functionalised microgels (**Figure 7**). Resuspension of functionalised microgels in Milli-Q water proved challenging even after 4 days of vigorous stirring. Creatine functionalisation, as we expected, increased the size of microgels, and this was particularly apparent comparing the fully functionalised ***MG9*** to the pristine ***MG2***. ***MG7*** was too prone to visible sedimentation for accurate size analysis, thus it was omitted from the graph (**Figure S11**). The resuspension process may have been unsuccessful if strong polymer-polymer interactions were formed in the dry state. Interestingly, the 0.5 and 1.0 equivalent functionalised microgels showed very similar average sizes across both comonomer compositions, implying similar degrees of functionalisation. Despite the expected additional hydrophilicity of the functionalised microgels, they did not exhibit the same degree of swelling as the thermoresponsive base microgels. Creatine is known to spontaneously form creatine monohydrate and precipitate from aqueous solutions.[39] The functionalised polymers may have inherited this property.

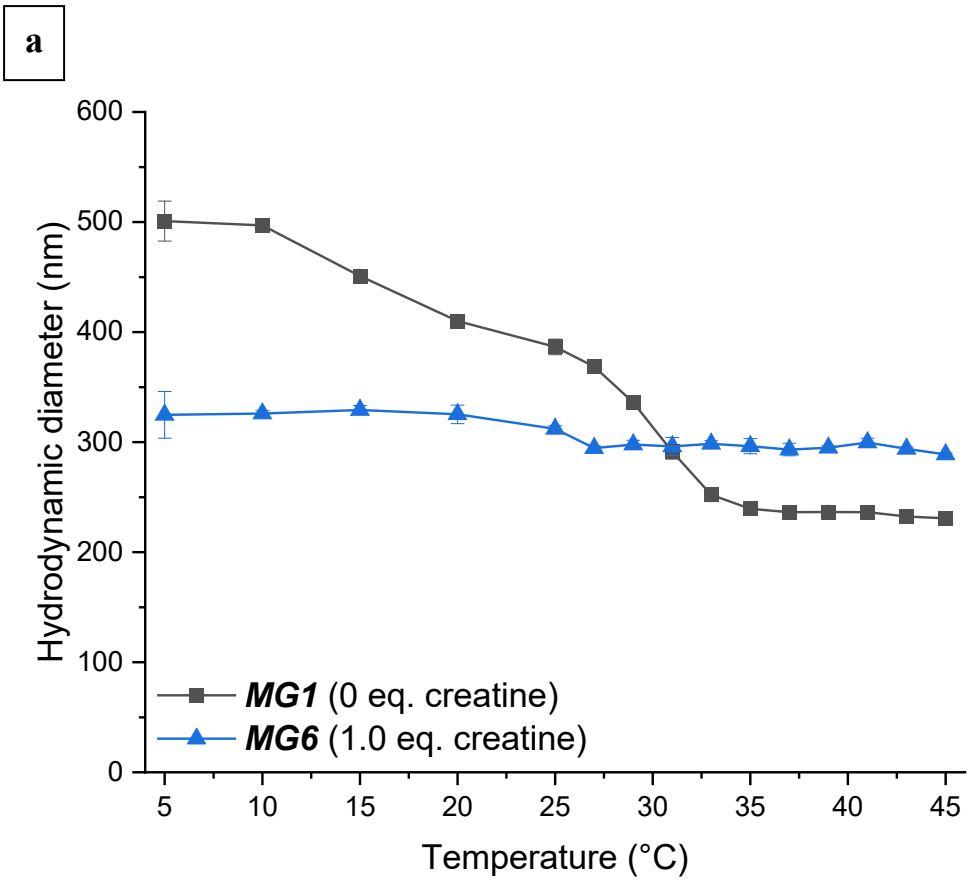
a
Hydrodynamic diameter (nm)
600
500
400
300
200
100
0
5
10
15
20
25
30
35
40
45
Temperature (°C)
MG1 (0 eq. creatine)
MG6 (1.0 eq. creatine)

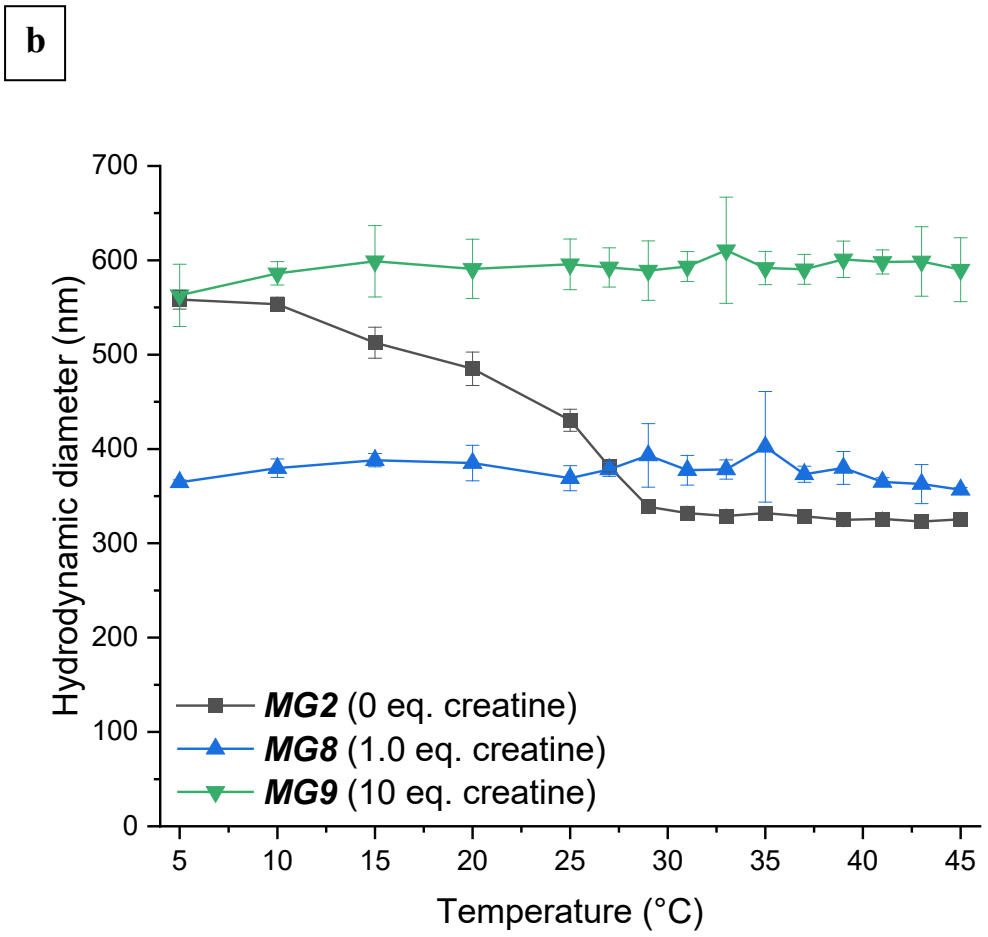

Figure 7: Hydrodynamic diameter measured from 5°C to 45°C, showing how functionalisation affected thermoresponsive behaviour starting with a (a) 7:3 composition and (b) 5:5 composition.

Size analysis showed virtually no thermoresponsive properties for all creatine-functionalised samples. Apart from hydrophilicity, charged side chains can flatten and erase thermoresponsive behaviour.[40] The guanidinium moiety of creatine has a pK_a of 12.7, thus the functionalised side chain would likely be charged at neutral pH.[41] The additional hydrophilicity and charge arising due to creatine functionalisation was likely the primary factor removing thermoresponsive behaviour. Thermoresponsive properties depend on an amphiphilic balance, thus these properties could potentially be restored by introducing hydrophobicity into the microgel.[40]

We then studied the water uptake of all functionalised samples over 1 hour (**Figure 8**). From the 7:3 microgel composition, functionalisation with 1.0 equivalent (***MG6***) of creatine reached adsorptive saturation after 10 minutes, then stabilised. The rate of uptake exceeded that of the non-functionalised microgel, which consistently adsorbed water over the entire hour (**Table 3**). These two samples had comparable total uptake after 1 hour at about 150

mg/g. The addition of creatine, even at our smallest equivalent attempted, noticeably improved the rate of water uptake. We found that ***MG7*** (10 eq.) exceeded both ***MG1*** and ***MG6*** in rate and total uptake. The average rate of uptake was 22 mg/g/min for ***MG7***, which was almost 7 times faster than the non-functionalised microgel. The total uptake of ***MG7*** exceeded 1000 mg/g after 1 hour. For the samples based on a 5:5 composition microgel, the results were very similar. The total uptake of ***MG9*** (10 eq.) was 1800 mg/g after 1 hour, presumably due to the higher degree of creatine-functionalised side chains. High water uptake is generally imparted by the use of hygroscopic salts in SAWH polymers. Uptake can range from about 0.5 to 2.5 g/g in 1 hour, at similar RH conditions, meaning creatine functionalisation is able to compete with hygroscopic salts.[5, 42] The results of ***MG7*** and ***MG9*** show that creatine functionalisation greatly improved water uptake capacity, though the reduction of HEMA self-association was also a potentially contributing effect. While the error bars on these two samples were large, even the lower end of the error bars showed a 490% and 965% increase in water uptake from the non-functionalised 7:3 and 5:5 composition microgels respectively after 1 hour. Anhydrous creatine spontaneously undergoes hydration to form creatine monohydrate at 70% RH, which translates into a maximum 14% increase in mass (**Figure S14**).[43, 44] When functionalised onto the microgel, the mechanism of hydration becomes largely dependent on the charged guanidinium groups present. This overall cationic charge enhances both the water uptake rate and capacity of the polymer. Microgel packing also contributed to the improved water uptake of the functionalised microgels. ***MG8*** and ***MG9*** packed as discrete spheres with visible inter-sphere voids, while ***MG2*** had no visible voids and showed tight, fused microgel packing (**Figure 9**). This correlates with the faster rate of uptake of the functionalised microgels. The diameter of all three microgels measured through SEM imaging ranged between 240–280 nm, i.e. exhibiting little-to-no size difference (**Table S1**). A minimal difference in packing between ***MG8*** and ***MG9*** indicated that creatine functionalisation was the major contributor to the change in water uptake. Because of the multiple changing variables between each functionalised microgel, a strong conclusion about the exact contribution of degree of functionalisation, size and packing to water uptake is difficult to make. Regardless, the effect of creatine functionalisation on water uptake is clearly significant.

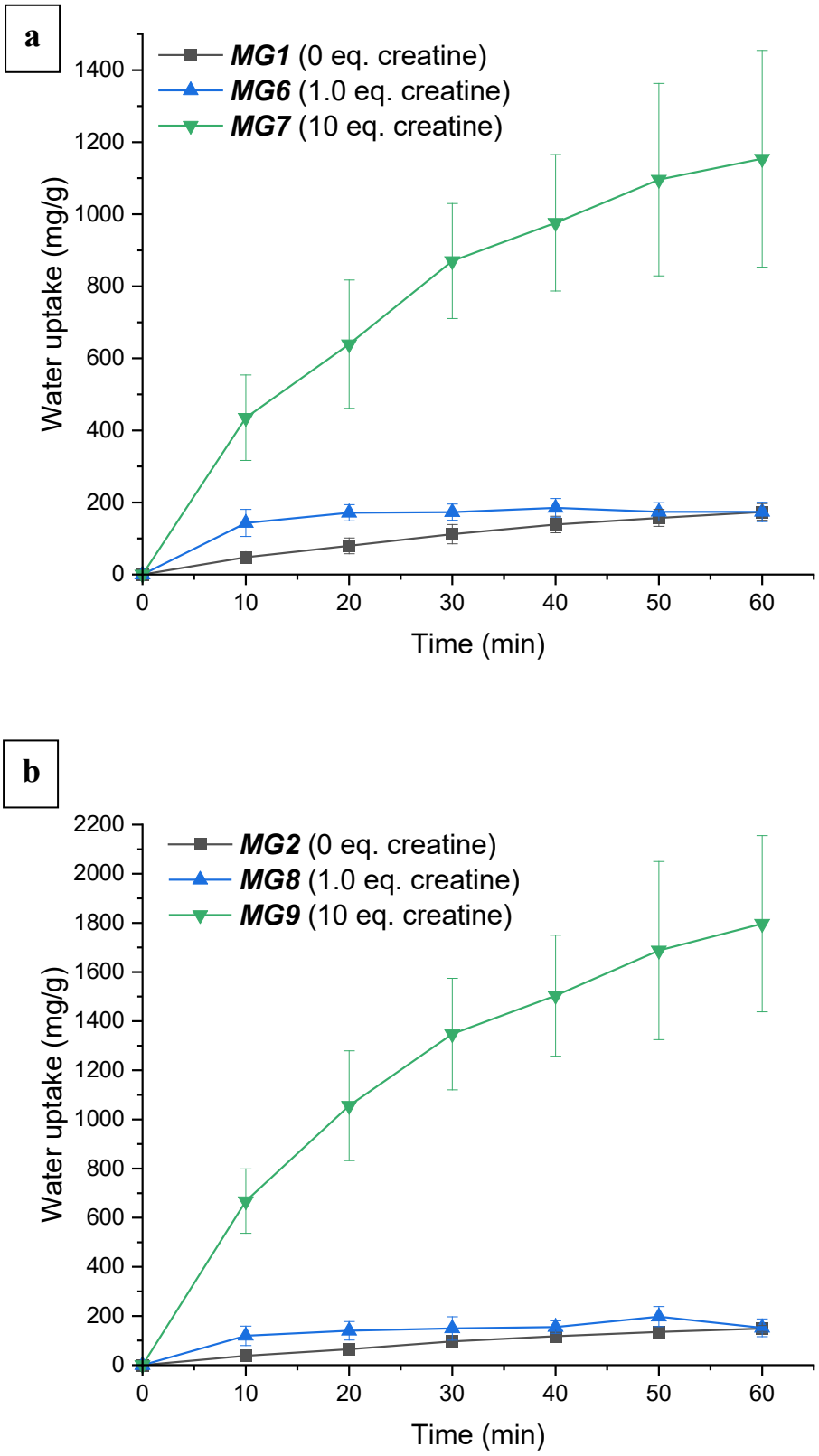

Figure 8: Water uptake over 1 hour, showing effects of degree of creatine functionalisation from a (a) 7:3 composition and (b) 5:5 composition microgel.

Polymer	*Original composition (molar ratio NIPAAm:HEMA)*	*Equivalents of creatine to HEMA*	*Uptake rate (mg/g/min)*
MG1	7:3	0	3.2
MG6		1	4.1
MG7		10	22
MG2	5:5	0	2.7
MG8		1	3.9
MG9		10	35

Table 3: Water uptake rate for ***MG1***, ***MG2*** and ***MG6***–***MG9***, showing effects of functionalisation.

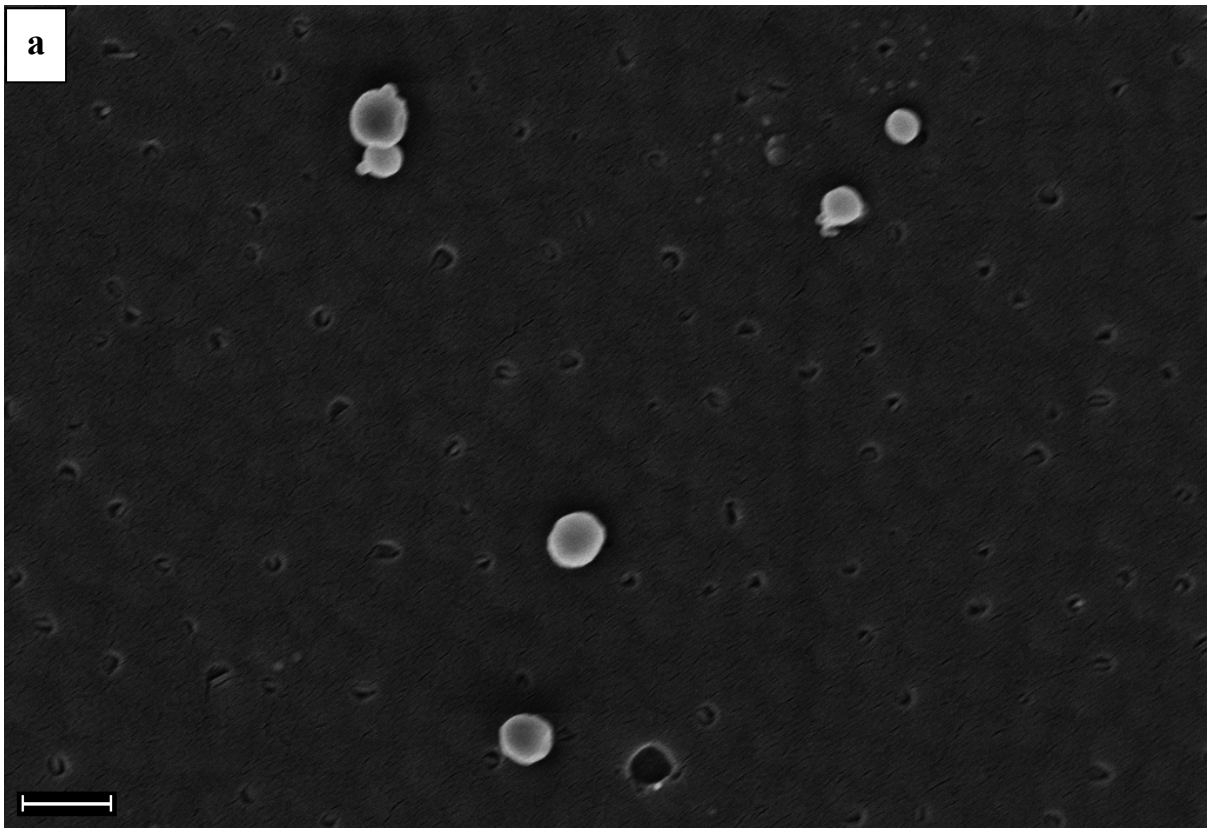

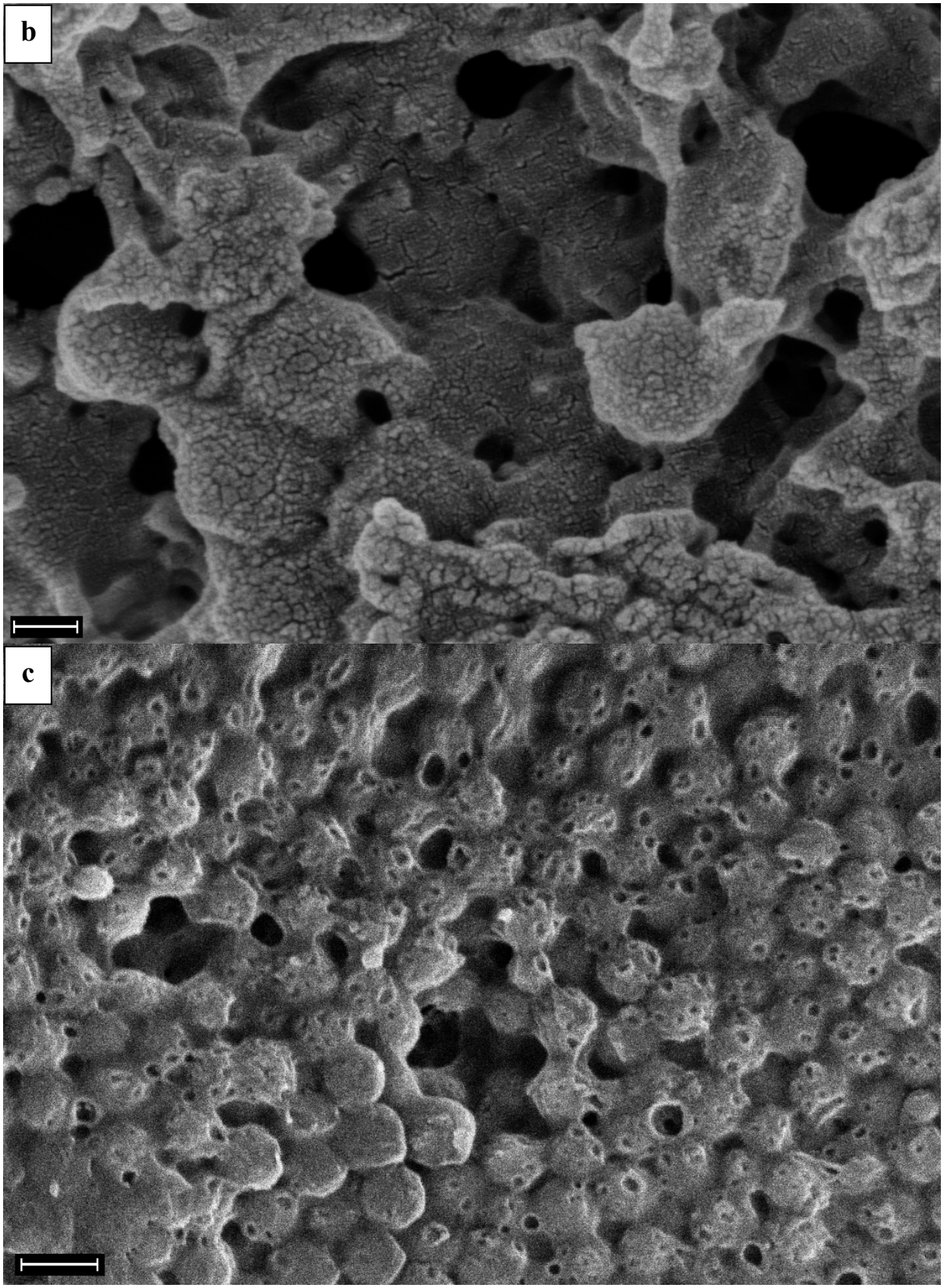

Figure 9: SEM images of dried ***MG2*** (a), ***MG8*** (b) and ***MG9*** (c). Scale bars are 500 nm, 100 nm and 300 nm respectively.

As creatine functionalisation improved water uptake, it simultaneously reduced the rate of release, which is critical for fast water harvesting. We used standard harvesting conditions of 30 minutes uptake (70% RH, 23°C) and 20 min release (70°C) to investigate the optimal systems. ***MG5*** (7:3 composition, 900 nm) had the strongest potential for water harvesting, with a projected water yield of 12.8 g/g/day with 50-minute cycles. Out of the functionalised samples, ***MG9*** (5:5 composition, 10 eq.) performed the best (11.1 g/g/day). These results, compared to the thermoresponsive ***MG5***, highlighted the importance of thermoresponsive properties in bypassing the trade-off between uptake and release performance.

We next investigated cycling experiments with ***MG5*** as the lead candidate. Cycling was performed with the previous harvesting conditions with about 200 mg of polymer (**Figure 10**). From these results, the projected yield was about 9.8 g/g/day based on an average observed cycle. Fluctuations in water release reduced the projected water yield compared to the previous set of experiments. We did not observe any overall decay in either water uptake or release over 10 cycles.

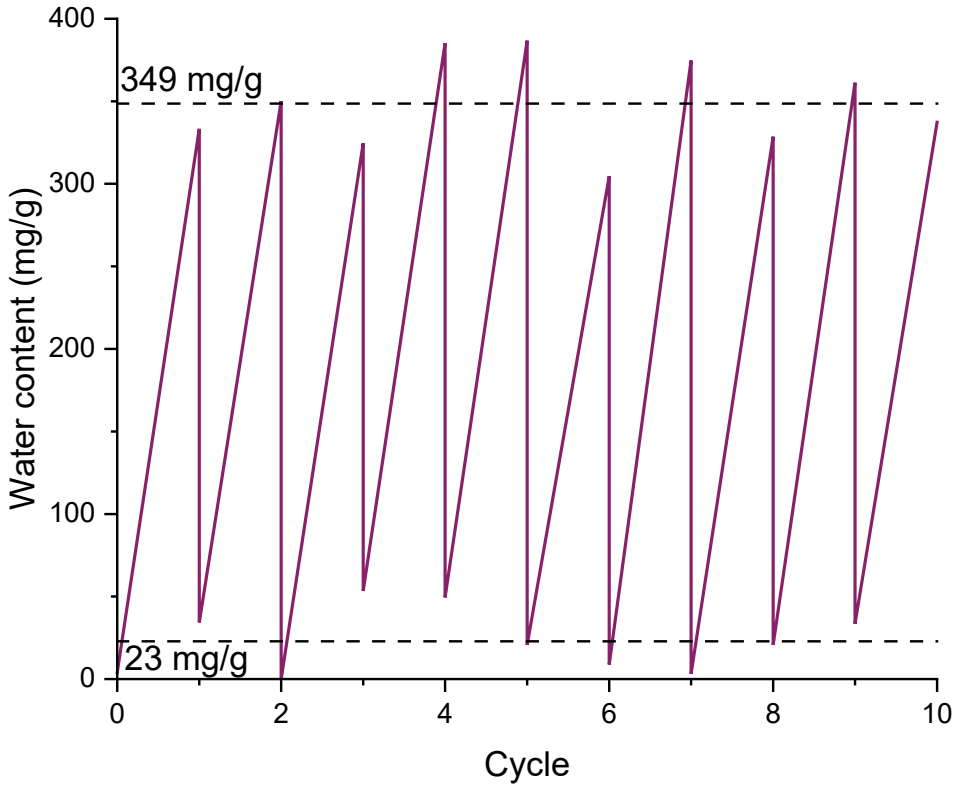

Figure 10: Water harvesting cycling data of ***MG5*** (7:3 composition, 900 nm) at sub-gram scale, showing minimal/no decay of performance. Uptake cycles were conducted at 70% RH at around 23°C for 30 minutes, while release cycles were conducted in a 70°C oven for 20 minutes. The mean water content is given for both uptake and release.

Comparison of our work to existing literature shows strong performance compared to other SAWH polymers prepared without hygroscopic salts (**Table 4**). Water harvesting yield is mainly dependent on the number of cycles conducted per day. Many of these polymers were envisioned for passive use (i.e. depending solely on the day-night cycle), which simplifies the field usage of the polymer by removing energy considerations (solar energy is free and in excess). Water uptake kinetics slow with longer absorption cycles which limits the potential of these passive systems. Shorter, more consistent water harvesting cycles require an external energy vector to maintain, but are able to maximise water yield.[33] To take full advantage of shorter harvesting cycles, rapid water harvesting kinetics are hence necessary. This can be achieved either through the incorporation of hygroscopic salts or by maximising polymer surface area. Very few authors have used spherical particles for SAWH polymers, and these generally accompany a ratcheted method of water harvesting.[6-8] The most direct comparison

to our work can be made with the PNIPAAm-based microgel by Guan and coworkers.[6] Even with the different RH for uptake, our work was able to achieve a comparable daily yield without the incorporation of hygroscopic salts.

Reference	*Daily Yield (g/g)*	*RH during uptake (%)*	*Cycles per day*	*Hygroscopic Component*
5	13	30	24	LiCl
6	11	60	12	LiCl
7	19	30	36	LiCl
8	3.0	90–100	1	Alg
17	2.0	70	~21	Arg
18	57	97	16	Alg and LiCl
42	1.3	40–80	1	PAAS
45	2.5	~60	1	LiCl
46	32 mg/cm^2	100	1	DOMA
47	0.3	43	1	Sulfonate groups
This work	9.8	70	29	NIPAAm/HEMA

Table 4: Comparison of SAWH polymers by daily yield.

We next attempted to demonstrate the potential of ***MG5*** as a SAWH material at a larger scale. ***MG5*** was synthesised at a 5 g scale, and the rate of uptake under 70% RH was tested under conditions identical to those employed throughout this body of work. It was confirmed that this new batch was physically and chemically identical to the first batch, gratifyingly demonstrating the reproducibility and scalability of our system, and on the sub-gram scale the cycling behaviour was essentially identical between the two batches. However, increasing the sample scale of the water harvesting test to a sample size of 5 g drastically reduced the rate of uptake and the total water uptake, with a maximum of 130 mg/g reached after one day which did not increase despite being held in humid conditions over several days. These results reflect limitations in the experimental set-up, which would require an engineering or a device-based solution to effectively conduct water harvesting at larger scales.

Conclusion

In summary, we presented poly(NIPAAm-*co*-HEMA) microgels as a viable thermoresponsive SAWH material. A series of microgels was synthesised to identify structure-property relationships for water harvesting. Notably, microgel size had significant effects on water harvesting. Water uptake reached 450 mg water per g polymer after 1 h at 70% RH for this set of microgels. Creatine functionalisation was also conducted in an attempt to increase the water harvesting capacity. Functionalisation greatly improved microgel water uptake, up to 1.8 g/g after 1 h at 70% RH. While thermoresponsive properties were erased after functionalisation, these microgels had strong desiccating potential. Preliminary water uptake-release cycling experiments of our best-performing microgel demonstrated a potential yield of 9.8 g/g after 24 hours with 50-minute cycles, which we hope to harness in the future through SAWH device development. These outcomes present not only one of the highest-performing additive-free SAWH hydrogels to date but also the potential of polymer microgels as an underutilised class of SAWH materials.

Experimental Section

Sodium dodecyl sulfate (SDS) was purchased from Fluka. Creatine monohydrate was purchased from MuscleTech and was dehydrated at 100°C before use. *N*-isopropylacrylamide (NIPAAm, stabilised with MEHQ) was purchased from TCI and a 1 M stock solution in RO water was used for synthesis. All other chemicals were purchased from Sigma-Aldrich and were used as purchased with the exception of 2-hydroxyethyl methacrylate (HEMA, containing ≤50 ppm MEHQ as inhibitor). For monomers containing MEHQ inhibitor, basic-alumina chromatography was conducted to remove inhibitors immediately prior to polymerisation.

Lyophilisation was conducted in a Buchi Lyovapor L-200 freeze dryer. Microgel suspensions were first frozen at -18°C until fully solid before lyophilisation, whereas samples with trace amounts of water were dried directly. FTIR spectroscopy was conducted on a Perkin Elmer Spectrum 2 using lyophilised samples. Dynamic light scattering measurements were conducted using a Malvern Zetasizer Ultra Red size and zeta potential analyser. Water uptake experiments were conducted inside a custom set-up as shown in our previous work.[30] Humidity and ambient temperature were measured using a RS PRO RS-1260 hygrometer. Field emission electron scanning microscopy (FESEM) images were taken at 3 kV using a

Zeiss Crossbeam 550 FIB-SEM. Samples were desiccated and coated with platinum before analysis.

Synthesis of poly(HEMA-*co*-NIPAAm) microgels

Microgels were formed using free radical precipitation polymerisation as described in a previous study.[14] NIPAAm, HEMA, SDS and N,N-methylenebisacrylamide (BIS) crosslinker were dissolved in RO water in a three-necked round bottom flask. The reaction was stirred at 600 rpm under a nitrogen atmosphere at 70°C with a condenser attached to the flask. After 1 hour, ammonium persulfate (APS) dissolved in 5 mL of RO water was added to the reaction mixture to initiate the polymerisation. The reaction was allowed to proceed for 5 hours. The resulting suspension was dialysed (cutoff 14 kDa) with twice-daily water changes for 2 days.

A detailed procedure for ***MG1*** with a NIPAAm:HEMA molar ratio of 7:3 is provided. NIPAAm (7.0 mL 1.0 M solution, 792 mg, 7.00 mmol), HEMA (390 mg, 3.00 mmol), BIS (30.8 mg, 0.20 mmol) and SDS (57.7 mg, 0.2 mmol) were added to 88 mL RO water (for a total of 95 mL water) in a 250 mL three-necked round bottom flask. A condenser was attached to the flask and the mixture was allowed to stir at 600 rpm under a nitrogen atmosphere at 70°C for one hour. APS (54.8 mg, 0.24 mmol) was dissolved in 5.0 mL water then added into the reaction mixture to initiate the polymerisation. The reaction mixture became turbid within the first half hour and was allowed to react for 5 hours. The resulting mixture was a white and turbid suspension. Dialysis was performed to remove surfactant and unreacted monomers over 2 days (cutoff 14 kDa). Some of the suspension was reserved for size analysis, with the rest lyophilised for subsequent experiments.

Creatine functionalisation procedure

The acyl chloride conversion was adapted from a previous work.[38] A three-neck round bottom flask containing creatine (1 eq.) and anhydrous dichloromethane (DCM) was sealed and placed under a nitrogen atmosphere. The flask was cooled to 0–5°C with stirring. Thionyl chloride (1.2 eq.) was added dropwise to the flask and the ensuing mixture was allowed to react for one hour to form the creatine acyl chloride. While still maintaining 0–5°C reaction conditions, one neck of the three-neck flask was opened while maintaining an internal nitrogen atmosphere in order to allow venting of the HCl vapour formed during the next step. A slurry of microgel (200 mg), triethylamine (TEA, 2 eq. relative to creatine) and anhydrous DCM was injected slowly into the flask. The reaction mixture changed from white to bright yellow and became turbid. Once the white HCl vapour had completely disappeared, the flask

was resealed while maintaining a nitrogen atmosphere. The functionalisation was then allowed to proceed at room temperature for 24 hours. The resulting brown mixture was concentrated under reduced pressure, and the solids were purified via dialysis for either two days, or until the dialysis water ran clear. The samples were then lyophilised to yield fine brown powders.

A detailed procedure for ***MG7***, using ***MG1*** as the parent polymer with ten equivalents of creatine relative to microgel HEMA content is provided. Creatine (644 mg, 4.91 mmol) was mixed with 100 mL anhydrous DCM in a 250 mL three-necked round bottom flask. The mixture was cooled to 0–5°C in an ice bath and was cycled under a nitrogen atmosphere. Thionyl chloride (534 µL, 7.37 mmol) was added dropwise, then the reaction was allowed to proceed for 1 hour. After 1 hour had passed, one neck of the flask was opened to vent HCl vapour formed during the next step, with the positive pressure from nitrogen flow maintaining the air-free conditions inside the flask. A mixture of ***MG1*** (200 mg, containing about 0.49 mmol HEMA side chains) and triethylamine (1.36 mL, 9.82 mmol) was wetted with 5.0 mL anhydrous DCM, and the resulting microgel slurry was injected slowly. The subsequent reaction was exothermic and generated voluminous HCl vapours, with the colourless reaction mixture becoming bright yellow. Once the slurry was added and HCl vapour ceased to form, the flask was sealed once again and the nitrogen flow maintained. The reaction was allowed to proceed for 24 hours at 23°C, during which time the bright yellow mixture changed to brown. The flask was opened to atmosphere, and the contents were transferred into a 200 mL round bottom flask to be dried under reduced pressure. The resulting brown solid was then purified by dialysis for two days with frequent water changes. After lyophilisation, the purified, functionalised microgel sample was afforded as a brown powder.

Water uptake measurements

Samples were lyophilised overnight prior to water uptake experiments to minimise residual water. Silicone moulds containing samples were then placed into a custom humidity chamber, in which the temperature was consistently 23°C and average humidity was 70% RH.[30] Samples were removed, weighed and returned to the box as quickly as possible. Water content was determined as the mass of water per gram of polymer. For the first hour, measurements were conducted every ten minutes, then once every hour for the next 5 hours, then once more 24 hours after the experiment was commenced. All samples after ***MG3*** were

only weighed over a 1-hour period in the manner described here. Mean values were taken from a minimum of three trials for each sample and no outliers were discarded.

Water uptake measurements were conducted for ***MG2***, ***MG8*** and ***MG9*** at 50% and 30% RH, and are presented in the Supplementary Information.

Microgel size and VPTT measurements

Microgel size measurements were measured using dynamic light scattering on a Malvern Zetasizer Ultra Red size and zeta potential analyser. Approximately 0.1 mg/mL suspensions in MilliQ water were used with a scattering angle of 90°. Samples were allowed to equilibrate at set temperatures for 2–5 minutes before commencing measurement. All data points were recorded in triplicate. VPTT was determined as the temperature with the highest first derivative, where the first derivative was calculated using the slopes with the two neighbouring points.

SEM microgel size analysis

SEM images were taken of the following microgels over several magnifications: ***MG1***, ***MG2***, ***MG4***, ***MG5***, ***MG8*** and ***MG9***. Microgel size of these polymers was measured using Adobe Photoshop. The mean average diameter for each microgel was determined by making a total of ten measurements using the ruler tool over several SEM images.

Water uptake-release cycling

For cycle optimisation, about 100 mg of lyophilised polymer was placed in a small silicone mould. 30 minutes of uptake was enough to reflect sample water harvesting kinetics while also maximising adsorption. Release time and temperature were determined using samples after 30 minutes of water uptake. Samples were placed in a lab oven maintained at 50°C, 60°C or 70°C. Sample mass was monitored over 1 hour, with measurements taken every 10 minutes. Optimal cycling conditions were determined by projected daily yield with 30 minutes of uptake. Water release was observed at all temperatures, with the greatest release occurring within the first 20 minutes. Cycling conducted at 70°C yielded the most complete release within 20 minutes and was the only temperature where full release was observed within 1 hour, thus this time and temperature were chosen for water release.

After cycle optimisation, ***MG5*** was lyophilised for 18 h. The water uptake method described immediately above was followed with measurements taken after 30 minutes. After this, the

sample was placed into an oven maintained at 70°C. After 20 minutes, the mass of the sample was recorded and then the sample was returned to the humidity box. This uptake-release cycle was repeated for another 9 cycles.

To test the uptake capabilities of the large-scale ***MG5***, an unsealed silicone tray was filled with the lyophilised polymer then placed into the humidity chamber and changes in mass monitored over time.

Reaction Schemes

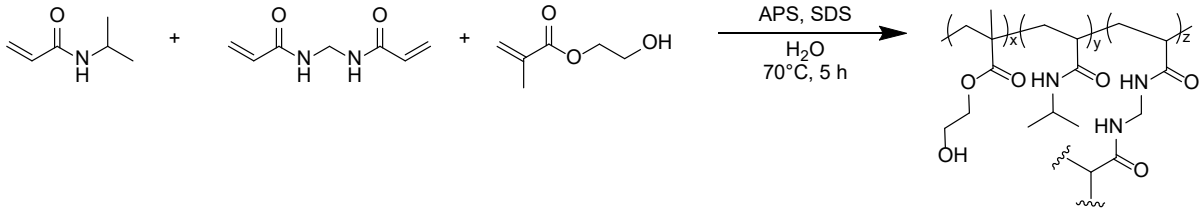

Scheme S1: Precipitation polymerisation of poly(NIPAAm-*co*-HEMA) microgels.

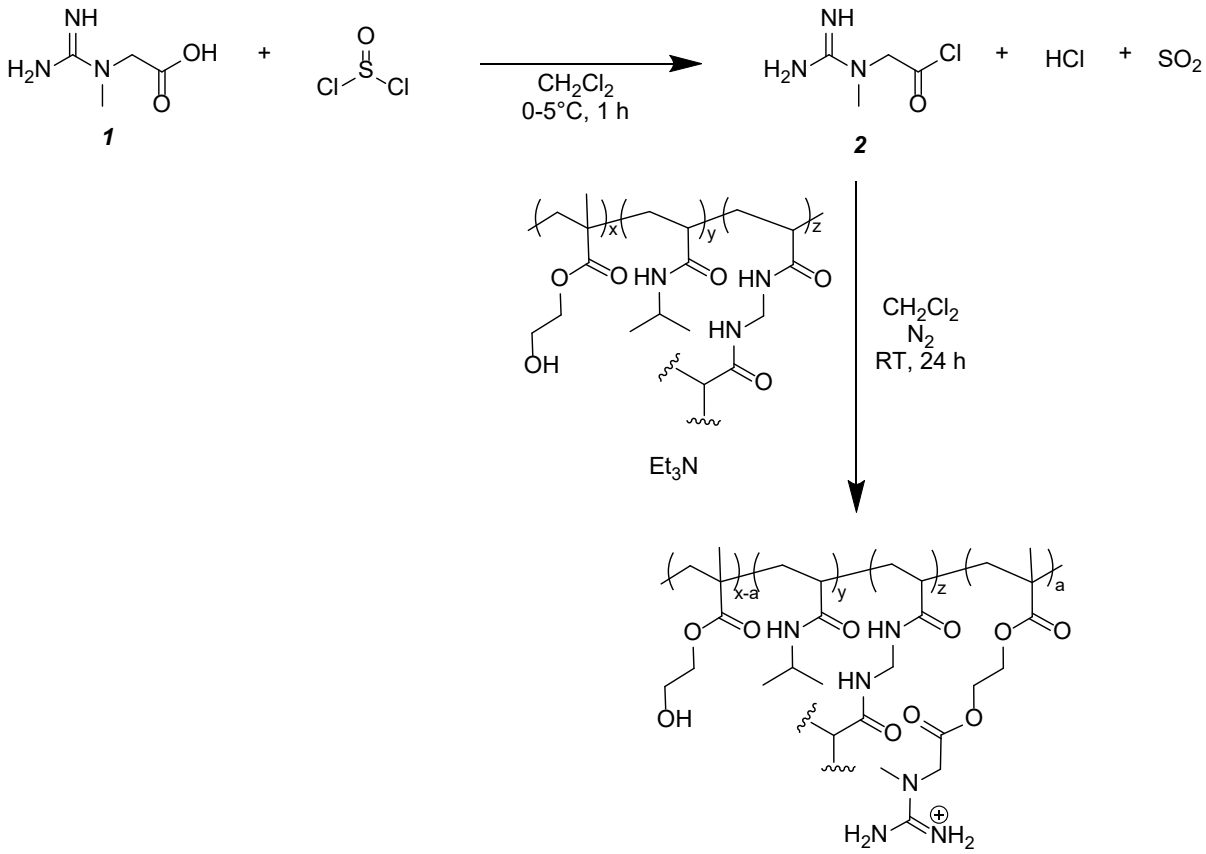

Scheme S2: Schemes showing conversion of creatine (***1***) to its acyl chloride (***2***) (top) and subsequent functionalisation of microgel HEMA side chains (bottom).

FTIR spectra

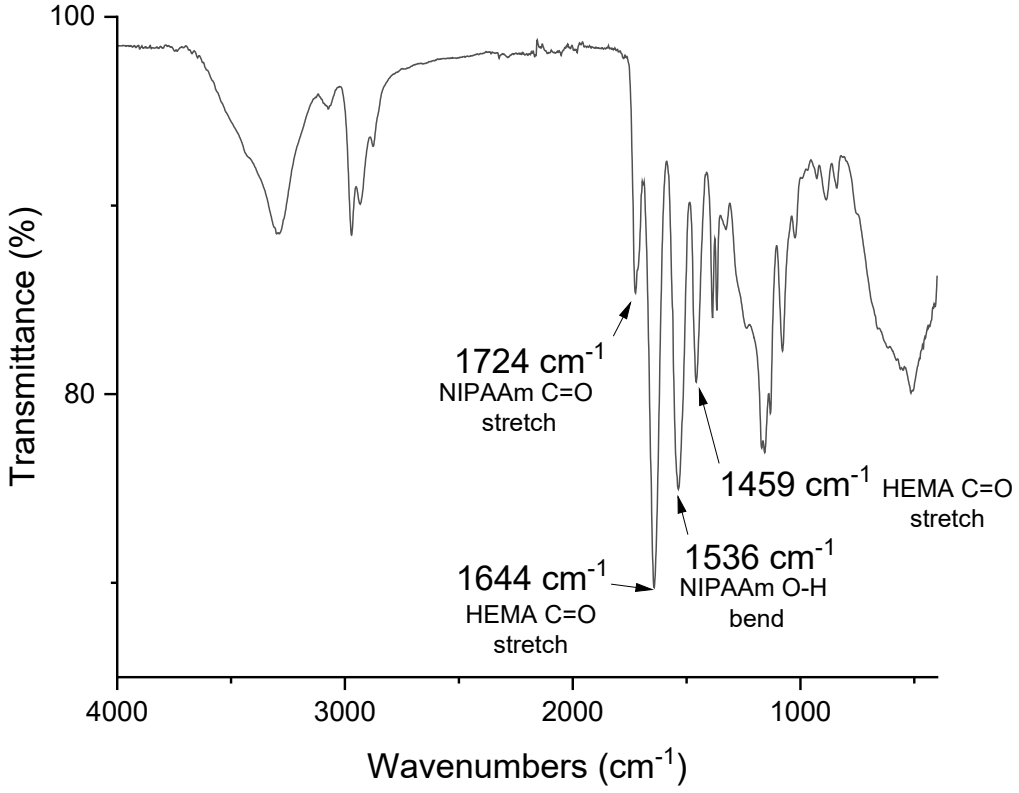

Figure S1: FTIR spectrum of poly(NIPAAm-*co*-HEMA) microgel with 7:3 NIPAAm:HEMA molar ratio (***MG1***)

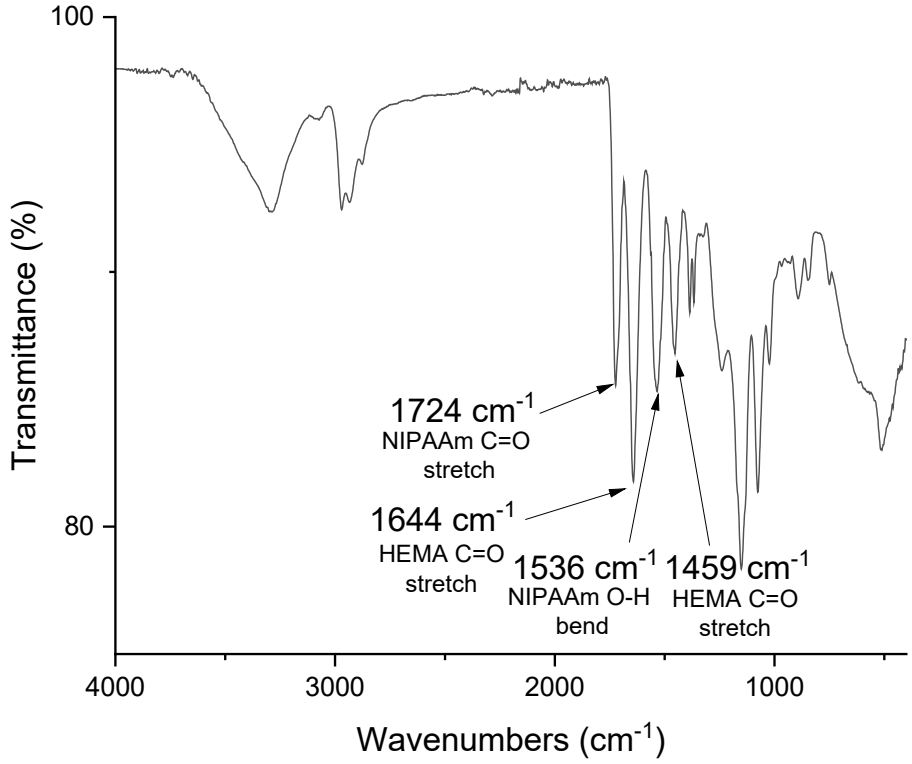

Figure S2: FTIR spectrum of poly(NIPAAm-*co*-HEMA) microgel with 5:5 NIPAAm:HEMA molar ratio (***MG2***)

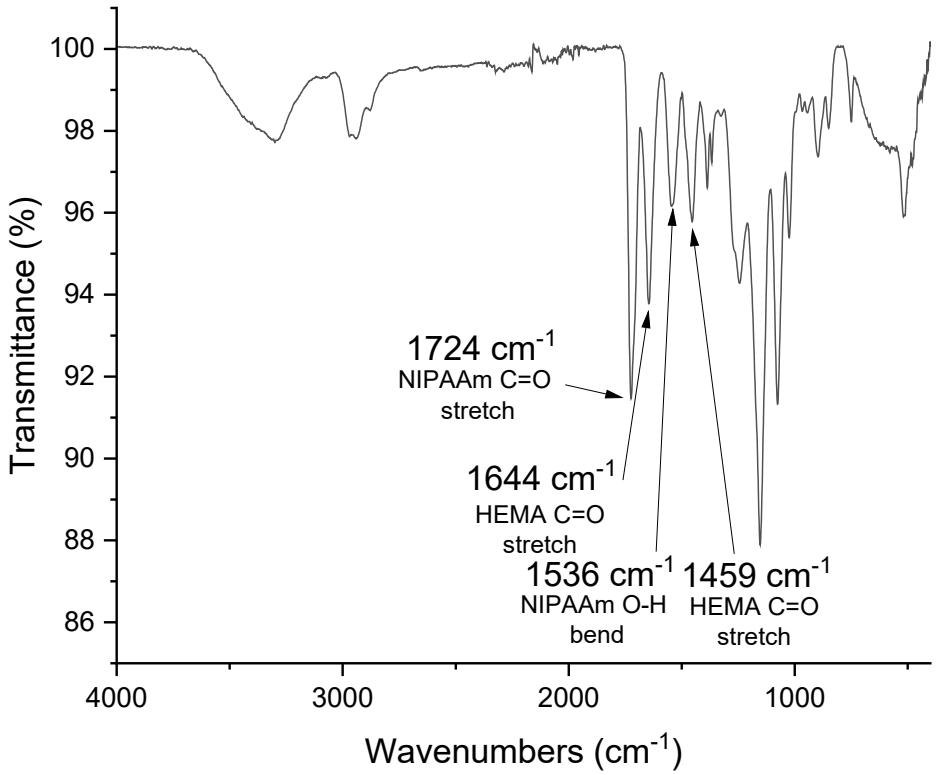

Figure S3: FTIR spectrum of poly(NIPAAm-*co*-HEMA) microgel with 3:7 NIPAAm:HEMA molar ratio (***MG3***)

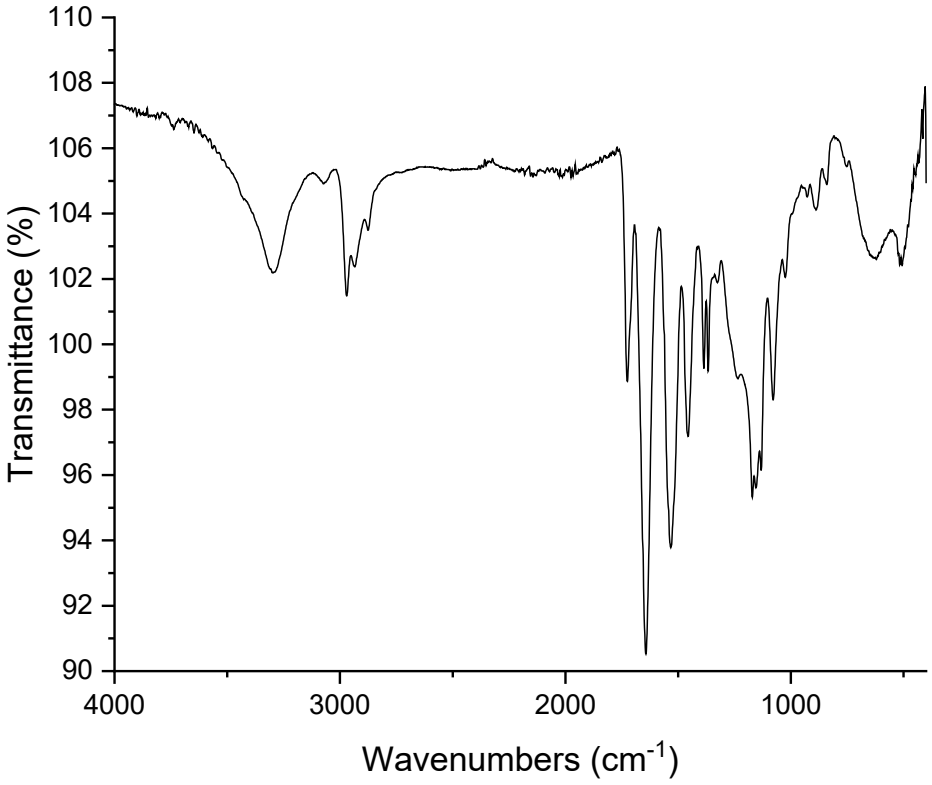

Figure S4: FTIR spectrum of poly(NIPAAm-*co*-HEMA) microgel with 7:3 NIPAAm:HEMA molar ratio and 1 mol% SDS concentration relative to monomer (***MG4***)

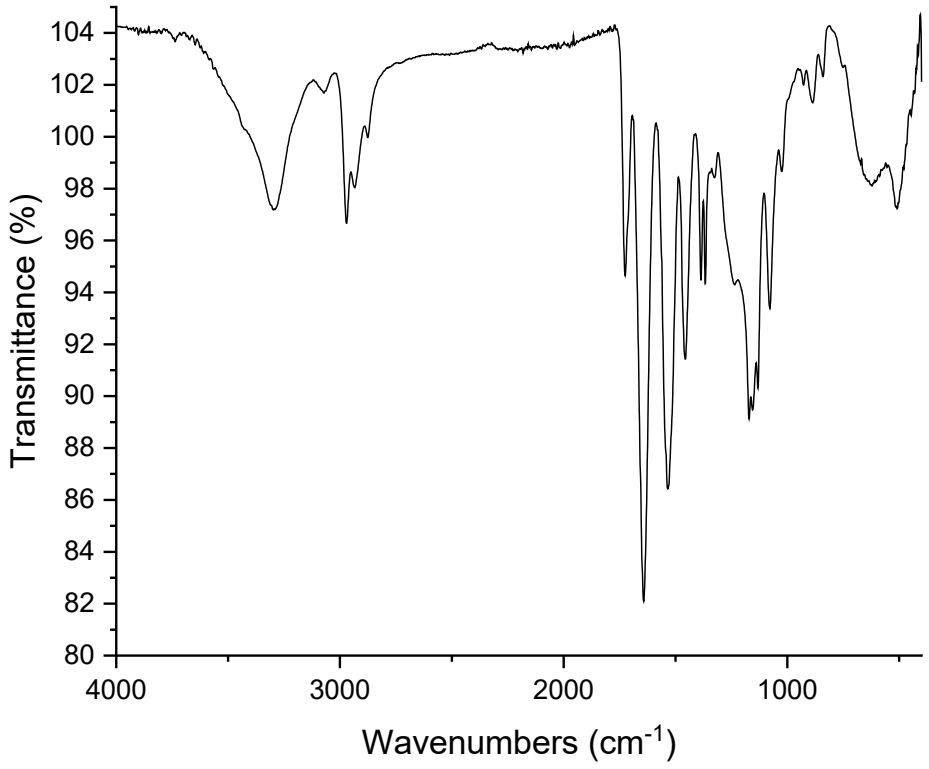

Figure S5: FTIR spectrum of poly(NIPAAm-*co*-HEMA) microgel with 7:3 NIPAAm:HEMA molar ratio and no added SDS (***MG5***)

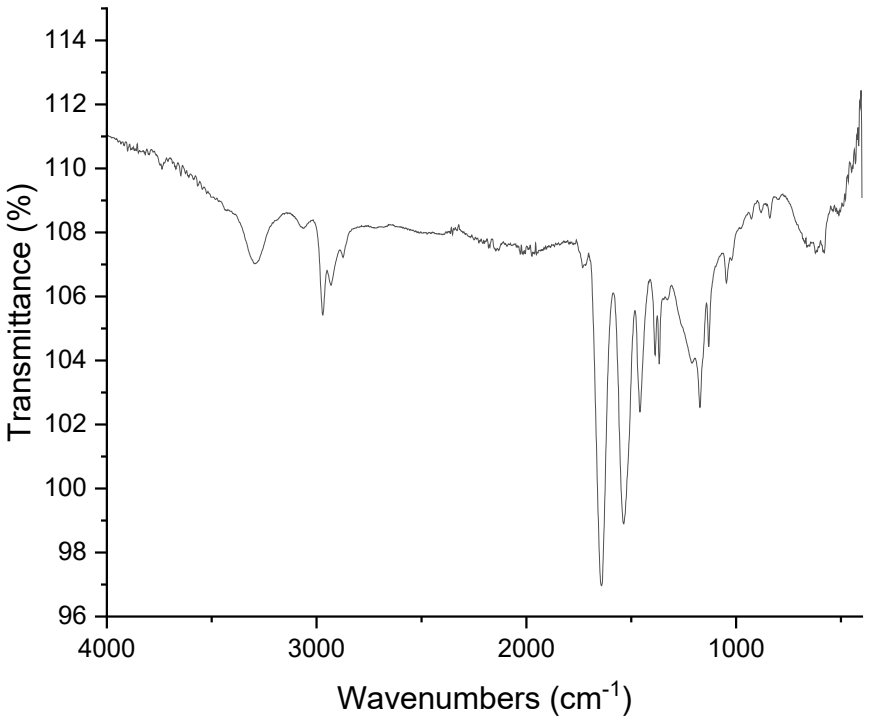

Figure S6: FTIR spectrum of creatine-functionalised poly(NIPAAm-*co*-HEMA) microgel with an original composition of 7:3 NIPAAm:HEMA and 1.0 equivalent of creatine functionalised relative to available HEMA (***MG6***)

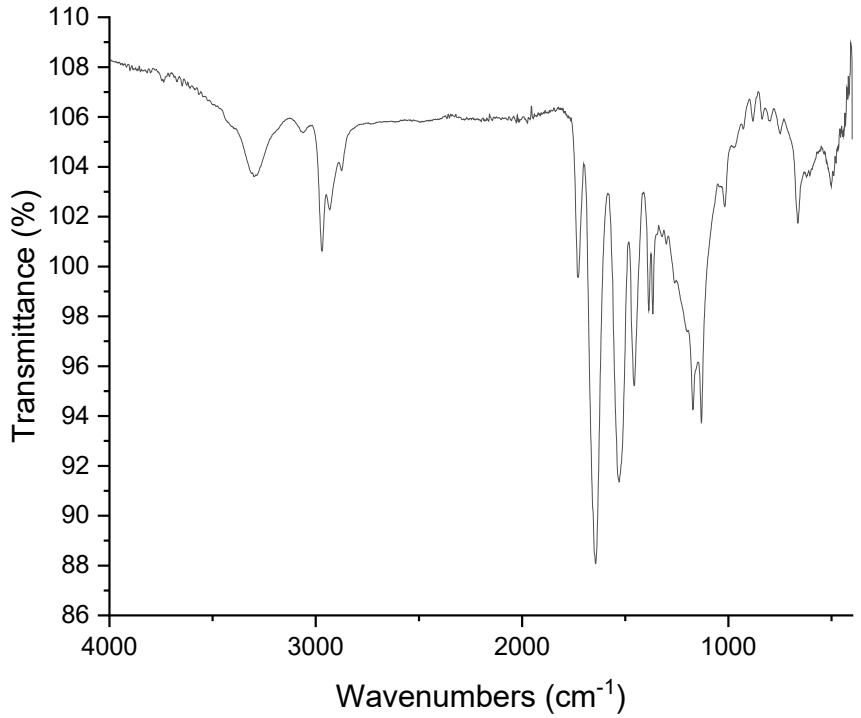

Figure S7: FTIR spectrum of creatine-functionalised poly(NIPAAm-*co*-HEMA) microgel with an original composition of 7:3 NIPAAm:HEMA and 10 equivalents of creatine functionalised relative to available HEMA (***MG7***)

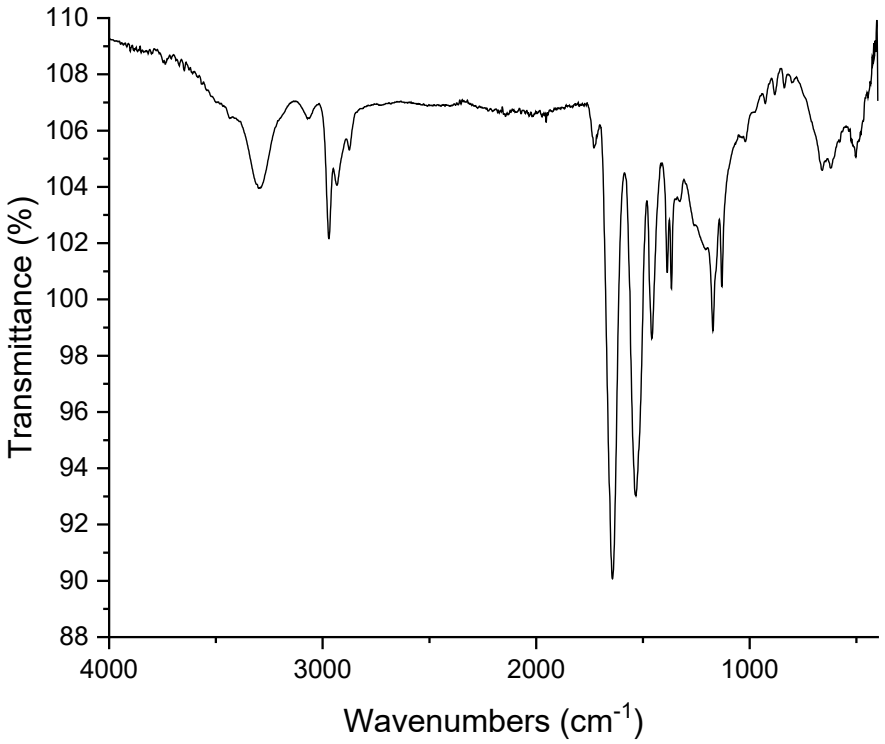

Figure S8: FTIR spectrum of creatine-functionalised poly(NIPAAm-*co*-HEMA) microgel with an original composition of 5:5 NIPAAm:HEMA and 1.0 equivalent of creatine functionalised relative to available HEMA (***MG8***)

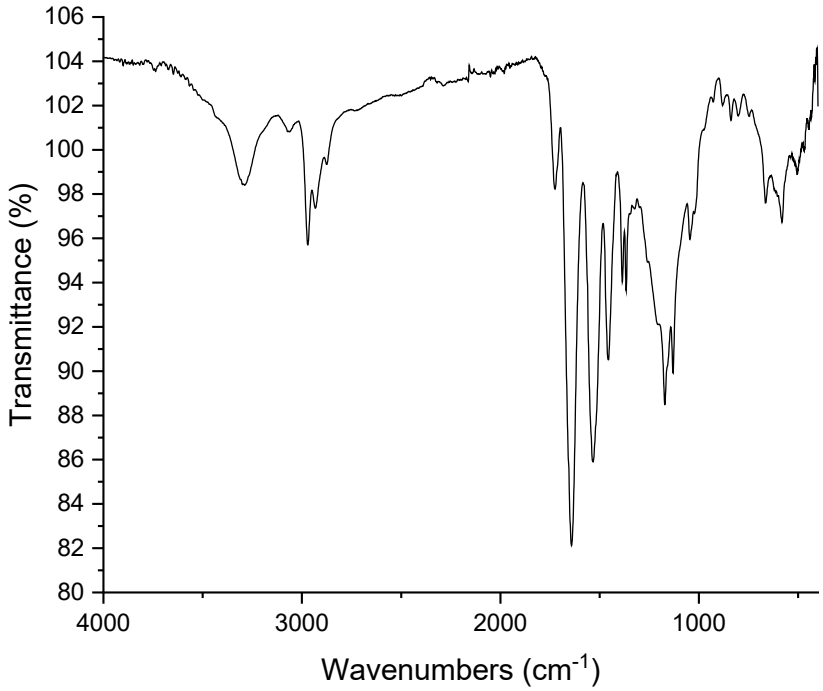

Figure S9: FTIR spectrum of creatine-functionalised poly(NIPAAm-*co*-HEMA) microgel with an original composition of 5:5 NIPAAm:HEMA and 10 equivalents of creatine functionalised relative to available HEMA (***MG9***)

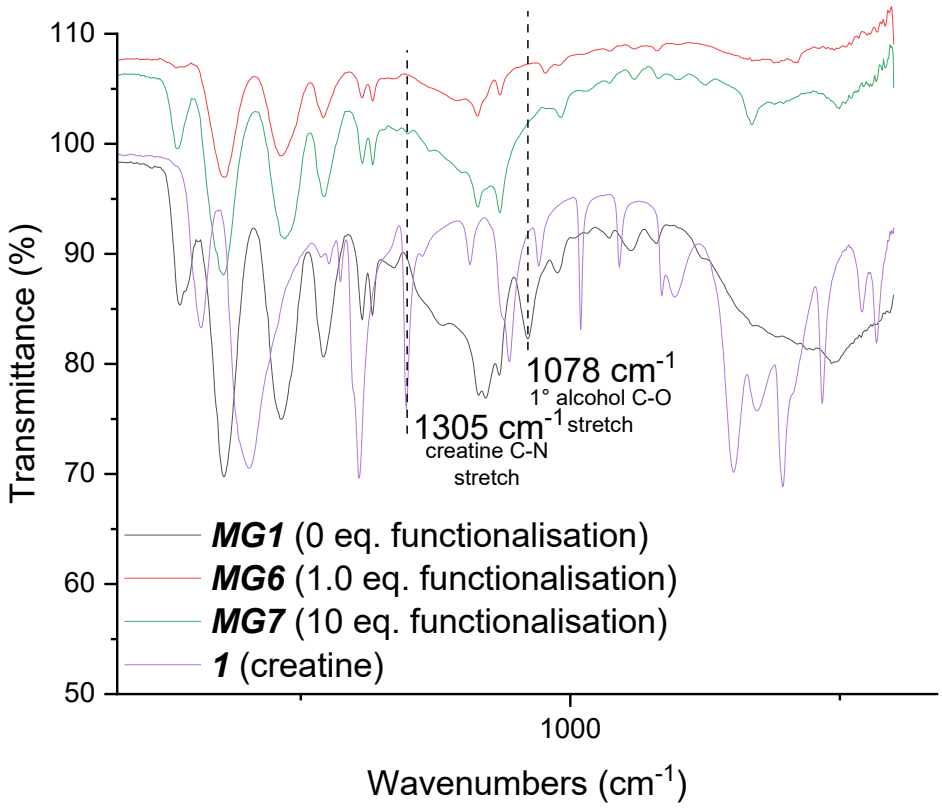

Figure S10: Superimposed FTIR spectra of ***MG1***, ***MG6***, ***MG7*** and ***1*** to show changes with functionalisation. Specifically, ***MG6*** and ***MG7*** gain a peak at 1305 cm^{-1} after functionalisation and lose a peak at 1078 cm^{-1}.

Miscellaneous

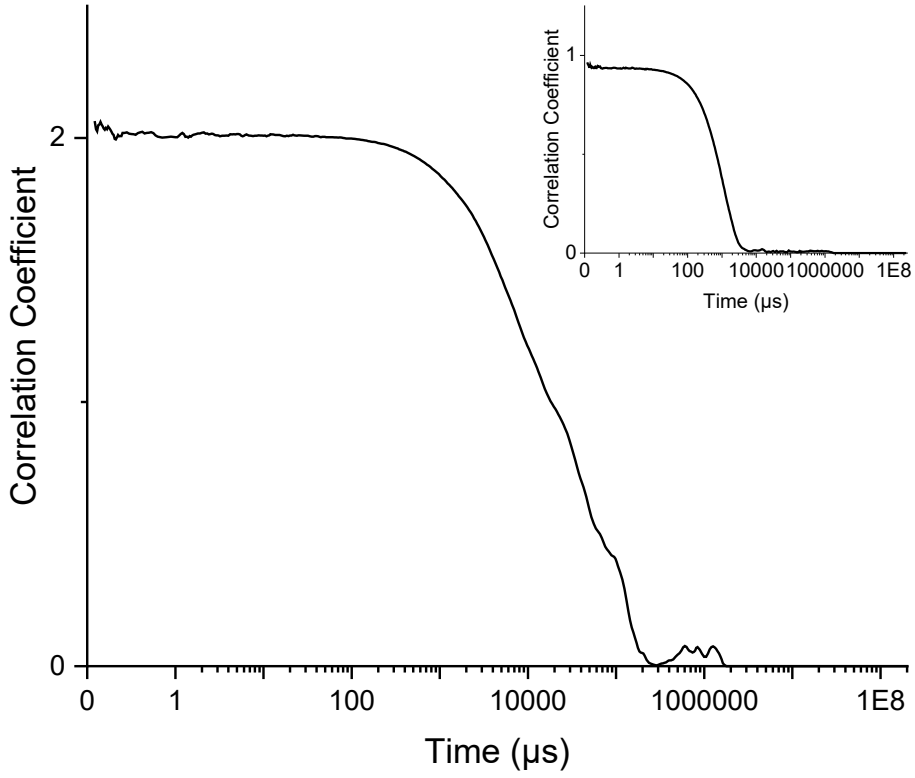

Figure S11: Correlogram of ***MG7*** at 25°C, showing the correlation function over time. Reliable DLS data has a smooth exponential decay in correlation over time, like with ***MG1*** (inset). The uneven nature of decay for ***MG7*** makes the associated DLS data questionable in quality. Thus, ***MG7*** DLS data was not used.

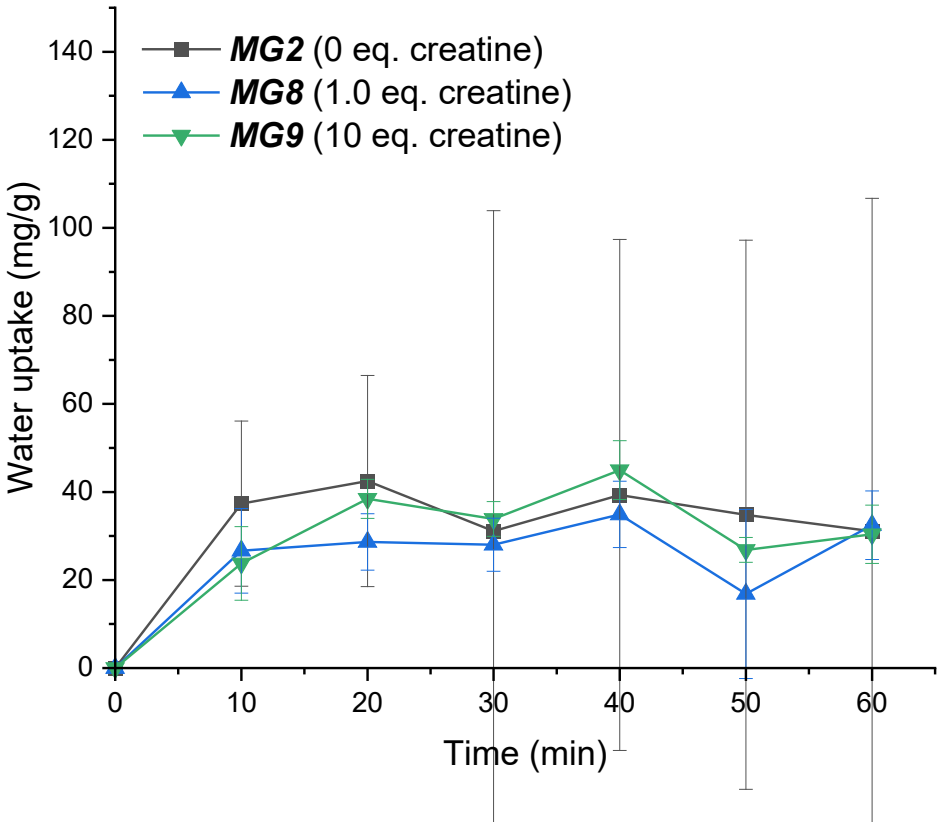

Figure S12: Water uptake over 1 hour, showing the effects of creatine functionalisation on a 5:5 composition microgel at 50% RH.

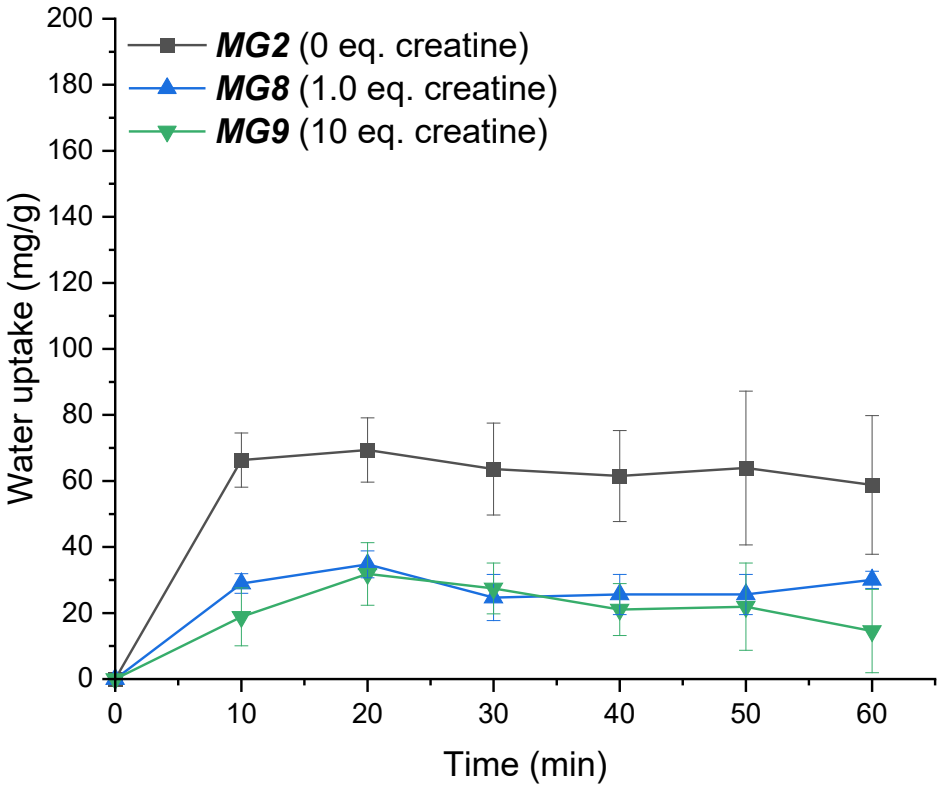

Figure S13: Water uptake over 1 hour, showing the effects of creatine functionalisation on a 5:5 composition microgel at 30% RH.

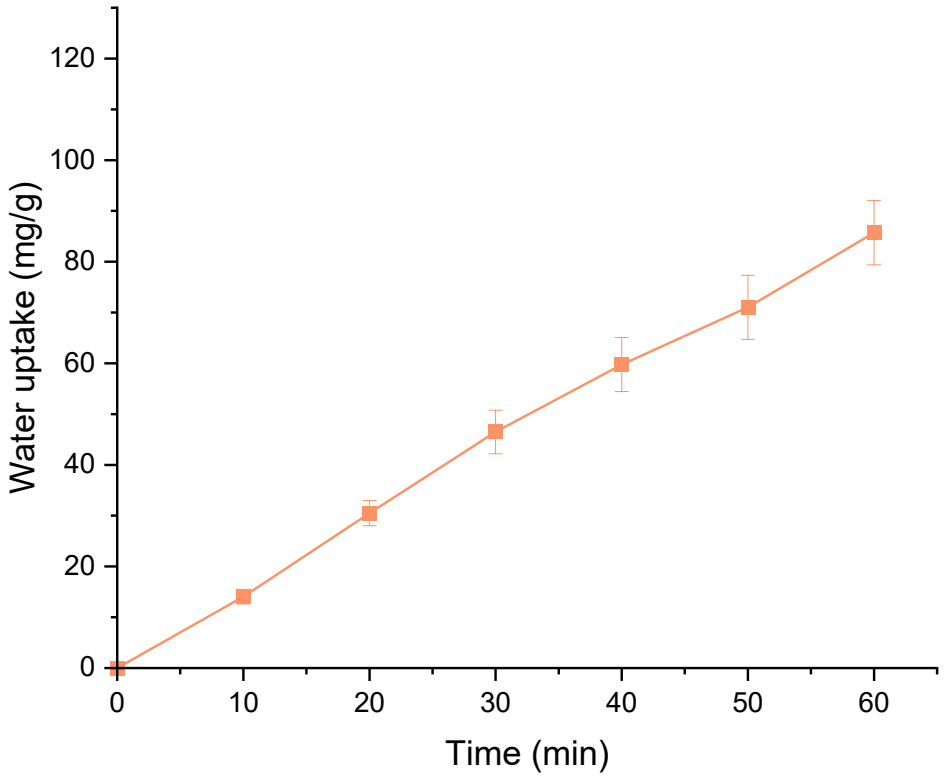

Figure S14: Water uptake over 1 hour of anhydrous creatine at 70% RH.

Sample	*Diameter (nm)*
MG1	175 ± 41
MG2	280 ± 26
MG4	292 ± 45
MG5	424 ± 33
MG8	243 ± 28
MG9	271 ± 23

Table S1: Diameter of dried microgels as measured via SEM.

References

(1) Díaz-Marín, C. D.; Zhang, L.; Lu, Z.; Alshrah, M.; Grossman, J. C.; Wang, E. N. Kinetics of Sorption in Hygroscopic Hydrogels. *Nano Letters* **2022**, *22* (3), 1100-1107. DOI: 10.1021/acs.nanolett.1c04216.
(2) Guo, Y.; de Vasconcelos, L. S.; Manohar, N.; Geng, J.; Johnston, K. P.; Yu, G. Highly Elastic Interconnected Porous Hydrogels through Self-Assembled Templating for Solar Water Purification. *Angewandte Chemie International Edition* **2022**, *61* (3), e202114074. DOI: https://doi.org/10.1002/anie.202114074.
(3) Mittal, H.; Al Alili, A.; Alhassan, S. M. Adsorption isotherm and kinetics of water vapors on novel superporous hydrogel composites. *Microporous and Mesoporous Materials* **2020**, *299*, 110106. DOI: https://doi.org/10.1016/j.micromeso.2020.110106.
(4) Wang, J.; Deng, C.; Zhong, G.; Ying, W.; Li, C.; Wang, S.; Liu, Y.; Wang, R.; Zhang, H. High-yield and scalable water harvesting of honeycomb hygroscopic polymer driven by natural sunlight. *Cell Reports Physical Science* **2022**, *3* (7), 100954. DOI: https://doi.org/10.1016/j.xcrp.2022.100954.
(5) Guo, Y.; Guan, W.; Lei, C.; Lu, H.; Shi, W.; Yu, G. Scalable super hygroscopic polymer films for sustainable moisture harvesting in arid environments. *Nature Communications* **2022**, *13* (1), 2761. DOI: 10.1038/s41467-022-30505-2.
(6) Guan, W.; Zhao, Y.; Lei, C.; Yu, G. Molecularly confined hydration in thermoresponsive hydrogels for efficient atmospheric water harvesting. *Proceedings of the National Academy of Sciences* **2023**, *120* (38), e2308969120. DOI: doi:10.1073/pnas.2308969120.
(7) Guan, W.; Lei, C.; Guo, Y.; Shi, W.; Yu, G. Hygroscopic-Microgels-Enabled Rapid Water Extraction from Arid Air. *Advanced Materials* **2024**, *36* (12), 2207786. DOI: https://doi.org/10.1002/adma.202207786.
(8) Chang, X.; Li, S.; Li, N.; Wang, S.; Li, J.; Guo, C.; Yu, L.; Murto, P.; Xu, X. Marine biomass-derived, hygroscopic and temperature-responsive hydrogel beads for atmospheric water harvesting and solar-powered irrigation. *Journal of Materials Chemistry A* **2022**, *10* (35), 18170-18184. DOI: 10.1039/D2TA04919H.
(9) Hartanto, Y.; Zargar, M.; Wang, H.; Jin, B.; Dai, S. Thermoresponsive Acidic Microgels as Functional Draw Agents for Forward Osmosis Desalination. *Environmental Science & Technology* **2016**, *50* (8), 4221-4228. DOI: 10.1021/acs.est.5b04123.
(10) Jangizehi, A.; Eckhardt, J.; Borkowska, K. I.; Dallos, Z.; Bauer, M.; Salehi, H.; Razavi, R.; Shakeri, A.; Hashemifard, S. A.; Seiffert, S. Thermo- and light responsive microgels for efficient brackish and seawater forward osmosis desalination. *Desalination* **2025**, *595*, 118314. DOI: https://doi.org/10.1016/j.desal.2024.118314.
(11) Hartanto, Y.; Yun, S.; Jin, B.; Dai, S. Functionalized thermo-responsive microgels for high performance forward osmosis desalination. *Water Research* **2015**, *70*, 385-393. DOI: https://doi.org/10.1016/j.watres.2014.12.023.
(12) Hartanto, Y.; Zargar, M.; Cui, X.; Jin, B.; Dai, S. Non-ionic copolymer microgels as high-performance draw materials for forward osmosis desalination. *Journal of Membrane Science* **2019**, *572*, 480-488. DOI: https://doi.org/10.1016/j.memsci.2018.11.042.
(13) Hwang, B. S.; Kim, J. S.; Kim, J. M.; Shim, T. S. Thermogelling Behaviors of Aqueous Poly(N-Isopropylacrylamide-co-2-Hydroxyethyl Methacrylate) Microgel–Silica Nanoparticle Composite Dispersions. *Materials* **2021**, *14* (5), 1212.
(14) Gan, T.; Zhang, Y.; Guan, Y. In Situ Gelation of P(NIPAM-HEMA) Microgel Dispersion and Its Applications as Injectable 3D Cell Scaffold. *Biomacromolecules* **2009**, *10* (6), 1410-1415. DOI: 10.1021/bm900022m.
(15) Gan, T.; Guan, Y.; Zhang, Y. Thermogelable PNIPAM microgel dispersion as 3D cell scaffold: effect of syneresis. *Journal of Materials Chemistry* **2010**, *20* (28), 5937-5944. DOI: 10.1039/C0JM00338G.
(16) Cui, X.; Tang, J.; Hartanto, Y.; Zhang, J.; Bi, J.; Dai, S.; Qiao, S. Z.; Cheng, K.; Zhang, H. NIPAM-based Microgel Microenvironment Regulates the Therapeutic Function of Cardiac Stromal Cells. *ACS Applied Materials & Interfaces* **2018**, *10* (44), 37783-37796. DOI: 10.1021/acsami.8b09757.

(17) Thanusing, M. K.; Pollard, B. L.; Connal, L. A. Arginine-functionalised hydrogels as a novel atmospheric water-harvesting material. *RSC Applied Polymers* **2025**, *3* (2), 480-487. DOI: 10.1039/D4LP00373J.
(18) Maity, D.; Teixeira, A. P.; Fussenegger, M. Hydratable Core–Shell Polymer Networks for Atmospheric Water Harvesting Powered by Sunlight. *Small* **2023**, *19* (47), 2301427. DOI: https://doi.org/10.1002/smll.202301427.
(19) Zhang, S.; Fu, J.; Xing, G.; Zhu, W.; Ben, T. Recent advances in porous adsorbent assisted atmospheric water harvesting: a review of adsorbent materials. *Chemical Synthesis* **2023**, *3* (2), 10.
(20) Pollard, B. L.; Thanusing, M. K.; Connal, L. A. WHO said what? Non-robust standards in citing WHO and EPA drinking water guidelines. *Molecular Systems Design & Engineering* **2026**. DOI: 10.1039/D5ME00181A.
(21) Antonio, J.; Candow, D. G.; Forbes, S. C.; Gualano, B.; Jagim, A. R.; Kreider, R. B.; Rawson, E. S.; Smith-Ryan, A. E.; VanDusseldorp, T. A.; Willoughby, D. S.; et al. Common questions and misconceptions about creatine supplementation: what does the scientific evidence really show? *Journal of the International Society of Sports Nutrition* **2021**, *18* (1), 13. DOI: 10.1186/s12970-021-00412-w.
(22) Zhao, F.; Zhou, X.; Liu, Y.; Shi, Y.; Dai, Y.; Yu, G. Super Moisture-Absorbent Gels for All-Weather Atmospheric Water Harvesting. *Advanced Materials* **2019**, *31* (10), 1806446. DOI: https://doi.org/10.1002/adma.201806446.
(23) Matsumoto, K.; Sakikawa, N.; Miyata, T. Thermo-responsive gels that absorb moisture and ooze water. *Nat. Commun.* **2018**, *9* (1), 2315. DOI: 10.1038/s41467-018-04810-8.
(24) Lee, S. J.; Ha, N.; Kim, H. Superhydrophilic–Superhydrophobic Water Harvester Inspired by Wetting Property of Cactus Stem. *ACS Sustainable Chem. Eng.* **2019**, *7* (12), 10561-10569. DOI: 10.1021/acssuschemeng.9b01113.
(25) Zhang, R.; Gao, R.; Gou, Q.; Lai, J.; Li, X. Precipitation Polymerization: A Powerful Tool for Preparation of Uniform Polymer Particles. *Polymers (Basel)* **2022**, *14* (9). DOI: 10.3390/polym14091851 From NLM.
(26) Shen, Z.; Terao, K.; Maki, Y.; Dobashi, T.; Ma, G.; Yamamoto, T. Synthesis and phase behavior of aqueous poly(N-isopropylacrylamide-co-acrylamide), poly(N-isopropylacrylamide-co-N,N-dimethylacrylamide) and poly(N-isopropylacrylamide-co-2-hydroxyethyl methacrylate). *Colloid and Polymer Science* **2006**, *284* (9), 1001-1007. DOI: 10.1007/s00396-005-1442-y.
(27) Feil, H.; Bae, Y. H.; Feijen, J.; Kim, S. W. Effect of comonomer hydrophilicity and ionization on the lower critical solution temperature of N-isopropylacrylamide copolymers. *Macromolecules* **1993**, *26* (10), 2496-2500. DOI: 10.1021/ma00062a016.
(28) Wang, Y.; Chu, X.; Sun, Y.; Teng, P.; Xia, T.; Chen, Y. A convenient approach by using poly-(HEMA-co-NIPAM)/Cu2+ solution sol–gel transition for wound protection and healing. *Journal of Biomedical Materials Research Part B: Applied Biomaterials* **2021**, *109* (1), 50-59. DOI: https://doi.org/10.1002/jbm.b.34679.
(29) Weaver, J. V. M.; Bannister, I.; Robinson, K. L.; Bories-Azeau, X.; Armes, S. P.; Smallridge, M.; McKenna, P. Stimulus-Responsive Water-Soluble Polymers Based on 2-Hydroxyethyl Methacrylate. *Macromolecules* **2004**, *37* (7), 2395-2403. DOI: 10.1021/ma0356358.
(30) Thanusing, M. K.; Shen, P.; Pollard, B. L.; Connal, L. A. Rational design of water-harvesting hydrogels. *Molecular Systems Design & Engineering* **2024**, *9* (1), 63-72. DOI: 10.1039/D3ME00132F.
(31) Newns, A. C. Sorption and Diffusion in Polymers. *Nature* **1968**, *218* (5139), 355-356. DOI: 10.1038/218355b0.
(32) Zhou, X.; Lu, H.; Zhao, F.; Yu, G. Atmospheric Water Harvesting: A Review of Material and Structural Designs. *ACS Materials Letters* **2020**, *2* (7), 671-684. DOI: 10.1021/acsmaterialslett.0c00130.
(33) Park, H.; Haechler, I.; Schnoering, G.; Ponte, M. D.; Schutzius, T. M.; Poulikakos, D. Enhanced Atmospheric Water Harvesting with Sunlight-Activated Sorption Ratcheting. *ACS Applied Materials & Interfaces* **2022**, *14* (1), 2237-2245. DOI: 10.1021/acsami.1c18852.
(34) von Nessen, K.; Karg, M.; Hellweg, T. Thermoresponsive poly-(N-isopropylmethacrylamide) microgels: Tailoring particle size by interfacial tension control. *Polymer* **2013**, *54* (21), 5499-5510. DOI: https://doi.org/10.1016/j.polymer.2013.08.027.

(35) McPhee, W.; Tam, K. C.; Pelton, R. Poly(N-isopropylacrylamide) Latices Prepared with Sodium Dodecyl Sulfate. *Journal of Colloid and Interface Science* **1993**, *156* (1), 24-30. DOI: https://doi.org/10.1006/jcis.1993.1075.
(36) Singh, D.; Kuckling, D.; Choudhary, V.; Adler, H.-J.; Koul, V. Synthesis and characterization of poly(N-isopropylacrylamide) films by photopolymerization. *Polymers for Advanced Technologies* **2006**, *17* (3), 186-192. DOI: https://doi.org/10.1002/pat.713.
(37) Gutiérrez-Hellín, J.; Del Coso, J.; Franco-Andrés, A.; Gamonales, J. M.; Espada, M. C.; González-García, J.; López-Moreno, M.; Varillas-Delgado, D. Creatine Supplementation Beyond Athletics: Benefits of Different Types of Creatine for Women, Vegans, and Clinical Populations—A Narrative Review. *Nutrients* **2025**, *17* (1), 95.
(38) Kandula, M. COMPOSITIONS AND METHODS FOR THE TREATMENT OF NEUROMUSCULAR DISORDERS. India 2014.
(39) Singh, S.; Dash, A. K. Chapter 1 - Creatine Monohydrate. In *Profiles of Drug Substances, Excipients and Related Methodology*, Brittain, H. G. Ed.; Vol. 34; Academic Press, 2009; pp 1-35.
(40) Ng, W. S.; Forbes, E.; Franks, G. V.; Connal, L. A. Xanthate-Functional Temperature-Responsive Polymers: Effect on Lower Critical Solution Temperature Behavior and Affinity toward Sulfide Surfaces. *Langmuir* **2016**, *32* (30), 7443-7451. DOI: 10.1021/acs.langmuir.6b00211.
(41) Tůma, P.; Sommerová, B.; Koval, D.; Šiklová, M.; Koc, M. Plasma levels of creatine, 2-aminobutyric acid, acetyl-carnitine and amino acids during fasting measured by counter-current electrophoresis in PAMAPTAC capillary. *Microchemical Journal* **2023**, *187*, 108426. DOI: https://doi.org/10.1016/j.microc.2023.108426.
(42) Zhang, Z.; Wang, Y.; Li, Z.; Fu, H.; Huang, J.; Xu, Z.; Lai, Y.; Qian, X.; Zhang, S. Sustainable Hierarchical-Pored PAAS–PNIPAAm Hydrogel with Core–Shell Structure Tailored for Highly Efficient Atmospheric Water Harvesting. *ACS Applied Materials & Interfaces* **2022**, *14* (49), 55295-55306. DOI: 10.1021/acsami.2c19840.
(43) Arlin, J.-B.; Bhardwaj, R. M.; Johnston, A.; Miller, G. J.; Bardin, J.; MacDougall, F.; Fernandes, P.; Shankland, K.; David, W. I. F.; Florence, A. J. Structure and stability of two polymorphs of creatine and its monohydrate. *CrystEngComm* **2014**, *16* (35), 8197-8204. DOI: 10.1039/C4CE00508B.
(44) Braun, D. E.; Orlova, M.; Griesser, U. J. Creatine: Polymorphs Predicted and Found. *Crystal Growth & Design* **2014**, *14* (10), 4895-4900. DOI: 10.1021/cg501159c.
(45) Kim, S.; Liang, Y.; Kang, S.; Choi, H. Solar-assisted smart nanofibrous membranes for atmospheric water harvesting. *Chemical Engineering Journal* **2021**, *425*, 131601. DOI: https://doi.org/10.1016/j.cej.2021.131601.
(46) Milatz, R.; Reink, C.; van den Berg, T. E.; Duvigneau, J.; Vancso, G. J.; Wurm, F. R. Water-harvesting polymer coatings for plant leaves. *RSC Applied Polymers* **2025**, *3* (1), 173-180. DOI: 10.1039/D4LP00249K.
(47) Schweng, P.; Mayer, F.; Galehdari, D.; Weiland, K.; Woodward, R. T. A Robust and Low-Cost Sulfonated Hypercrosslinked Polymer for Atmospheric Water Harvesting. *Small* **2023**, *19* (50), 2304562. DOI: https://doi.org/10.1002/smll.202304562.

Conclusions and Future Work

Atmospheric water harvesting is a promising method for alleviating water scarcity. **Chapter 1** provided an overview of the current landscape in atmospheric water harvesting, highlighting the lack of purely polymeric desiccants in the field. **Chapter 2** established a framework for rational design based on the relationship between polymer structure and water harvesting properties. Changes to polymer composition, crosslinking density and crosslinker length all had significant effects on water harvesting. Repeating these experiments on differing polymer systems would yield further insight on the robustness of the rational design framework. A well-developed rational design framework will be key to the efficient development of future SAWH hydrogels. In **Chapter 3**, *L*-arginine post-functionalisation was reported as a novel method of improving water harvesting performance. *L*-arginine is an accessible source of the guanidinium moiety which has significant effects on water uptake. The rapid water harvesting kinetics of this polymer could yield 2 g/g of water per day with 70-minute cycles. Optimisation of the functionalisation process would be a logical continuation to this research. Incorporation of other guanidinium-bearing or generally hygroscopic molecules through post-functionalisation would likely yield similar or even superior improvements in water uptake. **Chapter 4** presented microgel desiccants developed with the insights gained from previous chapters. These microgels could uptake as much as 1.8 g/g after 1 h at 60–70% RH, which exceeds the original benchmark of 1 g/g set in **Chapter 1**. While there remains ample room for optimisation, these systems are already highly promising for SAWH. The most immediate improvements could be made to functionalisation, where more elegant approaches (via functional group or reaction choice) would allow for better scalability. Beyond specific optimisations, exploring the design and implementation of SAWH devices incorporating these microgels is the salient continuation of this work. On a more general level, further research into microgels offers an interesting class of SAWH materials otherwise unexplored.

Two major directions for future research into fully polymeric SAWH hydrogels present themselves. One direction would be the further development of the rational design framework for streamlining new SAWH systems. To improve this framework, further research into structure-property relationships for SAWH is critical. Gathering structure-property data from a wide range of polymers will lead to the emergence of clear chemical patterns which may help identify new leads for SAWH, and these fundamental studies can serve as a foundation

to the development of new materials beyond SAWH. The second salient direction for research would be the development of fully polymeric SAWH hydrogels employing a wider variety of polymers and synthetic methods. I anticipate that this would be a fruitful exercise given the relative infancy of this field and the abundance of diverse materials available to the modern chemist. There is ample opportunity for novel and impactful research in this field regardless of which direction is taken.

Beyond the polymer chemistry aspects of SAWH hydrogel development, it is necessary to remain cognisant of systems-level considerations like sustainability or commercialisation. Each step of polymer production has a water and energy cost, and the final product must harvest water well enough to offset these costs. Additionally, life cycle assessment is necessary to evaluate the environmental effect of a material, from chemical feedstocks to degradation products. These systems-level considerations will become increasingly important as SAWH research further matures.

The current landscape for SAWH hydrogels has quickly converged to a dependence on functional additives without close examination of the nominal hydrogels themselves. I find it only natural to wonder what hydrogels could achieve on their own merits and properties both in this space and beyond. This compilation of work has established the significance and potential of fully polymeric materials for atmospheric water harvesting. I believe that these polymeric systems have a genuine chance to be at the forefront of SAWH research and I am optimistic towards their future developments.